JRC Scientific and Technical Reports

Structural Response of a Large Pressure Vessel to Dynamic Loading

Fast Transient 3-D Dynamic Analysis of the Effect of a Blast Wave

Elena Paffumi & Nigel Taylor

EUR 23451 EN - 2008

JRC EUROPEAN COMMISSION

Institute for Energy

The Institute for Energy provides scientific and technical support for the conception, development, implementation and monitoring of community policies related to energy. Special emphasis is given to the security of energy supply and to sustainable and safe energy production.

European Commission
Joint Research Centre
Institute for Energy

Contact information
Address: E. Paffumi
E-mail: elena.paffumi@jrc.nl
Tel.: +31 224 565082
Fax: +31 224 565641

http://ie.jrc.ec.europa.eu
http://www.jrc.ec.europa.eu

JRC 46828

EUR 23451 EN
ISSN 1018-5593

Luxembourg: Office for Official Publications of the European Communities

Printed in The Netherlands

Structural Response of a Large Pressure Vessel to Dynamic Loading

Fast Transient 3-D Dynamic Analysis of the Effect of Blast Wave

Elena Paffumi & Nigel Taylor

Contents

1 SCOPE

The potential of industrial plant to maintain its structural integrity when subject to fast transient dynamic loading, resulting from a blast wave caused either by accidental or a malicious event, is an issue of concern for vulnerability assessments. As part of the JRC's FP6 internal research project SAFELIFE, a study has been performed on the feasibility of performing reliable dynamic structural integrity analysis considering the effect of an external explosion on a steel vessel containing pressurized water[1]. The evaluation of pressures and impulses produced by blast loads has been studied using the EUROPLEXUS-SAMCEF FIELD and ABAQUS software codes [1,2,3]. This report describes the results of the investigation and the finite element simulations.

The work builds on a preliminary study [3], in which some examples of fast transient phenomena due to high pressure loads were considered as part of a familiarization process with the EUROPLEXUS/SAMCEF and ABAQUS Explicit programs and their standard dynamic input file options. A calibration analysis was run to compare the numerical results obtained by EUROPLEXUS with literature values and with those obtained with analytical expressions for different scaled distances and boundary conditions. In particular, the capacity to capture the effects of mesh size on pressure and impulse distribution was studied [4,5] (this calibration can be found also in Appendix A). However the main focus was on the 3-D simulation of a large vessel of hypothetical design containing pressurised water and subject to an explosive blast from a charge located directly underneath the lower domed end. The top of the vessel is closed by a flat lid arrangement. The properties of the explosive material, the air and water environments and the vessel steel were taken from the literature. An extensive series of computations were performed, principally with the EUROPLEXUS code since ABAQUS has limitations for modelling the fluid domain and fluid-structure interactions. Several aspects such as structural damping factors, elastic material properties, strain rate dependences of the material properties effects were considered, using the results of the elastic-plastic analysis at 20˚C as a baseline. The main conclusions were:

- The change in material properties between 20 and 400ºC has little effect on the global behaviour of the vessel (the temperature dependences of the material properties however has not been considered);
- Less deformation is predicted in the vessel if material damping is applied, due to the dissipation of energy in friction and mass effects. In general the material damping effects are neglected to have more conservative estimates of structural behaviour;
- Having absorbing boundary conditions (abso) at the walls of the bunker to simulate an infinite environment of air around the vessel leads to a smaller deformation of the vessel;
- The strain rate dependency of the material properties under high dynamic load was studied with both the Cowper-Symonds and Ispra models; both lead to the same behaviour. The resulting displacements are reduced from those of the standard elastic-plastic analysis and are close to the elastic case, for an analysis where the water is not in equilibrium inside the vessel.
- For the mesh the following points should be noted: for the explosive material modelled with the JWL equation, hexahedral elements were used. A 10 cm mesh appears accurate enough for the analysis of wave propagation in open environments.
- If the blast due to the 5 kg charge directly below the vessel is considered alone, the resulting deflections are well within in the elastic range. There is a slight upwards deflection at the bottom of the vessel, which receives the blast wave directly. The flat lid on the top of the vessel deflects downwards due to reflected pressure waves. It is noted that the dynamic deflections from the blast are more than an order of magnitude less than the static deflections due a 155 bar internal pressure.

[1] This topic is no longer part of the SAFELIFE work programme; however since the demonstration of computational feasibility was only completed at the end of 2007 the results are now being documented.

- The presence (inertia) of water inside the vessel but without pressure appears to have little effect on the predicted behaviour; the deformation levels are too small to reliably attribute physical effects to any differences observed with respect to the empty vessel case.

The current report deals with the analyses performed with a new release of EUROPLEXSUS (version, 2007), which allows delayed detonation times and therefore opens the possibility to directly combine an initial quasi-static damping analysis (to calculate the stresses due static loads in the structure) with a dynamic analysis of the fluid-structure interaction due to the explosion. The sensitivity of the predictions to the various factors, including the material properties, boundary conditions and the explosive model, has been considered. Finally the potential to simulate failure or fracture of the steel structure with a progressive damage model has been investigated.

2 3D MODEL OF THE VESSEL SUBJECT TO AN EXTERNAL BLAST

2.1 Mesh and boundary conditions

Figure 1 shows the geometry of the vessel modelled. It has a cylindrical body with a torispherical end and a flat top, containing high-pressure water (at 155 bar). It is located in an open bunker, as shown in Figure 2. The bunker is a box of dimensions 10m x 10m x10m.

An attempt was made during the preliminary study [4] to mesh the model using tetrahedral elements. These are easier for complex geometries and round shapes, but due to some limitations of the software in relation to these specific elements, hexahedrons elements had to be used. The mesh (Figure 3) was prepared by a rotation of a 2D mesh; details of the bottom and the explosive charge are given in Figure 4. As reported in [4], there were some convergence problems in the elements along the axis of rotation and around the explosive bubble. Moreover, it proved impossible to program a delay in the detonation time of the explosion to allow calculation of the static pre-stress in the vessel due to the high pressure water. This meant the results obtained did properly reflect the problem.

With the new release of the EUROPLEXSUS software it is possible to use a delay in the detonation time, but there was again the problem of convergence in the hex elements along the axis of rotation. Therefore the use of the tetrahedral elements was considered again for generating a refined mesh around the bubble (representing the explosive), due to the complex geometry. The problem with the tetrahedral elements had been fixed in the mean time and a detonation time delay was added in the high explosive routine for the JRC elements. It has to be specified, in fact, that in EUROPLEXUS two sets of elements are available, one set developed by JRC and one developed by CEA. The graphical interface, SAMCEF FIELD, uses as default the CEA elements and in the preliminary study [4] these elements were used together with their specific material models. To use the JRC elements from this interface, some dedicated command lines have to be put in the epilogue for the conversion between the two kinds of elements. This is also a new option in the new release of the software and it was used during the current work to take advantage of corrections to the JRC elements (mainly the detonation time delay not yet introduced for the CEA elements).

The main goal of this new work was to run three analyses in one, that is:

1. a quasi-static damping analysis up to an equilibrium state of the water-vessel system, to create the pre-stresses and strain in the vessel due to the water;
2. the blast and associated pressure waves;
3. and the final oscillations of the vessel to a post-explosion equilibrium state.

In [4] it had not been possible to consider the pre-stresses and pre-strains due to the high pressure of the water inside the vessel in a single analysis. A so-called re-start procedure was considered, but some limitations on the initialization of the element variables during the restart meant that the predicted structural behaviour of the vessel (which was the principal interest of the work) could not be considered realistic.

Figure 5 shows the mesh prepared with the tetrahedral elements. Figure 6 shows some details of this mesh. More precisely, in Figure 6a) the vessel and the charge box at 1 meter below the vessel are

shown, while Figure 6b) and c) provide details of the mesh of the charge box surrounded by the air elements. The charge box (0.145m x 0.145m x 0.145m) here corresponds to 5 kg of explosive. To give a compete overview of the tetrahedral mesh, a cut view for solid elements was used and the results are reported in Figure 7. The mesh is refined in and directly around the charge box, and then progressively enlarges towards the walls of the bunker, where there is no need for refinement.
One of the main objectives is to have a 3D conformed mesh (corresponding nodes at the interface between different domains) for the FSI calculation. In this case we have two such node interfaces:

- one internal between the water and metal of the vessel and
- one external between air and metal of the vessel wall.

To perform an ALE (Arbitrary Lagrangian Eulerian type) computation the interface nodes need to be in perfect correspondence. The graphical pre-processor in SAMCEF FIELD was used to produce the mesh, making a great effort to ensure exact correspondence between the different domains. It was a challenging work to achieve this for the various interfaces, considering also the different levels of mesh refinement needed at different locations.

For defining the properties of the elements, most of the work was done at the level of the epilogue, an interface that allows use of the EUROPLEXUS commands as well as the BACON language.

2.1.1 Vessel Boundary Conditions

The vessel is fixed rigidly at four equally-spaced points at the top flange, Figure 8, simulating possible clamping positions as shown in Figure 2. The different thicknesses of the vessel were modelled as shown in Figure 9. The transition section corresponding to the weld between the upper and lower part of the vessel (see Figure 1 and Figure 2) was modelled by a ring of thickness equal to the mean value of these two parts, Figure 9.

2.1.2 Bunker Boundary Conditions

Once a well-conformed mesh had been obtained, the bunker boundary conditions were defined. Two different approaches were considered:

a) completely rigid surfaces with reflection of the pressure waves applying the FSR (fluid sliding on the face) conditions;

b) an infinite bunker approximation, in which an infinite volume of air around the vessel is simulated by imposing absorbing conditions for the pressure waves at the walls.

2.2 Material Models

To run the 3 analyses consecutively, new command lines were added in the epilogue window (EUROPLEXUS command language) and JRC elements were used rather than CEA elements for the explosive and the fluids. This implied the change of the material models used up to now in [4]. First, a command line that converts CEA elements in JRC elements was added in the epilogue for all the fluid elements and groups. Specifically these commands were:

```
.ael group "Bubble_el" orde 1
.ael group "Air_el" orde 1
.ael group "Water_el" orde 1
```

The solid elements were kept as CEA elements since they give more accurate prediction of structural behaviour. Second, all the fluid material models were converted in JRC fluid material models, using the FLUT directive. This allows in fact the definition of a USER-DEFINED FLUID through the different values that can be assumed by its parameter NUM and it can be used to define not just the air and water, but also the JWL explosive equation.

To define the water and its initial pressure, the NUM=9 model was used. The general directive for fluid does not allow defining the initial pressure of water by the parameter pini. Also the internal

energy value (that could potentially be set equal to the value correlated to the 155 bar initial pressure) is not taken into account. Hence to define the initial pressure of the water the parameter PB (a constant used in the user-defined fluid models for the sound speed evaluation) has been used. The material model number 9 was modified in such a way so that PB defines the reference pressure. The following shows the commands in detail:

- Air

The air properties have been defined by the directive FLUT, at epilogue level imposing NUM=11.

```
.EPX
MATE
** air: eint  calculated for P=1bar
*
   flut ro 1.3 eint 0.21978e6 gamm 1.35 PB 0
      ITER 1 ALF0 1 BET0 1 KINT 0 AHGF 0 CL 0.5
      CQ 2.56 PMIN 0 PREF 1.e5 NUM 11
      a 3.738e11 b 3.747e9 r1 4.15 r2 0.90
      ros 1630
      LECT group "AIR"  TERM
```

- TNT

The high explosive material has been modelled by the directive FLUT, imposing NUM=11 and considering the modifications implemented for modelling the charge explosion as the JWL directive, at epilogue level

```
   flut ro 1630 eint 3.68e6 gamm 1.35 PB 0
      ITER 1 ALF0 1 BET0 1 KINT 0 AHGF 0 CL 0.5
      CQ 2.56 PMIN 0 PREF 1.e5 NUM 11
      a 3.738e11 b 3.747e9 r1 4.15 r2 0.90
      d 6930 pini 1e5
      TDET 40e-3
      xdet 0. ydet 0. zdet 0.07142857
         LECT group "BUBBLE" TERM
```

- Water

The water properties have been defined by the directive FLUT at epilogue level. In this case the value of the initial specific energy is set to 0, and the parameter PB, corresponding to the initial pressure for the model NUM 9, set equal to 155bar=15.5MPa.

```
FLUT RO 1000 EINT 0 GAMM 2.1316E9 PB 15.5e6
      ITER 1 ALF0 0.5 RREF 1000 BET0 0
      KINT 1 AHGF 0 CL 0  CQ 0
      PMIN 0 NUM 9 PREF 1.E5
      LECT group "Water_el"  TERM
```

- Vessel

The material of the vessel is A533B steel modelled by means of the stress-strain curve from experimental data. The temperature dependencies of the main parameters are defined as follows [6]:

- 0.2% proof stress σ_0 versus temperature for $20 \leq T(^{\circ}C) \leq 600$:

$$\sigma_0(MPa) = b[0] + b[1] \cdot T + b[2] \cdot T^2 + b[3] \cdot T^3 (^{\circ}C) \quad (1)$$

with: $b[0] = 484.18$, $b[1] = -0.604$, $b[2] = 2.487E\text{-}03$ and $b[3] = -3.571E\text{-}06$

- ultimate tensile stress, UTS, versus temperature for $250 \leq T(^{\circ}C) \leq 600$

$$UTS(MPa) = b[0] + b[1] \cdot T + b[2] \cdot T^2 (°C) \quad (2)$$

with: $b[0]$ = 543.26; $b[1]$ = 0.912 and $b[2]$ = -2.209E-03

- Young's modulus, E, versus temperature for -100≤ T(˚C) ≤600

$$E(MPa) = A + B \cdot T(°C) \quad (3)$$

with: A = 207200 and B = -57.1 (expression due to Oldfield).

Figure 10 shows the experimental stress-strain curve for different temperature conditions, 20˚C and 400˚C, for different strain rate and from SAMCEF Field interpolation calculation. As can be seen, the effect of the temperature is limited but that of strain rate can be important. The different available strain rate dependent constitutive equations were not considered in detail in this specific work. In [4] both the Symond-Cooper and Ispra law were used and it was shown that these two material models generate the same results. Hence, during the current work only von Mises stress criterion with the Cowper-Symonds strain rate dependent model was applied:

$$\dot{\varepsilon} = D\left(\frac{\sigma_0'}{\sigma_0} - 1\right)^q, \qquad \sigma_0' \geq \sigma_0 \quad (4)$$

where σ_0' is the dynamic flow stress at a uniaxial plastic strain rate $\dot{\varepsilon}$, σ_0 is the associated static flow stress and D and q are constants for a particular material. With D=40.4sec^{-1} and q=5, this gives reasonable agreement with the experimental data for mild steel assembled by Symonds [7,8]. For generalized multiaxial loading, the following form can be used:

$$\frac{\sigma_e'}{\sigma_0} = 1 + \left(\frac{\dot{\varepsilon}_e}{D}\right)^{1/q} \quad (5)$$

where

$$\sigma_e' = \left[\left(\sigma_x' - \sigma_y'\right)^2 + \left(\sigma_y' - \sigma_z'\right)^2 + \left(\sigma_z' - \sigma_x'\right)^2 + 6\left(\tau_{xy}'^2 + \tau_{yz}'^2 + \tau_{zx}'^2\right)\right]^{1/2} / \sqrt{2} \quad (6)$$

is the equivalent dynamic flow stress and

$$\dot{\varepsilon} = \sqrt{2}\left[\left(\dot{\varepsilon}_x - \dot{\varepsilon}_y\right)^2 + \left(\dot{\varepsilon}_y - \dot{\varepsilon}_z\right)^2 + \left(\dot{\varepsilon}_z - \dot{\varepsilon}_x\right)^2 + 6\left(\dot{\varepsilon}_{xy}^2 + \dot{\varepsilon}_{yz}^2 + \dot{\varepsilon}_{zx}^2\right)\right]^{1/2} / 3 \quad (7)$$

is the associated equivalent strain rate. The constants D and q are obtained from dynamic uniaxial tests on the material and σ_0 is the corresponding static uniaxial flow stress.

The vessel material properties were defined by the following directive in BACON language at epilogue level, as in the previous work [4]. The elements used to define the structure were in fact CEA elements, as mentioned above.

- Elastic behaviour:

```
.MAT NOM "M_Elastic"
   BEHAV "elastic"
   YT 206.058e09
   NT .3
   M 7800
.ael group "TANK" mat "M_Elastic"
```

- Elastic-plastic behaviour:

```
.FCT CRE FONCTION NOM "F_Harden"
   CRE VAL Y U
   COUPLES
     0.00E+00          4.63E+08
     3.00E-04          4.78E+08
     ……..          ……..

.MAT NOM "M_Plastic"
   BEHAV "Plastic"
   YT 206.058e09
   NT .3
   M 7800
   VONM
   XIT 1. NF "F_Harden"
   CAUC
.ael group "TANK" mat "M_Plastic"
```

In detail, the command lines used for Cowper-Symonds are:

```
.MAT NOM "M_Plastic"
   BEHAV "Plastic"
   YT 206.058e09
   NT .3
   M 7800
   VONMISES
   SYMO 40 5
   XIT 1. NF "F_Harden"
.ael group "Vessel_el" mat "M_Plastic"
```

3 SIMPLIFIED METHODS FOR ESTIMATION OF APPLIED LOADS AND VESSEL STRENGTH

Before describing the details of the FE simulations, this section presents selected "handbook" engineering formula which can be used to estimating the strength of the vessel and the level of the applied loads due to an explosion. Since in several cases these are based on empirical data, they provide a useful means for better understanding and cross-checking the values from the FE simulations.

3.1 Calculation of Critical Pressures for the Vessel

Assuming a free-end boundary condition for a thin-walled cylindrical tube, the static pressure required to distend it to its elastic limit is given by the simple engineering formula:

$$P_{\lim} = \sigma_y \frac{t}{r} \tag{8}$$

where σ_y is the stress at the elastic limit, t is the vessel thickness and r is the radius. By thin-walled it is generally meant a container whose wall thickness is less than 1/10 of the radius. Under this condition, the stresses in the wall may be considered uniform. In the current work the thickness of the upper part of the cylindrical vessel is 0.2 m while the radius is 2 m. In the transition ring the thickness is 0.1625 m with the same inner radius of 2 m. The criterion in Eq.(8) is derived from the equations for longitudinal and hoop stress in a thin-walled vessel under internal pressure P, Figure 11a) and b):

$$\sigma_L = \frac{\mathrm{Pr}}{2t} \tag{9}$$

$$\sigma_H = \frac{\mathrm{Pr}}{t} \tag{10}$$

The hoop stress is twice the value of the longitudinal stress and therefore this is used for the limiting case expressed in Eq.(8). The stresses in thin-walled spherical vessels can be considered with the same approach, as shown in Figure 12. Solving for the stress, we have:

$$\sigma = \frac{PR}{2t} \tag{11}$$

with P the internal pressure in the sphere, R the radius of the sphere and t is the wall thickness.
No distinction is made in a longitudinal or hoop stress as the symmetry means that the stresses are equal and biaxial.

The stresses in a thick-walled cylinder under a pressure are given instead by the Lamé equations and are of the form:

$$\begin{aligned} &\sigma_r = A - B/r^2 = -P_r \\ &\sigma_H = A + B/r^2 \\ &\sigma_L = (P_1 r_1^2 - P_2 r_2^2)/(r_2^2 - r_1^2) = A \end{aligned} \tag{12}$$

where A and B are constants for any given situation, σ_r , σ_H and σ_L are the radial, hoop and longitudinal stresses at r, r_1 is the inner radius, P_1 is the pressure at the inner radius, r_2 is the outer radius and P_2 is the outer pressure.

3.1.1 Elastic limit of an Empty Vessel Subject to Uniform External Pressure

Considering the vessel without inner water and using the equations described above, it is possible to estimate the static pressure required to distend the cylindrical vessel considered in this work to its elastic limit.

For the cylindrical part of the vessel with thickness t = 0.2 m and radius r = 2 m (here the inner radius is considered for simplicity), and assuming σ_y = 463 MPa, we have for a free-end case:

$$P_{\mathrm{lim}} = \frac{\sigma_y t}{r} = 46.3\ MPa \tag{13}$$

- in the transition ring of thickness, t = 0.1625 m and radius r = 2 m:

$$P_{\mathrm{lim}} = \frac{\sigma_y t}{r} = 37.6\ MPa \tag{14}$$

- and in the torispherical part of thickness t = 0.125 m and radius r = 2 m:

$$P_{\mathrm{lim}} = \frac{2\sigma_y t}{r} = 57.8\ MPa\ . \tag{15}$$

Considering the present scenario of an explosive charge 1 m directly beneath the torispherical bottom part of the vessel and assuming that the resulting explosion could produce a uniform pressure against the vessel, the above formula would imply that a pressure of approximated 58 MPa would be theoretically required to distend it to its elastic limit. Form this value the corresponding quantity of explosive can be calculated, as discussed in the next section.

The above assumes the maximum shear stress (Tresca) criterion. Alternatively the von Mises or maximum distortion energy criterion requires that:

$$\frac{1}{2}\left[(\sigma_1-\sigma_2)^2+(\sigma_2-\sigma_3)^2+(\sigma_3-\sigma_1)^2\right]\le\sigma_y^2 \qquad (16)$$

In the present case with principal stresses $\sigma_r = 0$, $\sigma_h = -Pr/t$ and $\sigma_l = -Pr/(2t)$ we have $\frac{Pr}{t}\frac{\sqrt{3}}{2}\le\sigma_y$, and hence the pressure for yielding is increased by a factor of $\frac{2}{\sqrt{3}}$ with respect to the Tresca value.

3.1.2 Elastic Limit of a Vessel with Pressurised Water Subject to Uniform External Pressure

Considering now that the vessel contains water at 155 bar, the above equations can be used to calculate the pre-stresses in the longitudinal and circumferential directions and then the external pressure needed to compress it to its elastic limit. For water pressure alone in the upper part of the cylindrical vessel of thickness t = 0.2 m and radius r = 2m we have:

$$\sigma_H=\frac{Pr}{t}=155\ MPa \text{ and } \sigma_L=\frac{Pr}{2t}=77.5\ MPa \qquad (17)$$

- in the middle ring of thinner thickness, t = 0.1625 m and radius r = 2 m:

$$\sigma_H=\frac{Pr}{t}=190.8\ MPa \text{ and } \sigma_L=\frac{Pr}{2t}=95.3\ MPa\ ; \qquad (18)$$

- and in the spherical part of thickness t = 0.125 m and radius r = 2m:

$$\sigma=\frac{Pr}{2t}=124\ MPa\ . \qquad (19)$$

These values are compared with the results obtained with ABAQUS static analysis [4] in Table 3. The values are in close agreement, even considering that ABAQUS modelled the full geometry (with a flat top and torispherical bottom) and boundary conditions. Table 4 shows the displacements, equivalent stresses and strain values obtained from ABAQUS for different locations on the vessel, together with the values obtained by a quasi-static EUROPLEXUS analysis, which is used in the first stage of the analysis to assess the effect of the pressurized water.

	Thin-wall vessel formula	ABAQUS static analysis
Axial Stress		
Upper cylindrical section	78 MPa	75MPa
Cylindrical transition	95 MPa	94 MPa
Hoop Stress		
Upper cylindrical section	155 MPa	160MPa
Cylindrical transition	191 MPa	157 MPa
Lower torispherical dome	124 MPa	123 MPa

Table 3: Comparison between the stress values from the thin-wall vessel formula and the ABAQUS static analysis for a vessel containing water at 155 bar internal pressure.

	EUROPLEXUS	ABAQUS
Displacement vertical axis		
Top node:	23.5 mm	24.78 mm
Bottom node:	-0.8 mm	-0.46 mm
Middle node:	-0.6 mm	-0.57 mm
Eq. Stress Vessel		
Top node:	453 MPa	468 MPa
Bottom node:	113 MPa	130 MPa
Middle node:	96 MPa	93 MPa
Eq. Plastic Strain		
Top node:	0.1 %	0.14 %
Bottom node:	0	0
Middle node:	0	0

Table 4: Comparison between results of the EUROPLEXUS quasi-static analysis and the ABAQUS static analysis for a vessel containing water at 105 bar internal pressure (in ABAQUS case the pressure of the water was substituted by a pressure load).

To be able to deform the vessel full of water at 155 bar to its elastic limit, these pre-stresses have to be taken into account. Hence for an external pressure, the value to be applied would need to equalise the pre-stresses plus an amount to create yield-level stresses. So, in this case:

- for the upper cylindrical part of thickness 0. 2m and radius 2 m:

$$P_H = \frac{(\sigma_H + \sigma_y)t}{r} = -61.8MPa \text{ and } P_L = \frac{2(\sigma_H + \sigma_y)t}{r} = -108.1MPa \quad (20)$$

- for the thinner transition ring of thickness 0.1625 m and radius 2 m:

$$P_H = \frac{(\sigma_H + \sigma_y)t}{r} = -53.1\ MPa \text{ and } P_L = \frac{2(\sigma_H + \sigma_y)t}{r} = -90.7\ MPa \quad (21)$$

- and in the torispherical part of thickness 0.125 m and radius 2 m:

$$P = \frac{2(\sigma + \sigma_y)t}{r} = -73.4\ MPa\ . \quad (22)$$

Summarising, since the explosive material is located 1 m underneath the torispherical part these values can be considered:

- vessel without water $P_{NoWater} = \frac{2\sigma_y t}{r} = -57.8\ MPa$ for reaching plasticity;

- vessel with water $P_{water} = \frac{2(\sigma + \sigma_y)t}{r} = -73.4\ MPa$ for reaching the plasticity;

3.1.3 Vessel Failure or Fracture Limit

Estimating the limit load for failure or fracture presents a number of difficulties. The first is to determine a realistic failure or fracture mode for the given loading conditions. Since the vessel is subject to external pressure and the stresses are globally compressive, so that a local or global buckling/collapse would be expected to determine the load bearing limit [9]. If the vessel contains pressurised water, which is close to being incompressible, this may also have an effect on the stability.

Notwithstanding these issues and considering the uncertainties which in any case are associated with fluid-structure analyses involving loads beyond yielding, an option for approximating an upper bound value is to simply use the nominal tensile strength properties in the above engineering equations Eq. (8) - (11). Even so, it should be noted that when a material is subjected to mixed tensile, compressive and shear loads, then the determination of the point of failure is more further complicated [10]. Finally it is noted that a progressive damage model, related to the work of Johnson-Cook [11] or Tuler-Butcher [12] can be considered generally for the simulation the fracture of the components. These approaches use an equivalent plastic limit strain value or energy value as a criterion for removing elements from the mesh. The engineering UTS for A533B steel is around 635MPa at room temperature.

A summary of all the critical values (Tresca criterion) can be found in Table 5.

Vessel location	Vessel Yielding		Vessel Failure (upper bound)	
	Empty [MPa]	Internal water at 155 bar [MPa]	Empty [MPa]	Internal water at 155 bar [MPa]
Upper cylindrical part	-46	-61.8	-64	-79
Torispherical dome (bottom part)	-58	-73	-79	-95

Table 5: Estimated values of uniform external pressure to produce a) compressive yielding and b) failure (assuming no buckling occurs).

3.2 Estimate of critical pressures from explosions

The most widely used approach for blast wave scaling is Hopkinson's law [13], which establishes that similar explosive waves are produced at identical scaled distances when two different charges of the same explosive and with the same geometry are detonated in the same atmosphere. Thus, any distance R from an explosive charge W can be transformed into a characteristic scaled distance Z:

$$Z = R/W^{1/3} \tag{23}$$

where W is the charge mass expressed in kilograms of TNT. The use of Z allows a compact and efficient representation of blast wave data for a wide range of situations.

There are many solutions for the wave front parameters from both numerical solution and experimental measurements [13, 14, 15]. The results are usually presented in condensed form based on experimental or numerical results, such as the tables given by Kinney and Graham [14] or the following equations presented by Smith and Hetherington [15]:

$$\begin{aligned} ps &= 1407.2/Z + 554.0/Z^2 - 35.7/Z^3 + 0.625/Z^4 \text{ kPa} && 0.05 \le Z \le 0.3 \\ ps &= 619.4/Z - 32.6/Z^2 + 213.2/Z^3 \text{ kPa} && 0.3 \le Z \le 1.0 \\ ps &= 66.2/Z + 405.0/Z^2 - 328.8/Z^3 \text{ kPa} && 1.0 \le Z \le 10. \end{aligned} \tag{24}$$

The accuracy in the near field is lower than in the far field, probably due to the complexity of blast phenomena [15]. Another way for calculating the peak overpressure P of a blast in air as a function of charge weight W and distance from the blast d is given by the following expression from Young et al [16]:

$$P = 1307.3(d/W^{1/3})^{-2.2715} \tag{25}$$

Here the charge weight is in pounds of TNT equivalent, the standoff distance is in feet and the pressure is in psi. This overpressure will break a concrete wall of thickness t (in feet) if:

$$t \leq \frac{W^{1/3}}{5.56(r/W^{1/3}) + 2.1}. \tag{26}$$

Table 6 summarises the predicted overpressure peaks as a function of quantity of explosive at a distance of 1, 5 and 6 metres. Figure 13 shows a comparison between these predictions at distances of 1, 5 and 6 m. For low quantities of explosive, at 1 m from the charge, the difference between the predicted values is relatively high but decreases as the amount of explosive is increased.

Quantity of Explosive kg	**Calculated pressure peak, MPa**					
	at 1 m		**at 5 m**		**at 6 m**	
	Eq. 24	**Eq. 25**	**Eq. 24**	**Eq. 25**	**Eq. 24**	**Eq. 25**
5	2.0	3.7	0.5	0.1	0.4	0.1
10	3.3	6.3	0.7	0.2	0.6	0.1
15	6.3	8.6	0.8	0.2	0.7	0.1
20	7.2	10.7	0.9	0.3	0.7	0.2
28	8.4	13.8	1.1	0.4	0.8	0.2
100	23.5	36.1	1.8	0.9	1.4	0.6
145	33.3	47.8	2.0	1.2	1.6	0.8
170	38.7	54.0	2.2	1.4	1.7	0.9
200	45.1	60.9	2.3	1.6	1.9	1.0
300	66.6	82.9	2.8	2.1	2.2	1.4
413	90.9	105.7	3.2	2.7	2.5	1.8
550	120.2	131.1	3.6	3.4	2.9	2.2
750	162.8	165.9	4.2	4.3	3.3	2.8
928	200.8	195.1	4.6	5.0	3.6	3.3
1116	240.9	224.3	5.0	5.8	3.9	3.8

Table 6: Calculation of the overpressure peak at 1, 5 and 6 m from the charge for increasing quantity of explosive with the Smith and Hetherington (Eq. 24) and the Young et al (Eq.25) equations.

In the previous work [4], a comparison between EUROPLEXUS results and some literature data [5] was carried out (see Appendix A). Overall EUROPLEXUS was found to reliably reproduce the values reported in Ref [5], those from empirical equations and experimental data. Hence these predicted values were considered rather close to those from EUROPLEXUS.

The most usual case of loading of large flat surfaces is represented by waves that strike at oblique incidence. For angles of incidence between 0˚ and 90˚, either regular or Mach reflection occurs depending on incident angle and shock strength [17, 18]. The evaluation of pressures resulting from multiple reflections on surfaces with different incidence angles is very complicated and difficult to perform by formula. In this case, the use of numerical methods is more appropriate.

If the blast wave reaches the ground or a wall it is reflected. Below a certain reflection angle the reflected wave and the direct wave merge and form a reinforced horizontal wave, the so-called Mach stem. For each goal overpressure there is a certain optimum burst height at which the blast range is maximized.

Two distinct, simultaneous phenomena are associated with the blast wave in air:

- Static overpressure, i.e., the sharp increase in pressure exerted by the shock wave. The overpressure at any given point is directly proportional to the density of the air in the wave.
- Dynamic pressures, i.e., drag exerted by the blast winds required to form the blast wave. These winds push, tumble and tear objects.

Most of the material damage caused by an air burst is caused by a combination of the high static overpressures and the blast winds. The long compression of the blast wave weakens structures, which are then torn apart by the blast winds.
The drag energies of the blast winds are proportional to the cubes of their velocities multiplied by the durations. These winds may reach several hundred kilometers per hour.

This blast effect is due to air movement as the blast wave propagates through the atmosphere. The velocity of the air particles and hence the wind pressure depend on the peak overpressure of the blast wave. In the low overpressure range for normal atmospheric conditions, the peak dynamic pressure can be calculated using the following empirical formula [19]:

$$q_0 = 2.5\left(\frac{P_{so}^2}{7P_0 + P_{so}}\right). \tag{27}$$

This is valid for $P_{so}<3.5$ bar. The dynamic pressure on a structure is the product of the dynamic pressure and the drag coefficient, C_d. Typical maximum values are 1.2 for a cylinder, 0.47 for a sphere and 2.05 for a rectangular box [19].

In a free field, the blast wave from an explosion travels above the acoustic speed for the propagating medium. For design purpose, it can be conservatively assumed that a pressure wave travels at the same velocity as the equivalent shock wave. In the low-pressure range and for normal atmospheric conditions the shock/pressure front velocity in air can be approximated using the following relationship [19]:

$$U \approx 340\sqrt{1+\frac{6P_{so}}{7P_0}}\ m/\sec \tag{28}$$

The propagating blast wave at any instant extends over a limited radial distance as the shock/pressure front travels outward from the explosion source. The pressure is largest at the front and trails off to ambient over a distance L_w, the blast wave length. In the low pressure range the length of the blast wave can be approximated from [19]:

$$L_W \approx Ut_d \quad . \tag{29}$$

Taking into account the iso-damage curves defined by other authors [20] the following numerical levels of reflected impulses were defined for different types of damage in structural and not-structural elements, in order to build the maps of damage:

- i_r > 3000kPa ms, reinforced concrete structure destroyed.
- 1000kPa ms < i_r < 3000kPa ms, masonry walls destroyed, reinforced concrete structure damaged.
- 500kPa ms < i_r < 1000kPa ms, masonry walls cracked
- 180kPa ms < i_r < 500kPa ms, most glass destroyed, external joinery, ceiling and tiling damaged.

Moreover, in order to obtain coherent maps, the structural configuration should also be taken into account.
A corresponding estimate for the peak overpressure values is the following:

- p > 1.379 atm = 0.1379MPa, reinforced concrete buildings destroyed; 800km/h wind ;
- p > 0.68046 atm = 68.94kPa, commercial buildings collapsed, 480 km/h wind;
- p > 0.34023 atm = 34.37kPa, brick and wood houses destroyed, 260 km/h wind (hurricane);
- p > 0.136atm = 13.79kPa, significant damage to houses, 115 km/h wind high fire hazard, destroyed 50% buildings;
- p > 0.0689 = 6.894kPa, moderate damage to civil buildings.

Hence, most buildings, except reinforced or blast-resistant structures, will suffer moderate to severe damage when subjected to overpressures of only 35.5 kPa or 0.35 atm. The blast wind may exceed several hundred km/h. The range for blast effects increases with the explosive yield of the weapon and also depends on the burst altitude. Contrary to what one might expect from geometry the blast range is not maximal for surface or low altitude blasts but increases with altitude up to an "optimum burst altitude" and then decreases rapidly for higher altitudes. This is due to the nonlinear behaviour of shock waves.

An overpressure fragility function can be also defined. It consists of a plot showing the component kill probability versus the peak overpressure experienced by the component. Typically functions are defined by specifying a minimum overpressure $P_{low,}$ below which the component kill probability is zero and a maximum overpressure P_{high}, above which it is unity. The fragility function for a component is then interpolated between P_{low} and P_{high} using either a linear approximation or a logarithmic fit of the form:

$$P_{kill}=log(P/P_{low})/log(P_{high}/P_{low}) \quad (30)$$

so that any component exposed to an overpressure p between P_{low} and P_{high} is assigned a fractional kill probability between 0 and 1.

4 FINITE ELEMENT ANALYSES

As described above, to realistically simulate the vessel behaviour a multi-step calculation is needed, first for the static pre-stresses due to the high pressure water, then the detonation and the interaction of the shock waves with the structure. The EUROPLEXSUS epilogue was therefore modified to perform three computations in one run. In particular this uses the detonation time command TDET to delay the detonation time. In this way the detonation starts only at the value imposed by TDET and an initial quasi-static damping analysis can be performed up to this time. During the present work TDET was set to 20 msec. In the QUASI STATIQU option two times can be specified, TINI and TEND, for applying a quasi-static analysis, or an open interval through the command UPTO …FROM. The latter is useful for applying the quasi-static analysis for two different interval of time. During the present work, UPTO 20e-3 FROM 60e-3 was used, which means that the quasi-static analysis is applied twice, once from time 0 sec (start of the analysis) to 20 msec when the detonation starts and from 60 msec (end of the detonation) up to the end of the analysis, TEND 85e-3. The command line CALCUL TINI 0 TEND 85e-3 gives the duration of the complete run, from 0 to 85 msec. In detail, the option lines added to the epilogue are the following:

```
OPTION
CSTA 0.4
DTDROP 0.002
AMOR QUAD 2
QUASI STATIQU 59 1 UPTO 20e-3 FROM 60e-3

CALCUL TINI 0 TEND 85e-3
PAS1 1.E-08
```

In the QUASI STATIQU line, 59 is the frequency of the first mode of oscillation of the system vessel plus high pressure water, as described previously in [4].

The effect of the gravity could be also evaluated by mean of the following command lines:

```
CHAR CONS GRAV 0 0 -9.80665     LECT group "water_n"
                                     group "tank_n"
                                     group "bubble_n"
                                     group "air_n"  TERM
```

Practically, a constant force equal to the gravitational force is applied to all the nodes of the model.

The following different simulations were performed:

- FSR boundary conditions (pressure waves reflecting on the walls of the bunker):
  - T=20˚C elastic-plastic analysis;
  - T=20˚C elastic-plastic analysis + gravity effect;
- ABSO boundary conditions (absorbing of the pressure waves at the walls of the bunker for simulating an infinite open area around the bunker):
  - T=20˚C elastic-plastic analysis, 5kg;
  - T=20˚C elastic-plastic analysis, 170kg.
- FSR boundary conditions (pressure waves reflecting on the walls of the bunker): T=20˚C elastic-plastic analysis with different quantities of high explosive material: 5, 15, 28, 170, 413, 928 and 1116 kg.

These cases were analysed both with and without water inside the vessel and some also used a constant pressure instead of the water. All the analyses were performed with a reference pressure of 1atm. A summary of the studied cases can be found in Table 9.

Explosive kg	Bunker boundary conditions	Water Pini=155bar	Vessel without water	Pini=155bar (water) + gravity effect	Pload of 155 and 140 bar inside the vessel instead of water
5	FSR	x	x	x	x
15	FSR		x		
28	FSR		x		
170	FSR		x		x
413	FSR	x	x		x
928	FSR	x	x		x
1116	FSR		x		
5	ABSO	x			
170	ABSO	x			

Table 9: Summary of the FE analyses performed; for all cases Pref = 1 atm and the vessel mechanical properties were elastic-plastic at 20˚C.

4.1 Influence of elements types and material models used for the explosive

A simple comparison was carried out between the two material models used for the solid explosive, JWLS and FLUT, which have been developed in EUROPLEXUS for the CEA and JRC elements respectively. The simulation used the model with a 5 kg charge at 1 m below the vessel, FSR bunker boundary conditions and Pref = 0. Figure 14 shows the pressure in some elements of the explosive

charge predicted by the JWLS (CEA implementation) and FLUT NUM=11 (JRC implementation) models. Tetrahedral elements were used in this case. A difference of around 5-6 MPa is present between the peaks predicted by the models, with the JWLS being approximately 25% higher.

Figure 15a) and b) show the pressure in the air element facing the bottom of the vessel with the mesh in a) tetrahedral elements and b) hex elements. Some difference can be noted between the overpressure peaks. Comparing the two figures (Figure 15a) and b)) it can also be noted that there is a difference due to the element type used, considering also that the case with hex elements is for 4.5 kg of explosive charge, while the tetrahedral case is for 5kg. The peak of the pressure values for all these cases are summarised in Table 12. The estimates reported in Table 6 from the Smith and Hetherington and the Young et al equations for 5kg at 1 m distance are respectively 2.1 and 3.7 MPa, which agree reasonably with the values obtained here.

Summarising, the peak pressure value is influenced by both the element type and the material model used for the high explosive charge, but the differences are modest for this amount of explosive and globally the peak overpressures are in agreement with the theoretic estimates.

	Explosive Charge, Kg	Tetra elements		Hex elements		Formula	
		FLUT N=11	JWLS	FLUT N=11	JWLS	Smith & Hetherington Eq.24	Young el al Eq. 25
Peak Pressure, MPa	4.5			2.2	4.5		
	5	1.5	2.8			2.1	3.7

Table 10: Peak overpressure values at 1 metre from EUROPLEXUS analyses with different element types and explosive models.

Figure 16 shows a comparison between analyses performed with two different reference pressures (pref = 0 atm and pref = 1 atm). There is no substantial difference in the peak overpressure values and hence also not in the vessel displacements (Figure 17), which are very small (< 1 mm). Figure 18 presents the displacement at different locations of the vessel for two meshes (hex and tetrahedral elements), again for a blast with 5kg of explosive material and no inner water. Little difference is present in the predicted displacement values (again very low for these blast conditions).

4.2 Pressure wave studies

To check the peak values of the pressure waves reaching the vessel, a series of analyses were run with different amount of explosive but without water in the vessel, as reported in Table 9. Table 11 gives the peak values obtained in the air element facing the bottom point of the vessel. The mesh used tetrahedral elements and the reference pressure was 1 atm. Figure 19 a) and b) shows the peak of pressure reaching the vessel for the different amounts of explosive material. The detonation point has been kept fixed at 0.073 above the bunker floor (at centre of the 5 kg box) for all the charge values. The higher the amount of explosive material, the higher is the peak of the pressure as expected. Figure 20 compares the formula predictions from Table 6 and the EUROPLEXUS results of Table 11. The values appear in good agreement up to a charge of 170 kg, while the next FE results for 928 kg is much higher than the trend indicated from the formula. This could be due to pressure wave reflections with this large amount of explosive.

Quantity of Explosive [kg]	Peak Overpressure [MPa]
5	1.5
15	4.8
28	6.5
170	47.9
413	164.3
928	650

Table 11: Peak overpressure values in an air element adjacent to the bottom of the vessel from EUROPLEXUS analyses with the FLUT NUM=11 explosive model.

The equivalent plastic strain at the bottom, top and middle of the vessel is shown for the different charges in Figure 21 and Figure 22 as a function of time. No substantial plastic deformation is predicted with charges up to 170 kg. For the 928 kg charge the bottom deforms significantly (Figure 21a) but no plasticity is present at the top or middle of the vessel (Figure 22), since the pressure peak at these locations is around 1 atm.

Figure 23 shows the pressure variation at different locations in the bunker, for explosive charges of 5kg, 170kg, 413kg and 928kg. The higher the amount of explosive, the higher the pressure peak reaching the different positions and the shorter the time needed for it to take place. In some cases the values could be high enough to damage the walls (or any ancilliary equipment in the bunker such as piping systems). For instance the empirical relations reported in the previous section, indicated that a pressure of 0.13 MPa can destroy reinforced concrete. On this basis a charge bigger than 170 kg could create substantial damage at the walls of the bunker.

Figure 24 shows the pressure variation due to 170 and 928 kg of explosive material in a line extending from the vessel top towards the bunker wall (as shown in Figure 24c), at the hypothetical location of a piping line.

Figure 25 to Figure 27 show the variation in time of the equivalent von Mises stress at the bottom, top and middle of the vessel, always for the case of a vessel without water and for increasing amounts of explosive material.

Figure 28 shows the components of the reaction forces at the clamps for charges of 5, 170 and 928 kg. The components correspond to the six degrees of freedom of the node: three translational and three rotational degrees i.e. three forces and three momentums. The forces in the axial (z) direction for different amount of explosive charge are compared in Figure 29.The axial (z) displacement at top, middle and bottom of the vessel for different amount of explosive charge is shown in Figure 30. The higher the amount of explosive, the higher the deformation of the vessel. The displacements are negligible except for the case of the 928 kg HE charge, at which they becomes rather high (~35 cm) at the bottom of the vessel, implying that the material would be at the point of collapse or fracture.

5 RESULTS AND DISCUSSION

5.1 Elastic-plastic analysis at 20˚C – FSR boundary - 5kg charge

The case described in this section is that of the vessel inside the bunker with FSR boundary conditions i.e. the pressure waves reflect on the bunker walls. The amount of high explosive charge is equal to 5 kg of TNT. After having reached stability in the quasi-static analysis phase, the explosion

takes place over 40 msec and then a final quasi-static analysis lasting 25 msec is imposed to reach a final equilibrium state.

For the quasi-static analysis, the previous investigation [4] showed that stabilised displacement and stress values are reached after 20 msec. A summary of the values obtained after a quasi-static analysis with EUROPLEXUS and a static analysis with ABAQUS can be found in Table 12. The quasi-static damping displacements, equivalent stress and plastic strain values from EUROPLEXUS are in broad agreement with the static ones, in particular at the top node of the vessel. Some differences are present at the bottom of the vessel. However allowing for the fact that EUROPLEXUS is essentially a dynamic rather than a static code, the results are considered in acceptable for the present study. Further preliminary studies of the equilibrium state of the water-vessel system showed a pressure drop of around 30% occurred during the quasi-static analysis due to fact that since the system is closed, when vessel expands under the pressure, the pressure has to fall to allow a similar expansion of the water. Therefore to arrive at a pre-stressed vessel with water at 155bar, an initial pressure of 228 bar was imposed to water at the start of the quasi-static analysis. Figure 31 shows the pressure in two elements of the water inside the vessel. The pressure starts from the imposed value of 228 bar and then due to the oscillation of the vessel during the quasi-static damping analysis drops down to a value of around 150-140bar, as prescribed. The incompressibility of the water means that the pressure is sensitive to even very small variation in the vessel volume.

In Figure 32 a) and b) the pressure in two elements of the explosive material is shown, respectively for the full duration of the computation and for a time interval around the detonation. The pressure is equal to the reference pressure of 1 atm (0.1 MPa) before and after the point at which the explosion takes place. The same variation can be noted in the air element directly below the vessel, Figure 33. The air has a pressure of 1 atm up to the explosion when a fast variation occurs. After this it drops below 1 bar but then appears to being to rise again at the end of the calculation at 5msec.

The displacement of a node at the top of the vessel, corresponding to the middle of the flat cover, is shown in Figure 34 for the x, y and z directions. Figure 34a) shows an increasing axial (z) displacement of up to 40 mm during the first 20 msec of quasi-static analysis, during which only the pressure of the water acts on the vessel. Once equilibrium is reached the explosion takes place from 20 up to 60msec. There is no evident effect on the z displacement history during this phase. From 60msec to 85msec another quasi-static analysis is run to reach an equilibrium status after the explosion. Again no effect is visible on the displacement at the top of the vessel in the z vertical direction. It is concluded that 5 kg of explosive charge is not enough to create a substantial displacement of the vessel. Figure 34b) shows the displacement of the top centre of the vessel in the x and y directions. This is negligible (order of ~μ m) as expected but it is interesting to note that oscillations occur during the initial quasi-static analysis of the pre-stress due to water pressure and then during the explosion.

Figure 35 shows the predicted displacement at the bottom of the vessel. Some oscillations are present during the explosion (from 20 msec up to 60 msec) but are very small (less than 0.5mm). During the initial quasi-static phase of the simulation negative z displacements occur of up to 2.5mm due to the pressure of the water. In the x and y directions the displacement are negligible (of the order of the μm), as expected.

The displacement at the transition ring in the middle of the vessel is shown in Figure 36. The displacement in the z direction is approximately 1 mm downwards due to the water pressure and overall movement of the vessel with respect to the anchoring points at the top. Oscillations of less than 0.1 mm are present due to the explosion.

Figure 37 shows the equivalent stress variation with time at the top, middle and bottom locations, while Figure 38 shows the calculated equivalent plastic strain values at the same locations. No plasticity is present at the bottom and middle of the vessel, where the corresponding stress values are about 150 MPa (well below the yield strength). At the top of the vessel almost 0.38% plastic strain is reached due to the pressure of the inner water, corresponding to an equivalent stress of around

470 MPa. Subsequently some oscillations can be seen during the explosion but these are very small. Again it is noted that the overall deformations are due to the water pressure rather than from any effects of the explosion below the vessel. As was seen above, the 5 kg charge of high explosive is not enough to create plasticity in the vessel configuration considered here.

Figure 39 to Figure 42 show the velocity components at the vessel top, bottom, middle and clamp locations. High velocities are present in the first quasi-static analysis, in particular at the top of the vessel and very small oscillations are evident during the explosion. The x and y components are reported even too small to have any significant.

Figure 43 shows the six components of the reaction forces at two locations of the clamped zone. As noted above these correspond to the 6 degrees of freedom of the nodes, three translational and three rotational degrees i.e. three forces and three momentums. The force in the negative z direction is quite high, but this is due to the water pressure against the flat top of the vessel. In fact, as shown in Figure 29, the clamp forces are much smaller for a vessel with water pressure subject to an explosion.

Vessel Location		EUROPLEXUS quasi-static (damping) analysis	ABAQUS static analysis
"z axis" displacement	Top: Bottom: Middle:	43.1 mm -1.4 mm -0.7 mm	43.9 mm -0.6 mm -0.75 mm
Eq. Stress	Top: Bottom: Middle:	463 MPa 116 MPa 110 MPa	486 MPa 175 MPa 124 MPa
Eq. Plastic Strain	Top: Bottom: Middle:	0.38 % 0 0	0.59% 0 0

Table 12: Comparison between results of the EUROPLEXUS quasi-static analysis and the ABAQUS static analysis for a vessel containing water at 140 bar internal pressure (in ABAQUS case the pressure of the water was substituted by a pressure load).

5.2 Elastic-plastic analysis at 20°C: different amounts of high explosive material

Here the effect of using larger amounts of explosive material was considered for the same basic scenario: the vessel with water at 155 bar, FSR boundary conditions at bunker walls, vessel material properties for 20°C. The displacement in the z direction of a node at the top of the vessel, corresponding to the middle of the flat cover, is shown in Figure 44 for different explosive charges. All the simulations show the same increasing displacement up to 40 mm during the first 20msec of quasi-static analysis where only the water pressure is acting. For explosion phase from 20 to 60 msec, an additional displacement is only evident for the cases with 170 kg and 413 kg. The case with 170 kg produces a modest increase, while that with 413 kg causes bigger oscillations reaching a maximum of 65 mm and a minimum of 55mm. In the final quasi-static phase to obtain an equilibrium state after the explosion, the final displacement is respectively ~48 mm for the 170 kg charge and ~60 mm for 413 kg charge. For all the other cases with lower charges the deformation is stable at the water pressure value of 40 mm.

Figure 45 shows the z displacement at the bottom of the vessel. Some oscillations are present during the explosion but are small for the lower charge values. In the case with 170kg of explosive a maximum of 3 mm deflection is reached at the start of the explosion. The case with 413 kg shows instead much bigger oscillations of up to 16 mm at the start of the explosion. The stabilised value reached after the explosion is around 3 mm. During the first phase of the calculation a slight negative displacement is evident of up to 2.5 mm due to the water pressure.

The displacement at the middle of the vessel, corresponding to the transition ring is shown in Figure 46. The displacement in the z direction is of the order of 1 mm due to the water pressure and ±0.7 mm of oscillations occur for the explosion with a 170 kg charge. For the lower charges the oscillations are less than 0.1 mm. For the 413 kg charge larger oscillations are present even though their amplitude is relatively small: 1mm and -1.5 mm.

Figure 47 shows the z displacement for a node near one of the clamps at the top of the vessel. Deformation up to 1.8 mm occurs due to the loads exerted by the closure plate subject to the water pressure. Also here no deformation occurs due to the blast load for the cases with explosive charges <170 kg. For the case with the 170 kg charge there is a displacement up to 2 mm (for the top of the vessel blast-related deformation became evident at this charge level, as shown in Figure 44), while the 413 kg charge generates a displacement up to 2.5 mm.

Figure 48 and Figure 49 show the equivalent stresses at different location while Figure 50 shows the equivalent plastic strain values at the same locations. No plasticity is present at the bottom and middle of the vessel (except for the case with 413 kg), with corresponding values of stress starting from around 120 MPa with oscillations of ±10 MPa for all the cases with charges < 170 kg and around ±150 MPa for the 170 kg charge and 50-450 MPa for 413kg. This behaviour is in agreement with the predictions of the section above, according to which these amounts of explosive are insufficient to create plasticity at the bottom of the vessel considered in this study. At the top of the vessel almost 0.38% of plastic strain is reached due to the water pressure, corresponding to an equivalent stress of around 470 MPa. During the explosion some stress oscillations can be seen. The higher is the explosive charge, the larger the amplitude of these oscillations. At the top the equivalent plastic strain for the case with the 170 kg charge reaches 0.6%, while for the 413 kg charge 1% plastic strain occurs. This latter case also produces 0.5% equivalent plastic strain at the bottom of the vessel (Figure 50b), as predicted by the analytical calculation ($p_{bottom}>p_{yield}$). The situation is still however some way from collapse, since experimental data indicate a UTS of 705 MPa with a true equivalent plastic strain of over 10%.

Figure 51 to Figure 53 show the velocity components at the different vessel locations. High velocities occur in the first quasi-static analysis. Significant oscillations are present during the explosion only for charge values greater than 170 kg. Similar considerations hold for the velocity of nodes at the top of the vessel near the clamped zone, as shown in Figure 54.

Figure 55 shows the third "z" component of the reaction force at a location of the clamps. The value is around -3000 kN, reached during the quasi-static calculation and therefore associated to the action of the water pressure on the flat top of the vessel. As noted earlier, this is in line with the previous results for a vessel under blast load without internal water, in which much lower forces occur at the clamps.

5.3 Consideration of gravity

A complete simulation including the effect of the gravity was run for a 5 kg charge. The gravity force was applied on all parts of the model, both the fluid and structural parts and also to the explosive charge elements. No noticeable effect was observed on the deformation of the vessel, but for completeness the results are reported here in any case. Figure 56 compares the pressure in the water for the cases with and without gravity effect, with FSR boundary conditions and 5 kg of explosive material. In Figure 57 the displacement at the top of the vessel in z direction is shown. As can be seen no difference between the case with and without gravity, even if the displacement scale is expanded (Figure 57b). Similar conclusions can be drawn from Figure 58 that shows the z component of the displacement at the bottom of the vessel and Figure 59 that depicts the displacement of a node placed at the top of the vessel near a clamping point. Figure 60 show the equivalent stress at the top a) and bottom b) of the vessel, while Figure 61 a) and b) show the equivalent plastic strain at the top of the vessel. Very little effect can be seen due to gravity. Finally Figure 62 reports the reaction force components at a location close to a clamped zone; again no significant effect is seen for the case with gravitational force.

5.4 Use of absorbing conditions at the bunker boundary

The results obtained using absorbing boundary conditions at the bunker walls, effectively simulating an infinite open environment around the vessel, are reported in this section. A calculation was run for 5 kg of explosive, with a total duration of 85 msec including the quasi-static analyses at the beginning. There appeared to be no significant effect on the deformation of the vessel. This agrees with the results of the studies reported in an earlier section which showed that the pressures at the walls of the bunker were close to atmospheric.

For completeness the results are reported from Figure 63 to Figure 67. Figure 63 shows the variation in water pressure for the cases with FSR and ABSO boundary conditions and 5 kg of explosive material. Figure 64 shows the pressure in an element of explosive material for an interval of time around the detonation. As expected, no differences are present for the two boundary conditions. In Figure 65 the displacements at the top of the vessel are shown.

Figure 66 shows the displacements at the bottom of the vessel and Figure 67 at the middle of the vessel. In all three the differences between the FSR and ABSO analyses are negligible. This can be explained considering the pressure history in the element facing the bottom of the vessel shown in Figure 68.The value of the pressure is identical in both cases since on the bottom of the bunker FSR conditions are imposed in both cases. In fact, the ABSO conditions are placed only on the lateral walls and roof of the bunker. This explains why the deformation of the vessel is identical in the two cases, being due mainly to the shock waves arriving from the bottom wall and the explosive charge. The pressure at different locations in the bunker has been plotted for both cases with ABSO and FSR boundary conditions in Figure 69 and Figure 70. The values of the pressure generated at these locations are different, with lower values for the ABSO case where no reflections of the pressure waves are present.

The same behaviour was verified in case of a larger quantity of explosive material, 170kg or 413kg. A short study, for the case of a vessel without water under a blast load of 413kg of explosive material and both FSR and ABSO boundary conditions, has been carried out to investigate the effect of these boundary conditions on an empty vessel. Figure 71 shows the pressure history in the element facing the bottom of the vessel for the two cases. The same peak value of pressure is reached, since the boundary condition at the ground floor is the same (FSR). Figure 72 shows the pressure at different locations in the bunker. The peak of pressure reached at the different locations is lower for the case with ABSO boundary conditions as expected, since no reflections are present at the walls of the bunker. The displacement at the top, bottom on middle position of the vessel for the two boundary conditions is shown in Figure 73 and no differences are evident.

5.5 Use of strain-rate dependent material properties

Blast and impact loaded structures experience a very rapid application of the load and a corresponding rise in member stresses. As a material is loaded rapidly, it cannot deform at the same rate at which the load is applied. This induces an increase in the yield stress and UTS in some materials. Strain rate sensitivity manifests itself typically as a strengthening effect in a structure but sometimes the fracture strain can decrease with increasing strain rate. Also the average yield strength of steel is generally greater than the specified minimum value given in codes and standards. The material characteristics of mild steel under dynamic uniaxial tension are generally such that:

- the upper and lower yield stress and UTS increase with increase in strain rate, the increase being more significant for the lower yield stress;
- the UTS increases less with increase in strain rate;
- little or no strain hardening at high strain rates;
- fracture strain decreases with increase in strain rate.

Consequently the use of strain-rate dependent material properties has also been considered based on the experience in the previous study [4] using literature data for mild steel, in which it was also shown that the Cowper-Symonds and the Ispra law generated similar results. Hence only the Cowper-

Symonds law was considered here, together with a 413 kg explosive charge and FSR boundary conditions.

Figure 74 and Figure 75 show the displacements at the top and bottom of the vessel respectively for the simulations with and without the strain-rate dependent material model. No significant difference is present at the top node, while the strain-rate model gives some peak displacement oscillations for the bottom node, and the final residual displacement is almost twice as large. Figure 76 shows the equivalent stress history at the top, bottom and middle position of the vessel. The different models affect the dynamic response. Figure 77 shows the corresponding equivalent plastic strain values. At the bottom where the blast wave first impinges on the vessel, the strain rate model leads to higher plastic strain values (about a factor of three). The velocity in the z direction for the top of the vessel is shown in Figure 78 for both cases. The evolution is more or less the same despite some higher peaks for the case without strain rate. Finally for the clamped zone the third component of the reaction force is shown in Figure 79.

5.6 Different types of pressure load

A study of the effect of different pressure loads on the vessel was carried out substituting the water at high pressure with a direct pressure load on the inner walls of the vessel. Precisely, a constant pressure equal to 155 bar minus the reference pressure for the water of 1 bar was applied on the inner wall of the vessel. A case was always run for 85 msec comprising the starting quasi-static analysis, an explosion period of 40 msec with a 5 kg explosive charge and a final quasi-static analysis of stabilization. Figure 80 compares the displacements obtained for the two cases i.e. for internal water at 155 bar and for pressure loads on the inner walls. The constant applied pressure produces significantly higher deformations. However it should be noted that in the case of internal water at 155 bar there is a drop of the pressure due to the variation of the volume of the vessel, while in the case of the pure pressure the load is constant throughout the analysis. Hence a reduced pressure of 140 bar was used to reproduce the same deformation in the vessel as in the case with water. This is also reported in Figure 80.

The equivalent plastic strains at the top of the vessel were also checked. Figure 81 shows that there is a large difference between the values obtained applying 155 bar of pressure load and the water at high pressure (as noted elsewhere, the plastic strains at the bottom and middle location of the vessel are zero. Figure 82 compares the equivalent stress at the top of the vessel for the case with water at 155 bar and with the applied pressure load. Again the case with a pressure load of 140 bar reproduces the stresses generated by the water rather well. Figure 83 and Figure 84 show the displacements and equivalent plastic strains for cases with 170 kg of explosive material. Good agreement in the history values of the case with water is reached using 140bar pressure load.

In detail, the commands lines used are:

```
.FCT CREE FONCTION  NOM "pressure"
   CREE VALEUR Y U
   COUPLES
    0.      0.
    0.0001   (14e06-1.e05)
    0.1      (14e06-1.e05)
    100.     (14e06-1.e05)
   CREE
.clm pre group "Vessel_el" val 1. nf "pressure" time
```

5.7 Failure model

EUROPLEXSUS offers the possibility to simulate local failure or rupture of a structure via a the progressive damage model. This is implemented for von Mises material model both for shell and for

solid elements. In the current application CEA structural elements were used for the vessel and bunker, while the fluid was modelled as always with JRC elements. The progressive damage model is based on the verification at the element integration points of some specific criteria. In this case, for metallic material behaviour, the equivalent plastic strain value is taken as the screening criterion. When this reaches the nominal level recorded at fracture in tensile tests, the corresponding element is no longer considered to contribute anymore to the rigidity of the system, its internal energy is not computed anymore and it is deleted from the mesh. In this way it is possible to generate a fracture hole in the vessel surface, corresponding to the ultimate tensile strength from experimental data.

The problem of the water in the vessel is still open. The progressive damage model is not compatible with an ALE computation since the software does not understand that a hole is generated in the mesh and an error in the flow of fluid would be generated. This problem is being studied by the software developers to prescribe an eventual flow of fluid (air, water etc.) through such a hole or fracture. Therefore another option has been considered to overcome this problem. A pressure field was applied directly on the structure to simulate the pressure due to the water and the water itself was removed from the mesh. The ALE computation of the water is in this way avoided, allowing a simulation to be performed. In the previous section it was shown that by applying a internal pressure load of 140 bar gives a similar vessel deflections to the case with water. In details the commands lines used are the followed:

```
[…]
    .FCT CREE FONCTION  NOM "pressure"
       CREE VALEUR Y U
       COUPLES
        0.      0.
        0.0001   (14e06-1.e05)
        0.1      (14e06-1.e05)
        100.     (14e06-1.e05)
       CREE
    .clm pre group "Vessel_el" val 1. nf "pressure" time

    .MAT NOM "M_Plastic"
       BEHAV "Plastic"
       YT 206.058e09
       NT .3
       M 7800
       VONM
       XIT 1. NF "F_Harden"
       DT 0.1027
    .ael group "Vessel_el" mat "M_Plastic"
[…]
```

where DT is the screening criteria, equivalent plastic strain.

Three cases were considered: one with 170 kg of explosive material, one with 413 kg and one with 928 kg. The results show that with the 170 kg charge no plasticity occurs at the bottom of the vessel. With the 413 kg charge even though some plasticity is generated, the fracture strain level is not reached, while with the 928 kg charge the fracture limit is reached and a hole is generated at the bottom of the vessel. The material data used were always those from [6], where the true UTS value is 705 MPa and the true equivalent plastic strain is 10.3%.

Figure 85 and Figure 86 show, respectively, the equivalent plastic strain and corresponding equivalent stress values for the three cases at both the top and the bottom of the vessel. As usual the runs had three phases: 20 msec of quasi-static pre-stress calculation, 40 msec of explosion and 25 msec of quasi-static calculation of the final stabilised state. It is seen that while the evolution of plasticity at the top of the vessel is similar for the 413 kg and 928 kg charges, at the bottom of the vessel the value increases as the charge increases, reaching the plastic limit level, when failure occurs. A series of contour plots with the results of the progressive damage model for increasing time steps is shown in

Figure 87 for the simulation with the 928 kg charge. The hole generated at the bottom of the vessel when the plastic strain limit value is reached is visible.

6 SUMMARY AND CONCLUSIONS

This report presents a feasibility study on structural analysis of pressure-containing structures subject to external blast loads using finite element and volume simulation software. A basic understanding of the main factors influencing the results of such analyses was established in an earlier study [4]. However analysis of combined static and dynamic loads only became possible with the latest release of the EUROPLEXUS software. An extensive series of computations have now been performed and the results are presented and discussed in detail in this report. These involve a 3-D simulation of a large steel vessel of hypothetical design containing pressurised water and subject to an explosive blast from a charge located directly underneath the lower torispherical end. The top is closed by a flat lid arrangement. The properties of the explosive material, the air and water environments and the vessel steel were taken from the literature. For the latter, elastic-plastic material properties at 20˚C have been considered. The vessel is located in a bunker and by using FSR boundary conditions the reflections of the pressure waves on the bunker walls are also considered. To provide a cross-check on the computational results, some simplified analyses were performed using engineering and empirical formulae to estimate the pressure loads need to produce yielding and failure of the vessel, as well as of the corresponding quantities of explosives that would be needed to produce sufficient shock wave pressures.

The main findings are as follows:

- The capability of the 2007 release of EUROPLEXSUS to simulate combined static and dynamic loads was successfully demonstrated. The procedure uses an initial quasi-static phase from 0 to 20 msec, then the explosion over 40 msec and finally a quasi-static analysis lasting 25 msec to reach a final equilibrium state.
- For explosive charges of up to 170 kg, the simulations predict no damage to the vessel. With a charge of 413 kg plasticity occurs at the bottom of the vessel. These values agree with the simplified engineering estimates that predict yielding in the bottom part of the vessel above approximately 350 kg explosive charge.
- With the EUROPLEXSUS progressive damage model is possible to simulate a local rupture in the lower part of the vessel for a high explosive charge of 928 kg. Again this is broadly in line with predictions from simple analytical formulae, but it should be noted that neither approaches consider buckling phenomena. For this type of simulation it was necessary to replace the internal water with an internal pressure value, so the water inertia effects or pressure changes are not taken into account.

The sensitivity of the predictions to several modelling assumptions were considered in detail, and the following summarises the findings:

- Several factors affect the accuracy of the quasi-static analysis. However, the overall values of predicted displacement, stresses and strains can be considered in broad agreement with the static calculations done by ABAQUS. The presence of the internal water presents a further complication, since the corresponding elements cannot expand to accommodate the expansion of the vessel created by the pressure. This could be compensated by using an artificially higher starting pressure.
- The gravity effect was also considered applying a constant force corresponding to the gravity value on all the nodes of the elements of the model. No substantial difference is present in the deformations values at different location of the vessel, although only the case with 5 kg of explosive was considered in this case.
- Both FSR (pressure waves reflecting on the bunker walls) and ABSO (pressure waves absorbed at the bunker walls to simulate a infinite open environment around the vessel) boundary

conditions were considered. No substantial difference in the response of the vessel is present for the case with 5 kg of explosive material, although the FSR conditions lead to higher pressure values at the sides and top of the bunker.

- Strain rate dependence of the material properties was also considering in the case with 413 kg of explosive material, when significant plasticity is induced. Both models considered (Symonds-Cowper and Ispra) give similar predictions, with three times higher plasticity than for the standard material law (without strain rate dependence). It was shown that these models can also be combined with the progressive damage model to simulate fracture.

In conclusion, the series of studies on fast transient simulations of the interaction between explosive blast waves and pressure-containing structures have successfully demonstrated the capability of the EUROPLEXSUS software tool to consider a wide range of effects, including structural damping factors, elastic and elastic-plastic material properties, strain rate dependences of the material properties effects, different explosive material models, mesh dependencies and optimisation, inertia effects, gravitational effects and also progressive damage models to simulate local rupture. To provide confidence in the predictions and to further study and optimise the above aspects, a priority would be to identify a suitable experimental benchmark to allow direct comparisons.

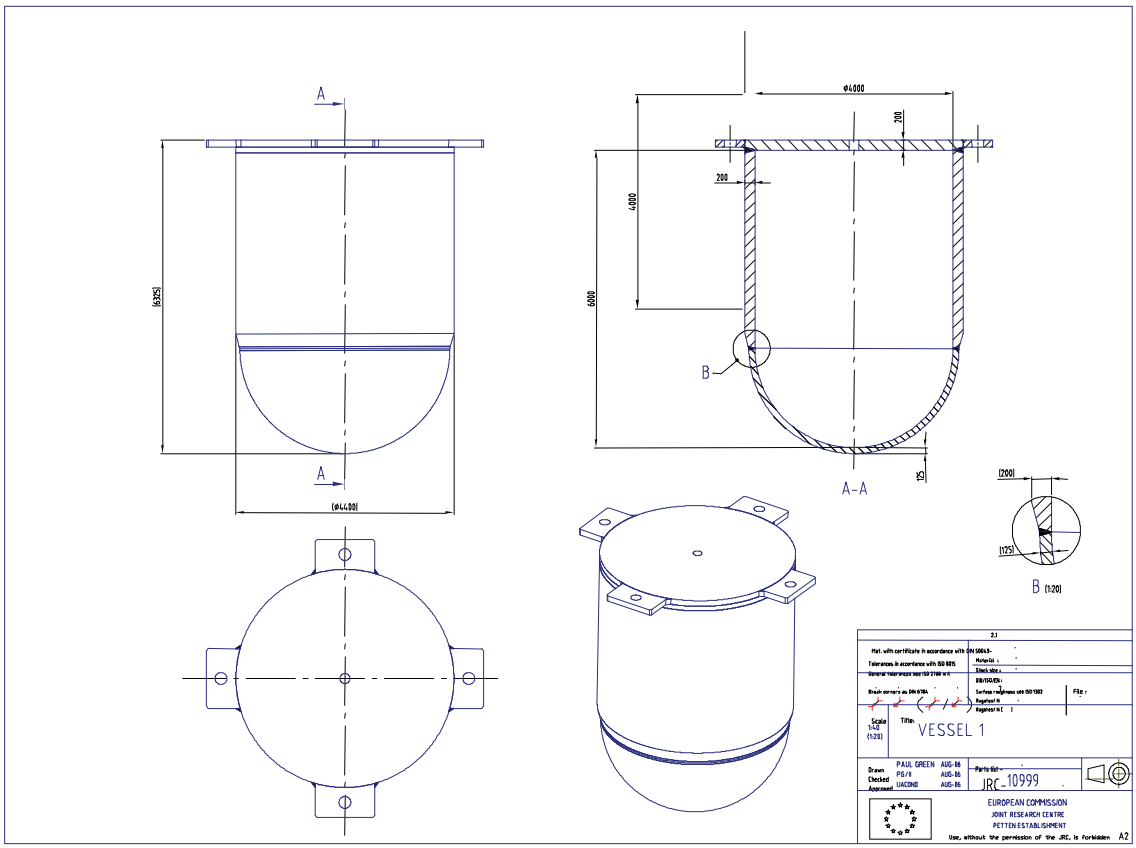

Figure 1 Geometry of the 3D FE case: high pressurised vessel in a bunker.

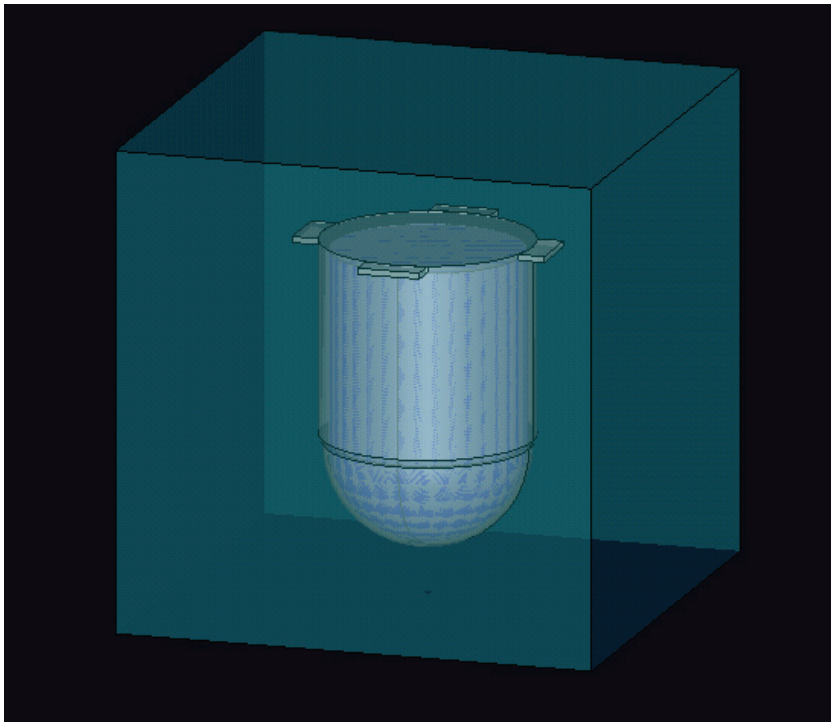

Figure 2 Vessel, with high pressurised water inside (155bar) and air at 1 atm around. Cubic bunker of 10x10x10 m of dimension.

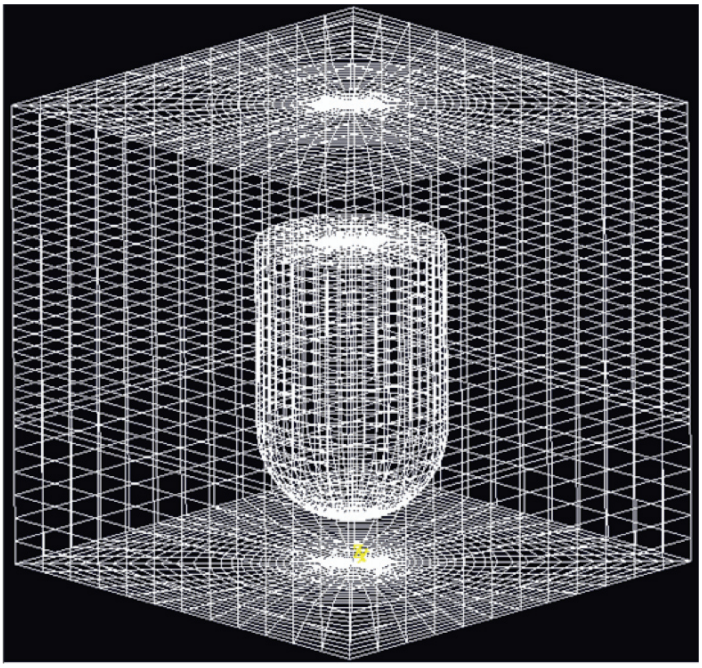

Figure 3 Mesh of the vessel and of the bunker of air. Hexahedrons elements.

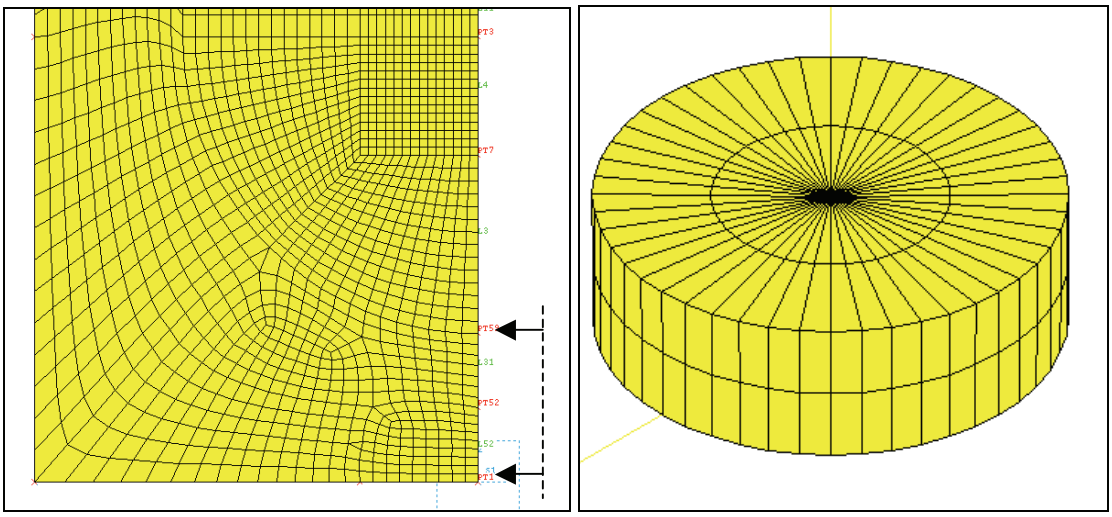

a) **b)**

Figure 4 a) Details of the mesh of the bottom of the vessel and of the high explosive (HE) charge at 1 m below the vessel (inside the indicate square) and b) mesh of the HE box (5kg). The length from Point 1 to Point 59 is 1 meter. Point 59 is the bottom of the tank.

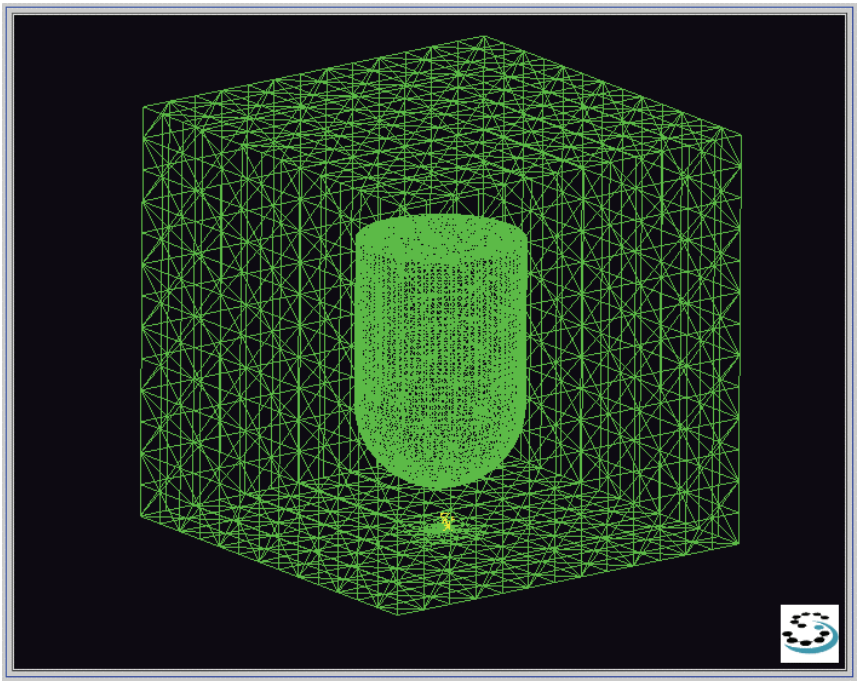

Figure 5 Mesh of the vessel and of the bunker of air. Tetrahedral elements.

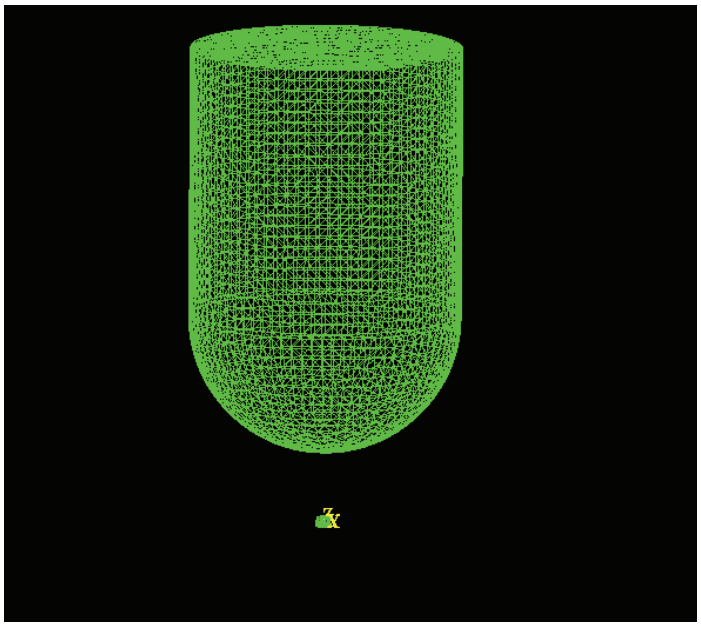

a)

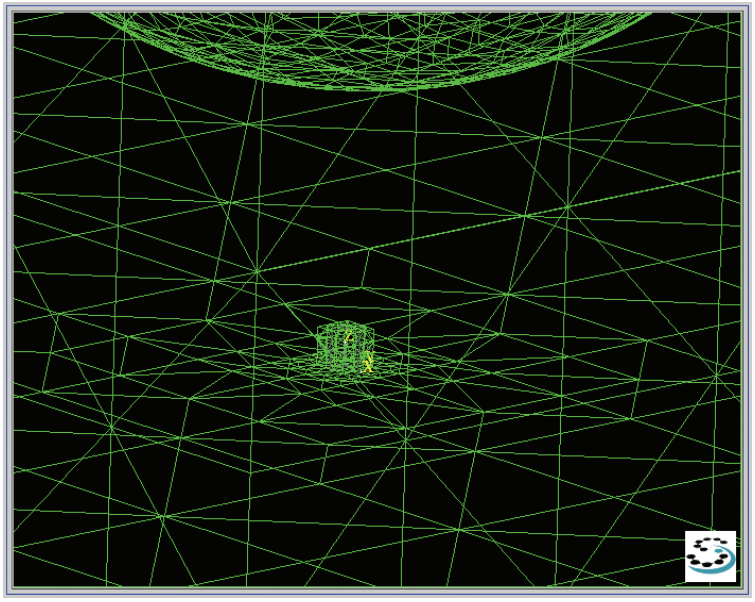

b)

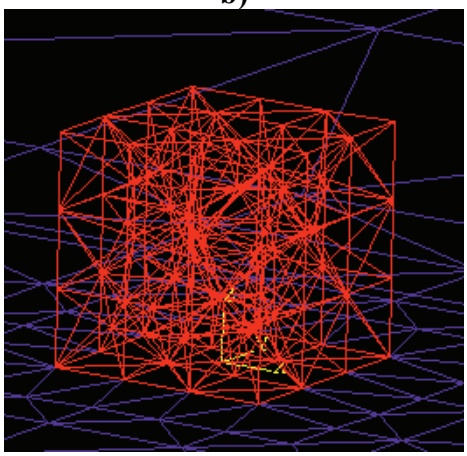

c)

Figure 6 Particulars of the mesh: a) vessel and b) and c) explosive charge box (5kg) below the vessel. Tetrahedral elements.

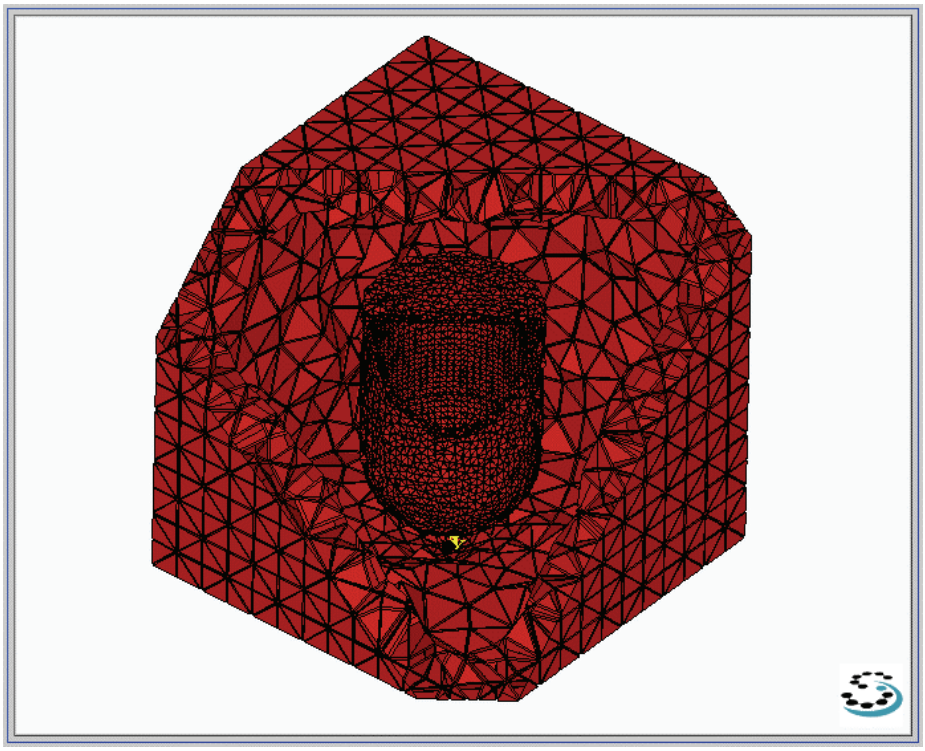

a)

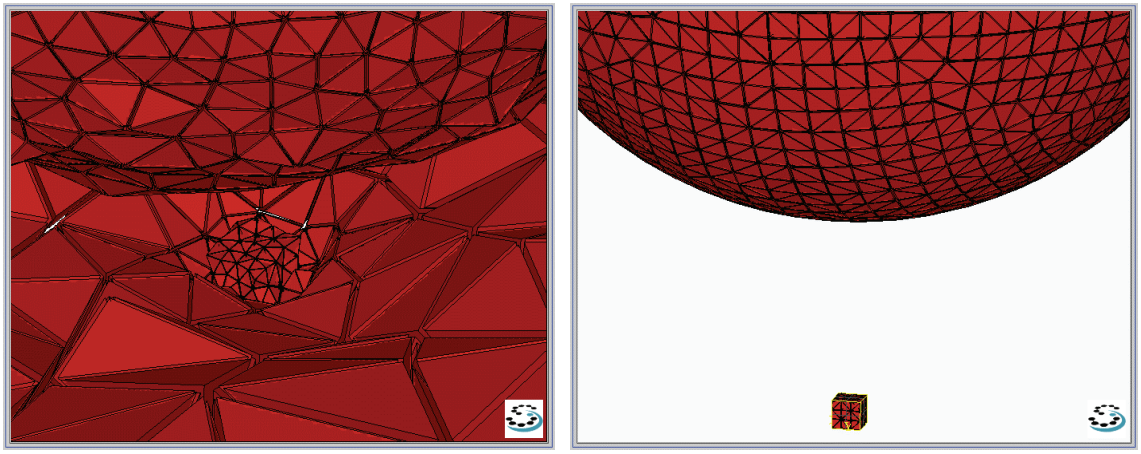

b)

Figure 7 Cut view of the tetrahedral mesh: a) vessel in the bunker of air and b) explosive charge box below the vessel.

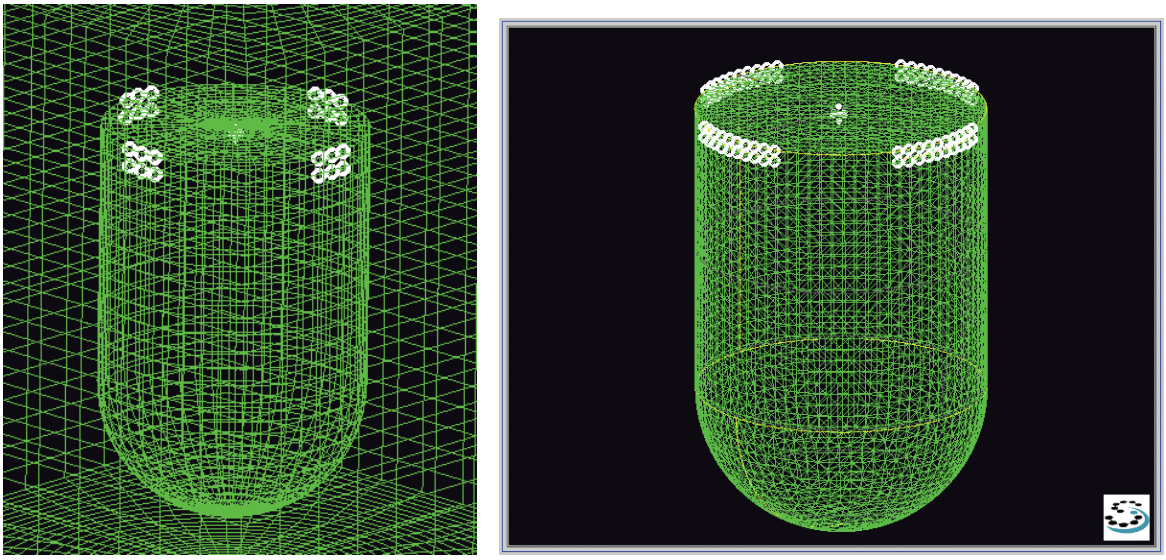

a) b)

Figure 8 Boundary conditions of the vessel: the nodes of the four sides of the top of the vessel fixed to simulate the clamps of the vessel (Figure 2); a) hexahedrons mesh, b) tetrahedral elements.

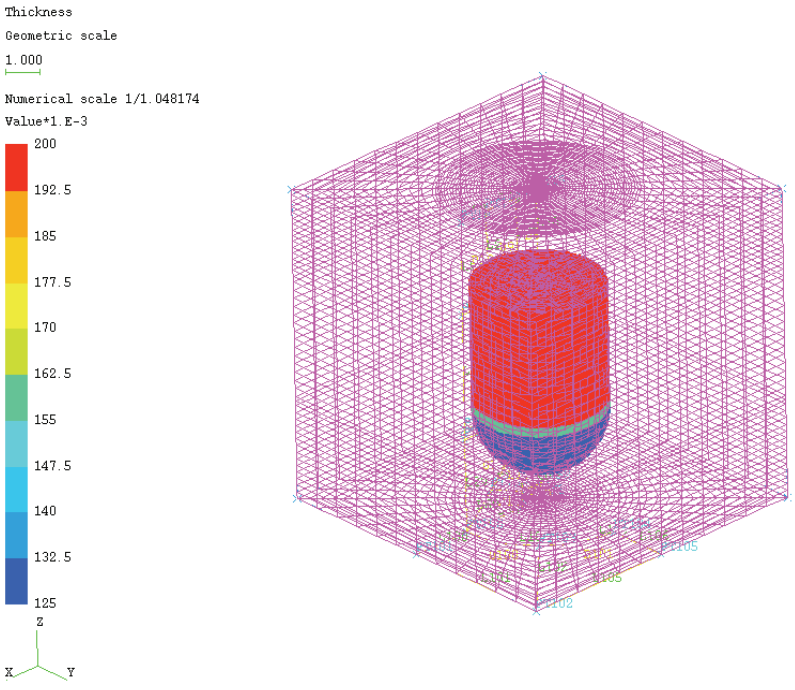

Figure 9 Thickness of the vessel

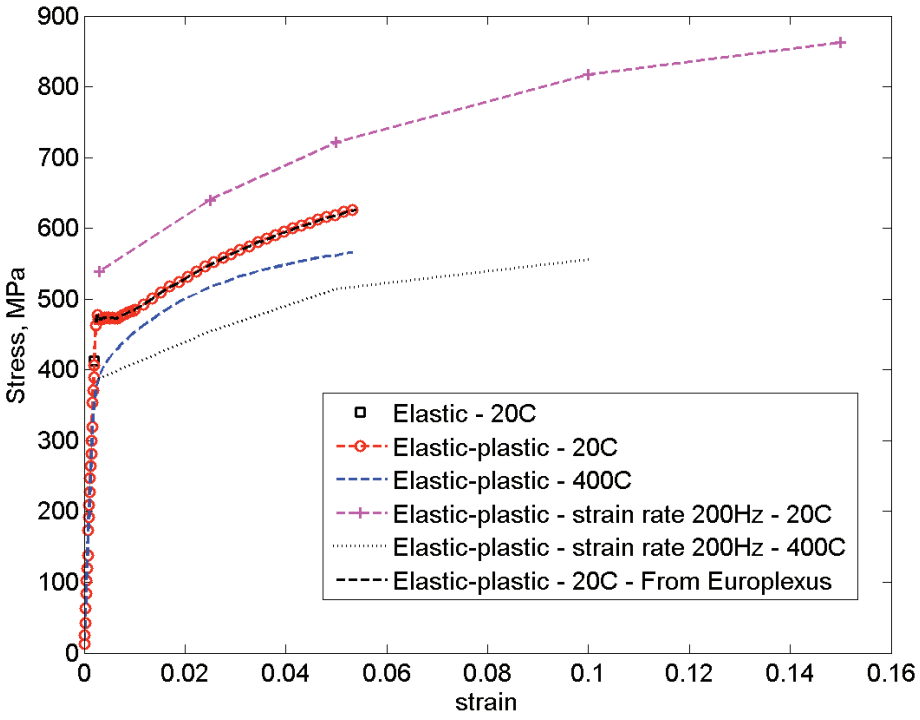

Figure 10 Stress-strain curve from the experimental tests at different temperature [6] and EUROPLEXUS output at 20°C.

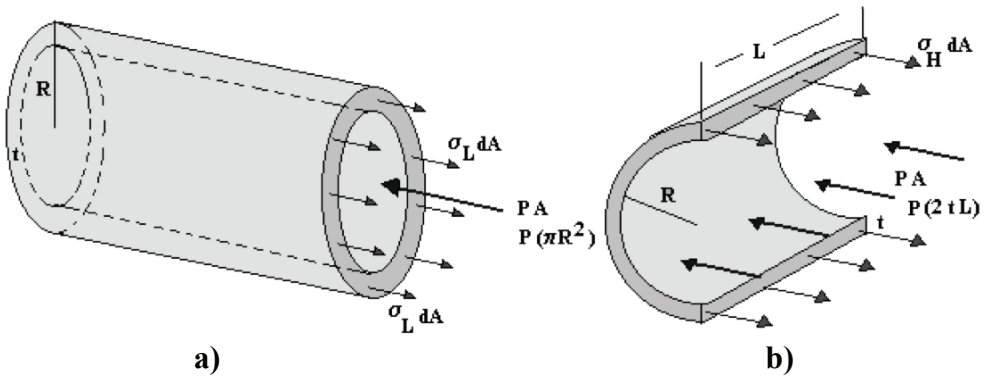

Figure 11 Cylindrical pressure vessel a) and section view b).

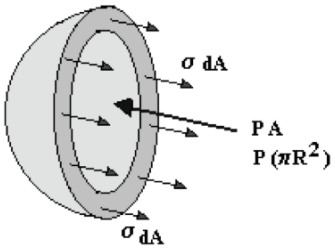

Figure 12 Spherical pressure vessel section.

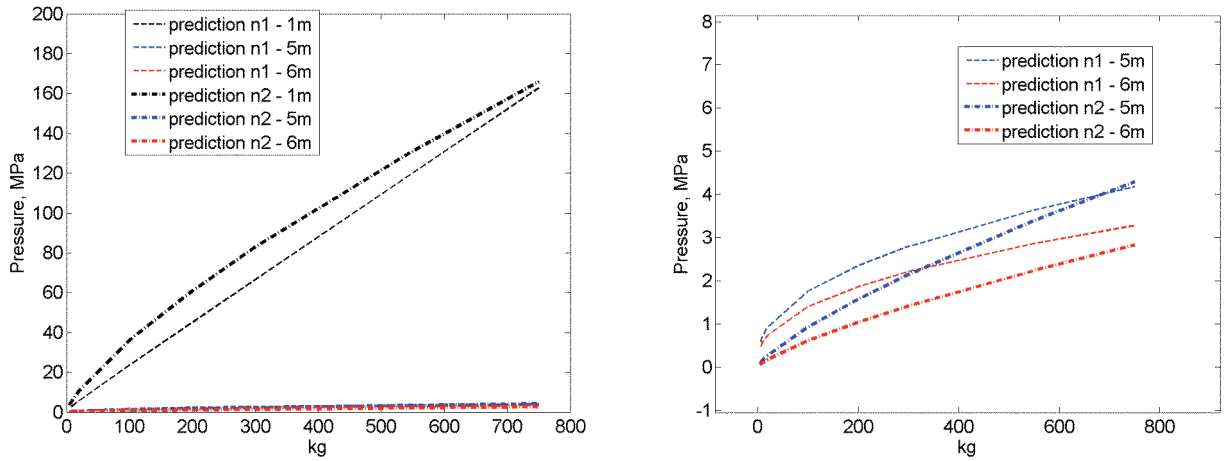

Figure 13 Comparison between the predicted values at a distance equal to 1, 5 and 6 meters from the ground where the charge is located.

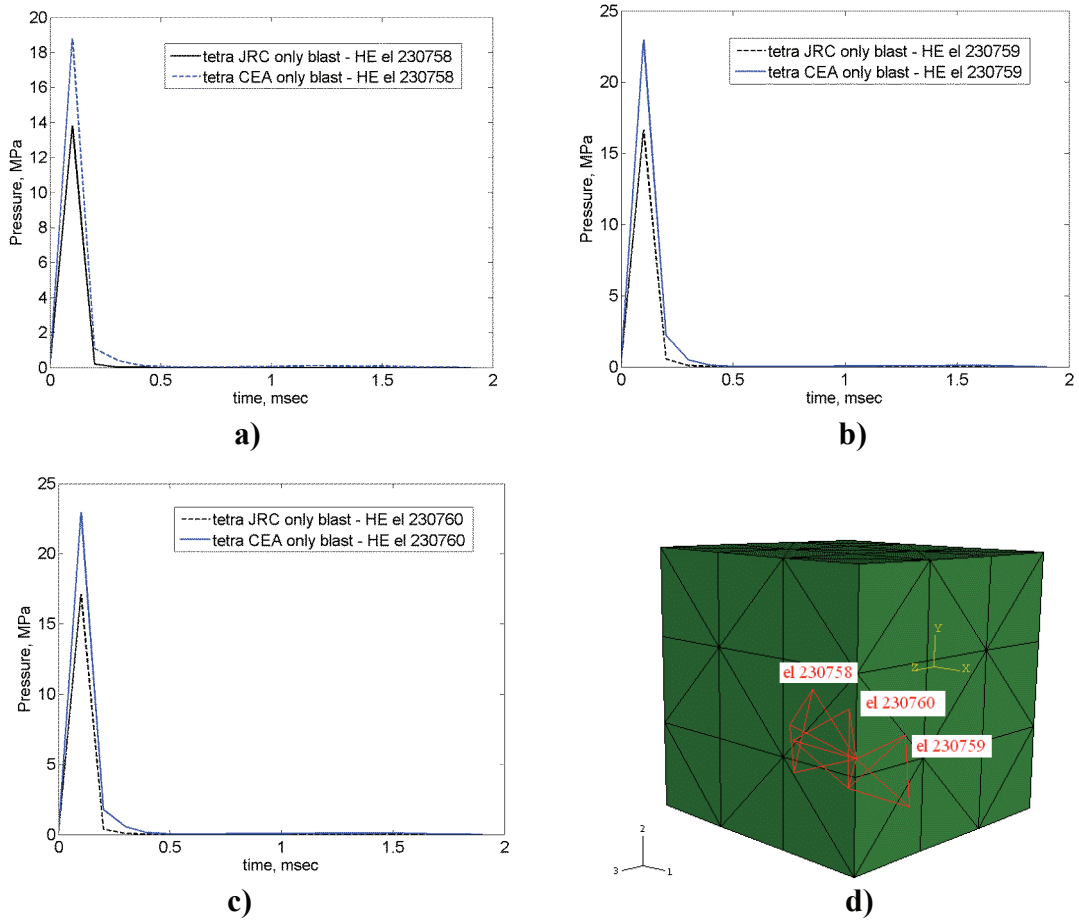

Figure 14 Pressure evolution in different elements of the explosive charge a), b) and c) for the two kinds of tetrahedral elements implemented in the software (Pref=0atm). 5kg of explosive charge d).

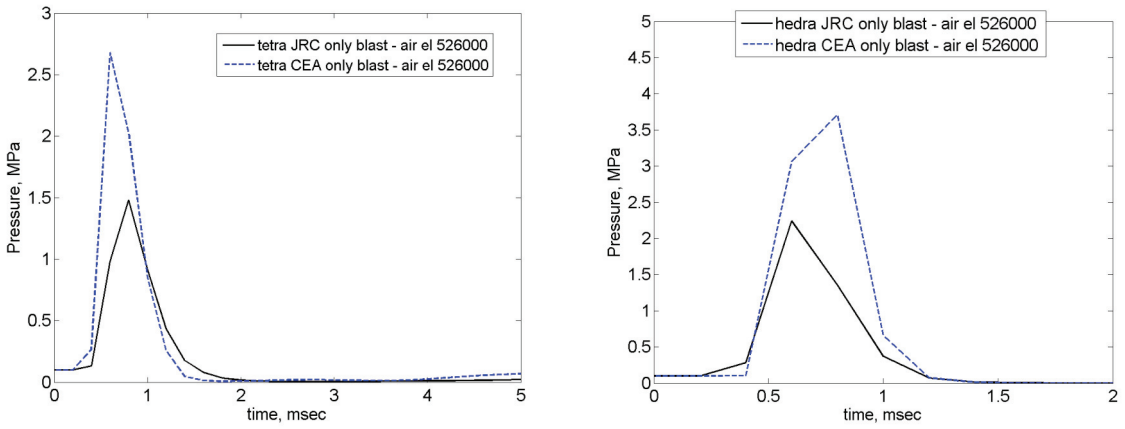

a) b)

Figure 15 Pressure evolutions in the air element facing the vessel for a) tetrahedral elements and b) hexahedrons elements and the two material model for explosive material. (pref=1atm)

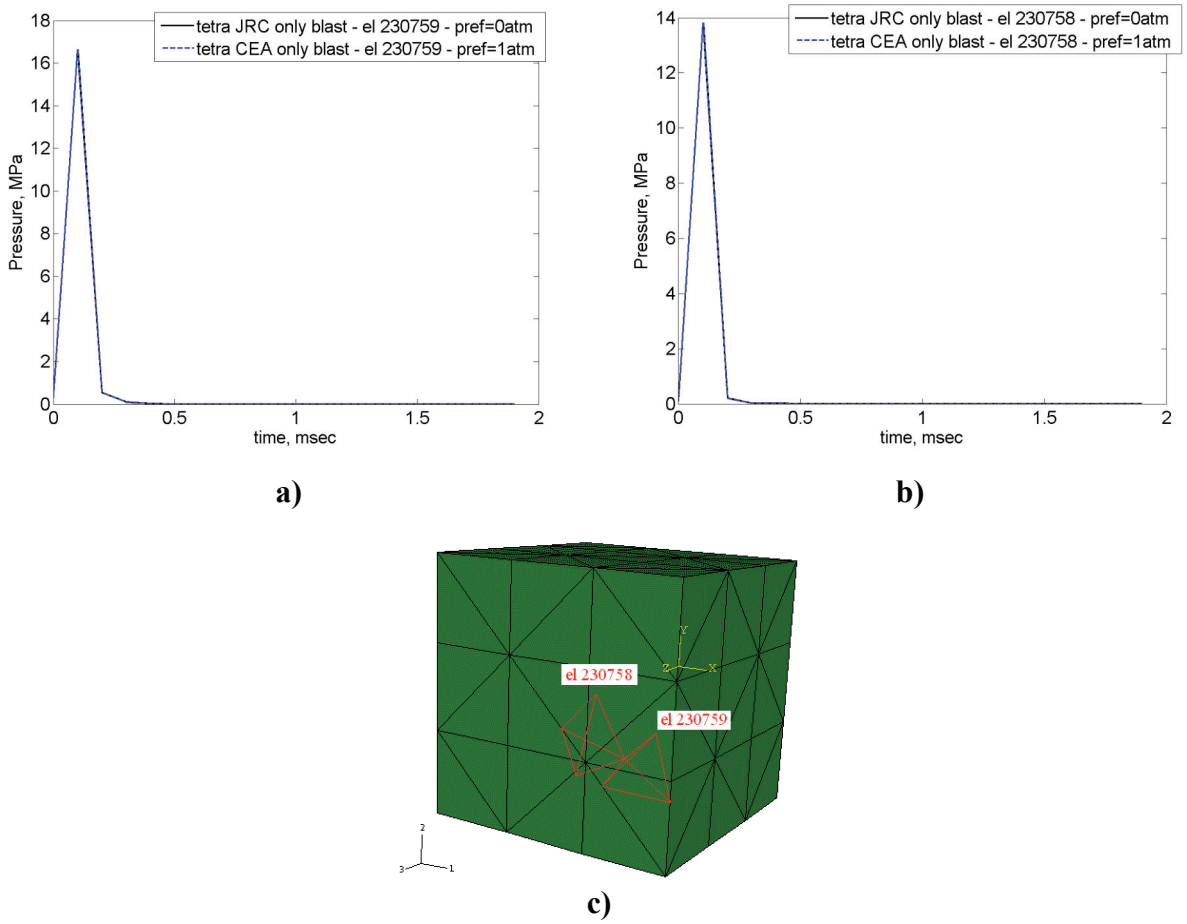

a) b)

c)

Figure 16 Pressure evolution a) and b) in two elements of the explosive charge c) for two reference pressures: pref=0atm and pref=1atm.

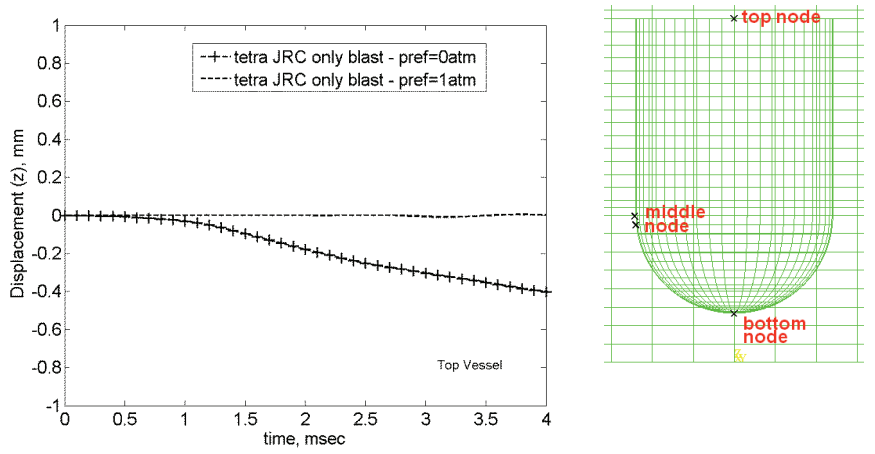

a)

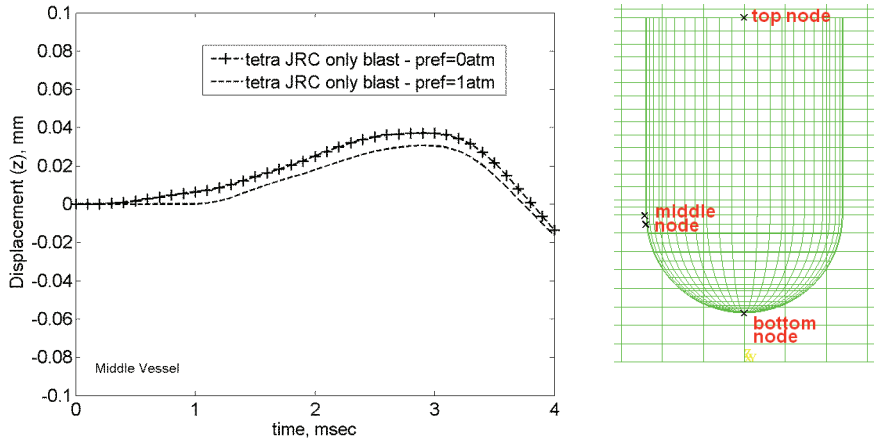

b)

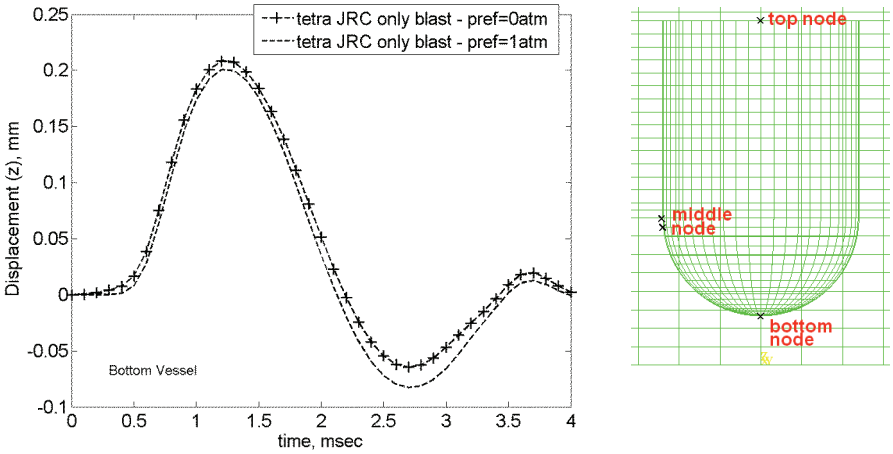

c)

Figure 17 Displacement in the z direction at a) top, b) middle and c) bottom of the vessel, with the different reference pressure value. Vessel without water.

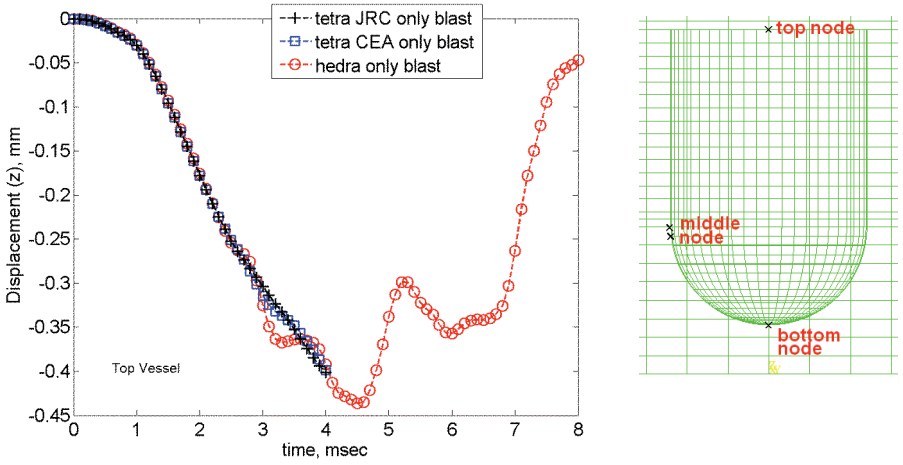

a)

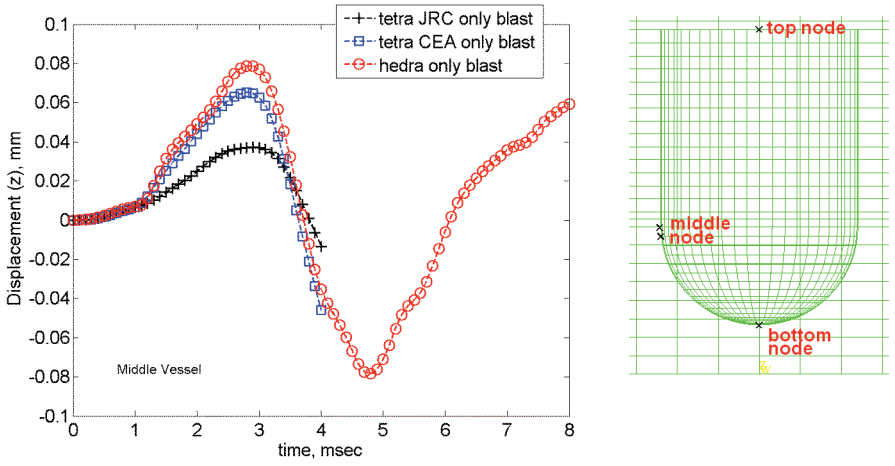

b)

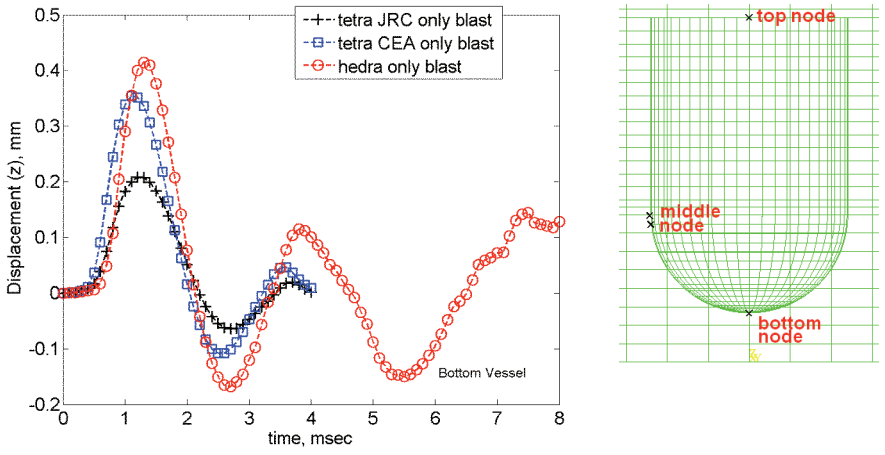

c)

Figure 18 Displacement in the z direction at a) top, b)middle and c) bottom of the vessel, with the different elements type implemented in the software. Vessel without water.

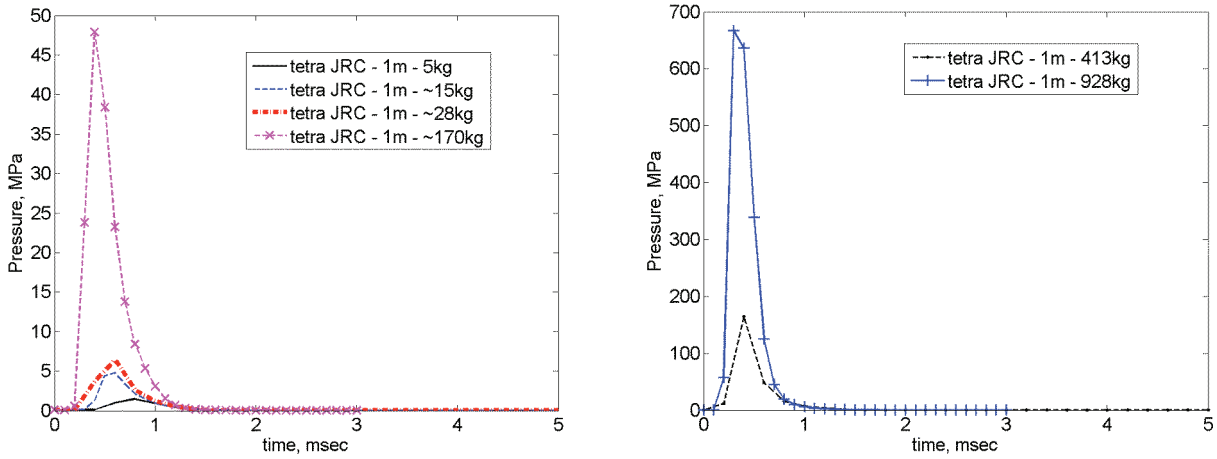

Figure 19 Pressure overpressure reaching the bottom of the vessel (1m distance from the explosive charge) for different amount of explosive charge.

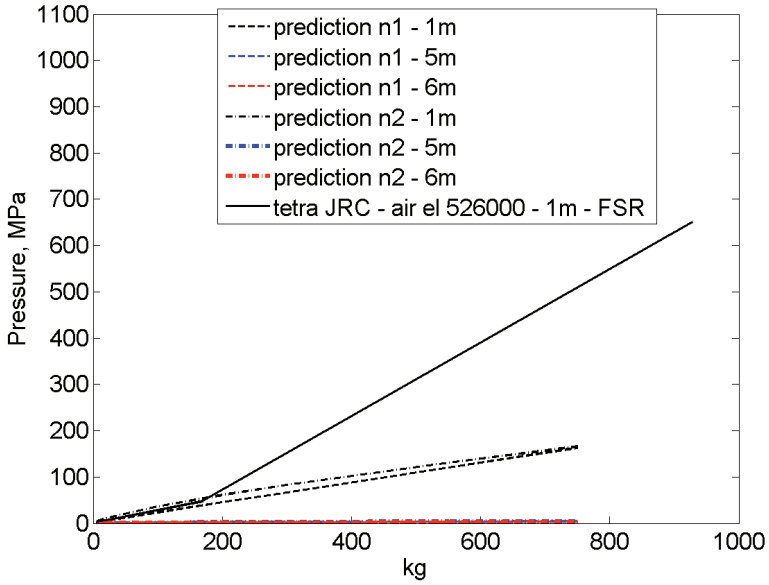

Figure 20 Comparison between the predicted values and the analysis values.

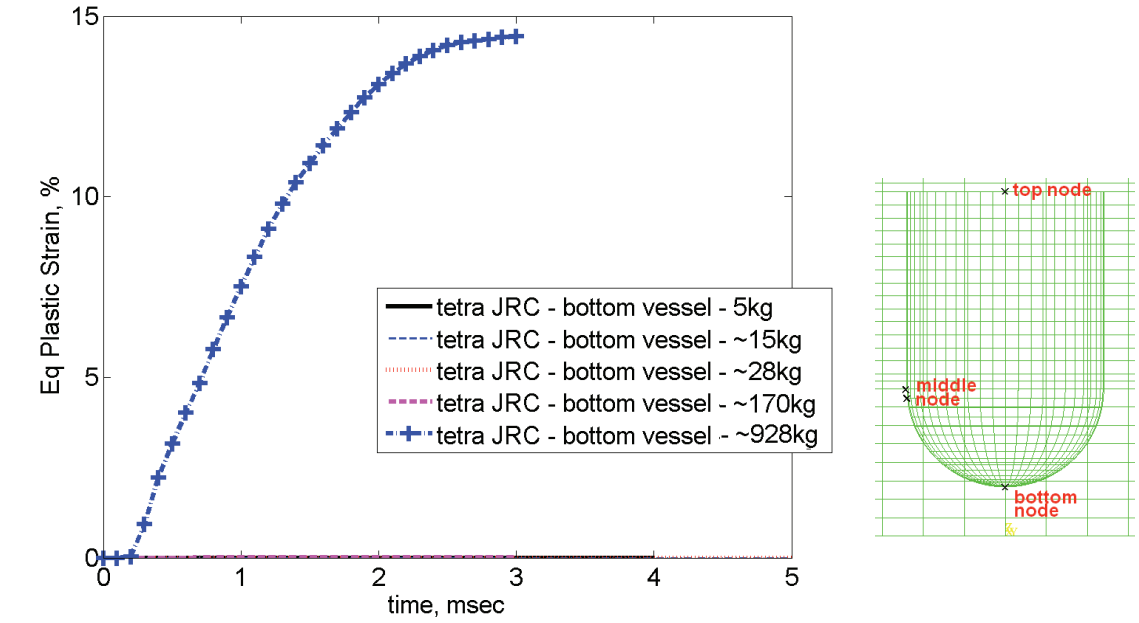

a)

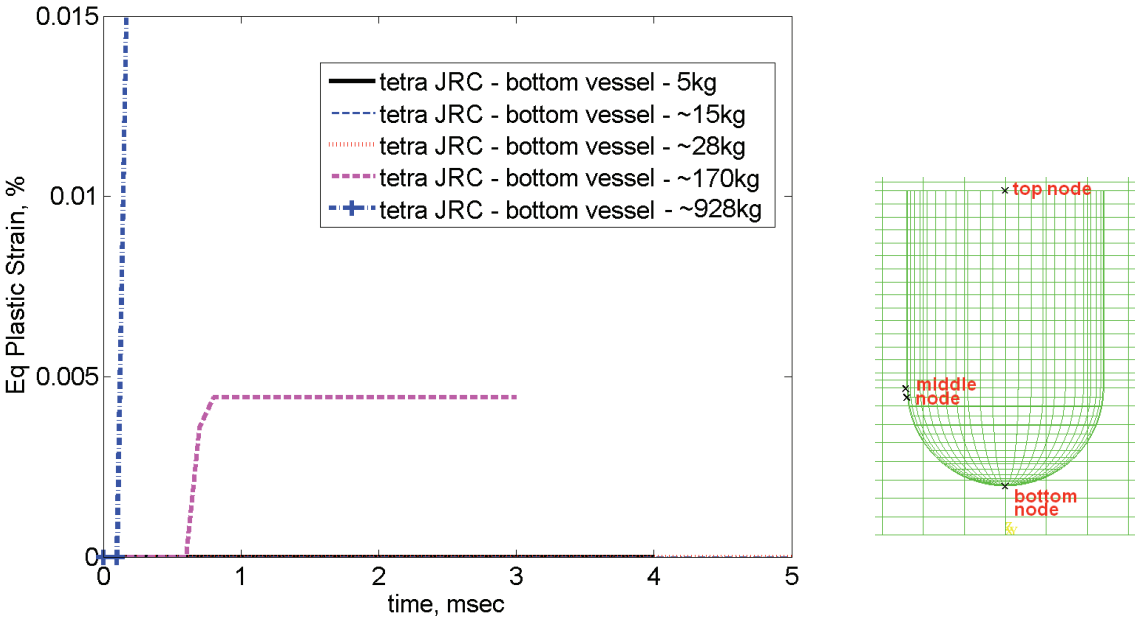

b)

Figure 21 Equivalent plastic strain at the bottom of the vessel for different amount of explosive charge a) and related detail b). Vessel without water.

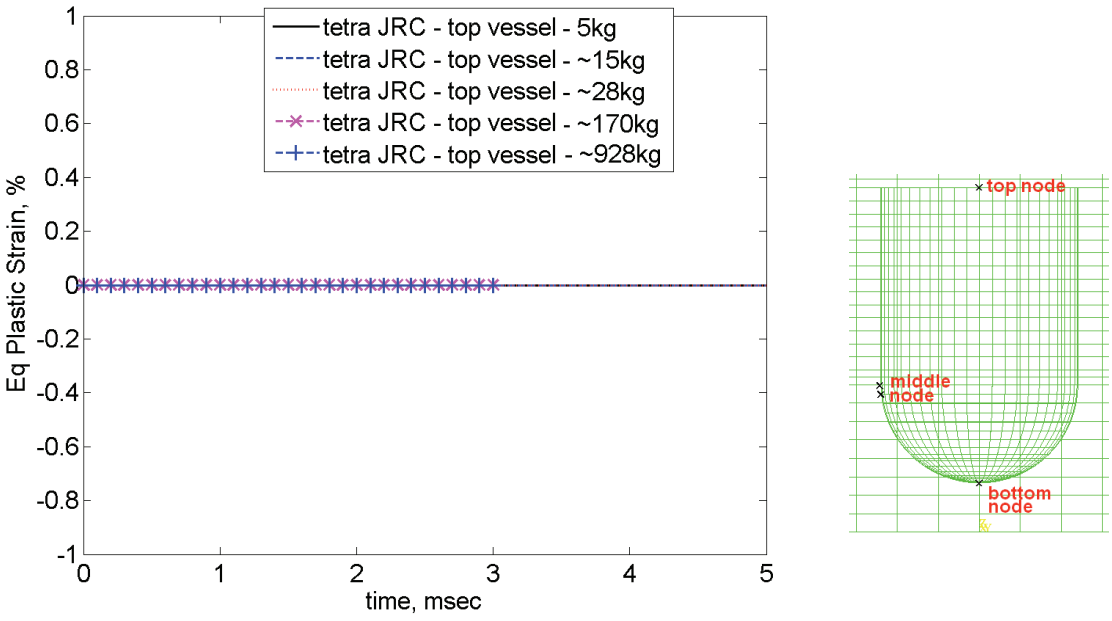

a)

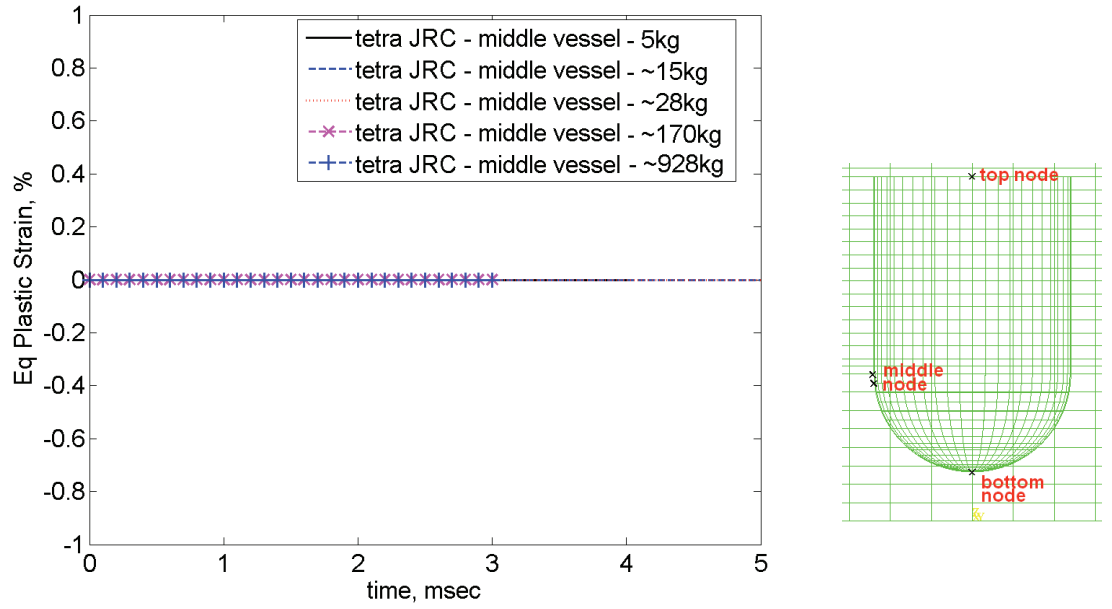

b)

Figure 22 Equivalent plastic strain a) at the top of the vessel and b) middle of the vessel for different amount of explosive charge. Vessel without water.

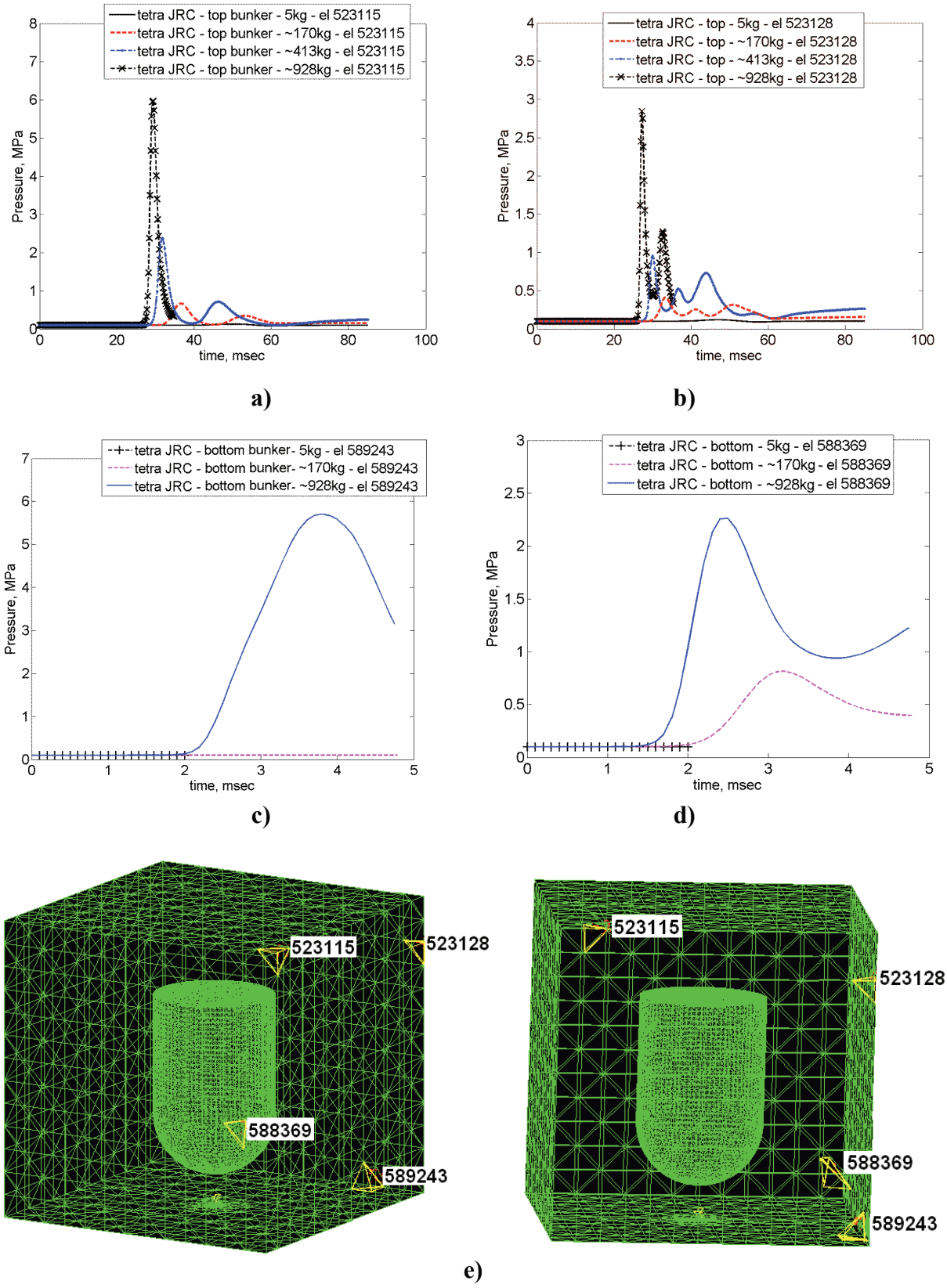

Figure 23 Pressure at different location in the bunker: a) top of the bunker, b) top of the vessel level, c) bottom of the bunker, d) bottom of the vessel level, as shown in e).

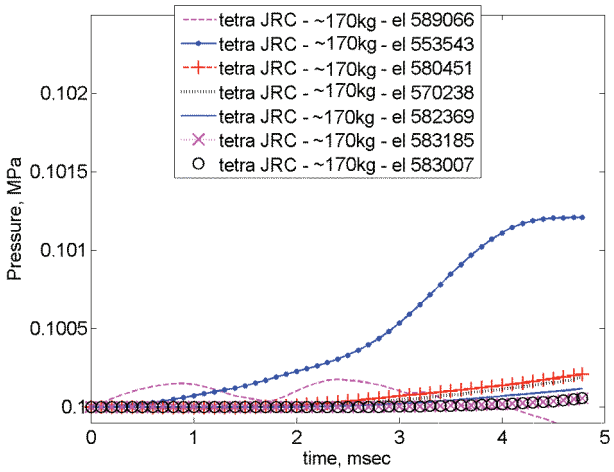

a)

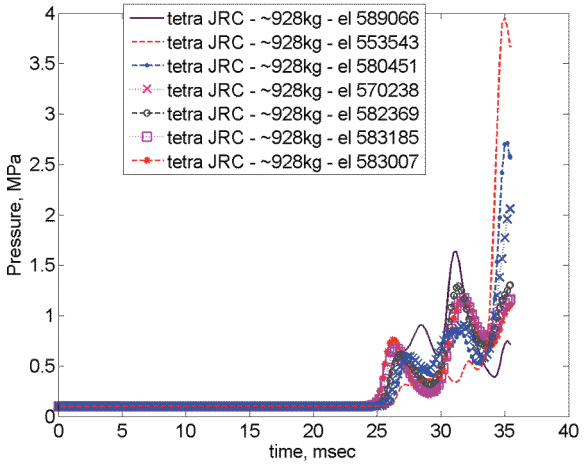

b)

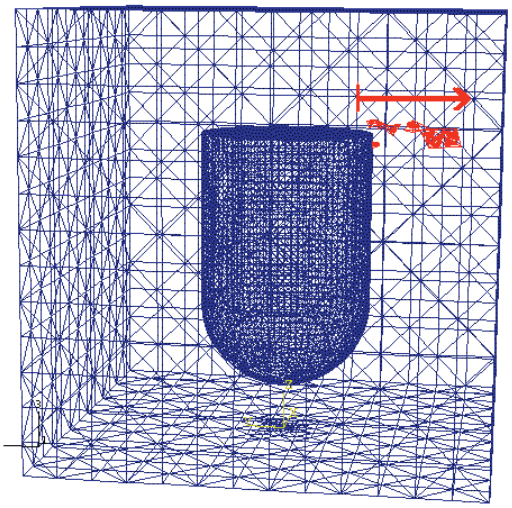

c)

Figure 24 Pressure at different location in the bunker a) for ~170 kg of explosive material, b) for ~928 kg of explosive material, from the vessel to a bunker wall as shown in c) (starting element 589066 near the vessel).

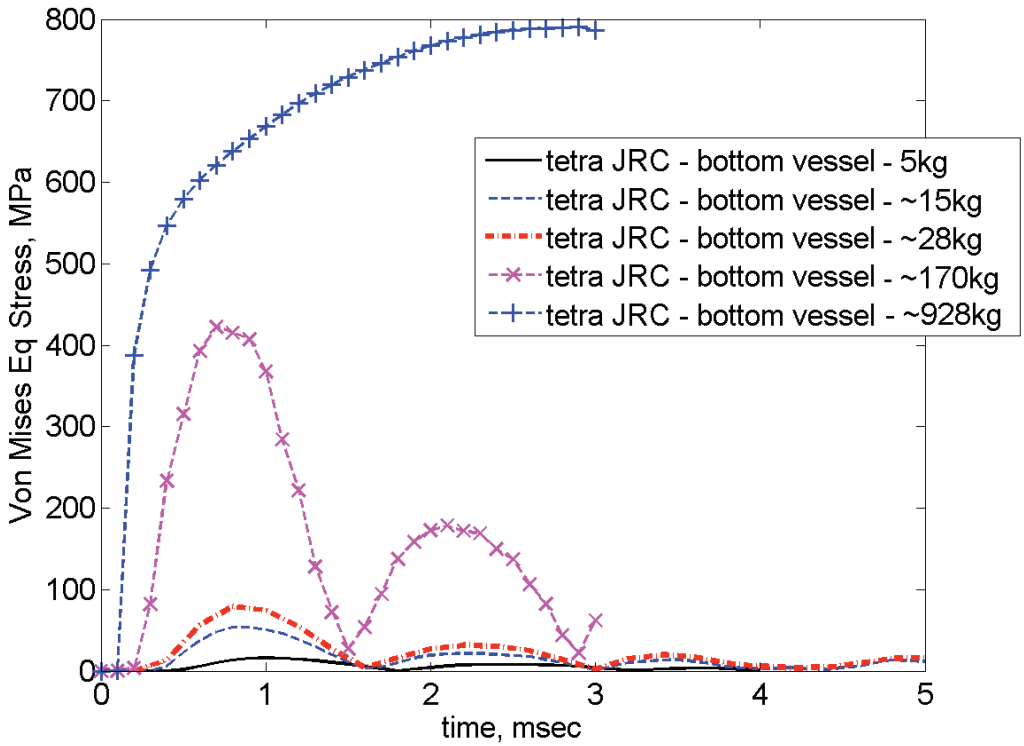

Figure 25 Von Mises equivalent stress at the bottom of the vessel for different amount of explosive charge. Vessel without water.

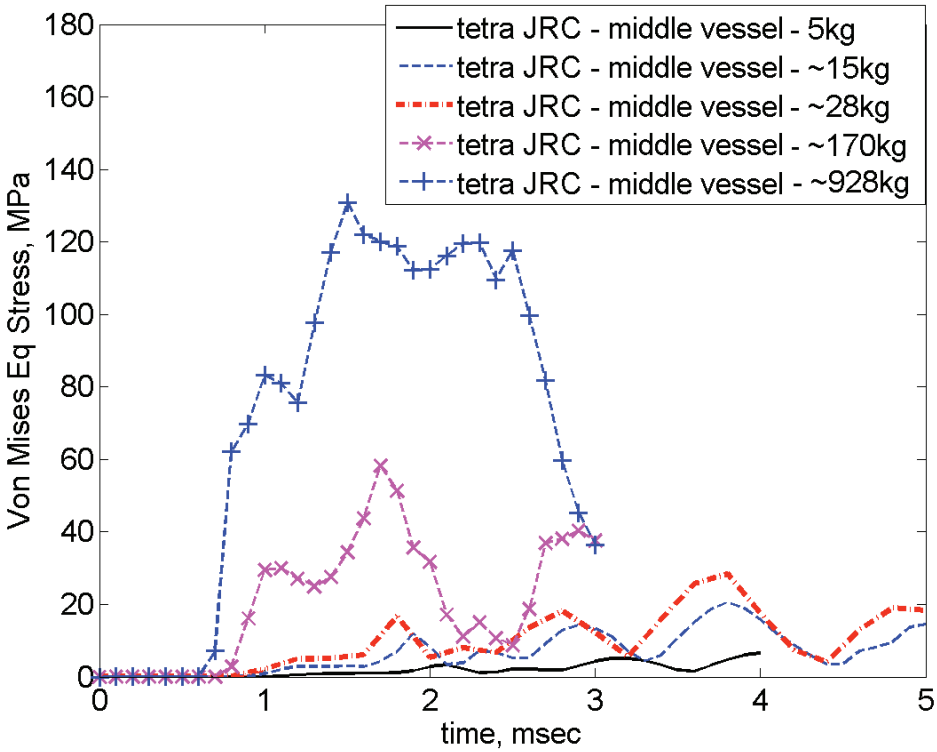

Figure 26 Von Mises equivalent stress at the middle of the vessel for different amount of explosive charge. Vessel without water.

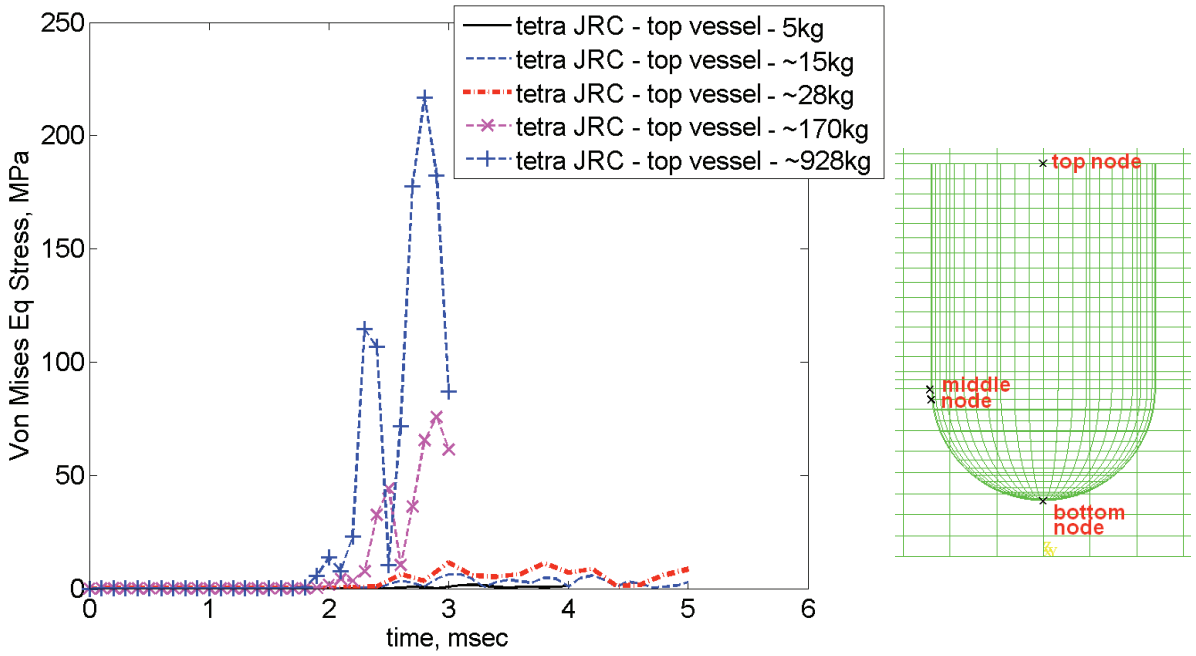

a)

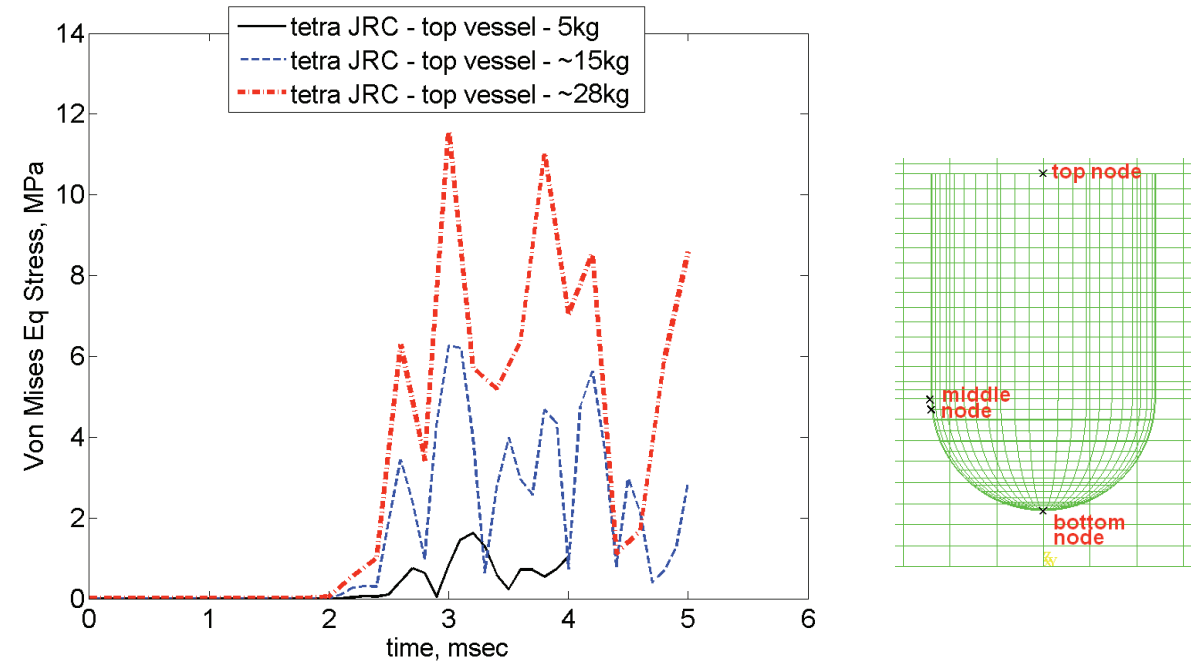

b)

Figure 27 Von Mises equivalent stress at the top of the vessel for different amount of explosive charge a) and related detailed b). Vessel without water.

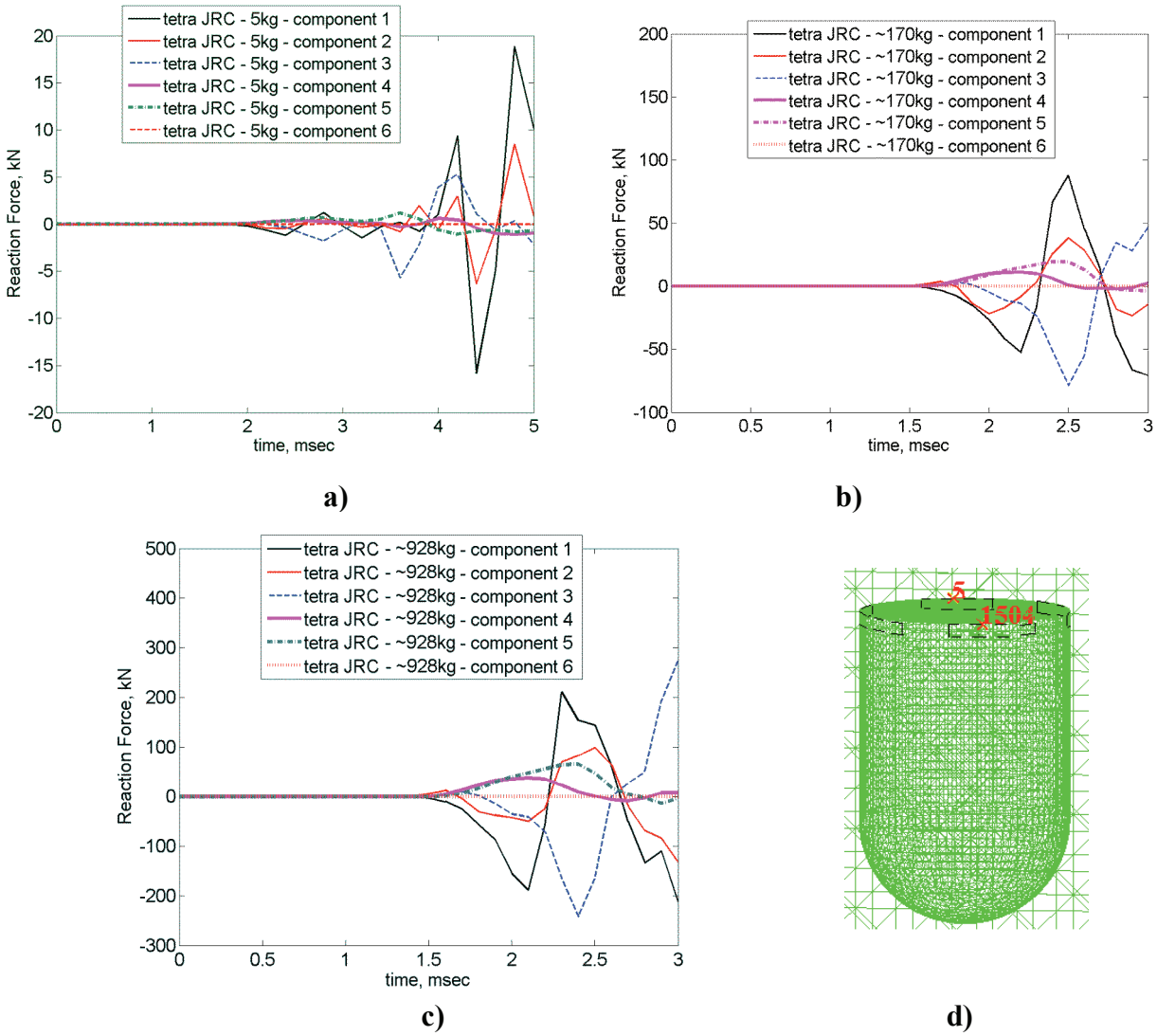

Figure 28 Reaction forces components at a location of the clamped zone (node 1504) for a) 5 kg, b) 200kg and c) 550 kg. Vessel without water.

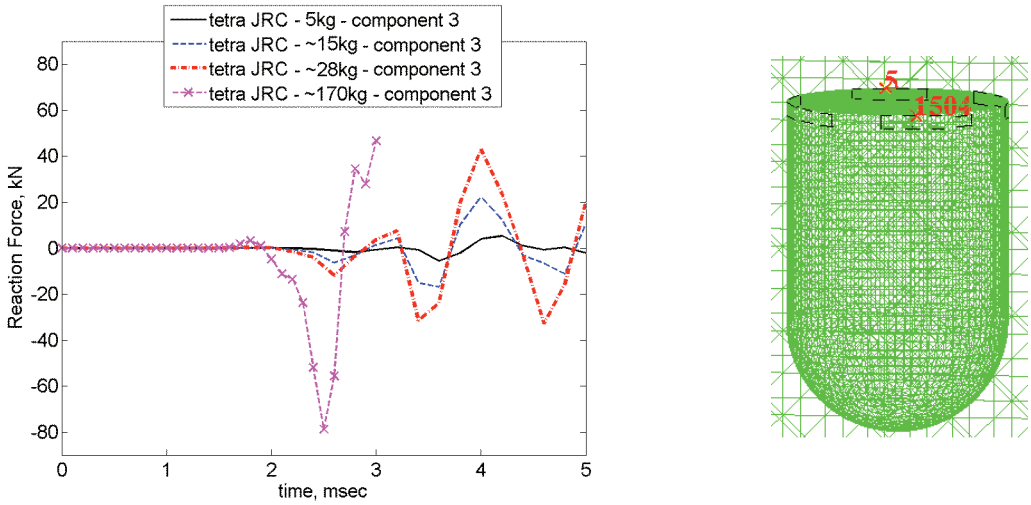

Figure 29 Reaction force z component at a location of the clamped zone (node 1504) for different amount of explosive charge. Vessel without water.

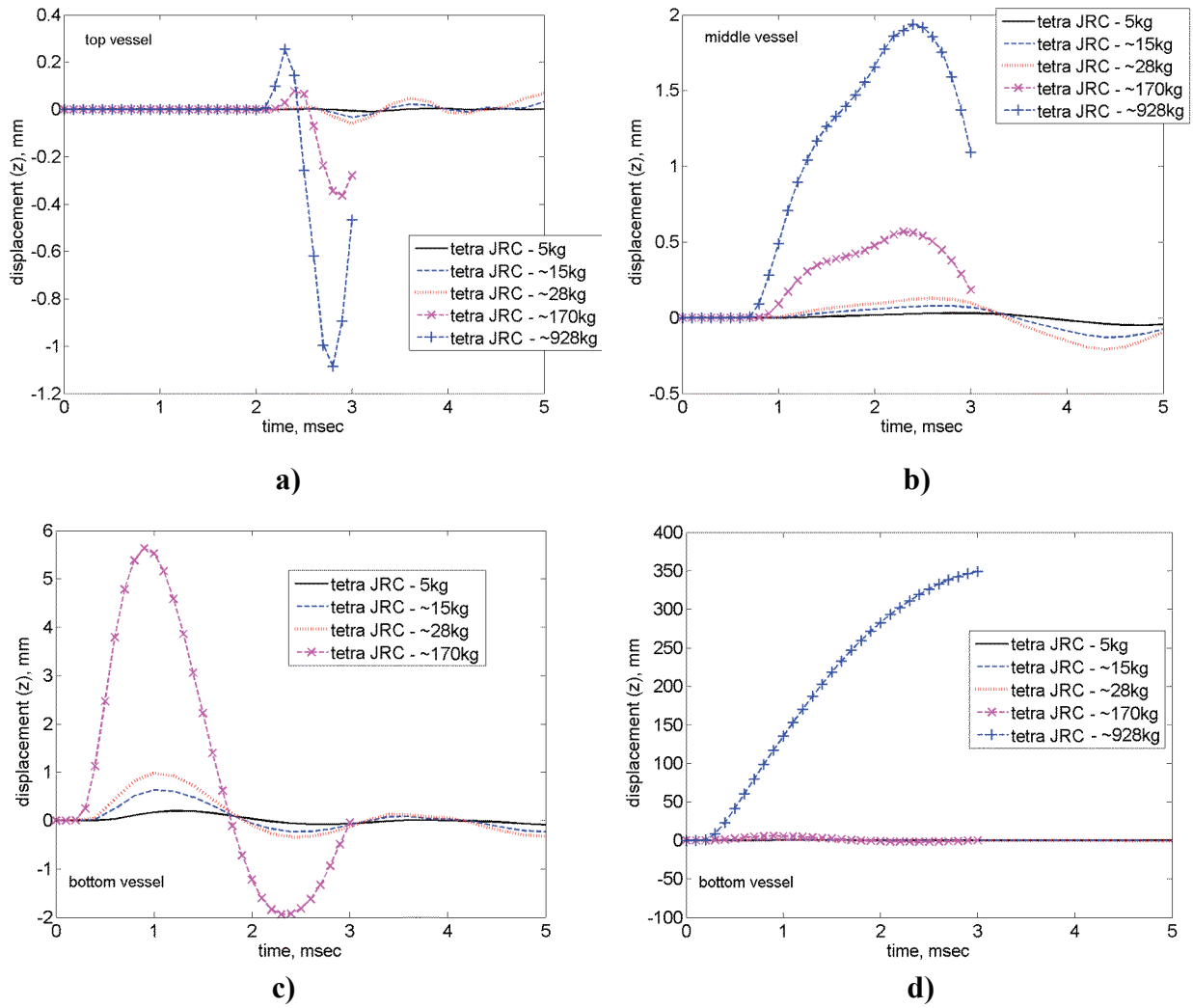

Figure 30 Displacement in the z direction at a) top, b) middle and c) and d) bottom of the vessel, for different amount of charge. Vessel without water.

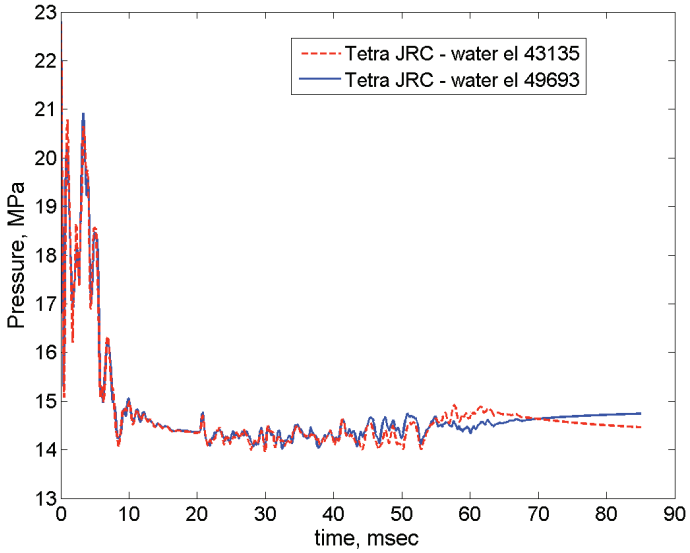

Figure 31 Pressure in the water.

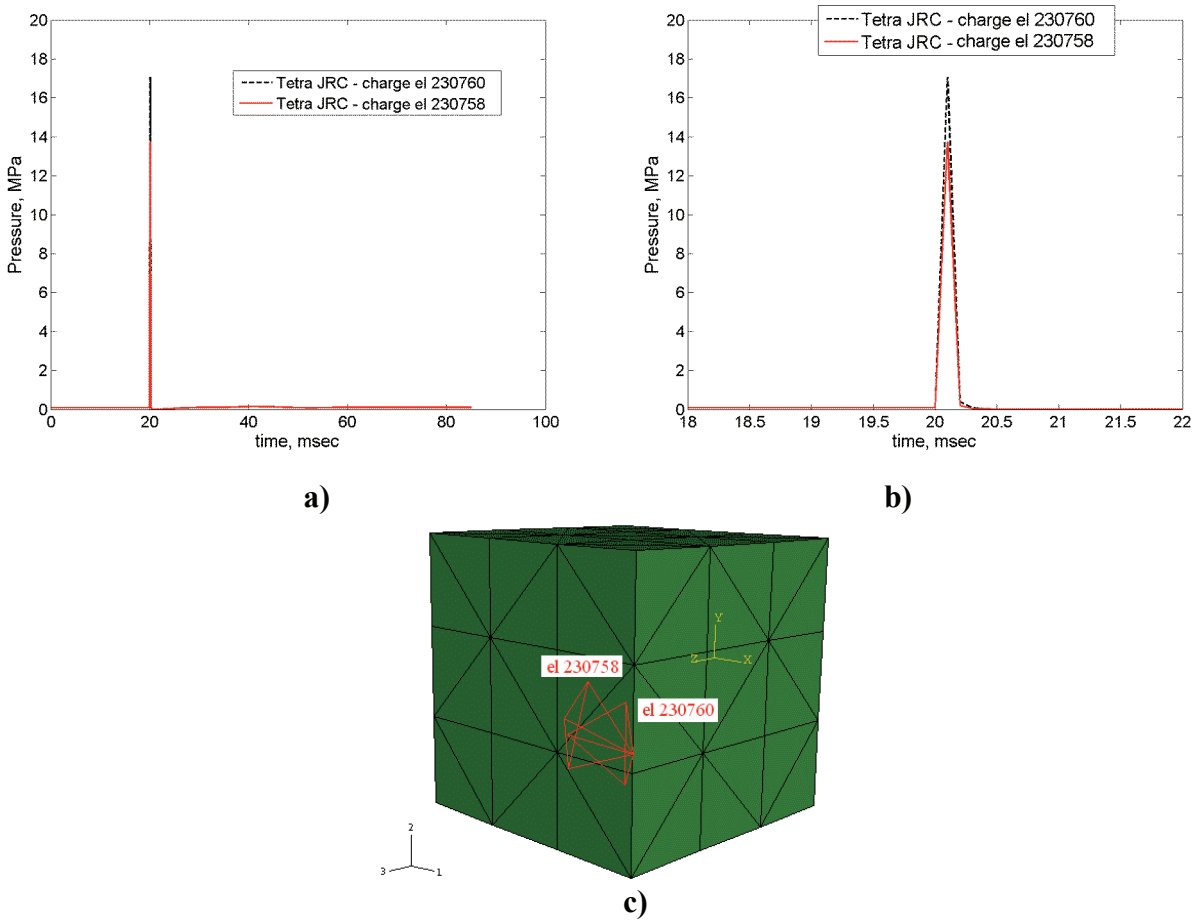

Figure 32 Pressure in some elements of explosive material a) for the total computation time and b) detail for an interval of time around the detonation time. 5kg of explosive charge c).

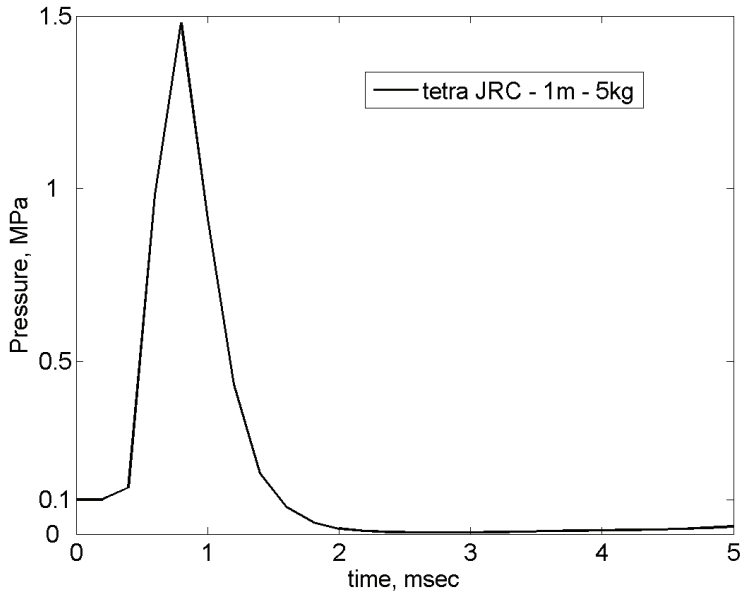

Figure 33 Pressure in the element of air below the vessel. 5kg of explosive charge.

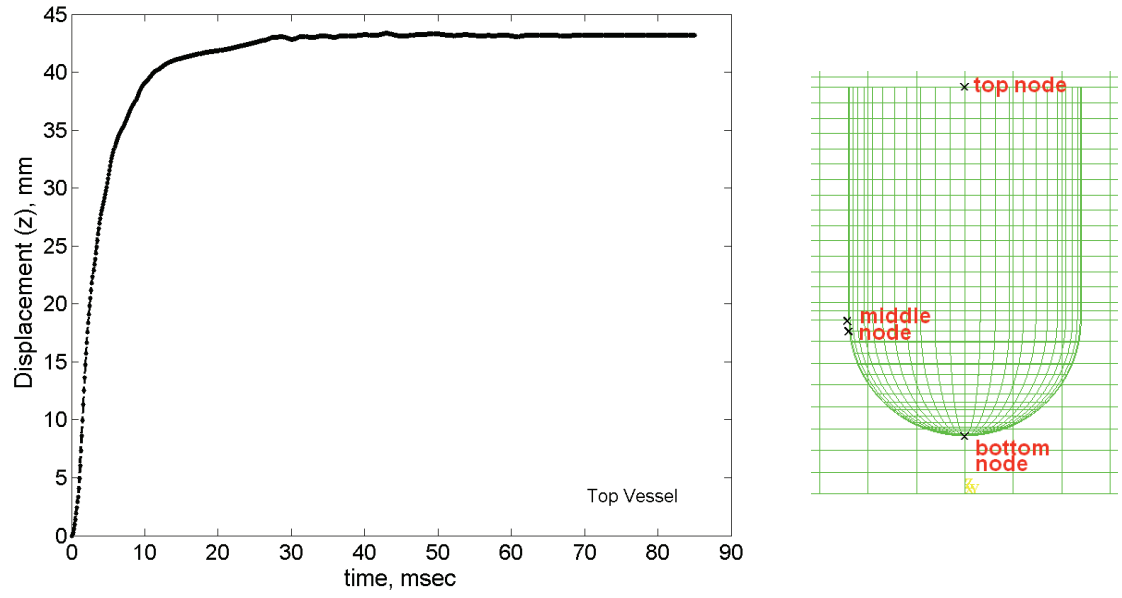

a)

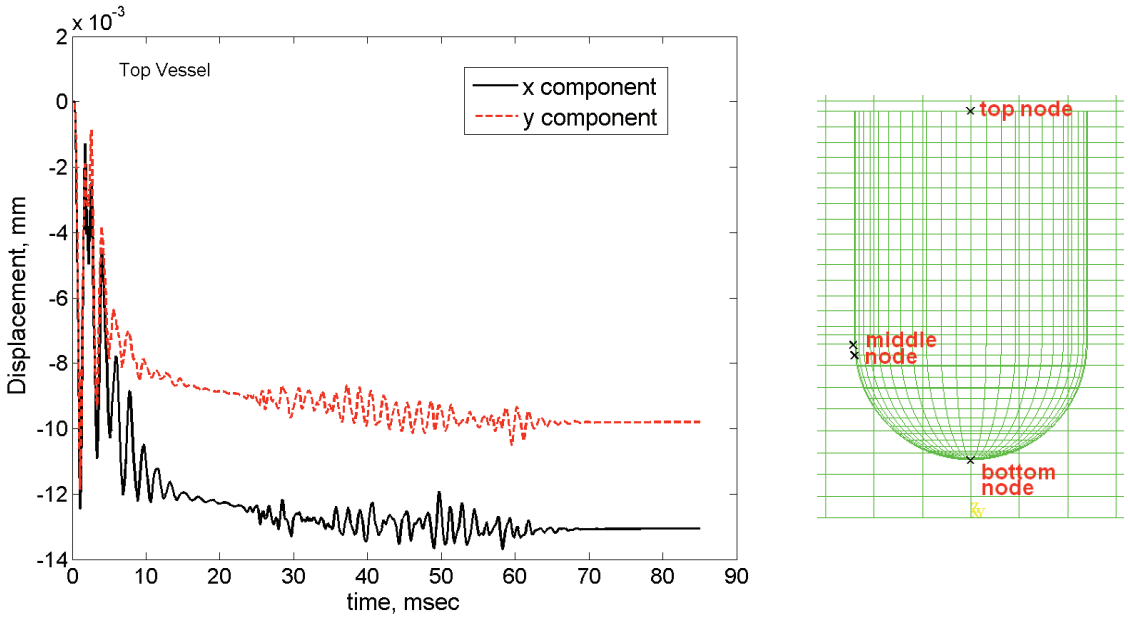

b)

Figure 34 Displacement at the top of the vessel a) z component and b) x and y components for the case with FSR boundary conditions and 5 kg of explosive material.

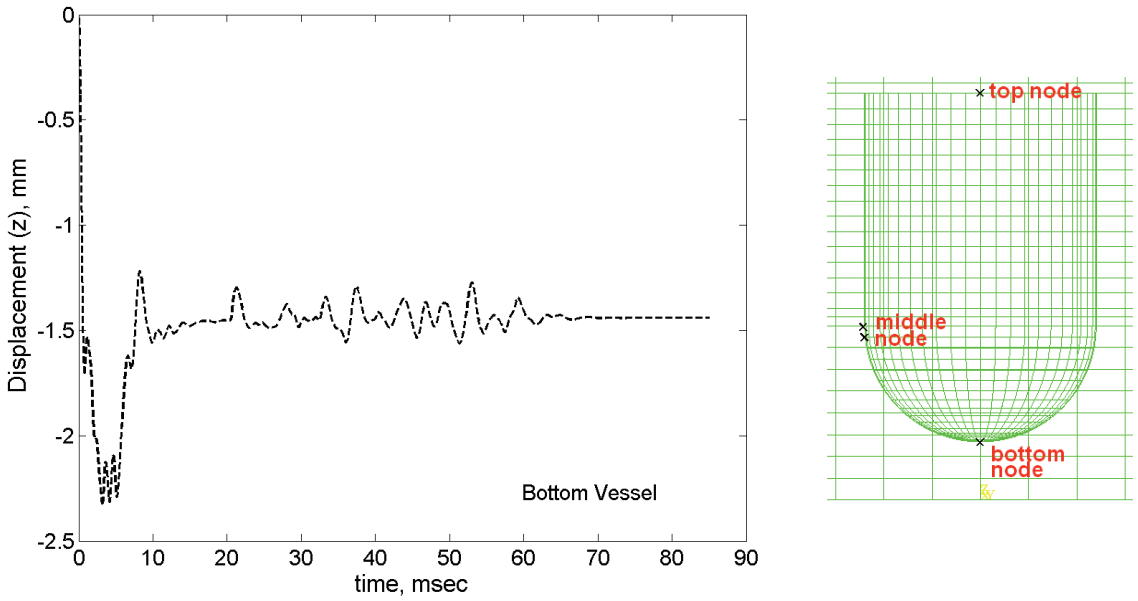

a)

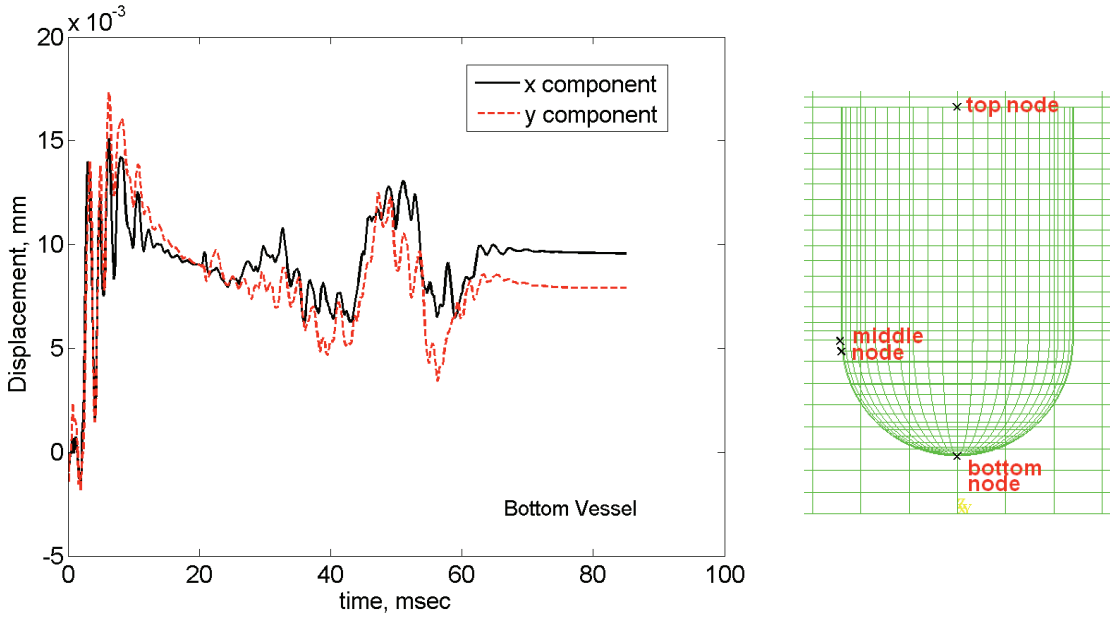

b)

Figure 35 Displacement at the bottom of the vessel a) z component and b) x and y components for the case with FSR boundary conditions and 5 kg of explosive material.

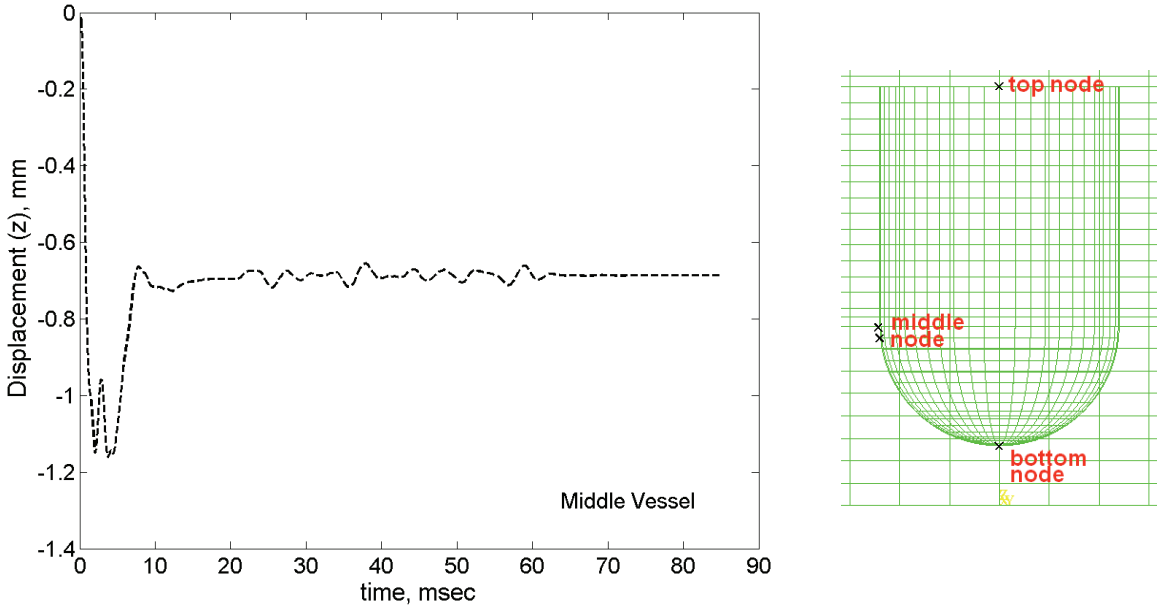

a)

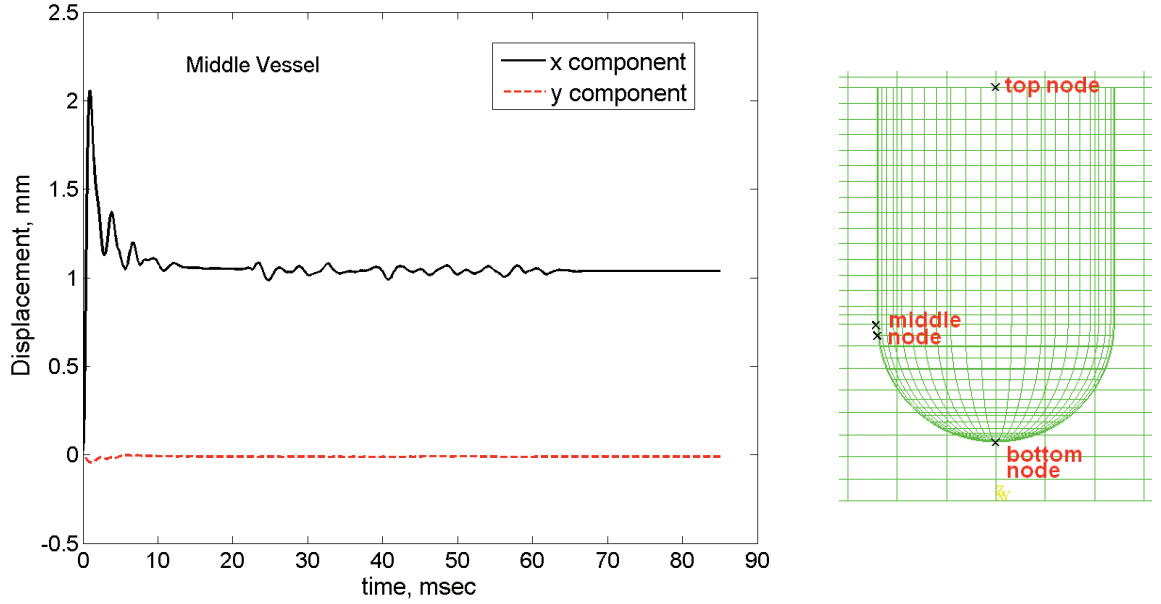

b)

Figure 36 Displacement at the middle of the vessel a) z component and b) x and y components for the case with FSR boundary conditions and 5 kg of explosive material.

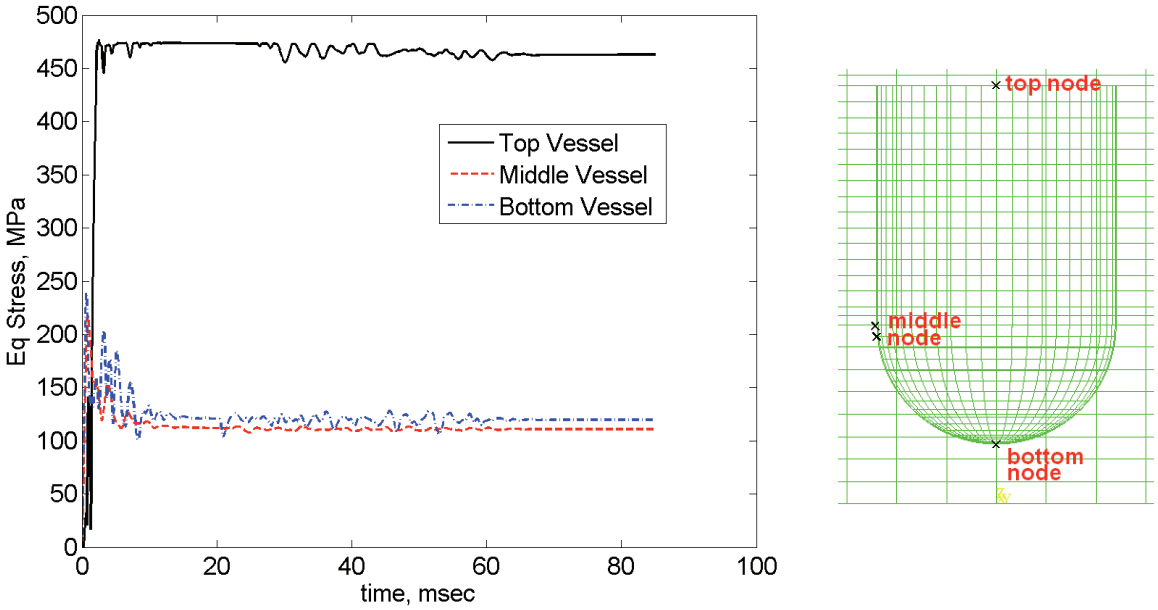

Figure 37 Equivalent stress at the top, bottom and middle of the vessel for the case with FSR boundary conditions and 5 kg of explosive material.

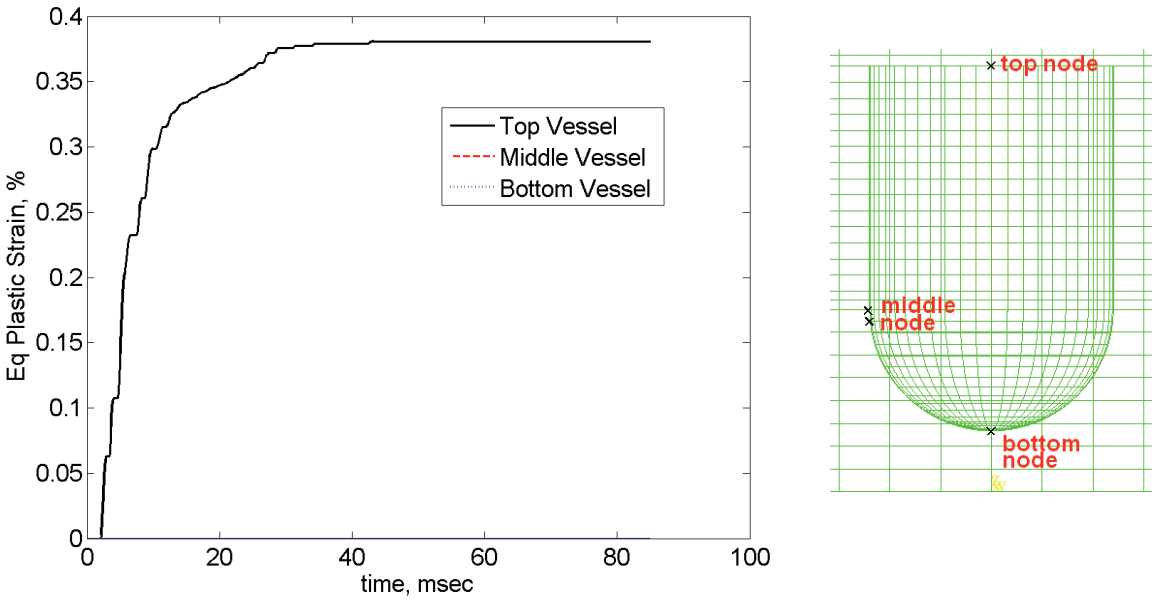

Figure 38 Equivalent plastic strain at the top, bottom and middle of the vessel for the case with FSR boundary conditions and 5 kg of explosive material.

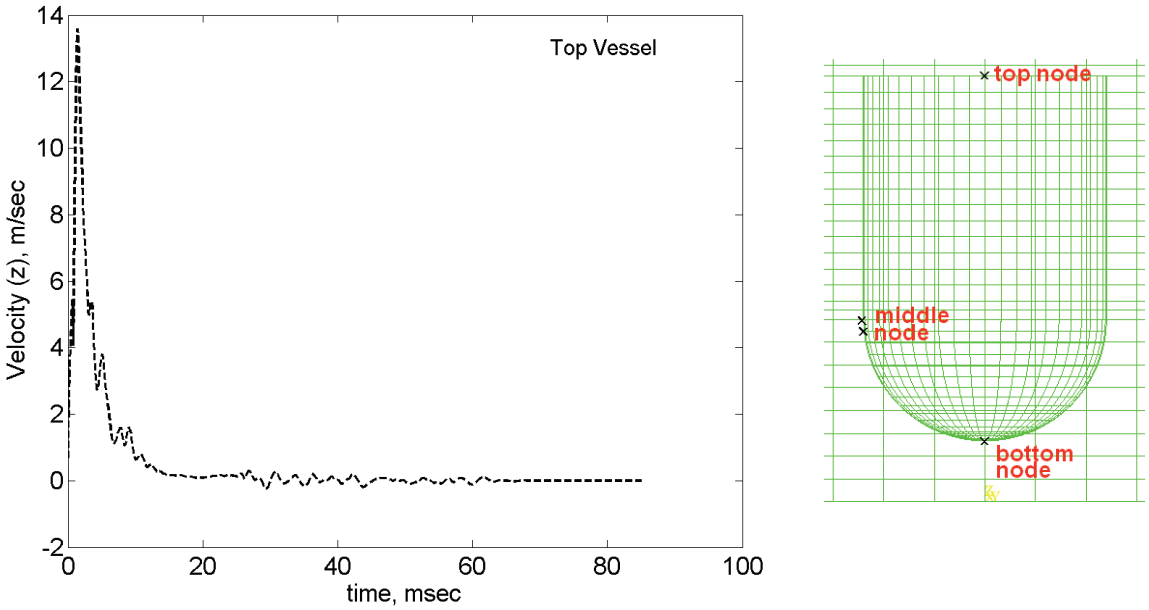

a)

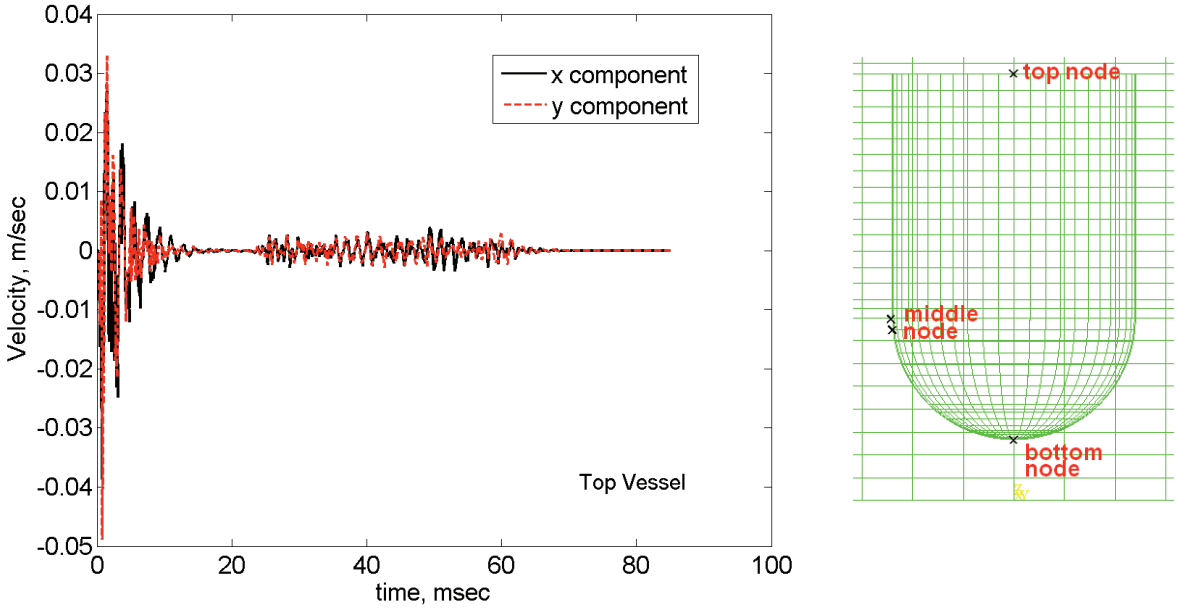

b)

Figure 39 Velocity at the top of the vessel a) z component and b) x and y components for the case with FSR boundary conditions and 5 kg of explosive material.

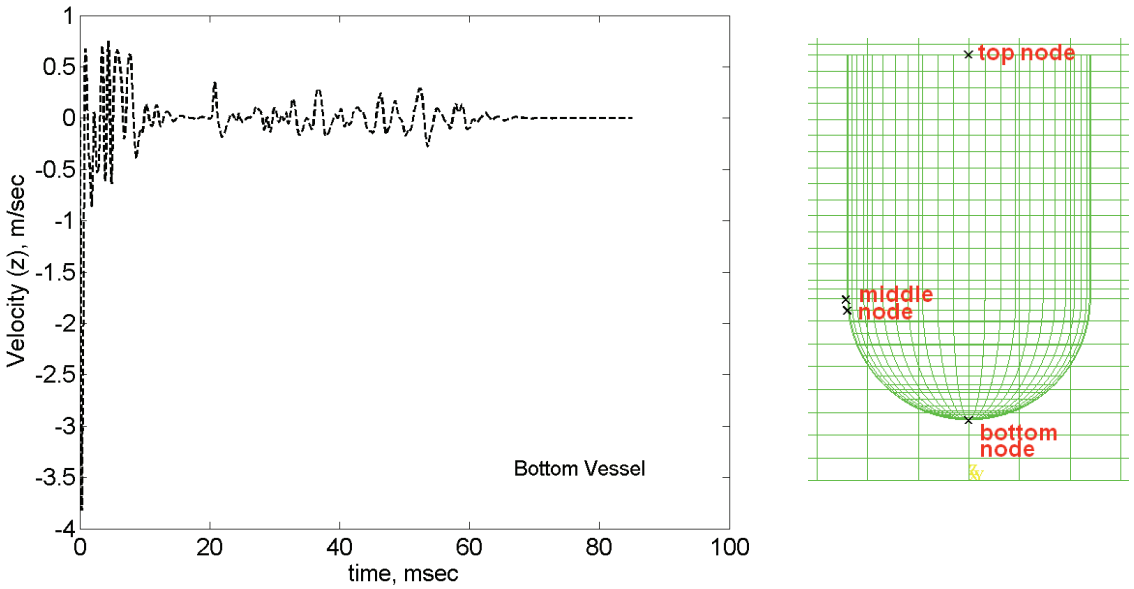

a)

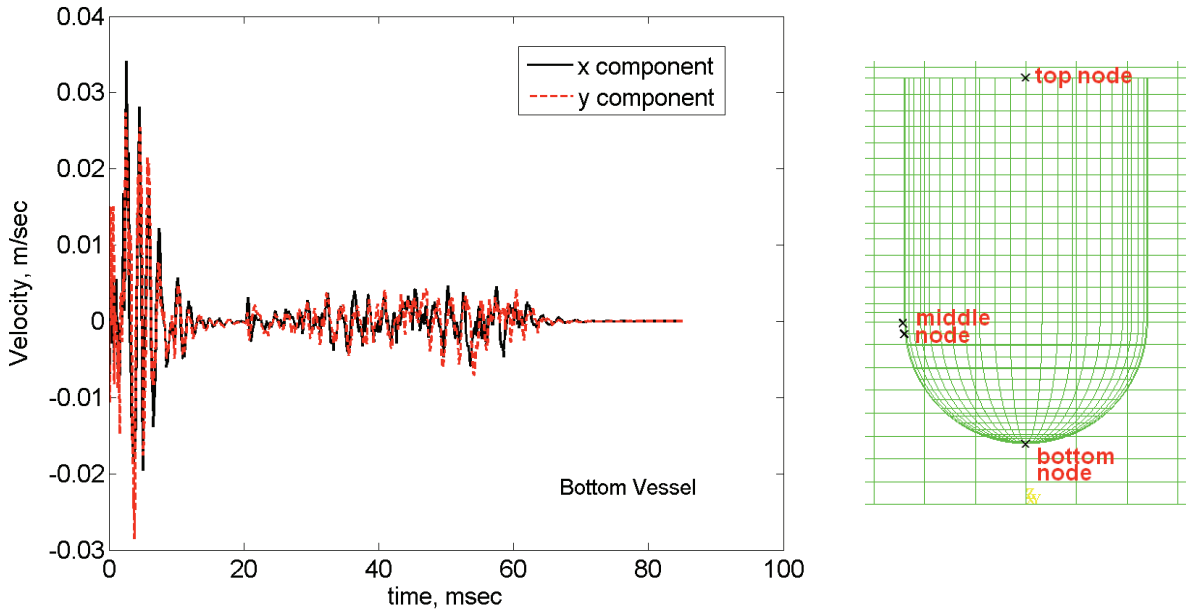

b)

Figure 40 Velocity at the bottom of the vessel a) z component and b) x and y components for the case with FSR boundary conditions and 5 kg of explosive material.

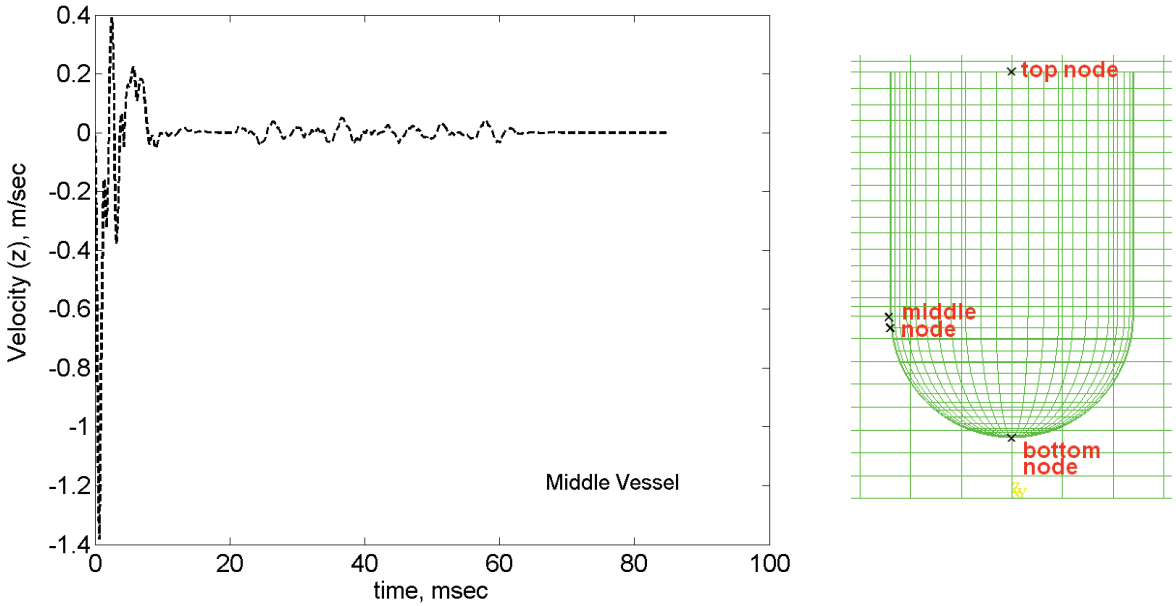

a)

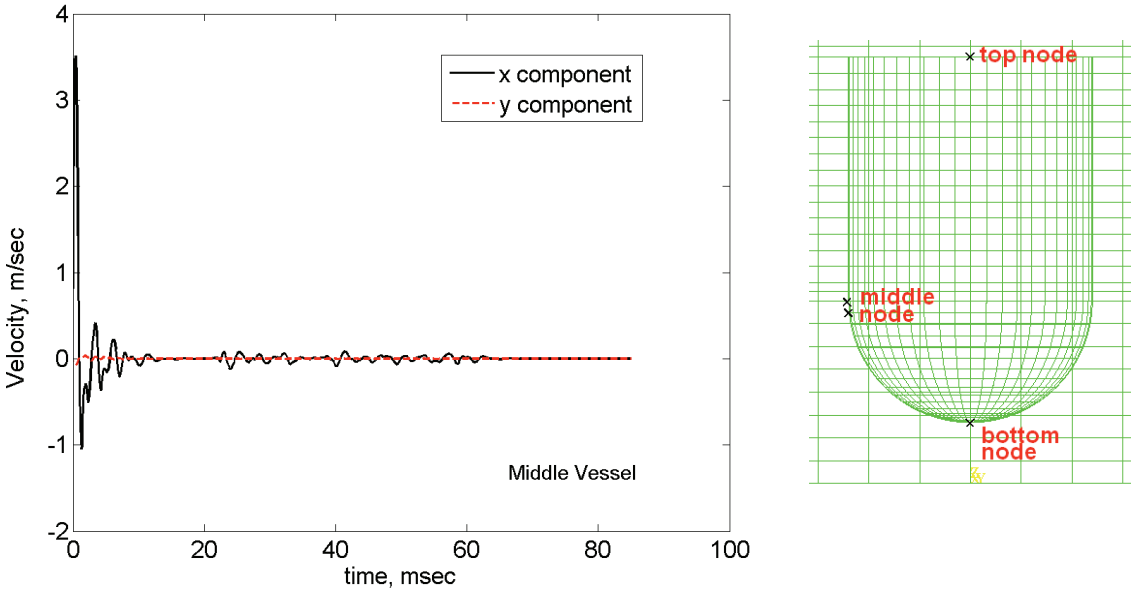

b)

Figure 41 Velocity at the middle of the vessel a) z component and b) x and y components for the case with FSR boundary conditions and 5 kg of explosive material.

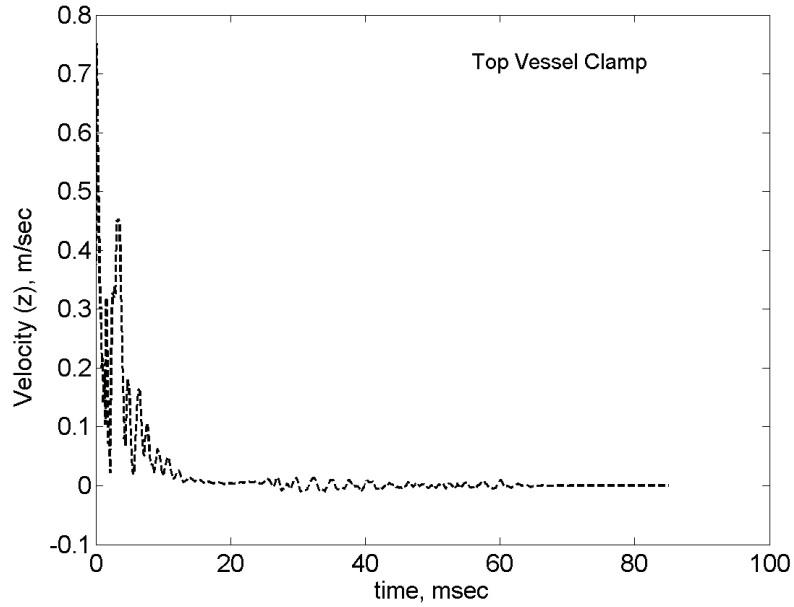

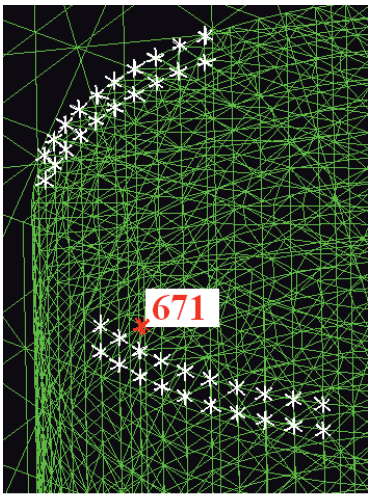

a)

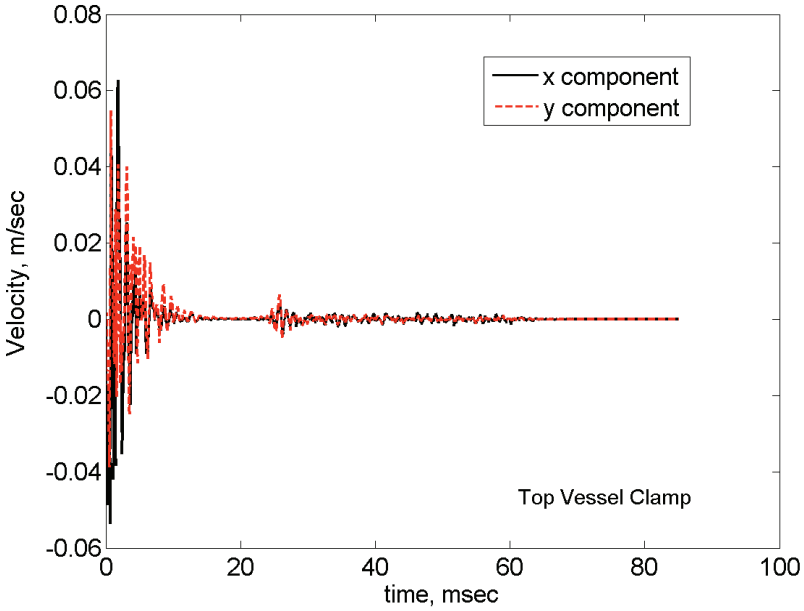

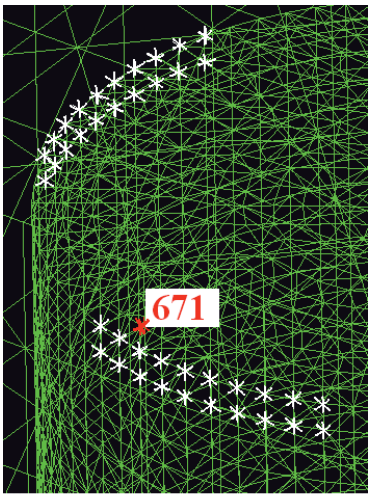

b)

Figure 42 Velocity in a node placed at the top of the vessel near the clamped zone (N671) a) z component and b) x and y components for the case with FSR boundary conditions and 5 kg of explosive material.

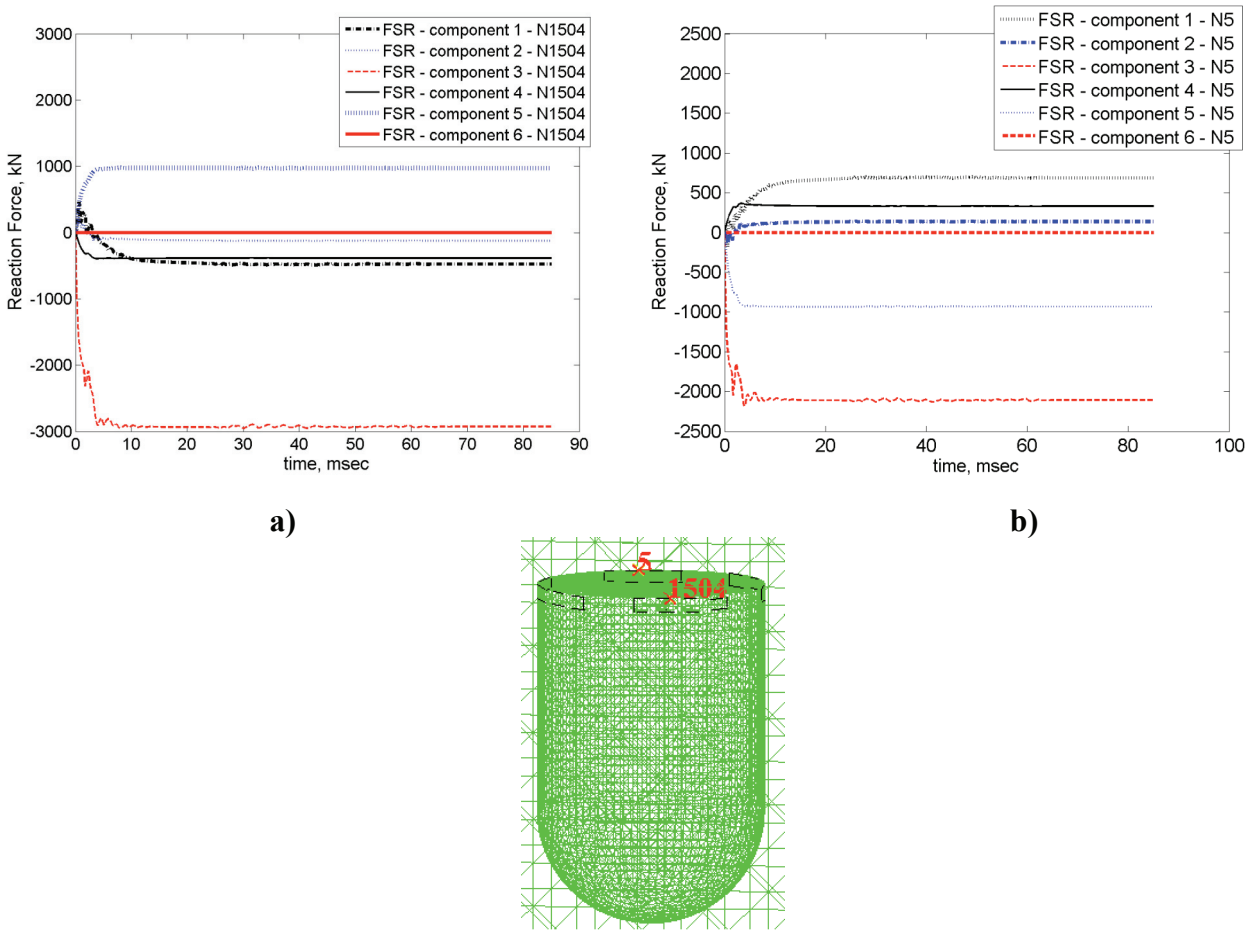

Figure 43 Reaction force components a) and b) at two different locations in the clamped zone as shown in c) .

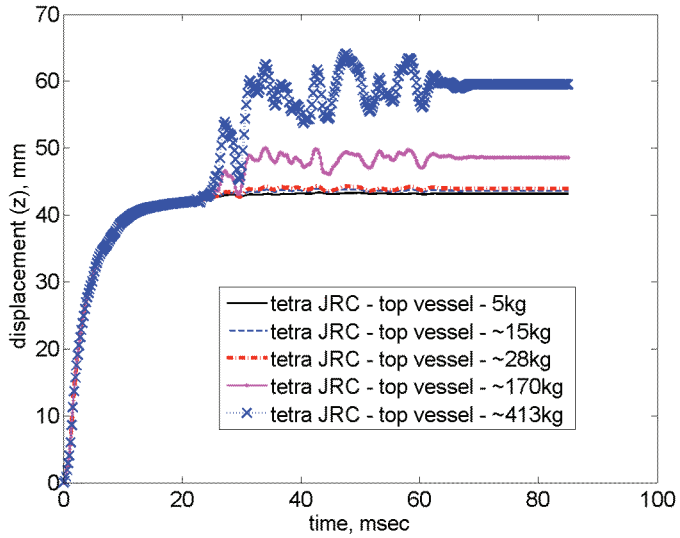

Figure 44 Displacement at the top of the vessel (z component) for the case with FSR boundary conditions and different amount of explosive material. Vessel with water.

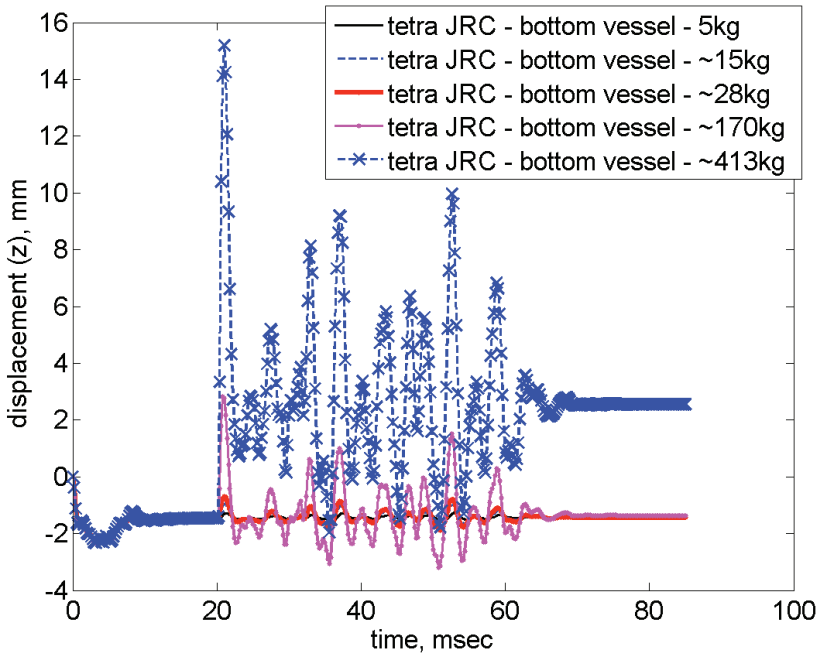

Figure 45 Displacement at the bottom of the vessel (z component) for the case with FSR boundary conditions and different amount of explosive material. Vessel with water.

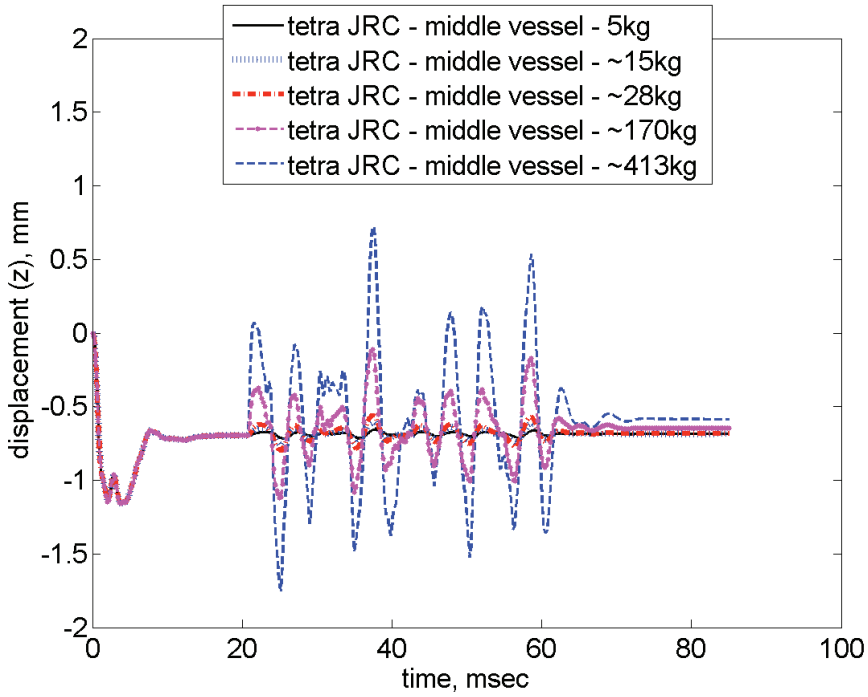

Figure 46 Displacement at the middle of the vessel (z component) for the case with FSR boundary conditions and different amount of explosive material. Vessel with water.

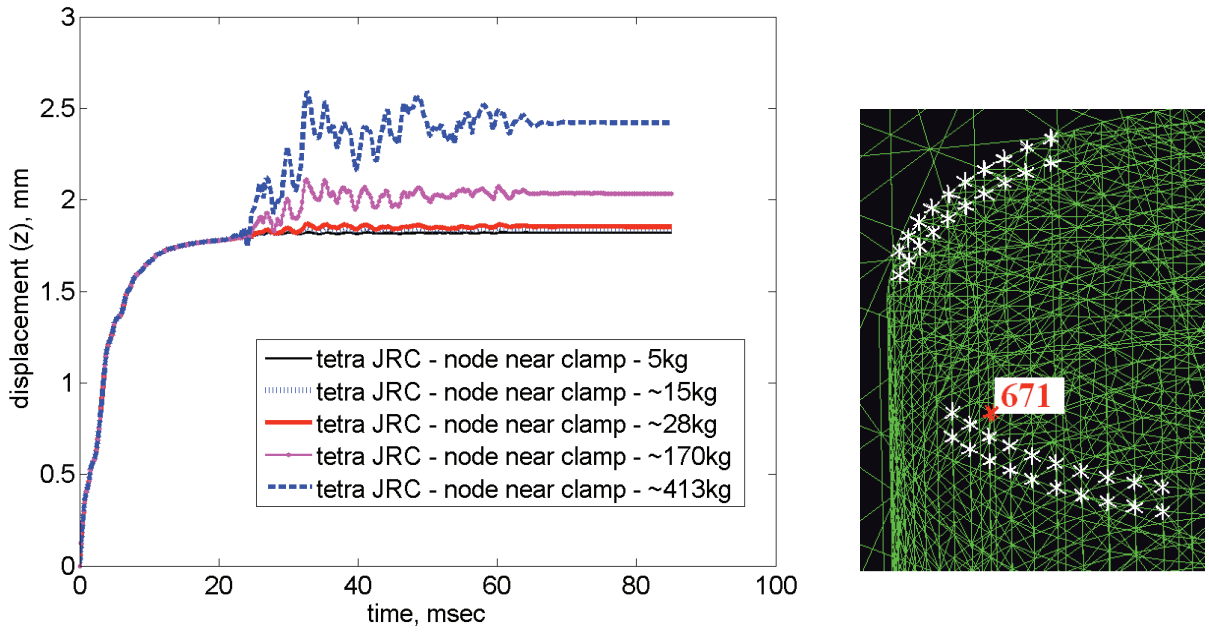

Figure 47 Displacement of a node placed at the top of the vessel near the clamped zone (z component) for the case with FSR boundary conditions and different amount of explosive material. Vessel with water.

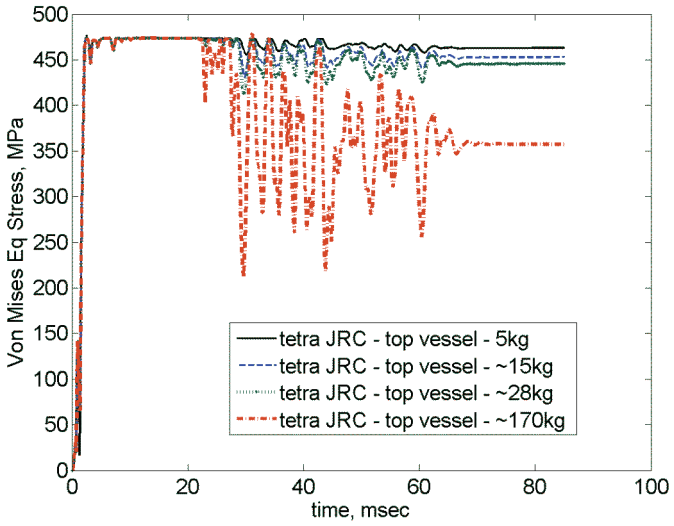

a)

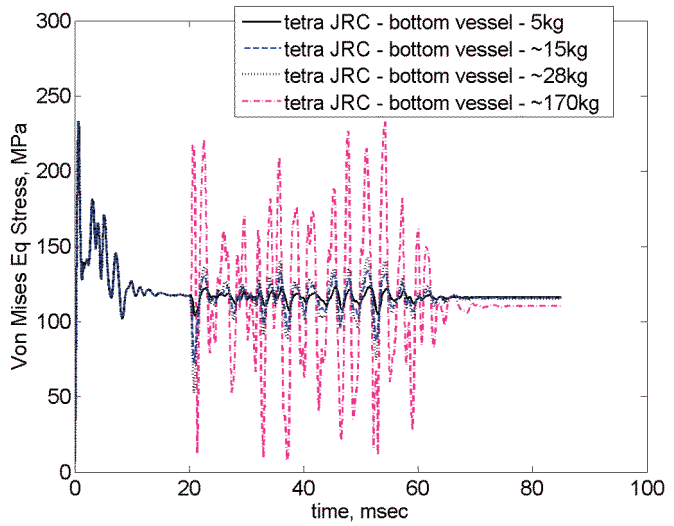

b)

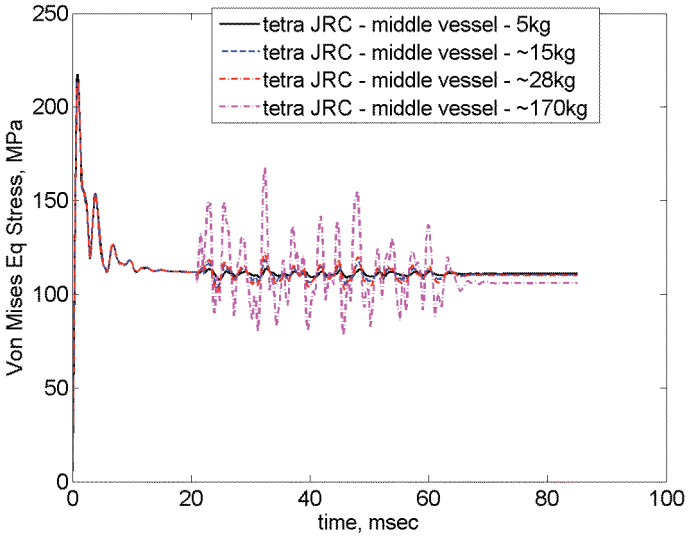

c)

Figure 48 Equivalent stress at the a) top, b) bottom and c) middle of the vessel for the case with FSR boundary conditions and different amount of explosive material. Vessel with water.

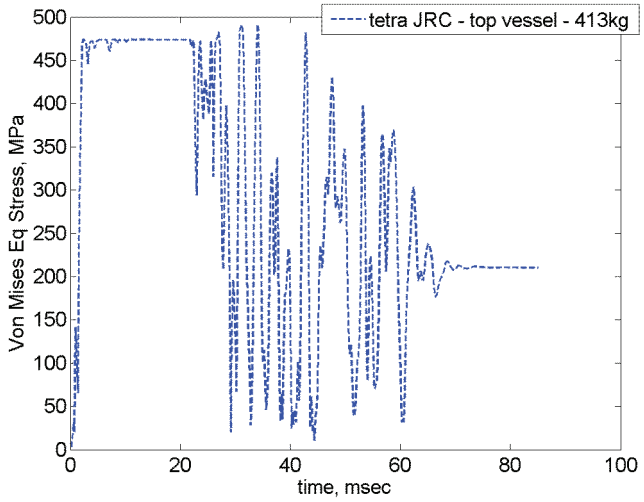

a)

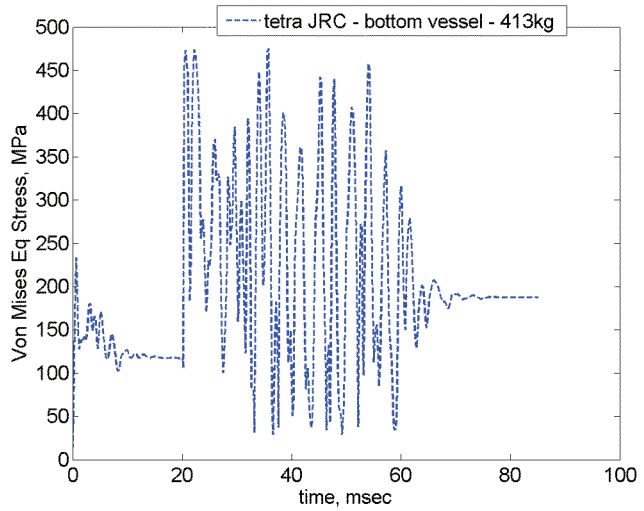

b)

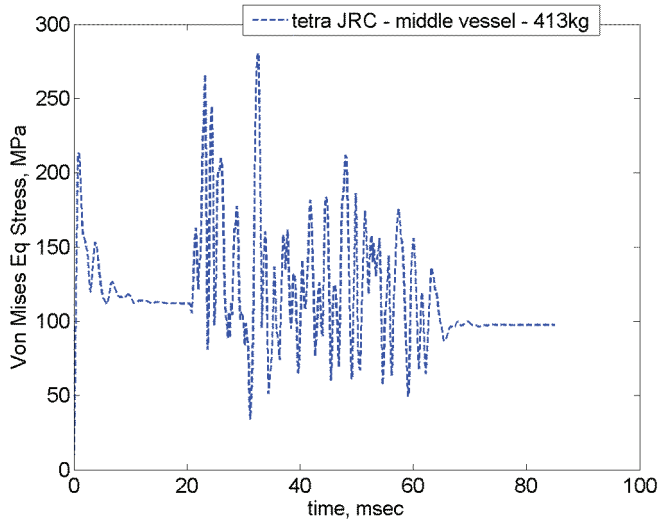

c)

Figure 49 Equivalent stress at the a) top, b) bottom and c) middle of the vessel for the case with FSR boundary conditions and 413kg of explosive material. Vessel with water.

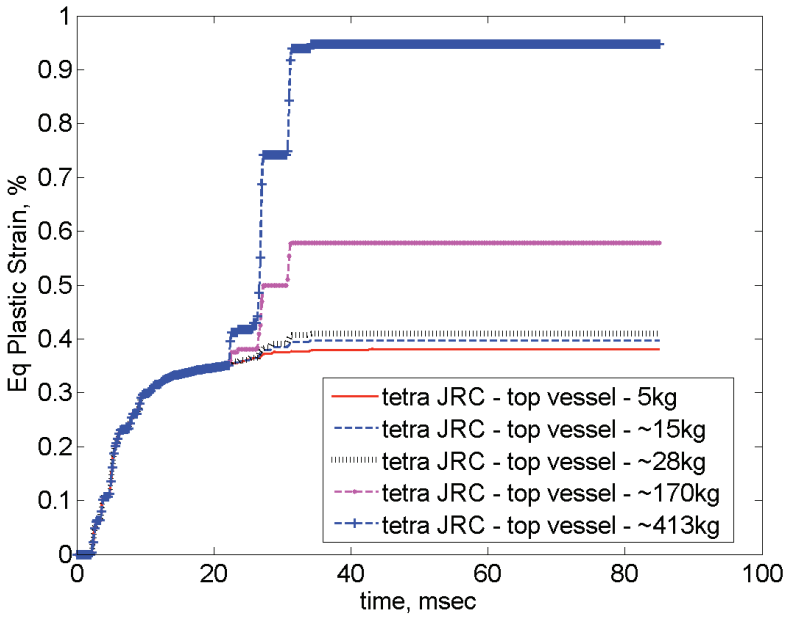

a)

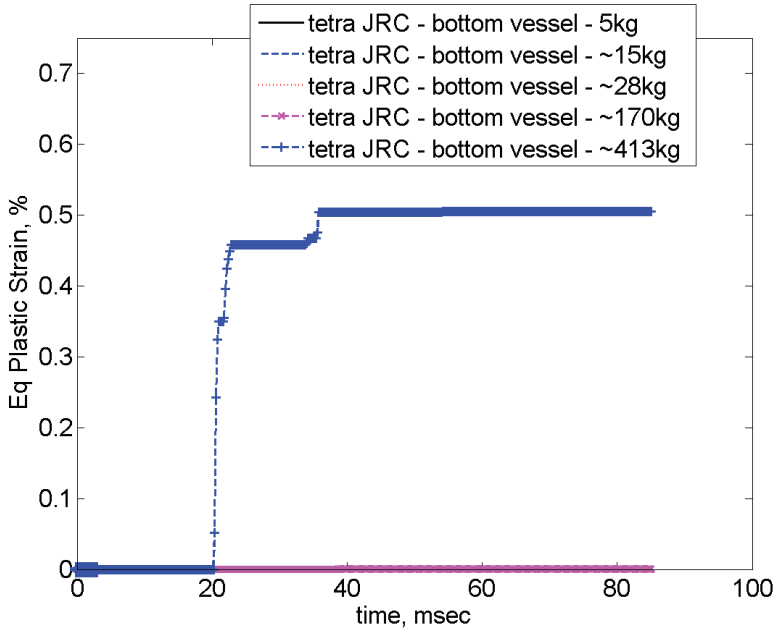

b)

Figure 50 Equivalent plastic strain for different amount of explosive charge a) at the top of the vessel and b) at the bottom of the vessel. Vessel with water.

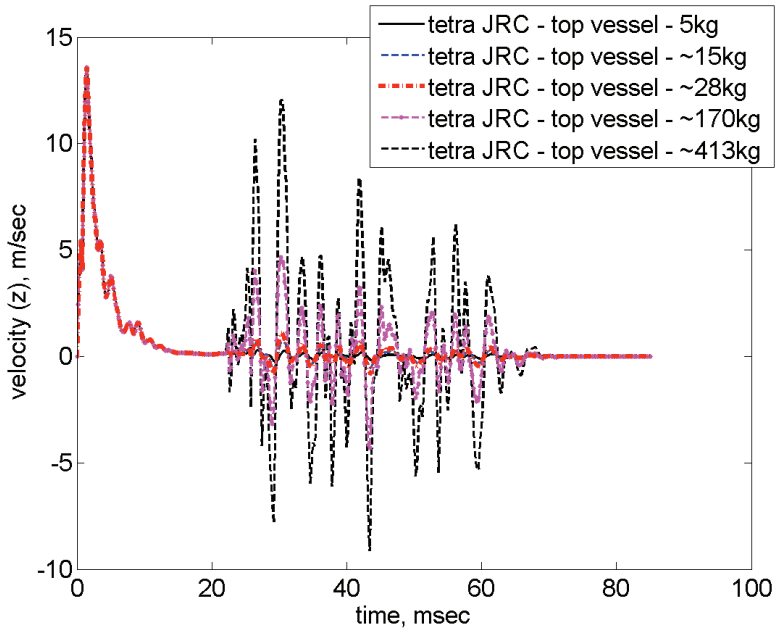

Figure 51 Velocity at the top of the vessel (z component) for the case with FSR boundary conditions and different amount of explosive material. Vessel with water.

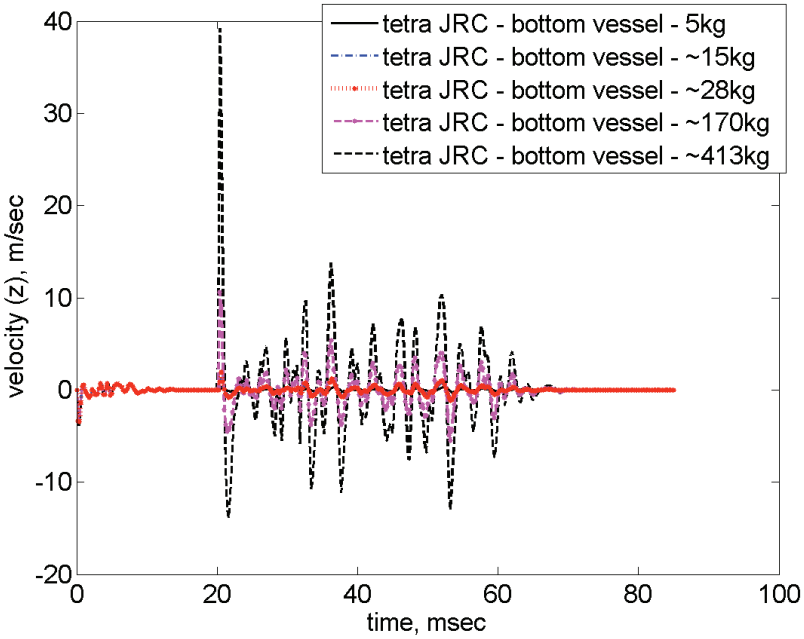

Figure 52 Velocity at the bottom of the vessel (z component) for the case with FSR boundary conditions and different amount of explosive material. Vessel with water.

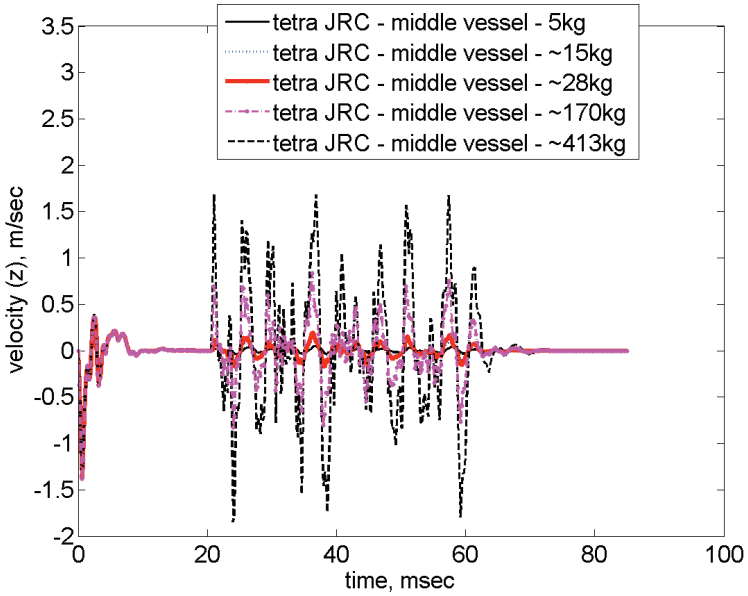

Figure 53 Velocity at the middle of the vessel (z component) for the case with FSR boundary conditions and different amount of explosive material. Vessel with water.

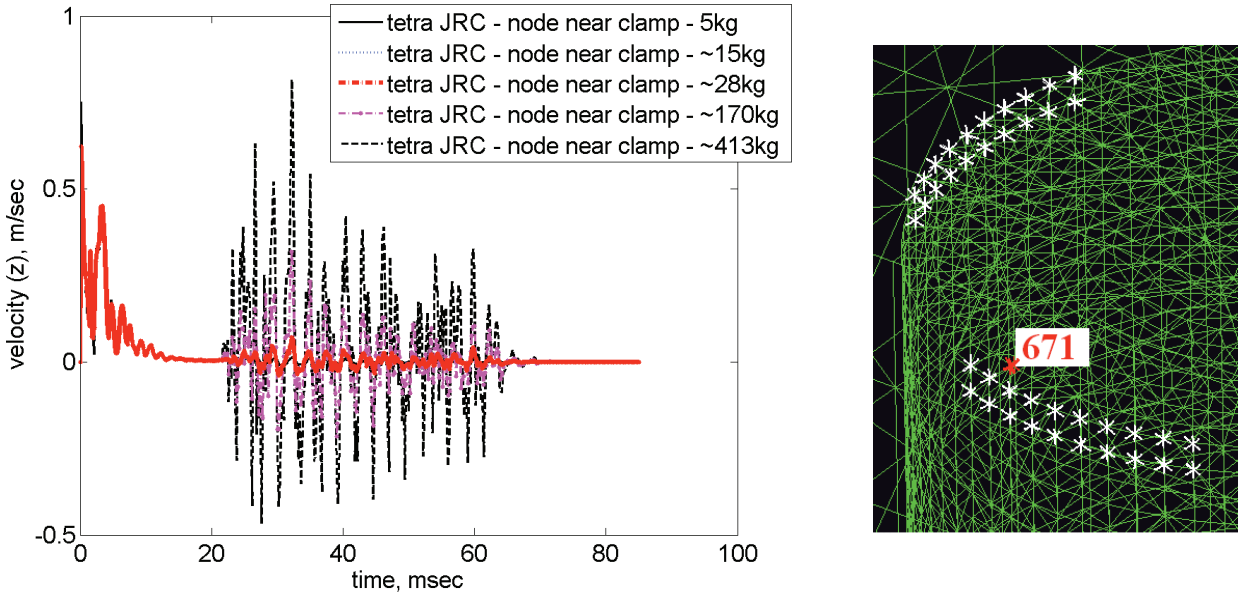

Figure 54 Velocity in a node placed at the top of the vessel near the clamped zone (z component) for the case with FSR boundary conditions and different amount of explosive material. Vessel with water.

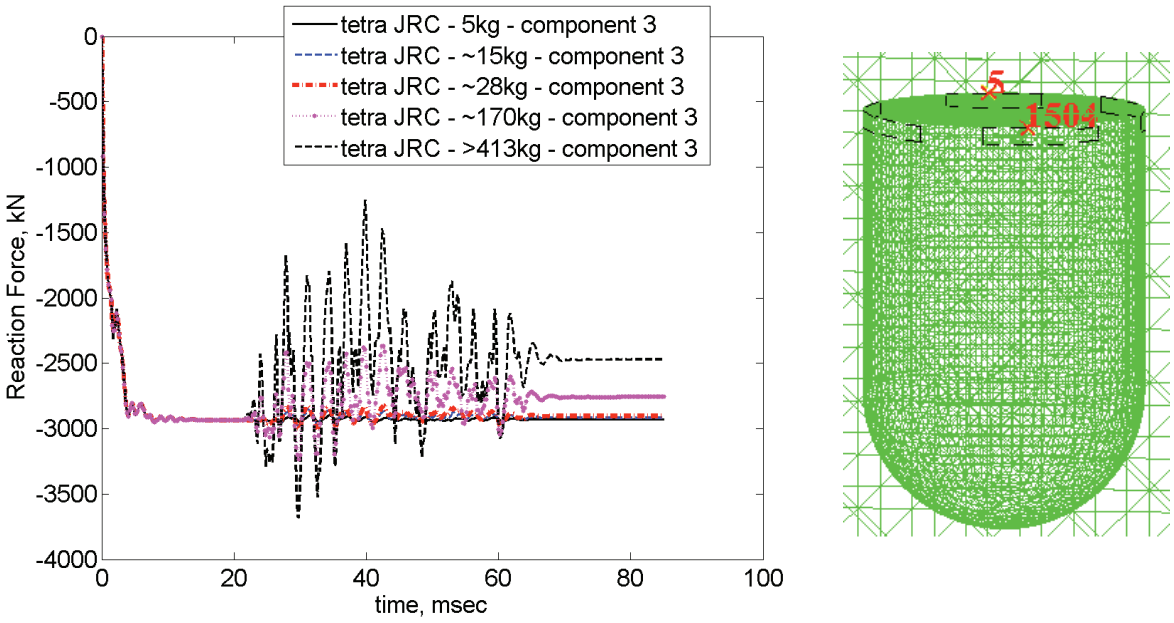

Figure 55 Reaction force in the z direction at a location of the clamped zone (node 1504) for the case with FSR boundary conditions and a) different amount of explosive material and b) 413kg. Vessel with water.

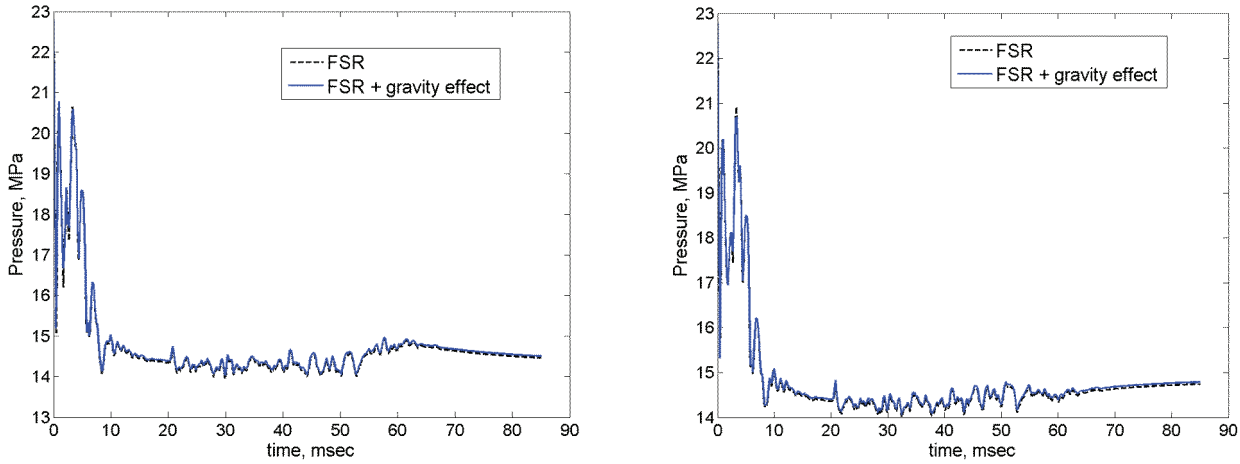

Figure 56 Pressure in the water for the cases with and without gravity effect, FSR boundary conditions and 5kg of explosive material.

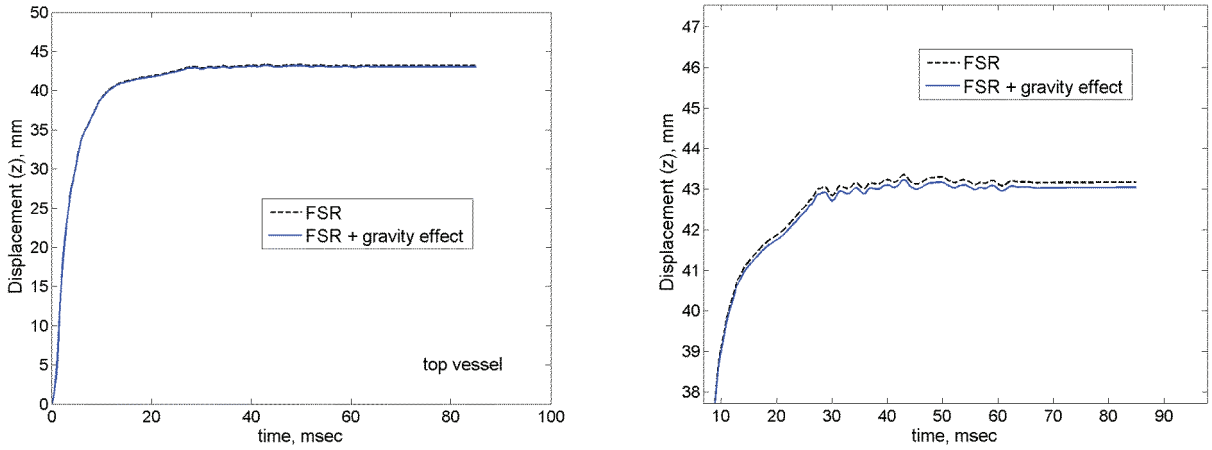

a) b)

Figure 57 a) Displacement at the top of the vessel z component and b) enlargement for the cases with and without gravity effect, FSR boundary conditions and 5 kg of explosive material.

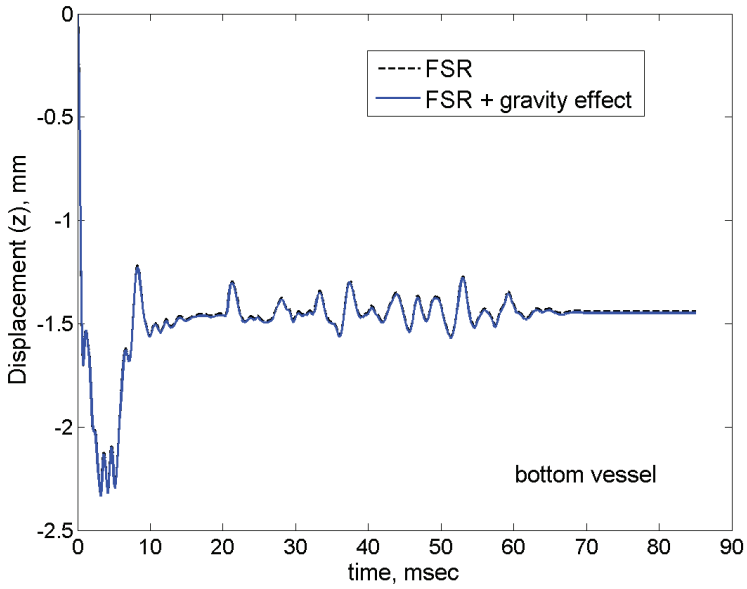

Figure 58 a) Displacement at the bottom of the vessel z component for the cases with and without gravity effect, FSR boundary conditions and 5 kg of explosive material.

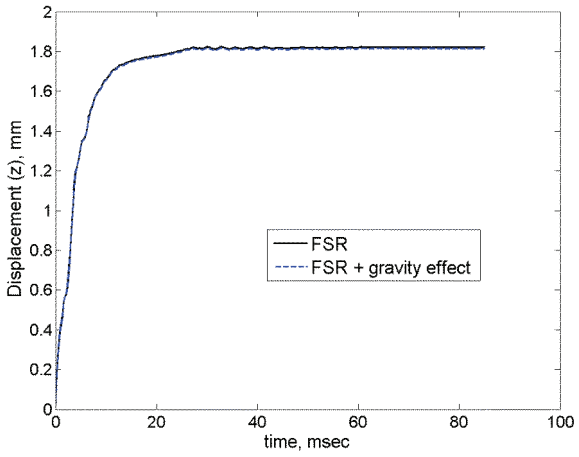

a)

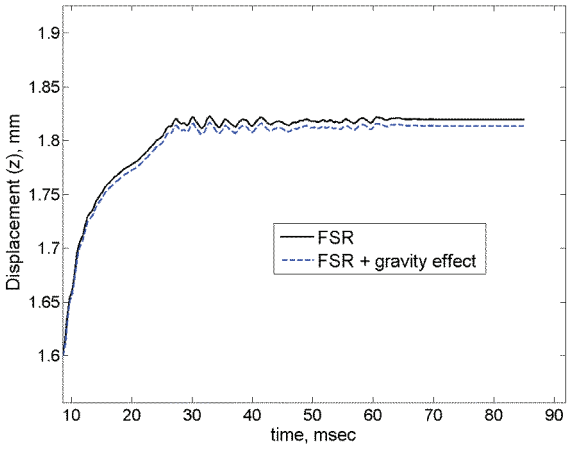

b)

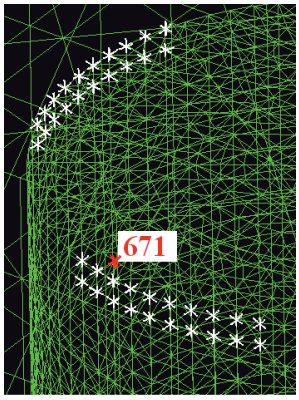

c)

Figure 59 a) Displacement of a node placed at the top of the vessel near the clamped zone in the z direction for the cases with and without gravity effect, FSR boundary conditions and 5 kg of explosive material and b) enlargement.

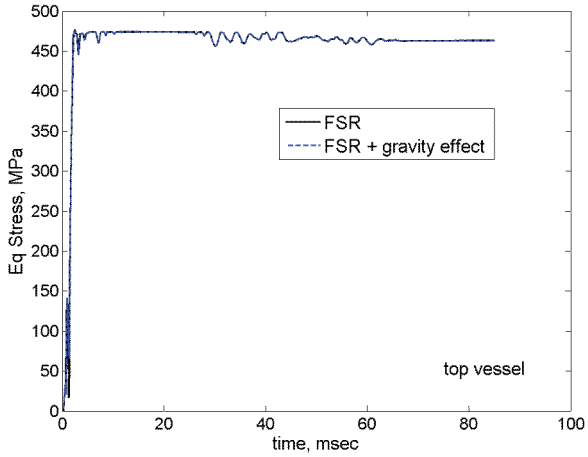

a)

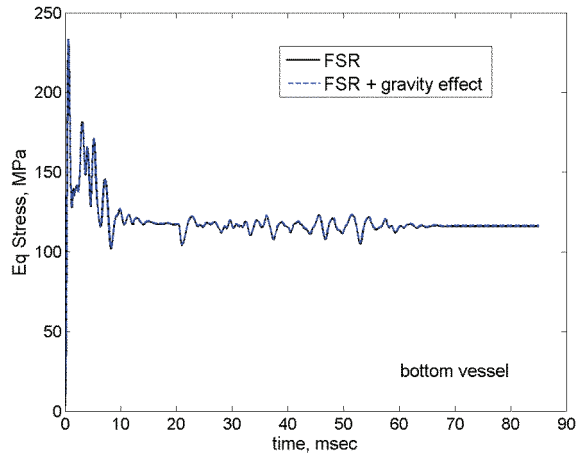

b)

Figure 60 Equivalent stress at the top a) and bottom b) of the vessel for the cases with and without gravity effect, FSR boundary conditions and 5 kg of explosive material

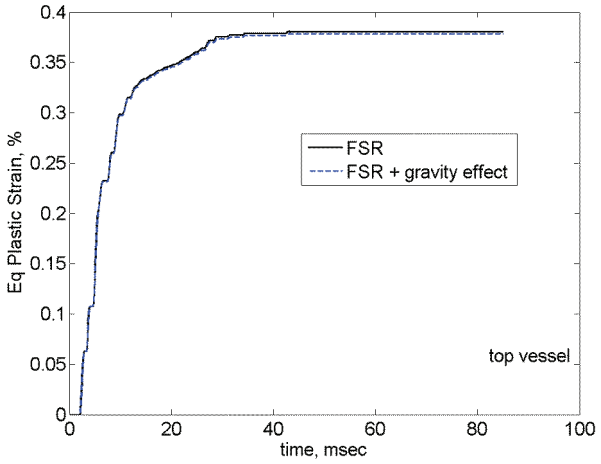

a)

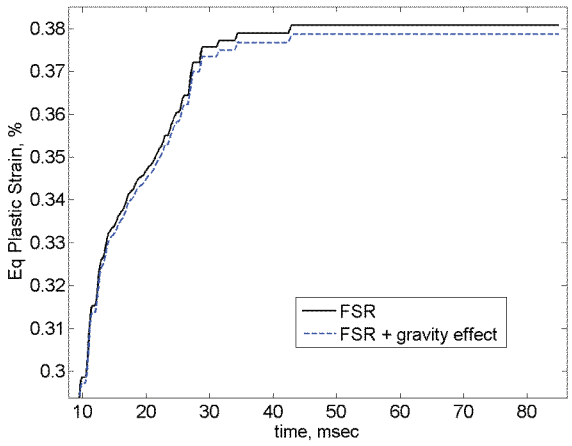

b)

Figure 61 Equivalent plastic strain at the top of the vessel a) and its enlargement b) for the cases with and without gravity effect, FSR boundary conditions and 5 kg of explosive material.

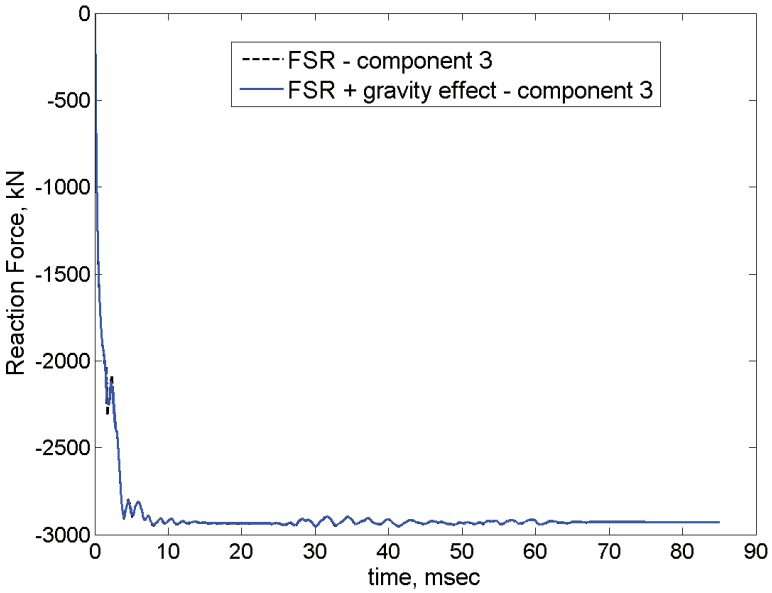

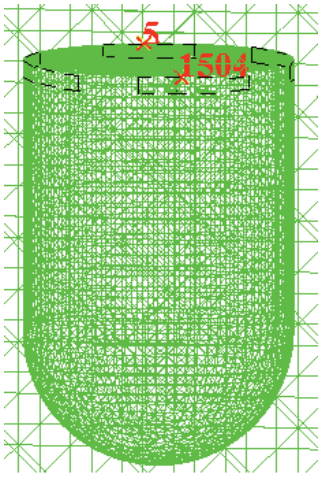

Figure 62 Reaction force components at a location in the clamped zone (N 1504) for the cases with and without gravity effect, FSR boundary conditions and 5 kg of explosive material.

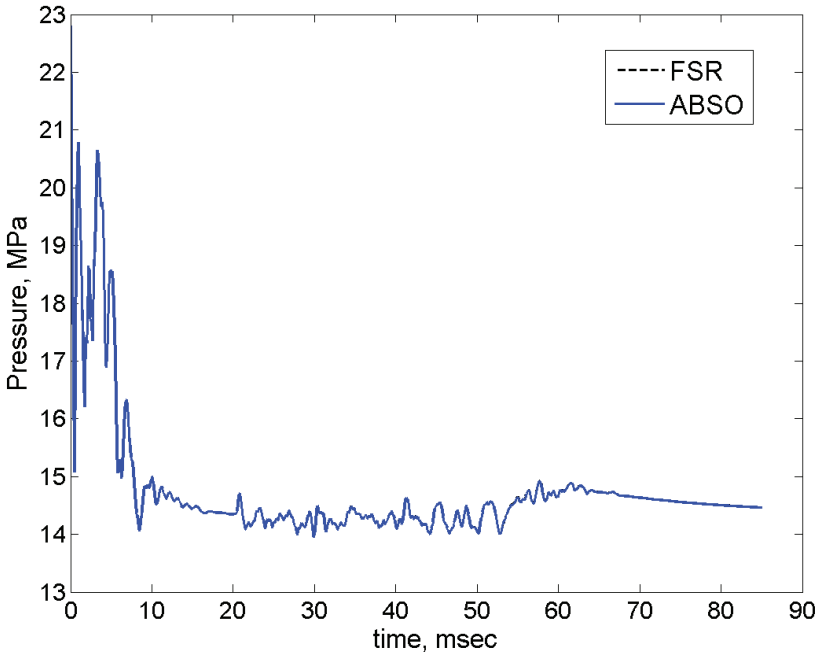

Figure 63 Pressure in the water for the case with FSR and ABSO boundary conditions and 5kg of explosive material.

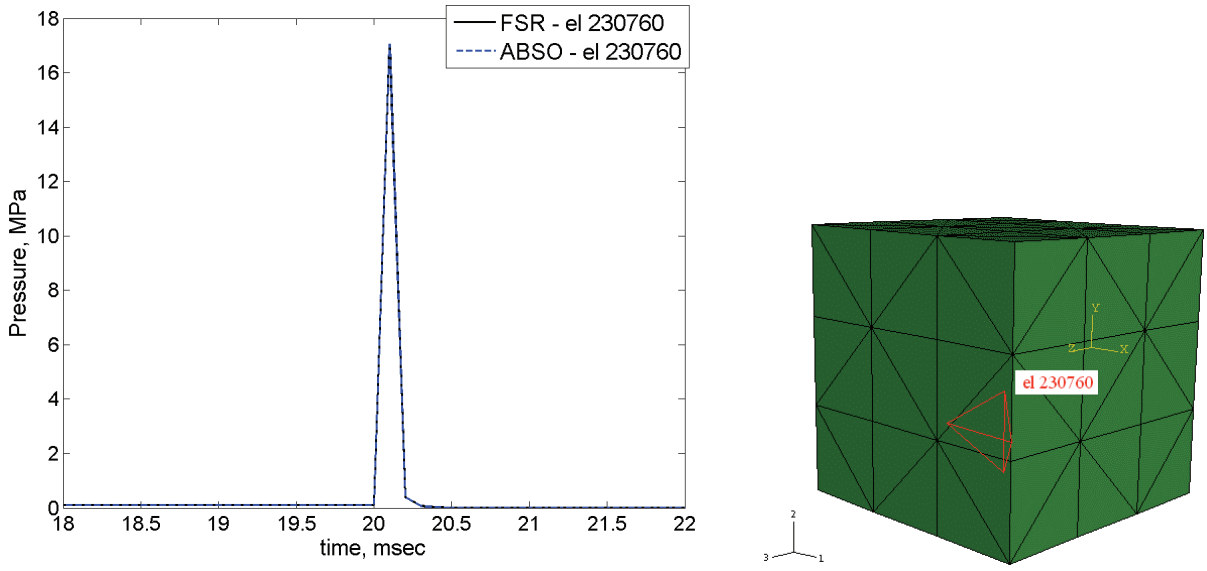

a) **b)**

Figure 64 Pressure in an elements of explosive material a) for an interval of time around the detonation time for the case with FSR and ABSO boundary conditions and 5 kg of explosive material b).

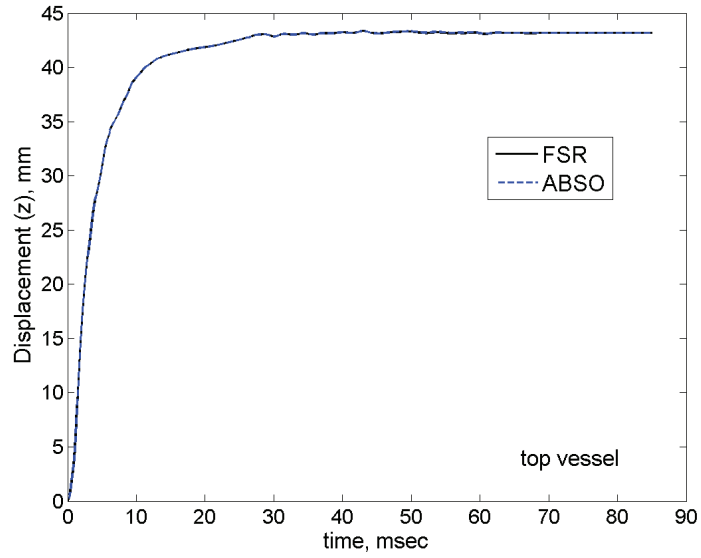

a)

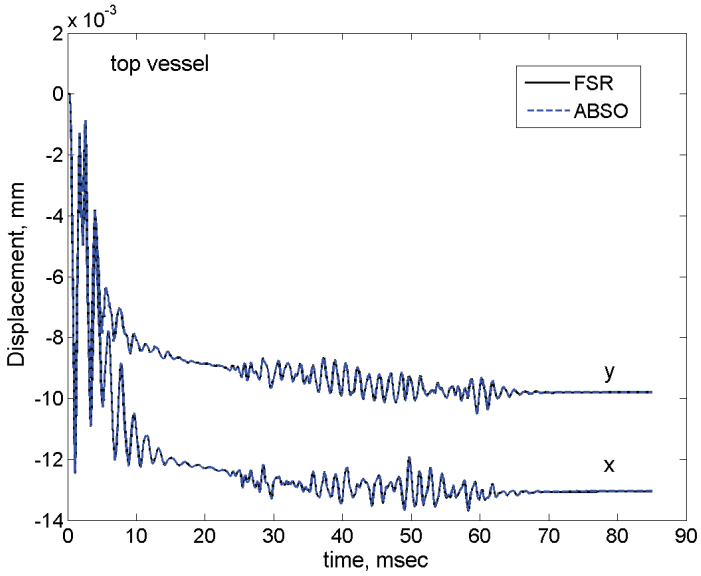

b)

Figure 65 Displacement at the top of the vessel a) z component and b) x and y components for the case with FSR and ABSO boundary conditions and 5 kg of explosive material.

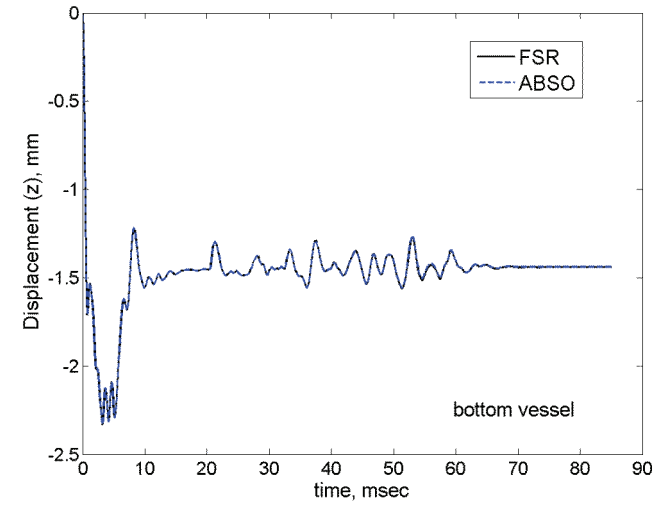

a)

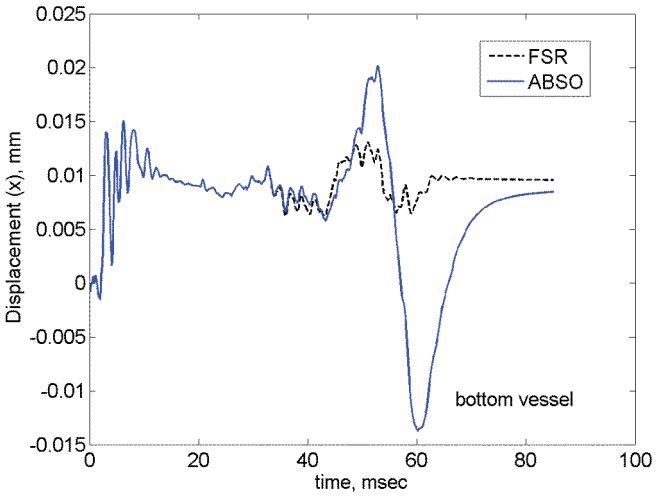

b)

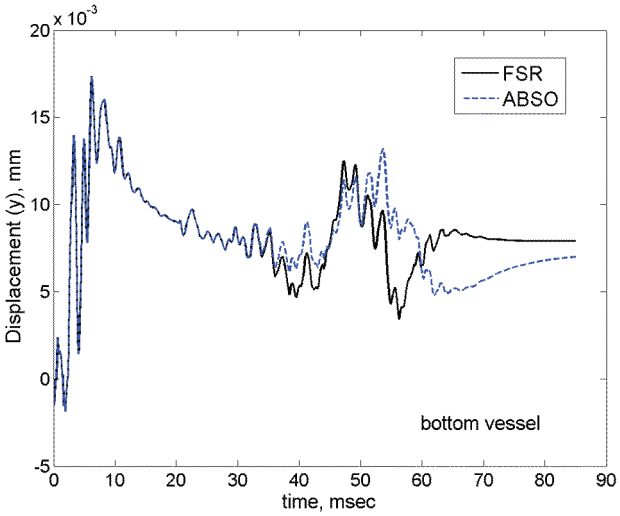

c)

Figure 66 Displacement at the bottom of the vessel a) z component and b) x and c) y components for the case with FSR and ABSO boundary conditions and 5 kg of explosive material.

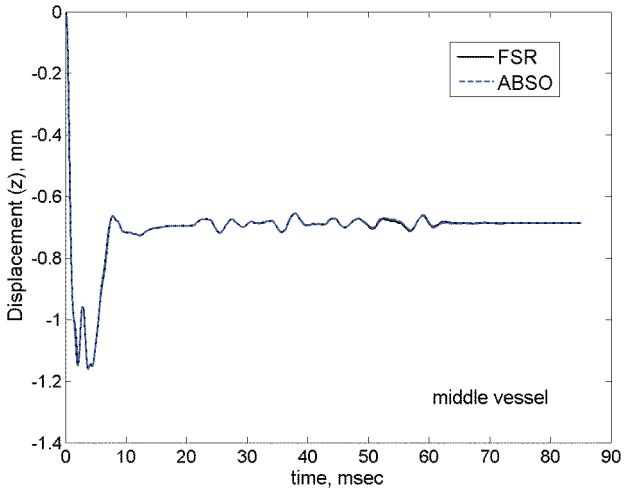

a)

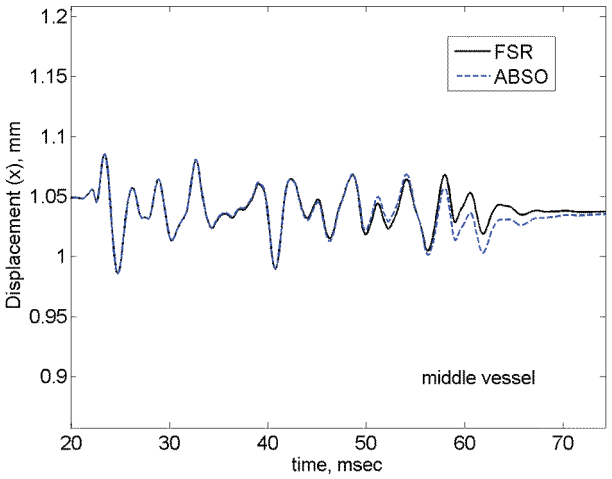

b)

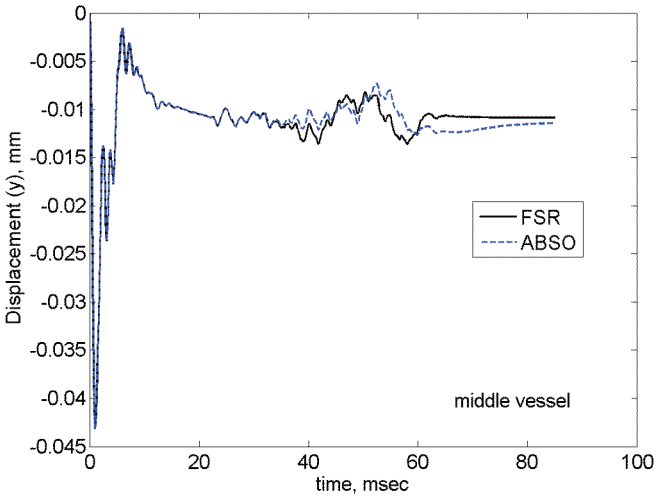

c)

Figure 67 Displacement at the middle of the vessel a) z component and b) x and c) y components for the case with FSR and ABSO boundary conditions and 5 kg of explosive material.

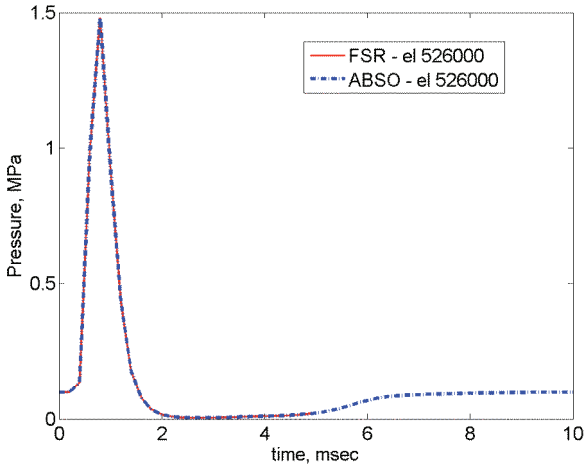

Figure 68 Pressure overpressure reaching the bottom of the vessel (1m distance from the explosive charge) for both the FSR and the ABSO boundary conditions and 5kg of explosive material.

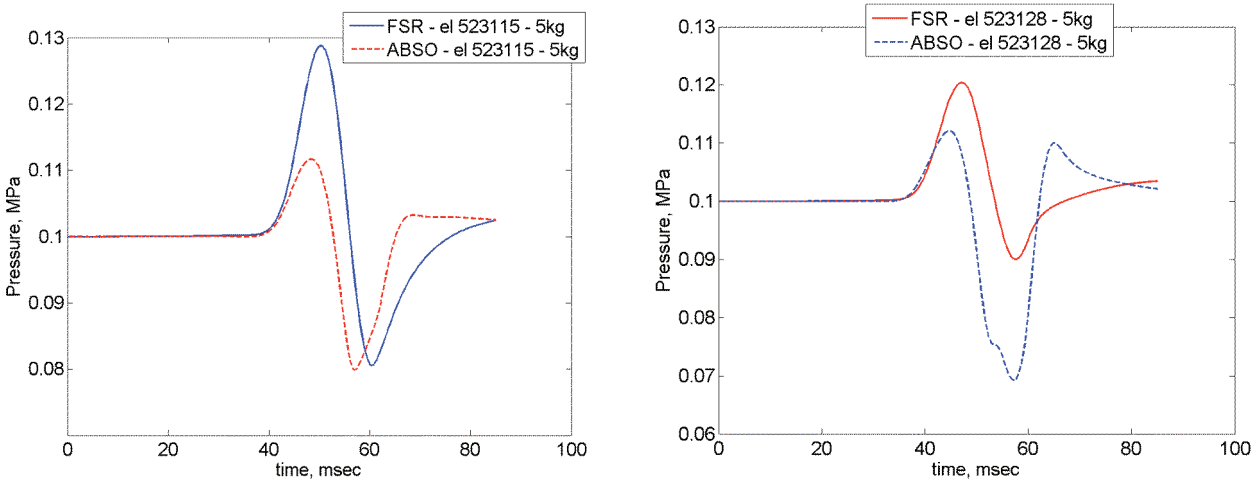

a) **b)**

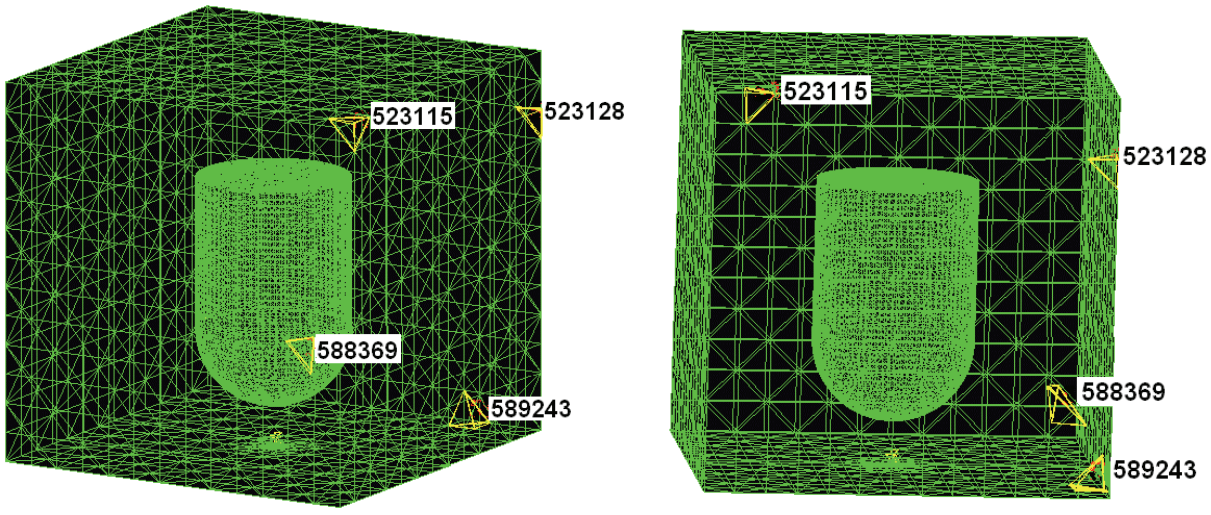

c)

Figure 69 Pressure at different location in the bunker: a) top of the bunker, b) top of the vessel level, as shown in c). FSR and ABSO boundary condition at the walls of the bunker and 5 kg of explosive material.

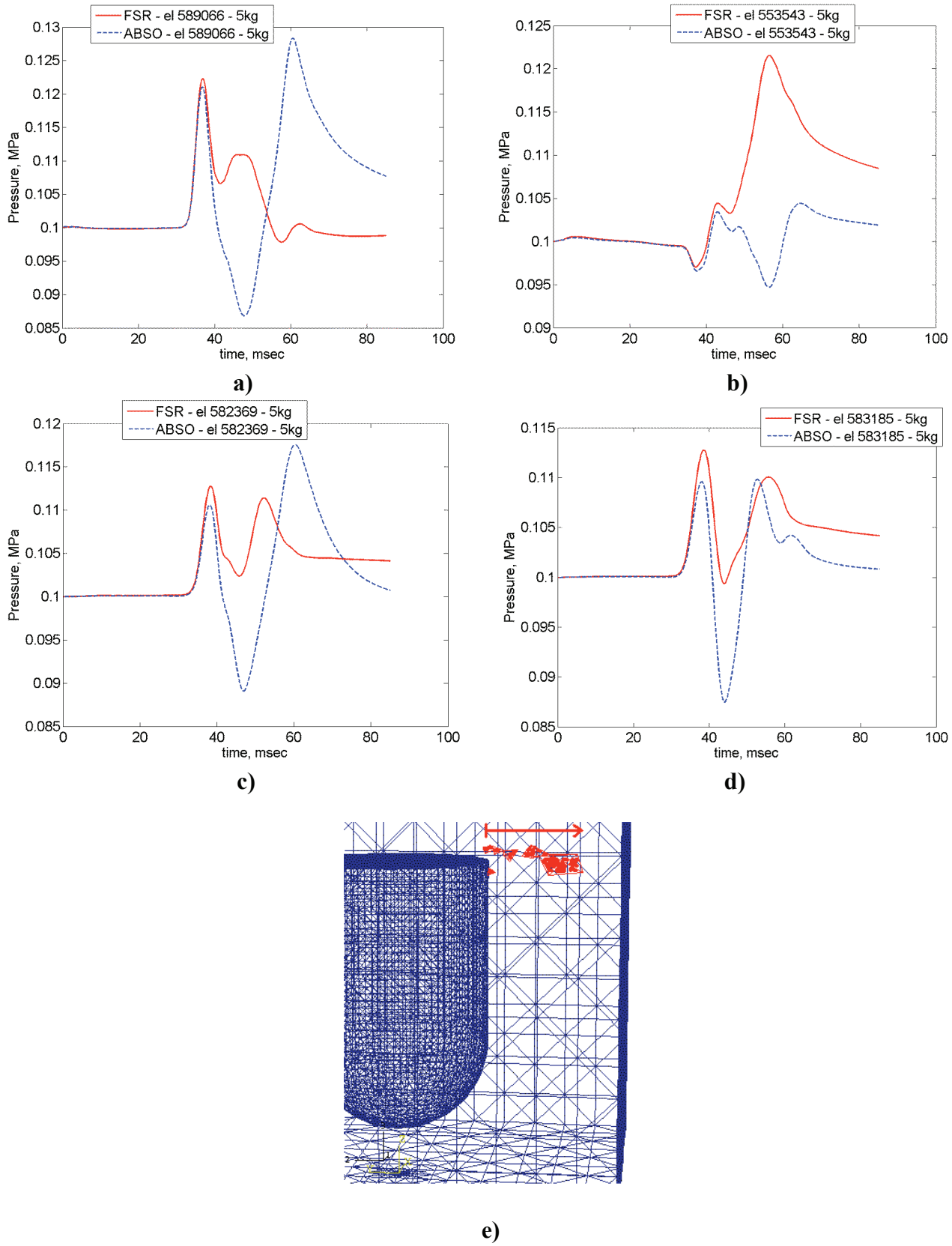

Figure 70 Pressure at different location in the bunker for 5 kg of explosive material as shown in e) (starting element 589066 near the vessel; element 583185 near the bunker wall).

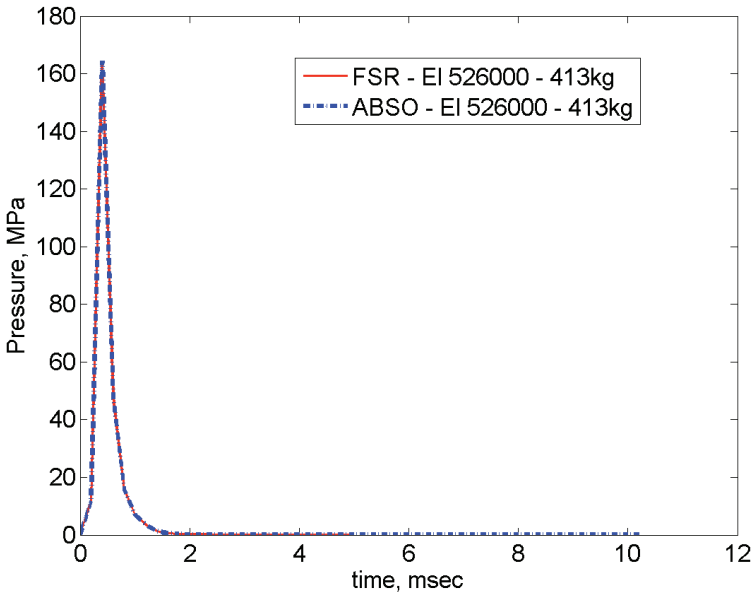

Figure 71 Pressure overpressure reaching the bottom of the vessel (1m distance from the explosive charge) for both the FSR and the ABSO boundary conditions and 413kg of explosive material.

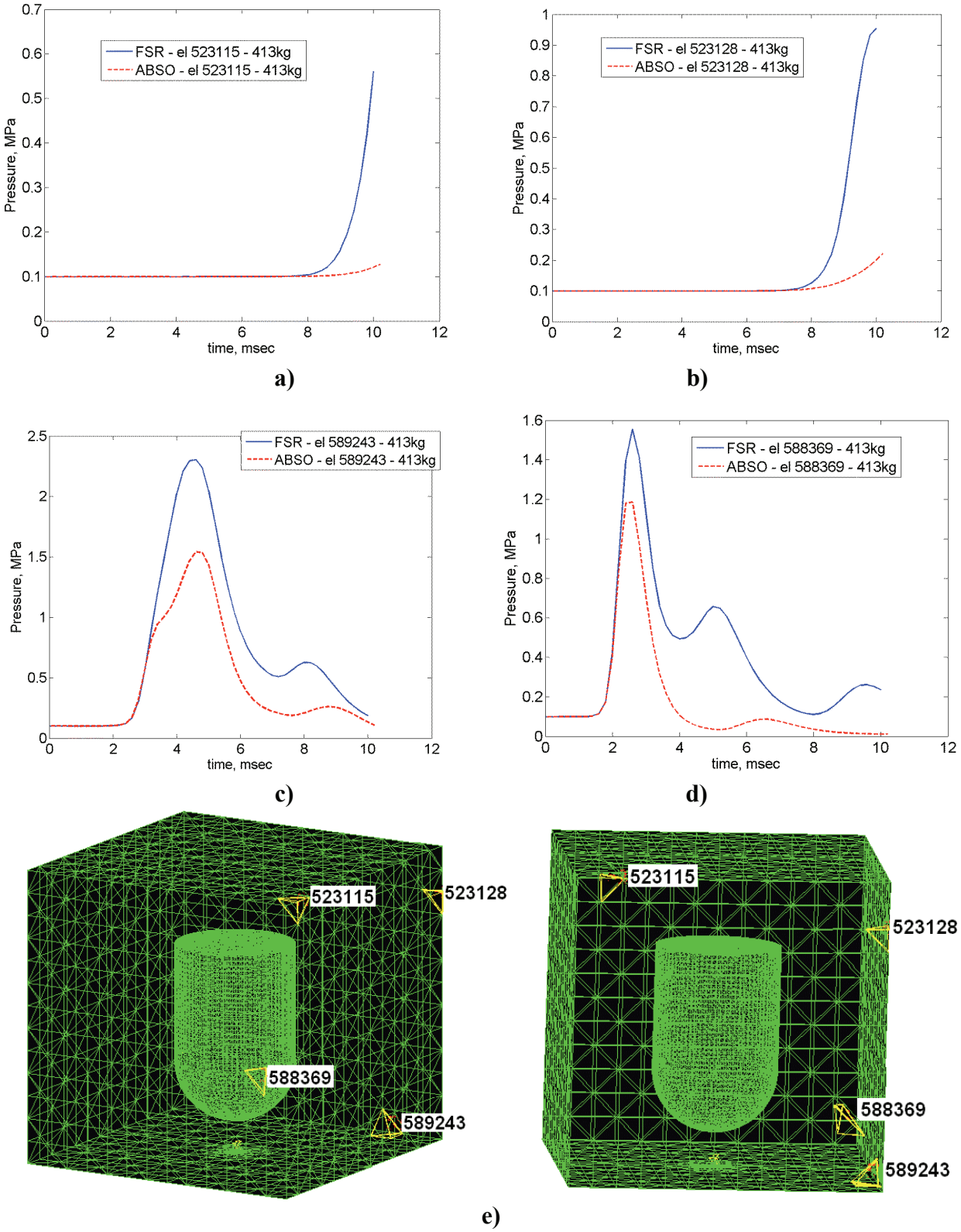

Figure 72 Pressure at different location in the bunker: a) top of the bunker, b) top of the vessel level, c) bottom of the bunker, d) bottom of the vessel level, as shown in e). FSR and ABSO boundary condition at the walls of the bunker and 413kg of explosive material.

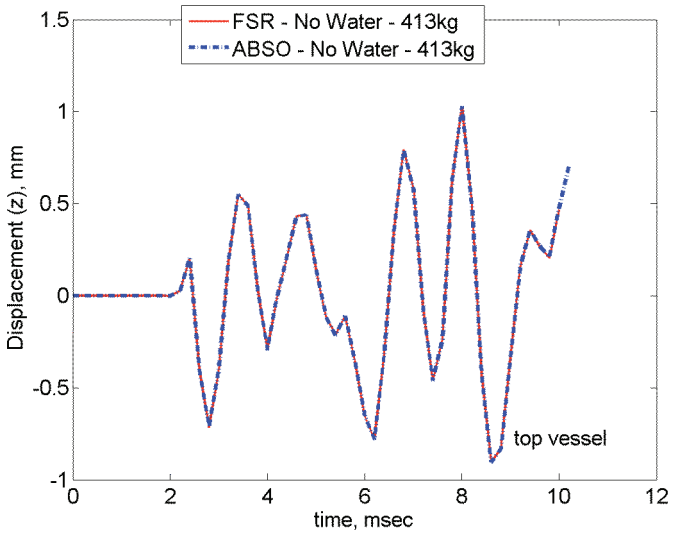

a)

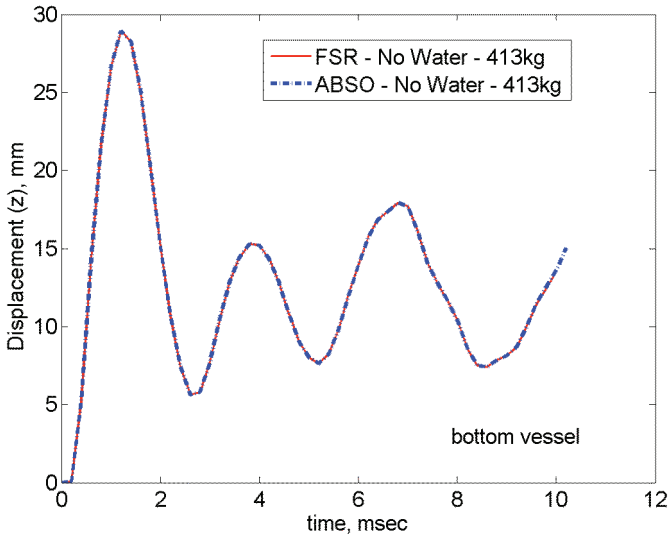

b)

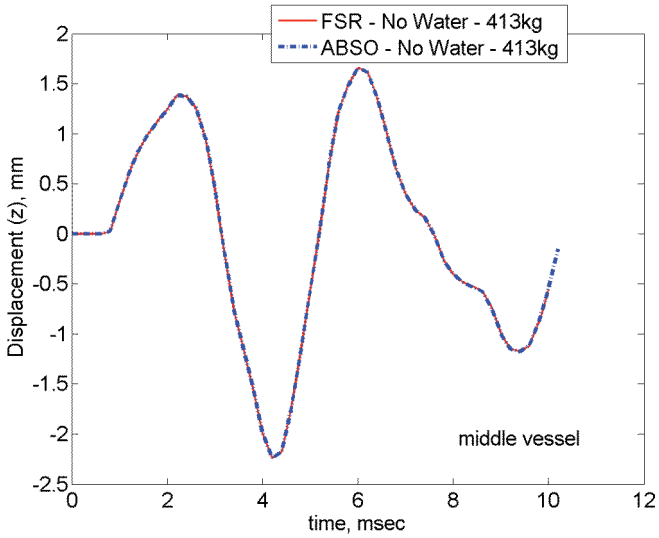

c)

Figure 73 Displacement (z component) at the top a), bottom b) and middle c) of the vessel for the case with FSR and ABSO boundary conditions and 413 kg of explosive material.

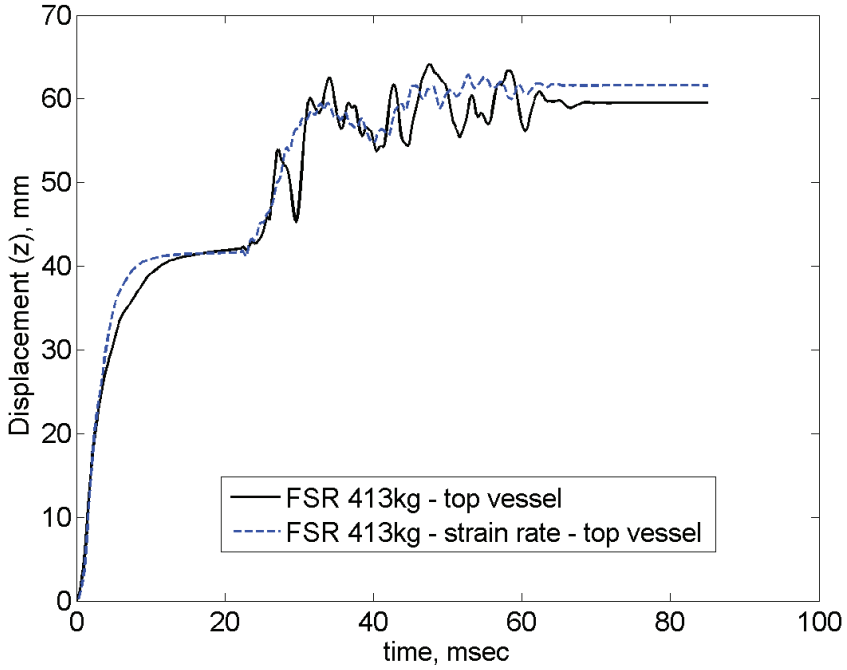

Figure 74 Displacement at the top of the vessel z component for the case with and without strain rate dependences of the material model. FSR boundary conditions and 413 kg of explosive material.

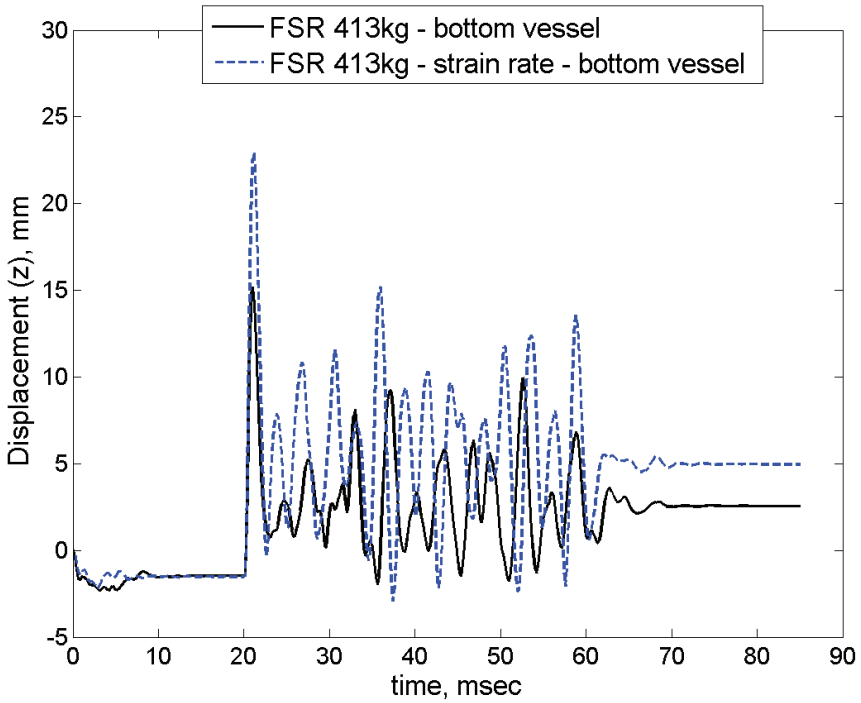

Figure 75 Displacement at the bottom of the vessel z component for the case with and without strain rate dependences of the material model. FSR boundary conditions and 413 kg of explosive material.

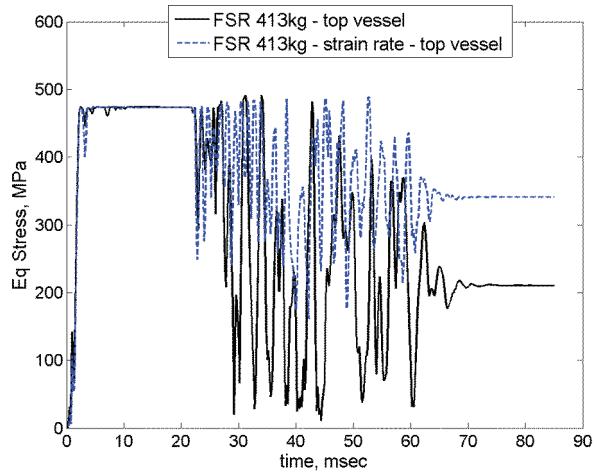

a)

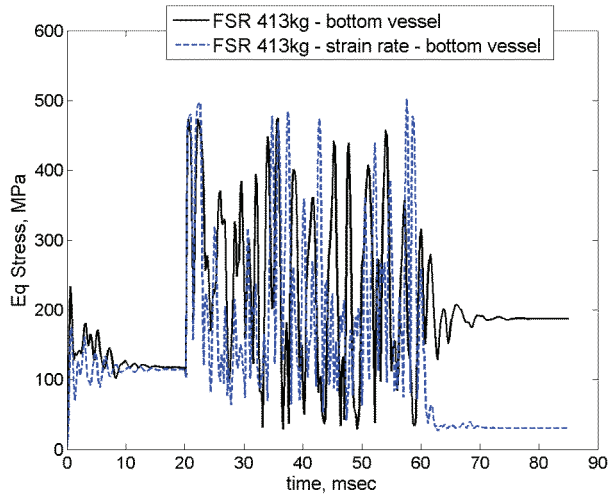

b)

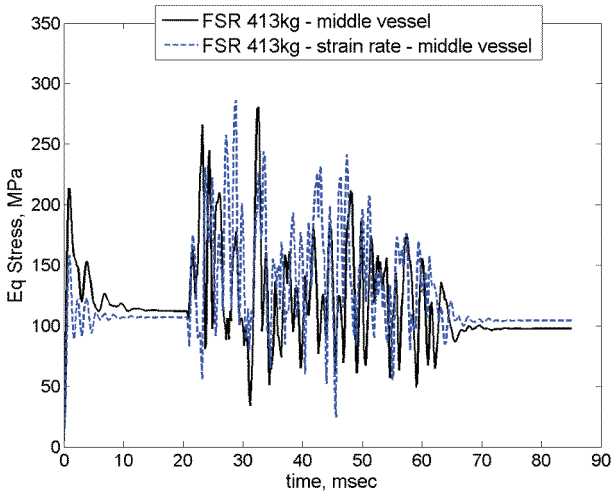

c)

Figure 76 Equivalent stress at the top a), bottom b) and middle c) of the vessel for the case with and without strain rate dependences of the material model. FSR boundary conditions and 413 kg of explosive material.

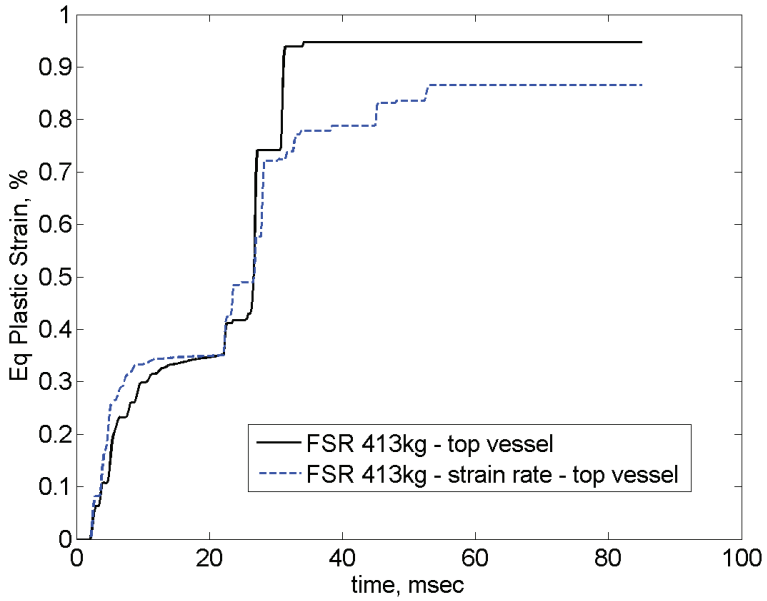

a)

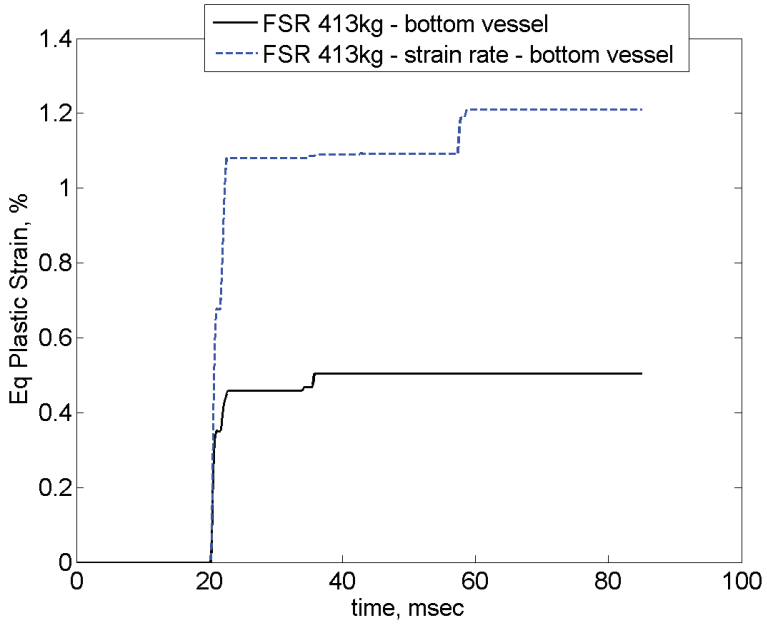

b)

Figure 77 Equivalent plastic strain at the top a) and bottom b) of the vessel for the case with and without strain rate dependences of the material model. FSR boundary conditions and 413 kg of explosive material.

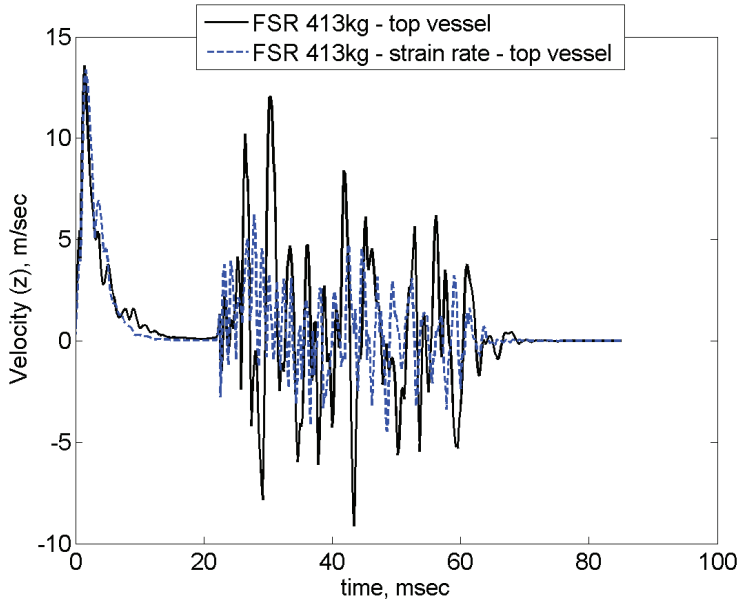

Figure 78 Velocity at the top of the vessel (z component) for the case with and without strain rate dependences of the material model. FSR boundary conditions and 413 kg of explosive material.

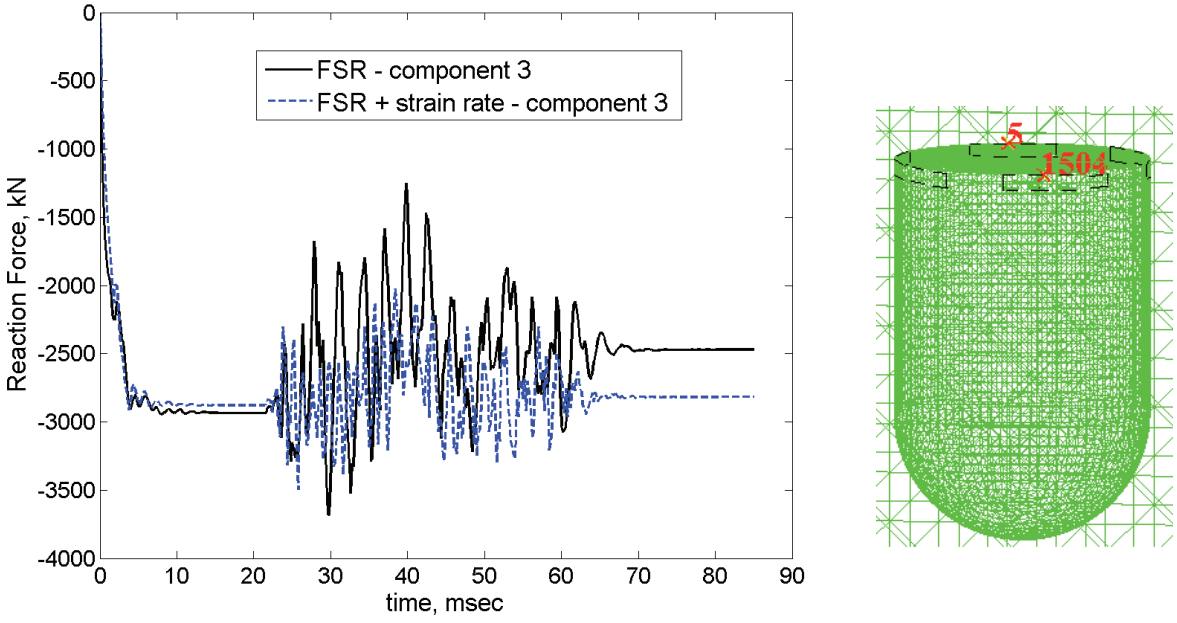

Figure 79 Reaction force third component at a location in the clamped zone (N 1504) for the case with and without strain rate dependences of the material model. FSR boundary conditions and 413 kg of explosive material.

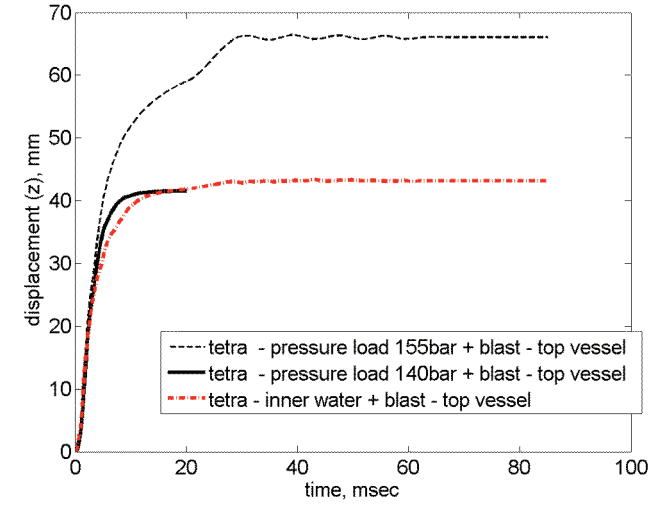

a)

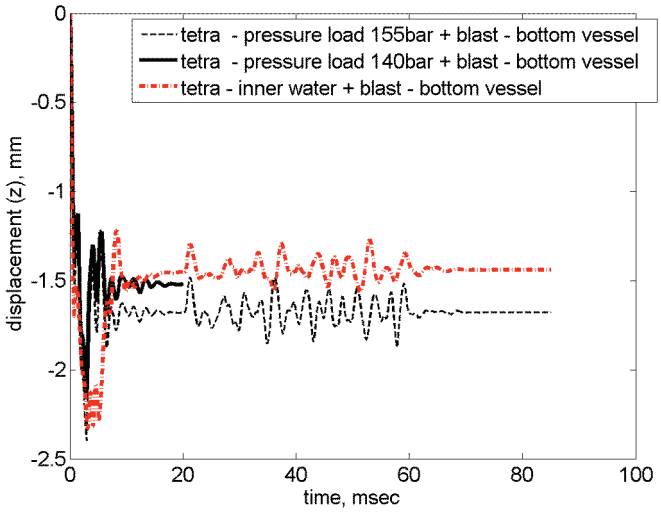

b)

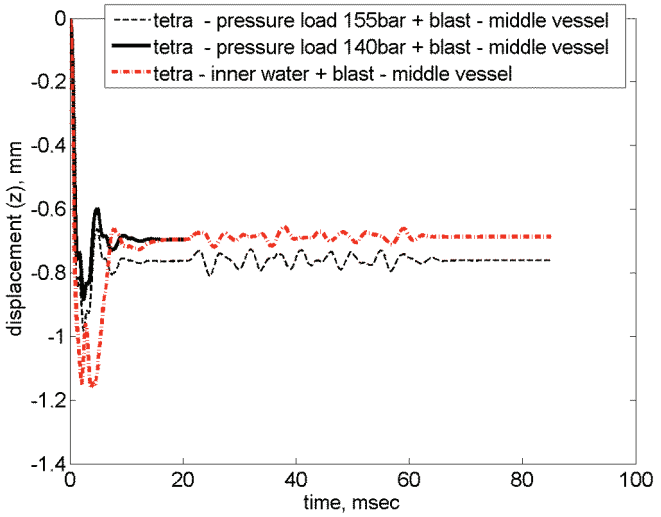

c)

Figure 80 Comparison between the displacement a) at the top, b) bottom and c) middle position of the vessel for the case with water at 155bar and without water but pressure load applied on the walls of the vessel. Case with 5kg of explosive charge.

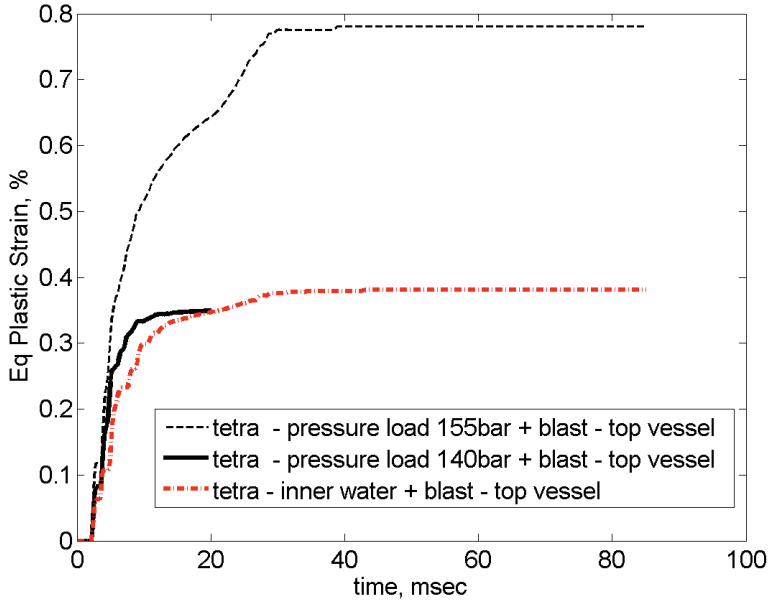

Figure 81 Comparison between the equivalent plastic strain at the top of the vessel for the case with water at 155bar and without water but pressure load applied on the walls of the vessel. Case with 5kg of explosive charge.

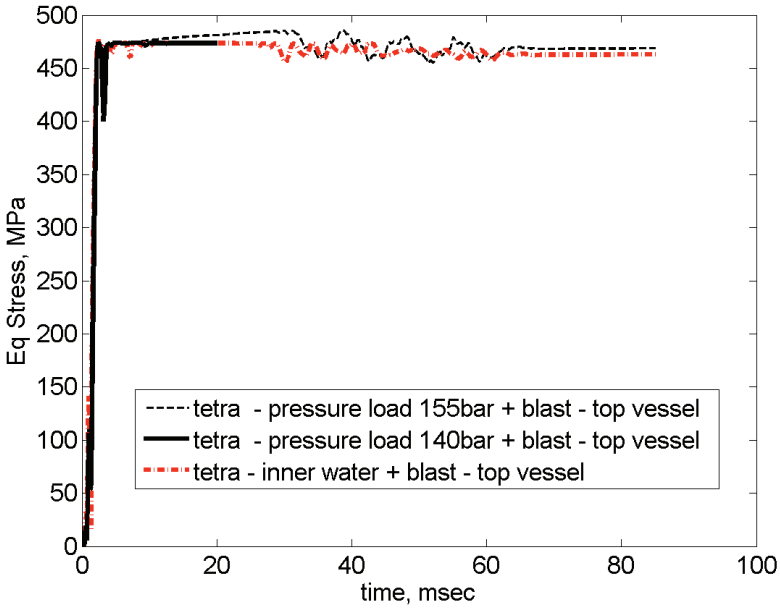

Figure 82 Comparison between the equivalent stress at the top of the vessel for the case with water at 155bar and without water but pressure load applied on the walls of the vessel. Case with 5kg of explosive charge.

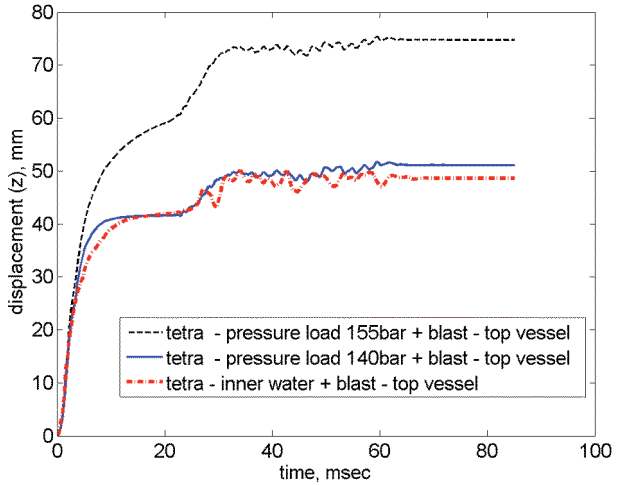

a)

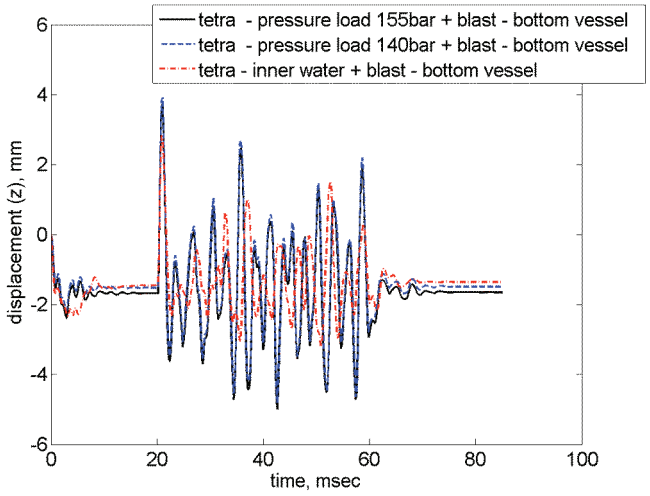

b)

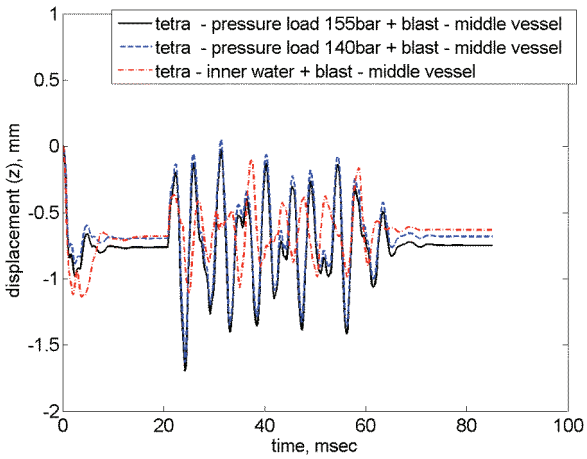

c)

Figure 83 Comparison between the displacement a) at the top, b) bottom and c) middle position of the vessel for the case with water at 155bar and without water but pressure load applied on the walls of the vessel. Case with 170kg of explosive charge.

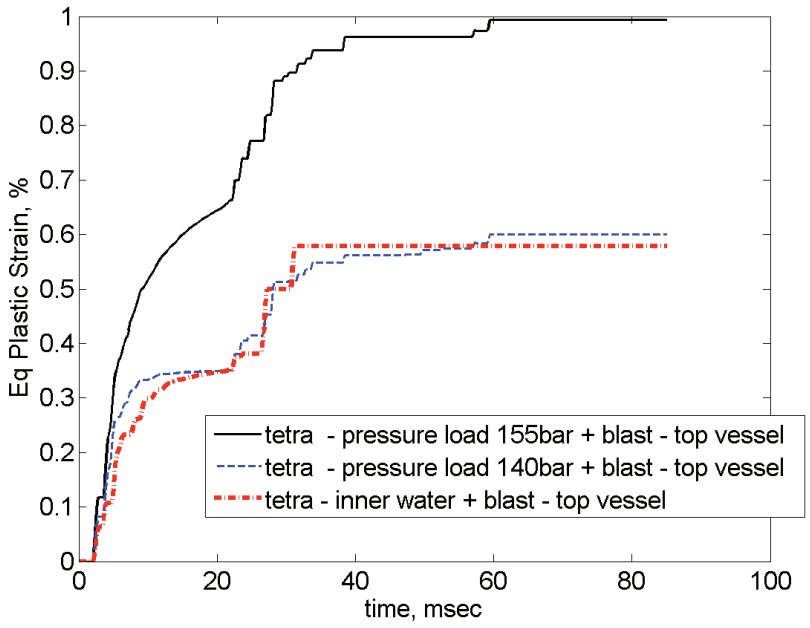

Figure 84 Comparison between the equivalent plastic strain at the top of the vessel for the case with water at 155bar and without water but pressure load applied on the walls of the vessel. Case with 170kg of explosive charge.

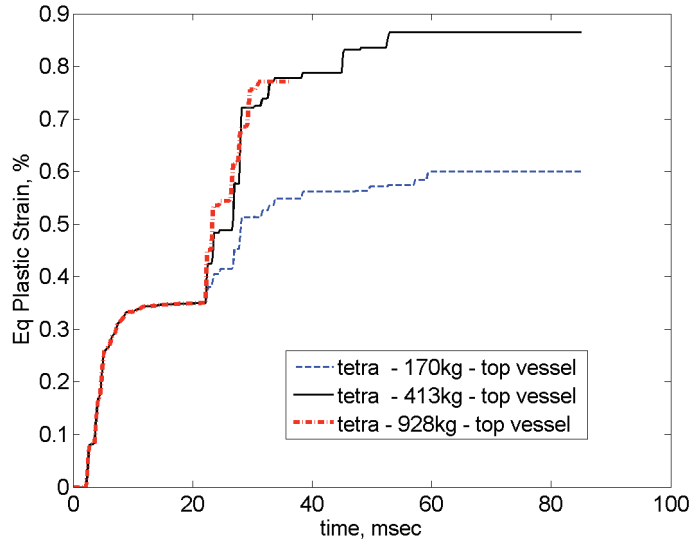

a)

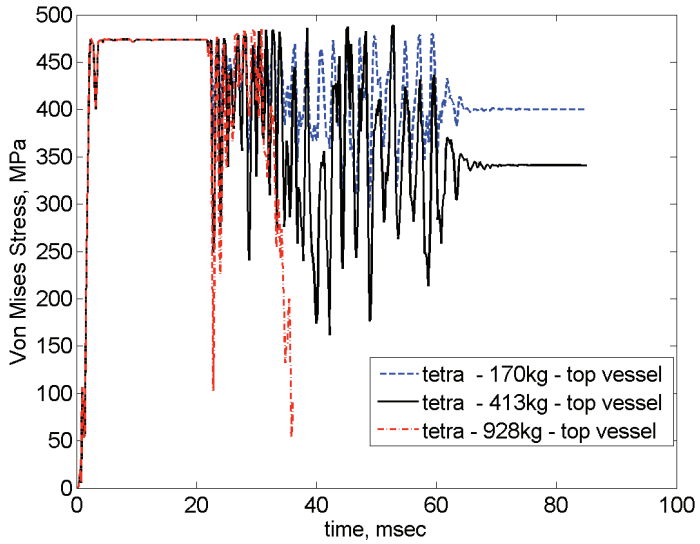

b)

Figure 85 a) Equivalent plastic strain and b) stress variation for 170kg, 413kg and 928kg of explosive material and the progressive damage and fracture material model at the top of the vessel.

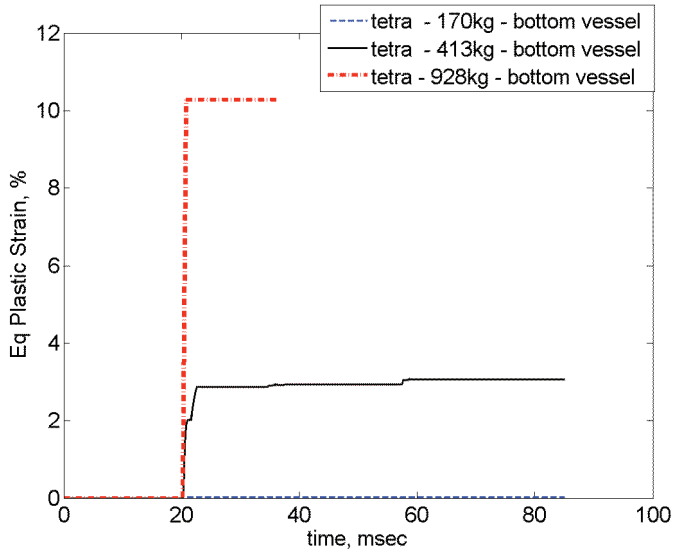

a)

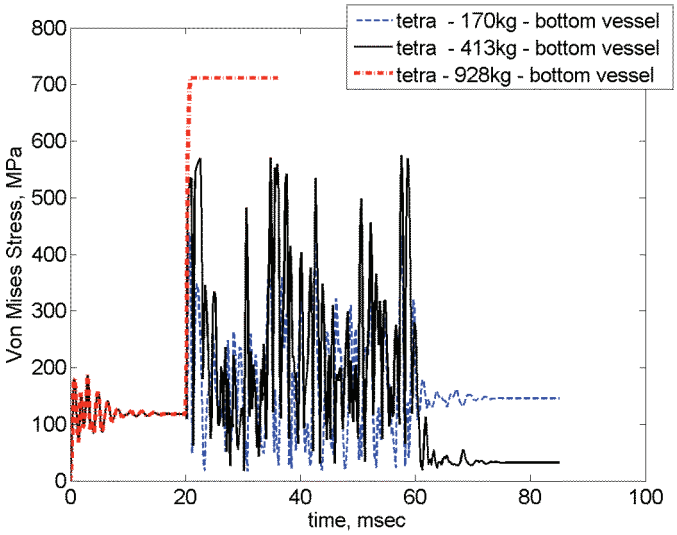

b)

Figure 86 a) Equivalent plastic strain and b) stress variation for 170kg, 413kg and 928kg of explosive material and the progressive damage and fracture material model at the bottom of the vessel.

CONTOUR PLOTS

Figure 87 Progressive damage and fracture model. Equivalent plastic strain and stress, pressure and nodal speed for 928 kg of explosive material.

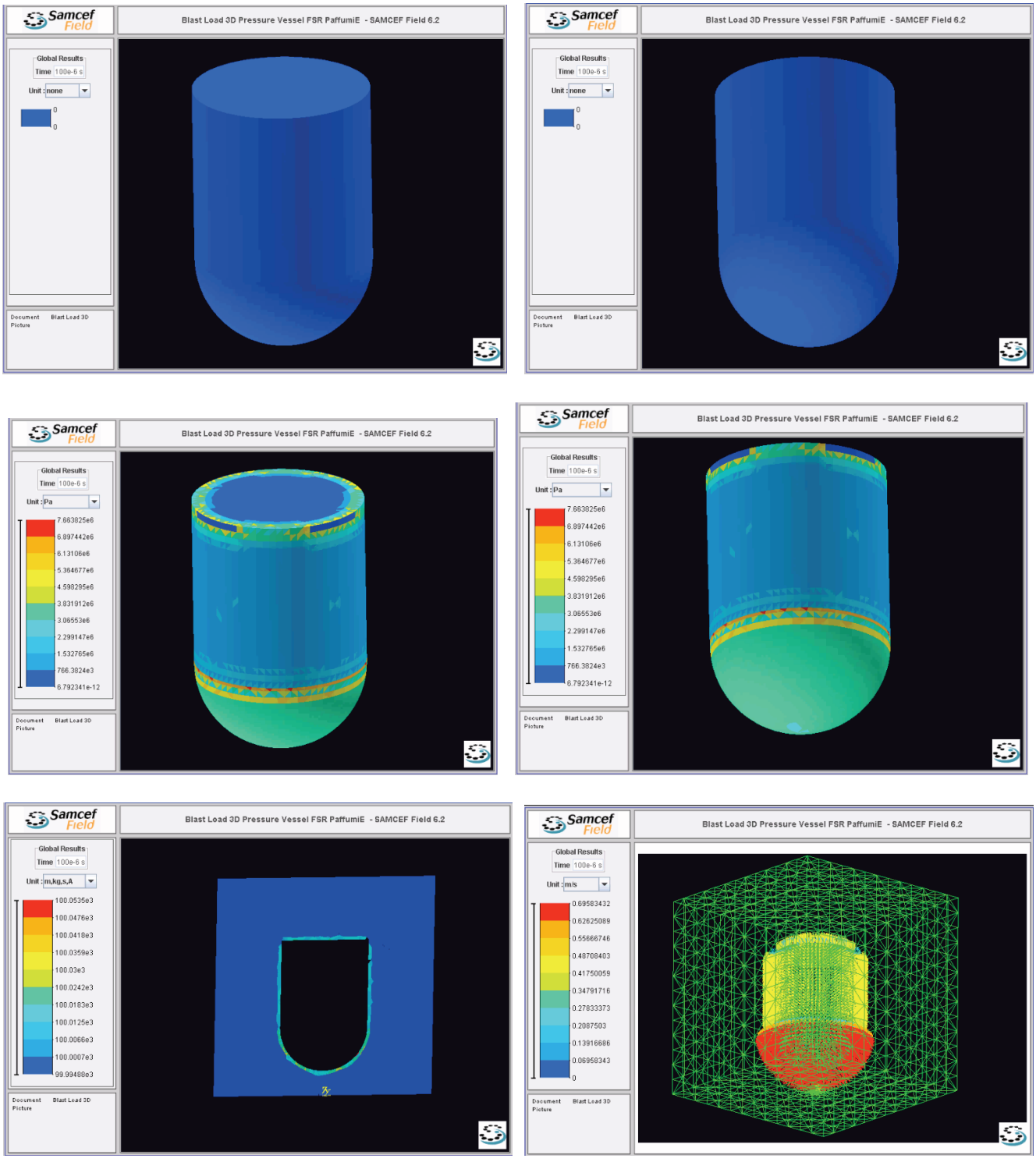

928 kg of explosive material
Equivalent Plastic Strain and Equivalent Stress
Pressure and Nodal Speed: 100µsec of analysis

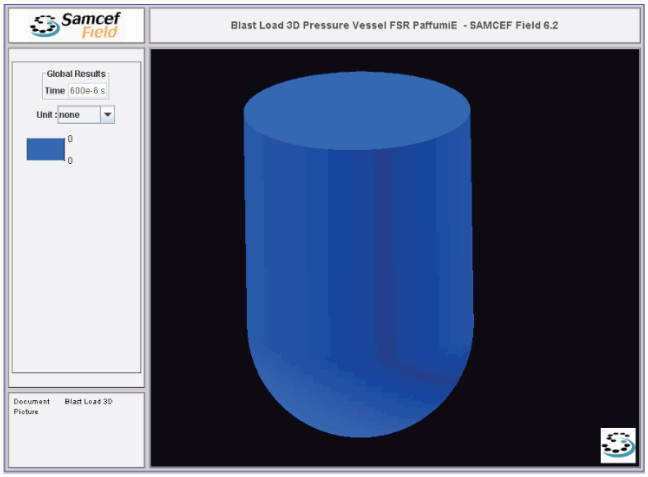

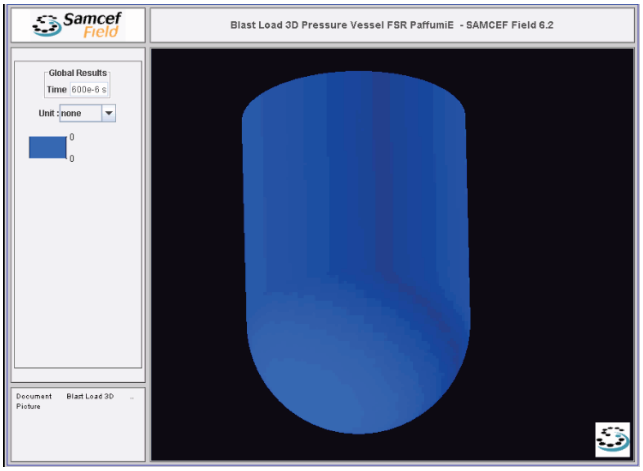

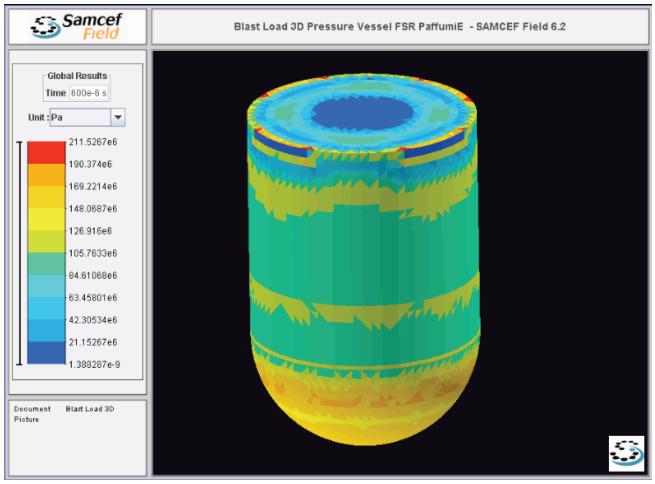

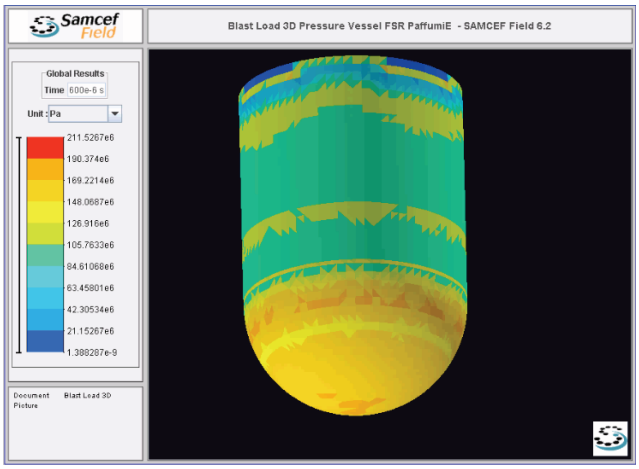

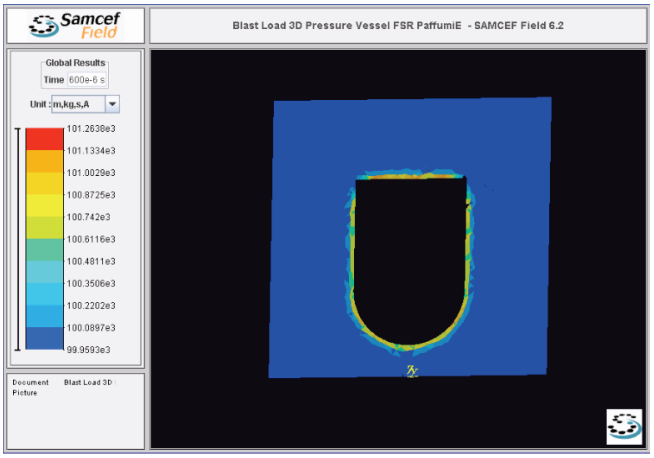

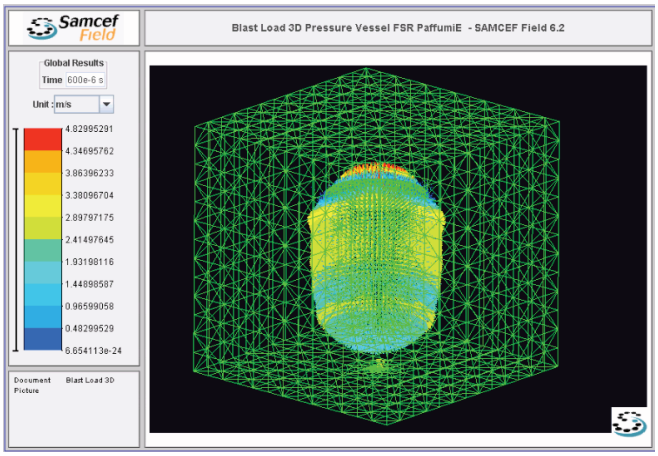

928 kg of explosive material
Equivalent Plastic Strain and Equivalent Stress
Pressure and Nodal Speed: 600µsec of analysis

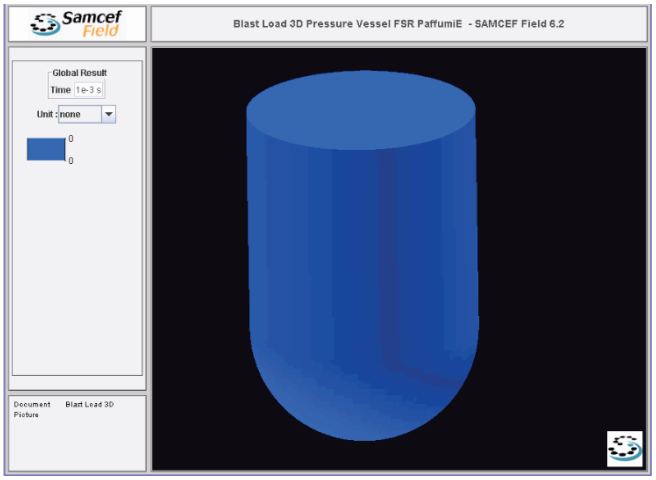

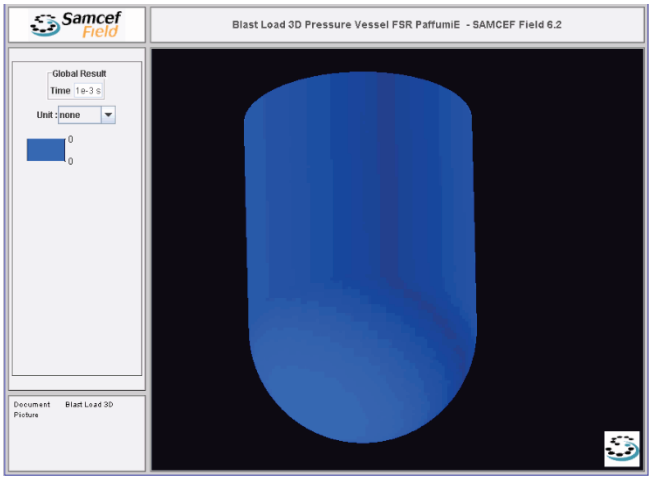

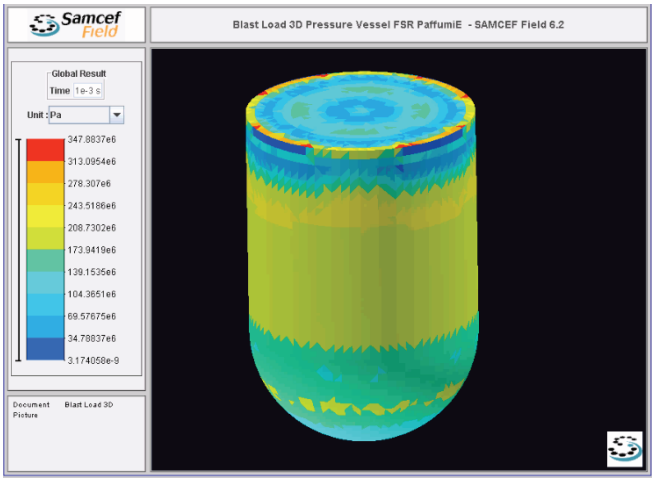

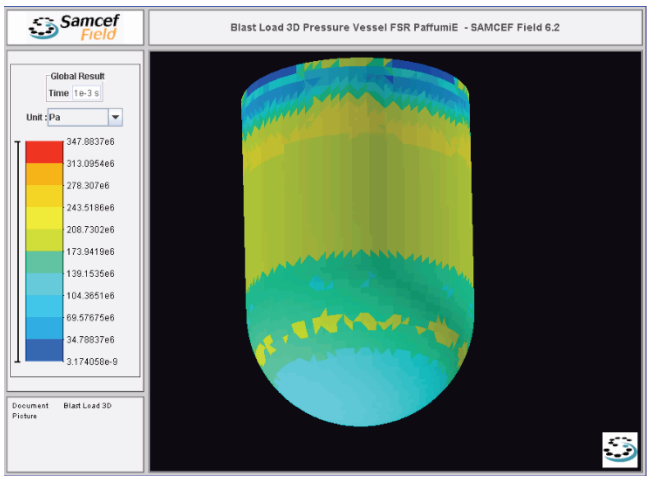

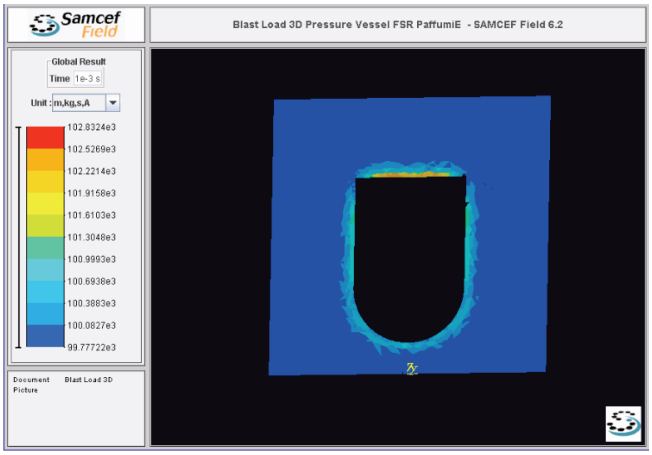

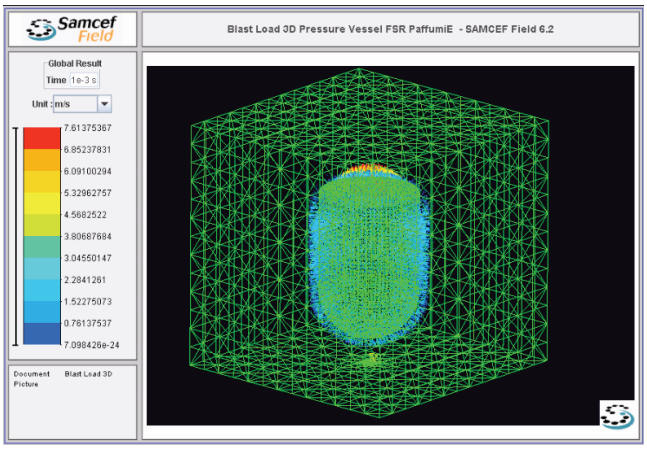

928 kg of explosive material
Equivalent Plastic Strain and Equivalent Stress
Pressure and Nodal Speed: 1msec of analysis

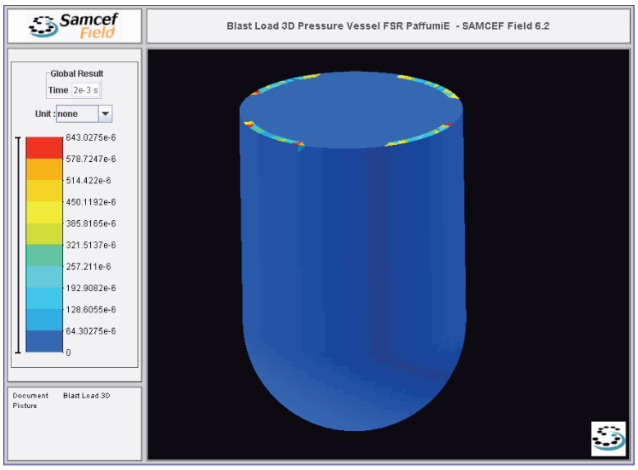

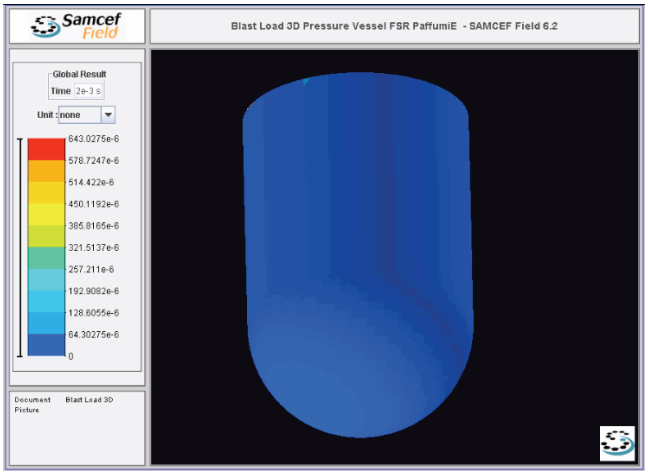

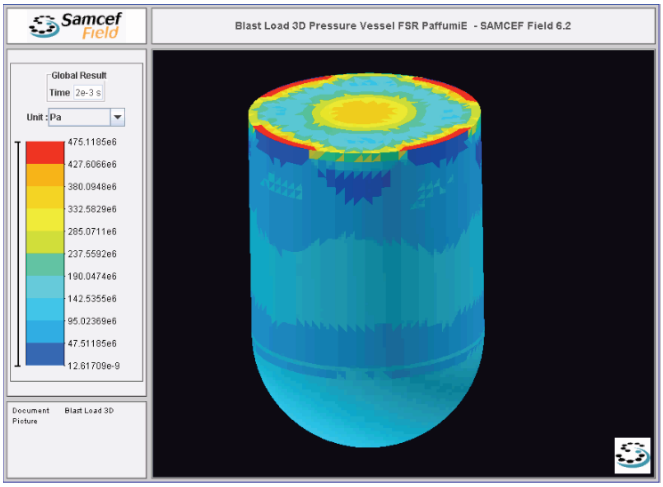

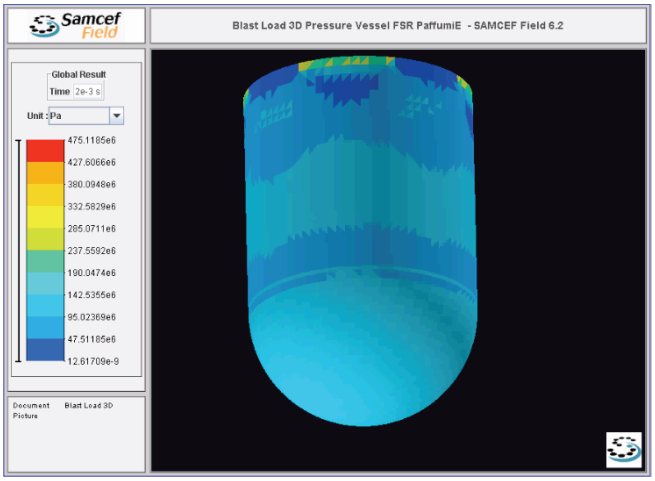

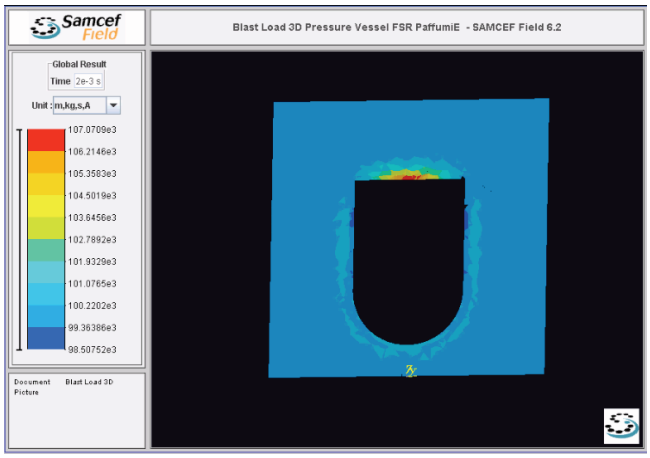

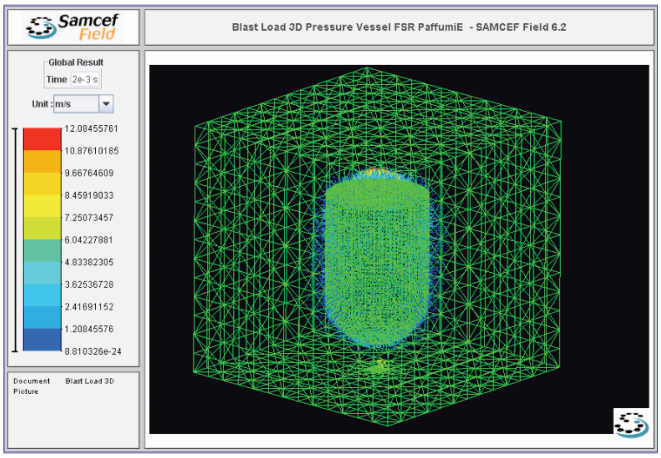

928 kg of explosive material
Equivalent Plastic Strain and Equivalent Stress
Pressure and Nodal Speed: 2msec of analysis

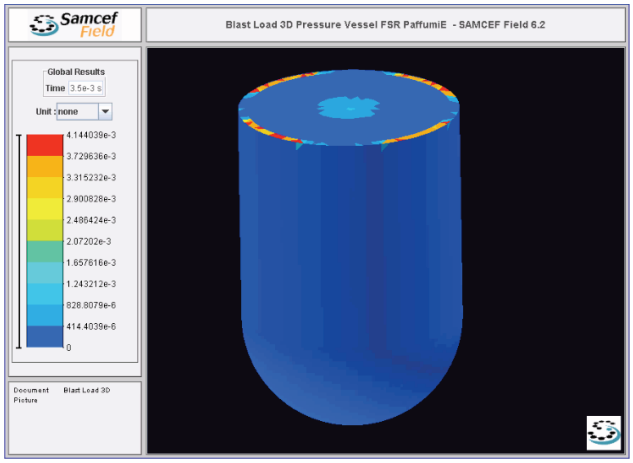

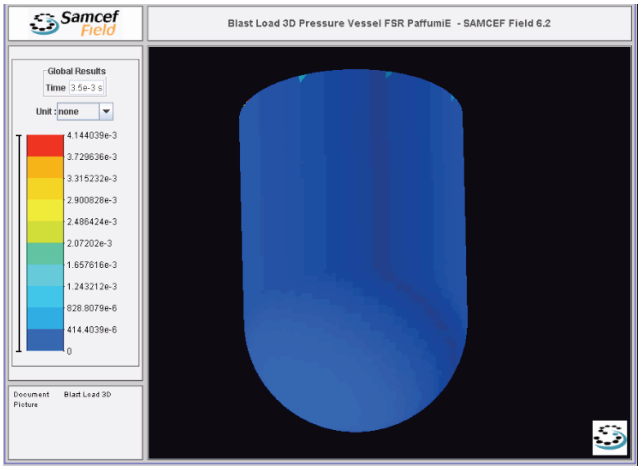

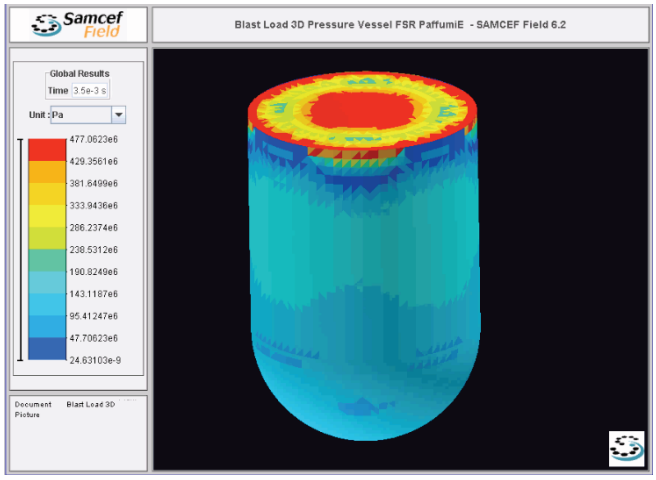

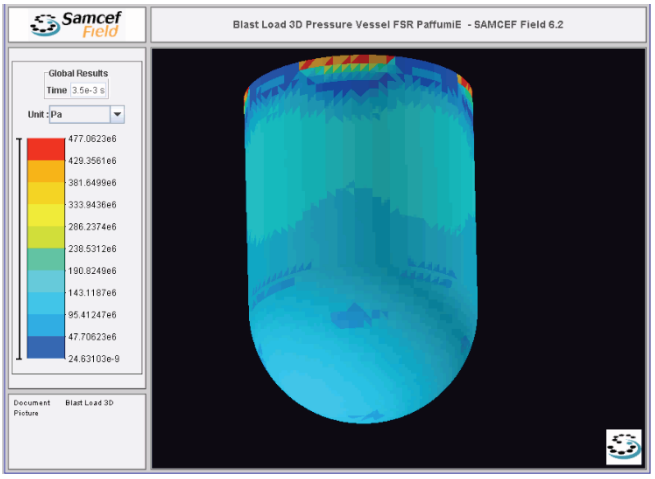

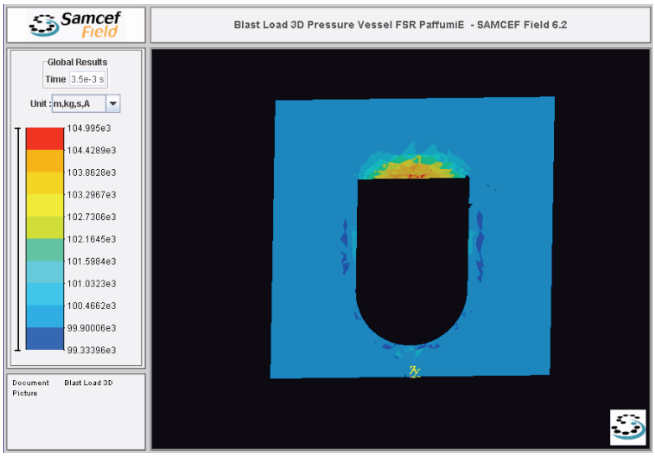

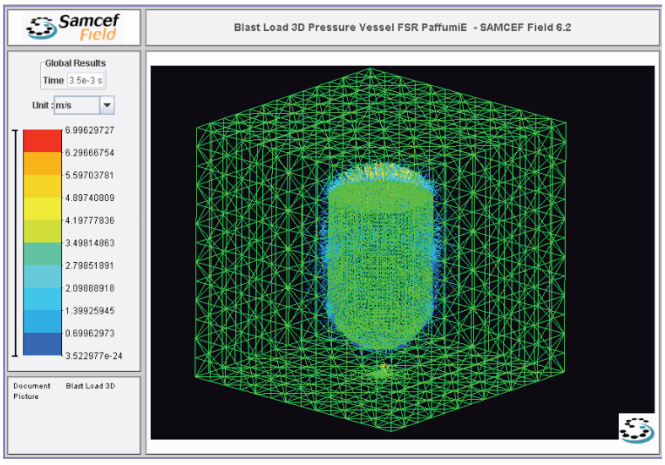

928 kg of explosive material
Equivalent Plastic Strain and Equivalent Stress
Pressure and Nodal Speed: 3.5msec of analysis

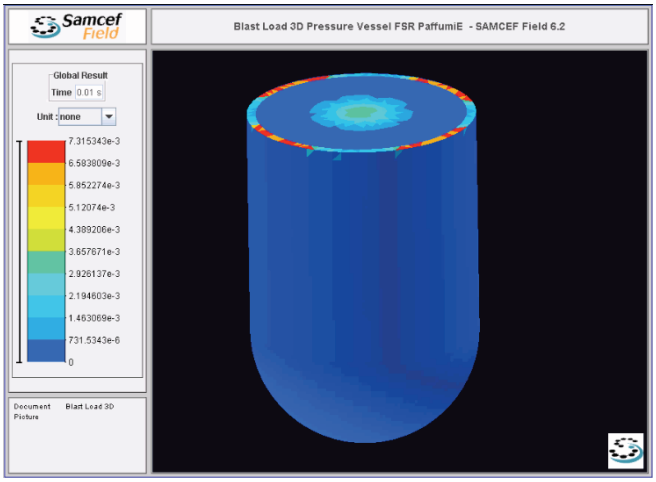

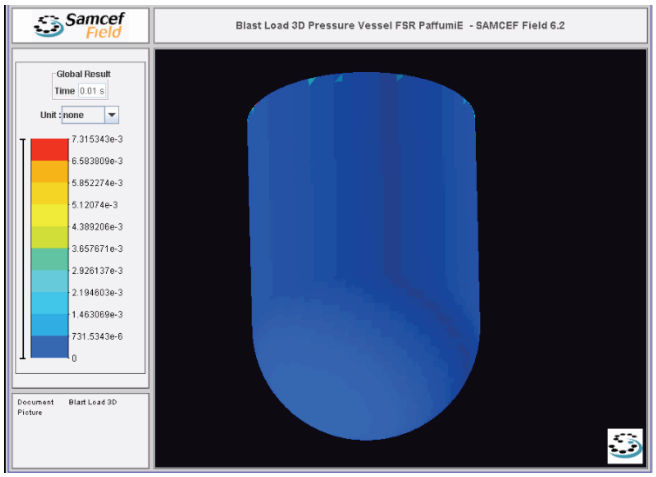

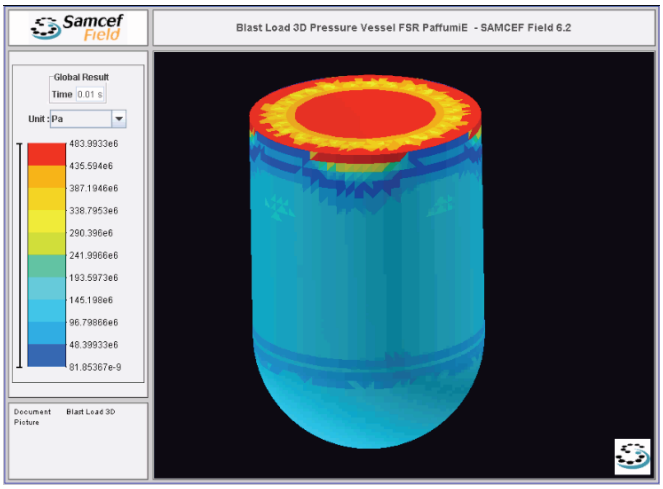

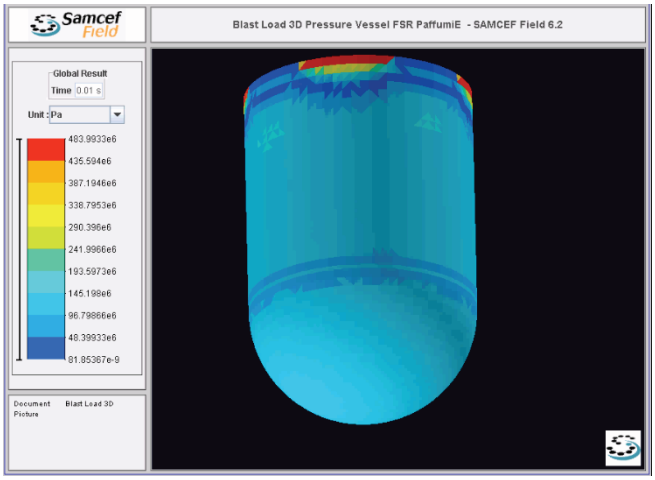

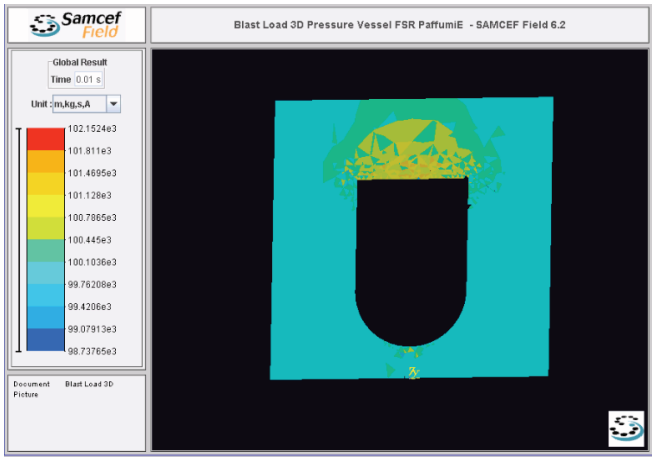

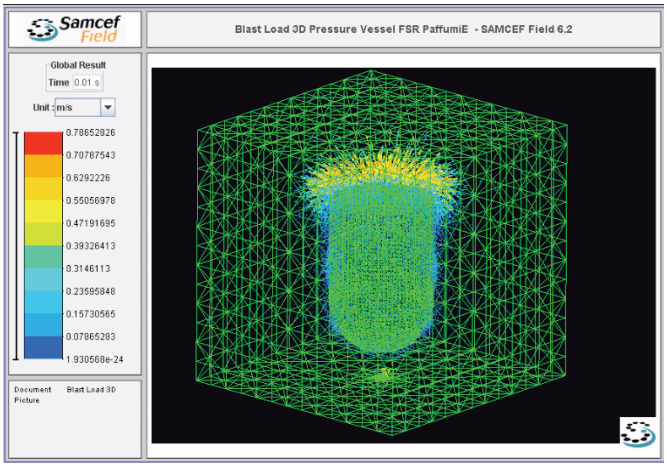

928 kg of explosive material
Equivalent Plastic Strain and Equivalent Stress
Pressure and Nodal Speed: 0.01sec of analysis

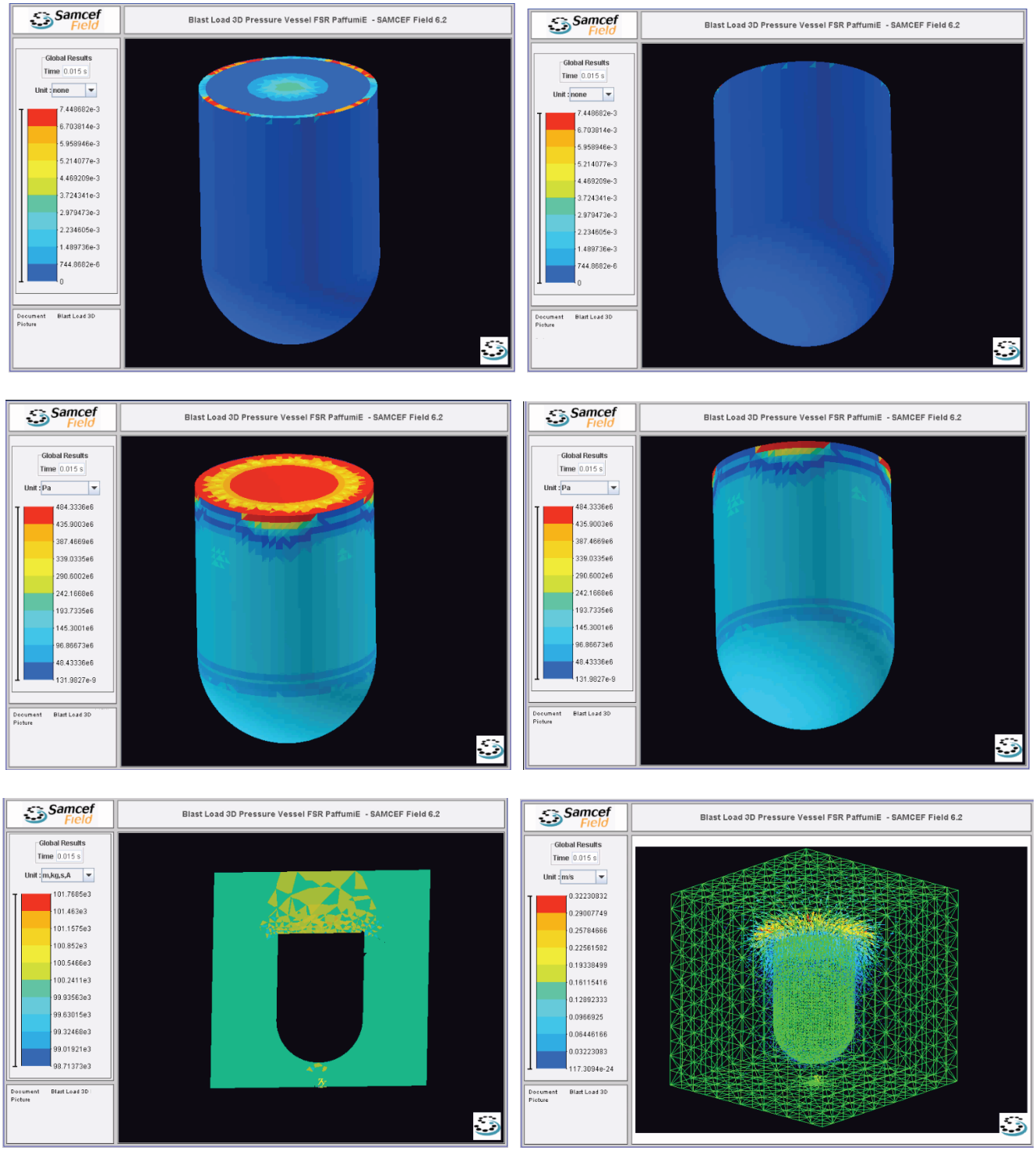

928 kg of explosive material
Equivalent Plastic Strain and Equivalent Stress
Pressure and Nodal Speed: 0.015sec of analysis

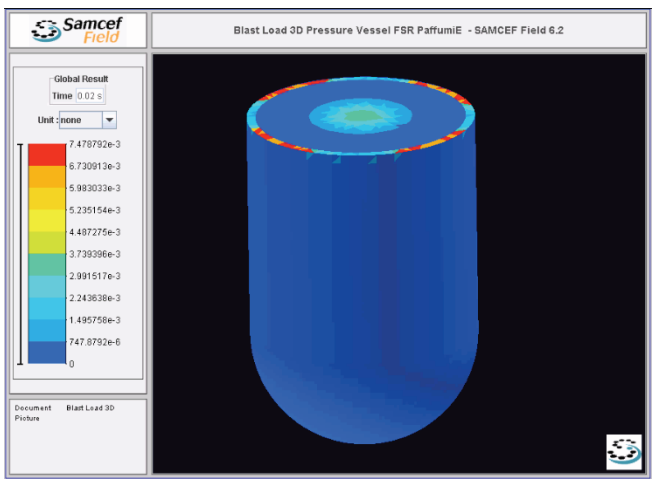

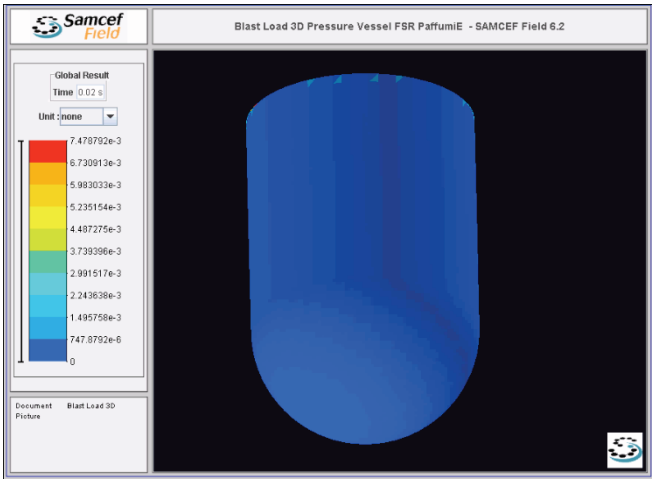

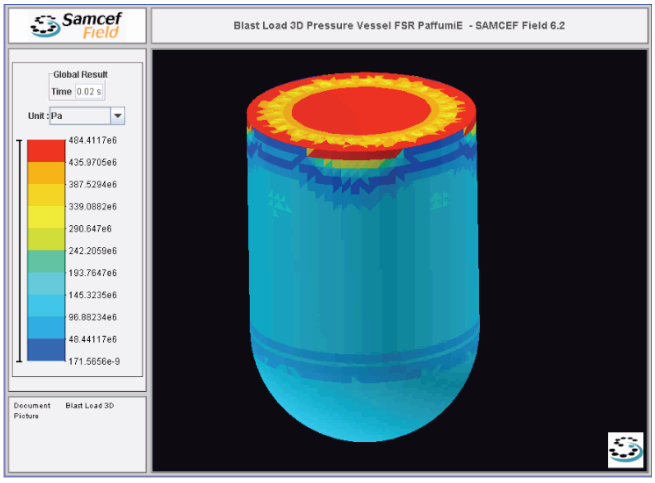

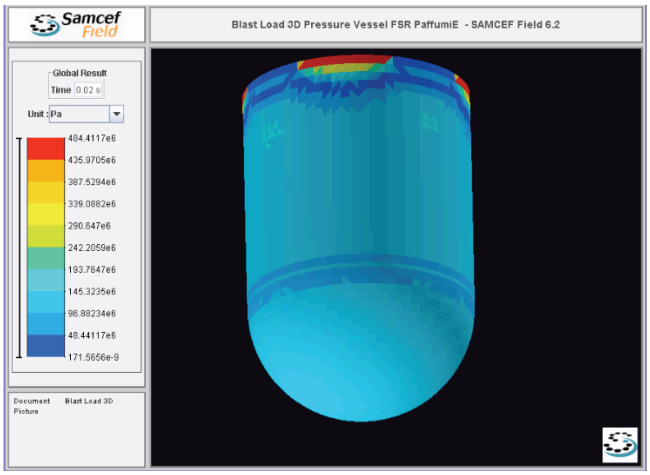

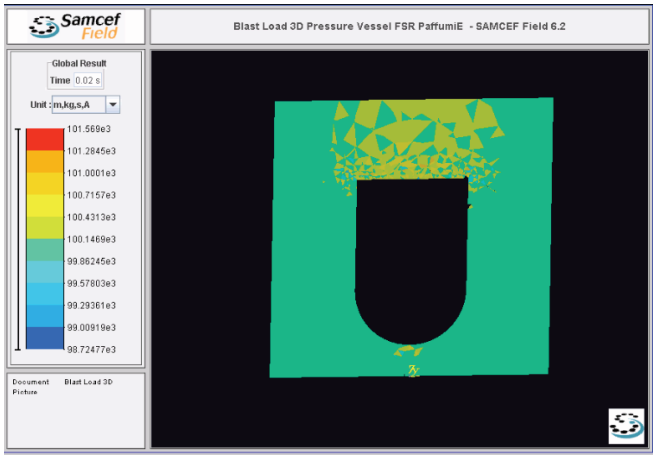

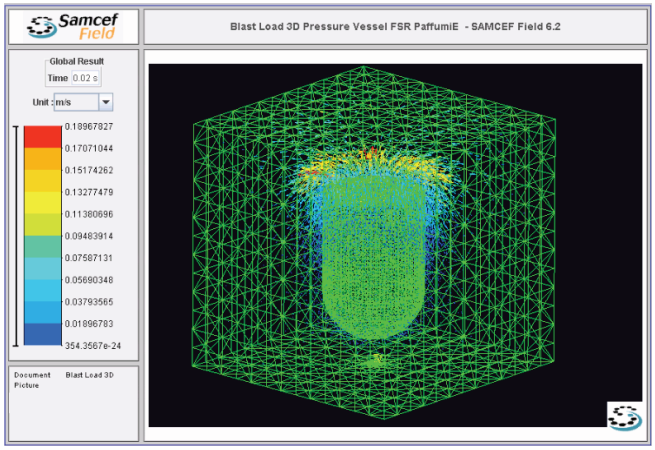

928 kg of explosive material
Equivalent Plastic Strain and Equivalent Stress
Pressure and Nodal Speed: 0.02sec of analysis

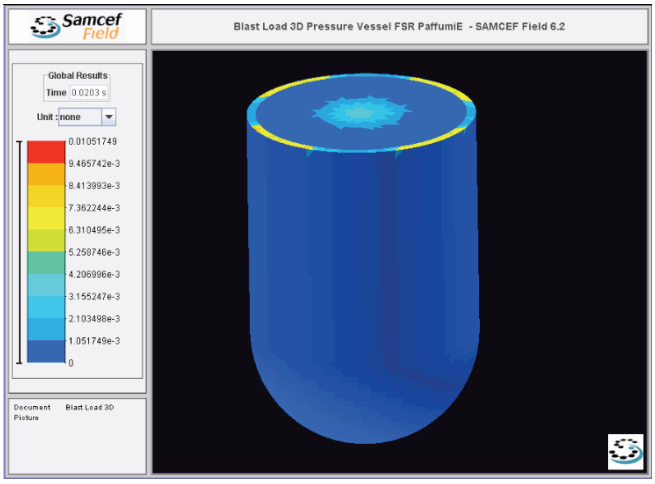

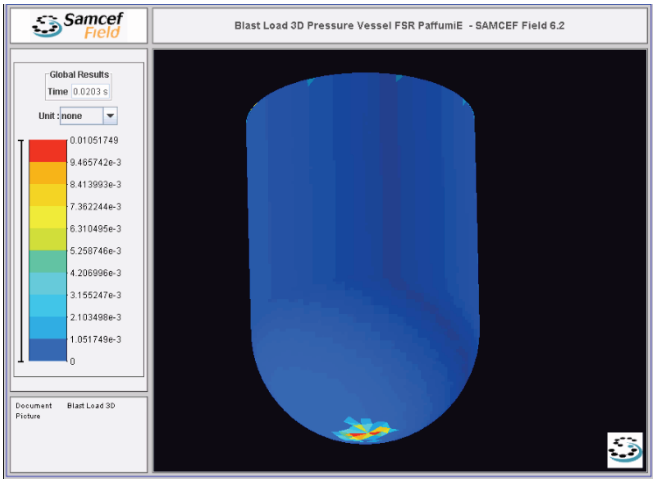

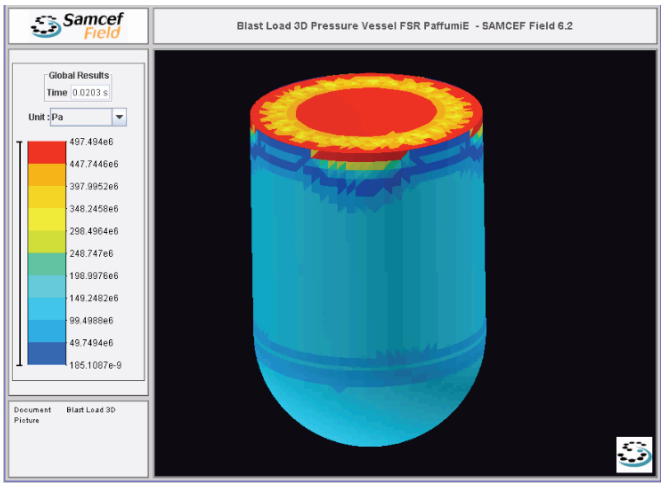

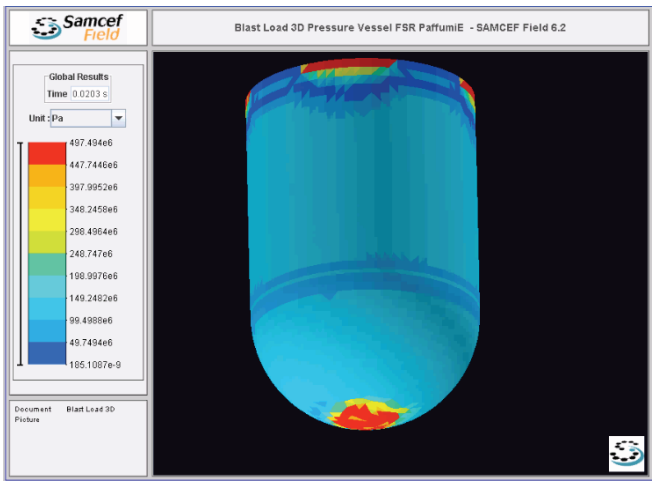

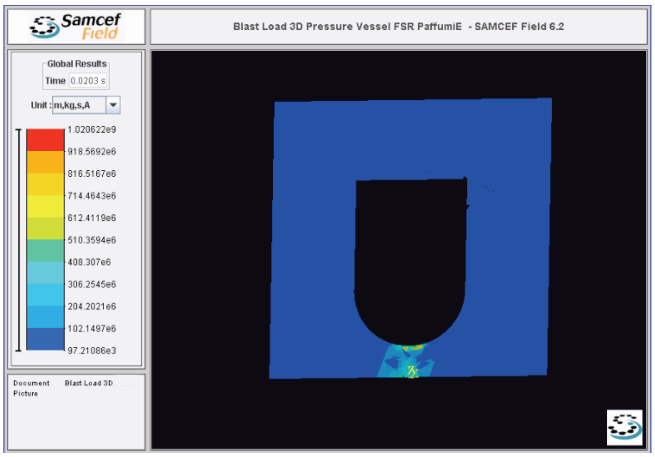

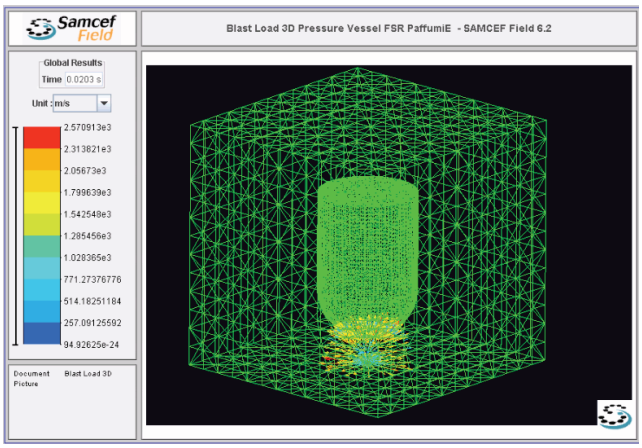

928 kg of explosive material
Equivalent Plastic Strain and Equivalent Stress
Pressure and Nodal Speed: 0.0203sec (explosion starts at 20msec)

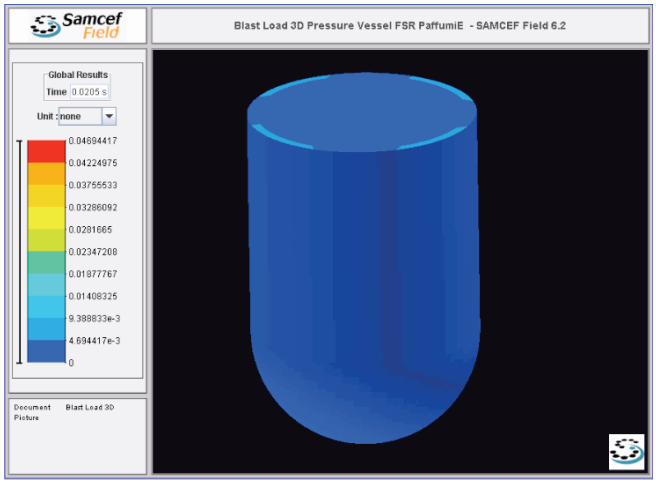

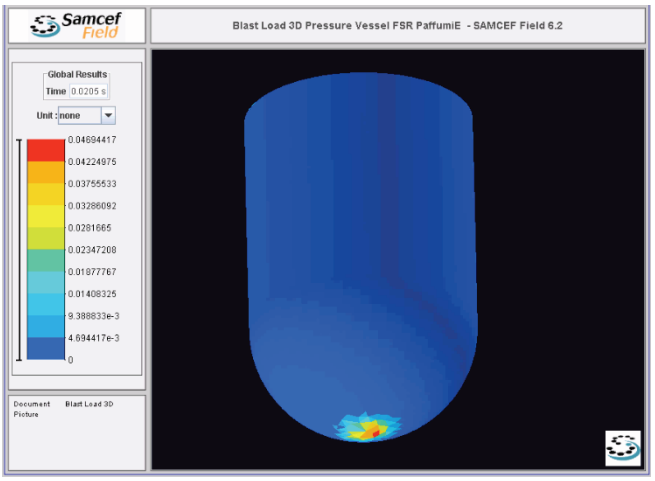

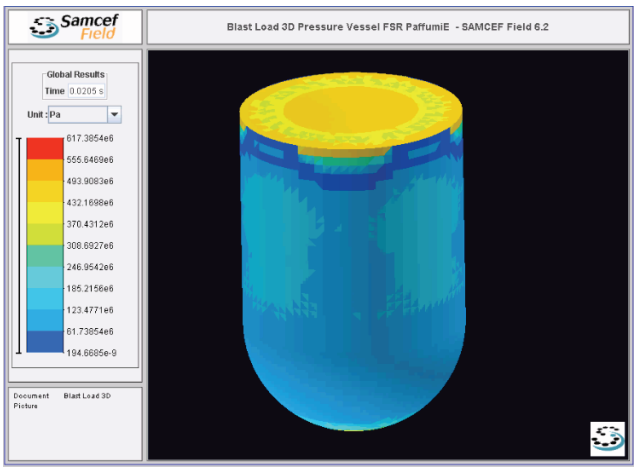

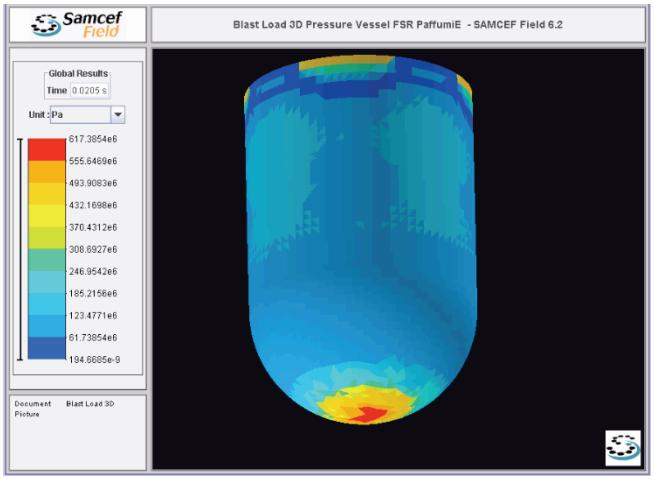

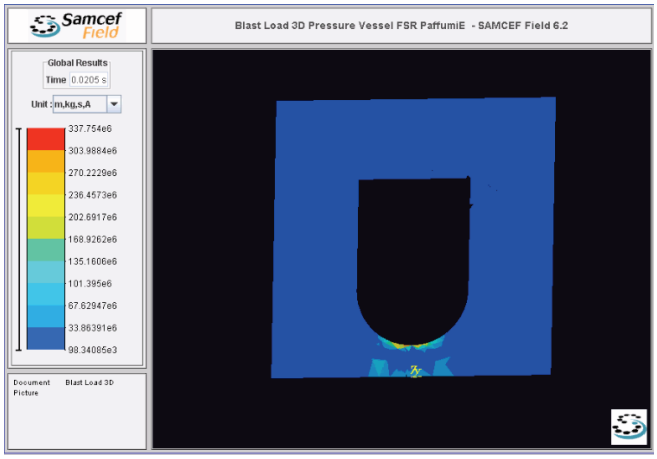

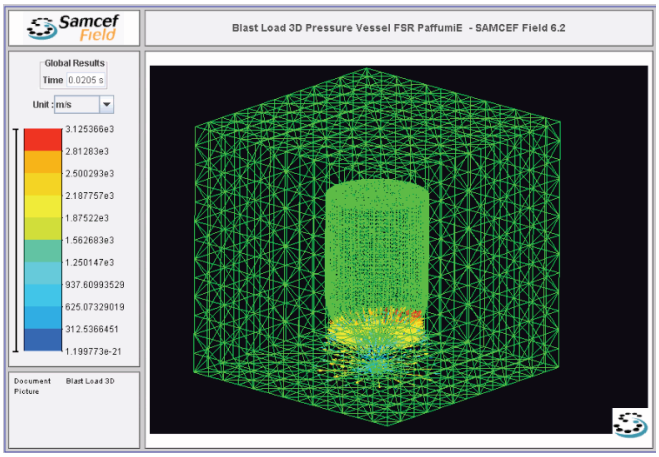

928 kg of explosive material
Equivalent Plastic Strain and Equivalent Stress
Pressure and Nodal Speed: 0.0205sec (explosion starts at 20msec)

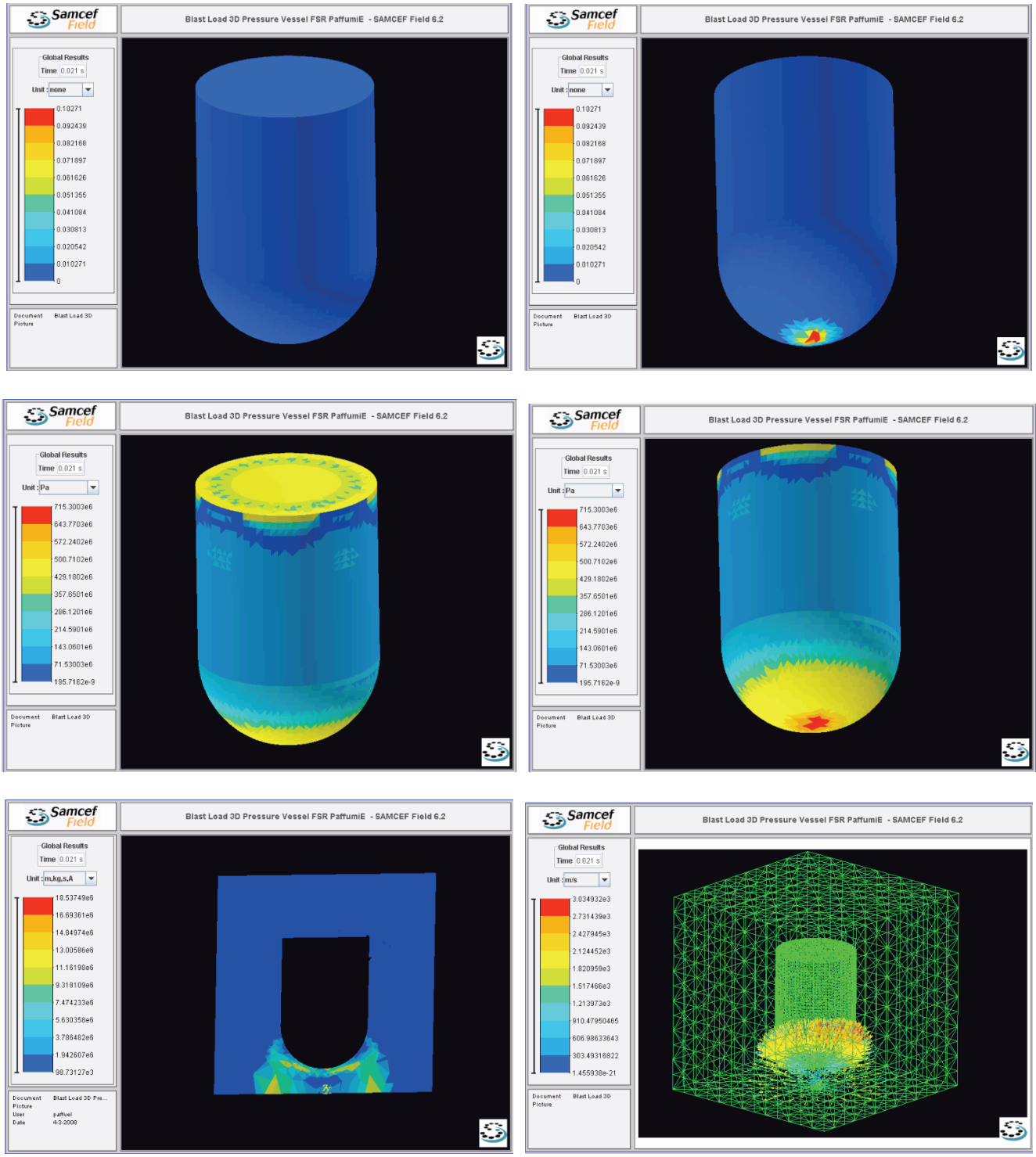

928 kg of explosive material
Equivalent Plastic Strain and Equivalent Stress
Pressure and Nodal Speed: 0.021sec (explosion starts at 20msec)

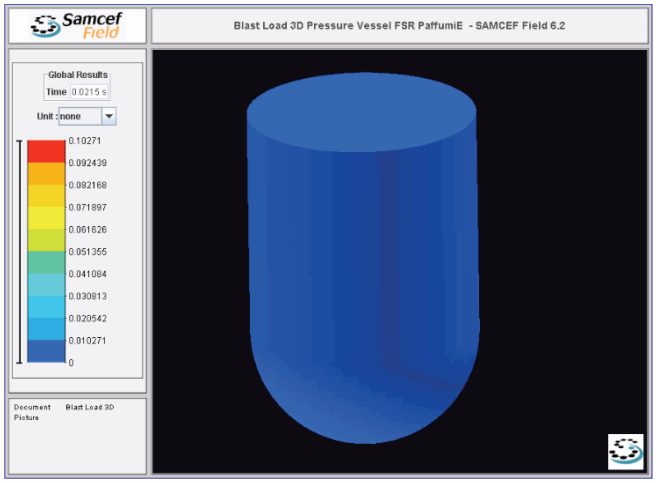

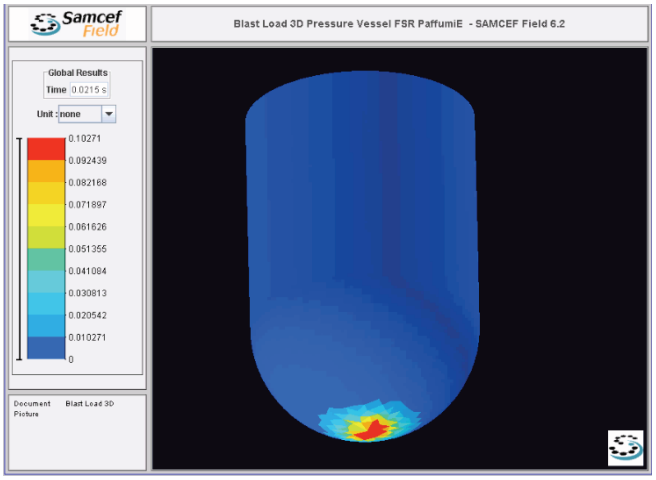

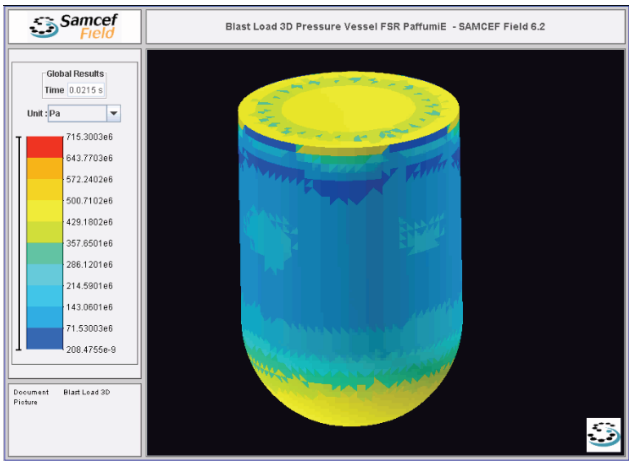

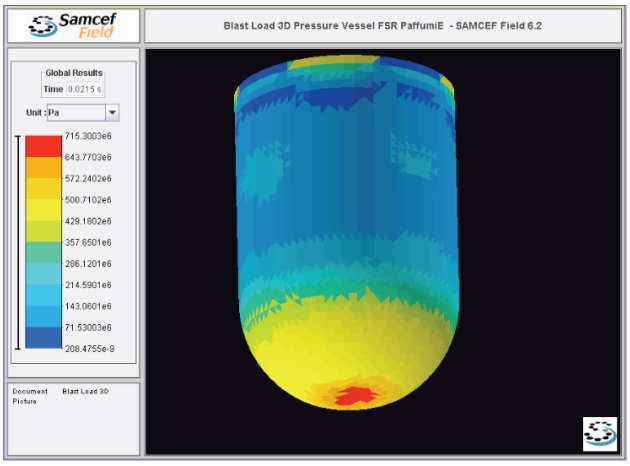

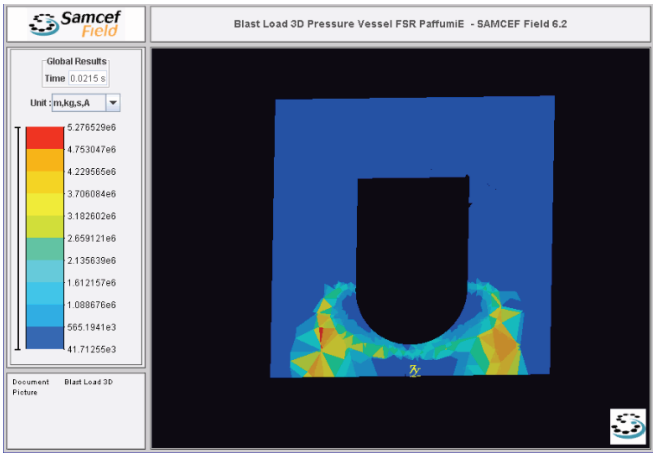

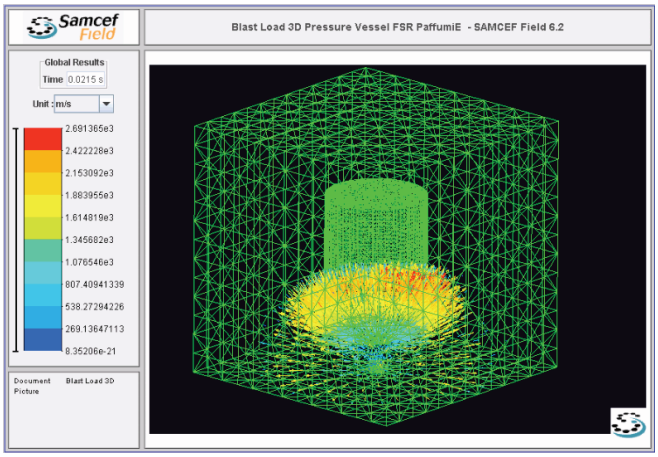

928 kg of explosive material
Equivalent Plastic Strain and Equivalent Stress
Pressure and Nodal Speed: 0.0215sec (explosion starts at 20msec)

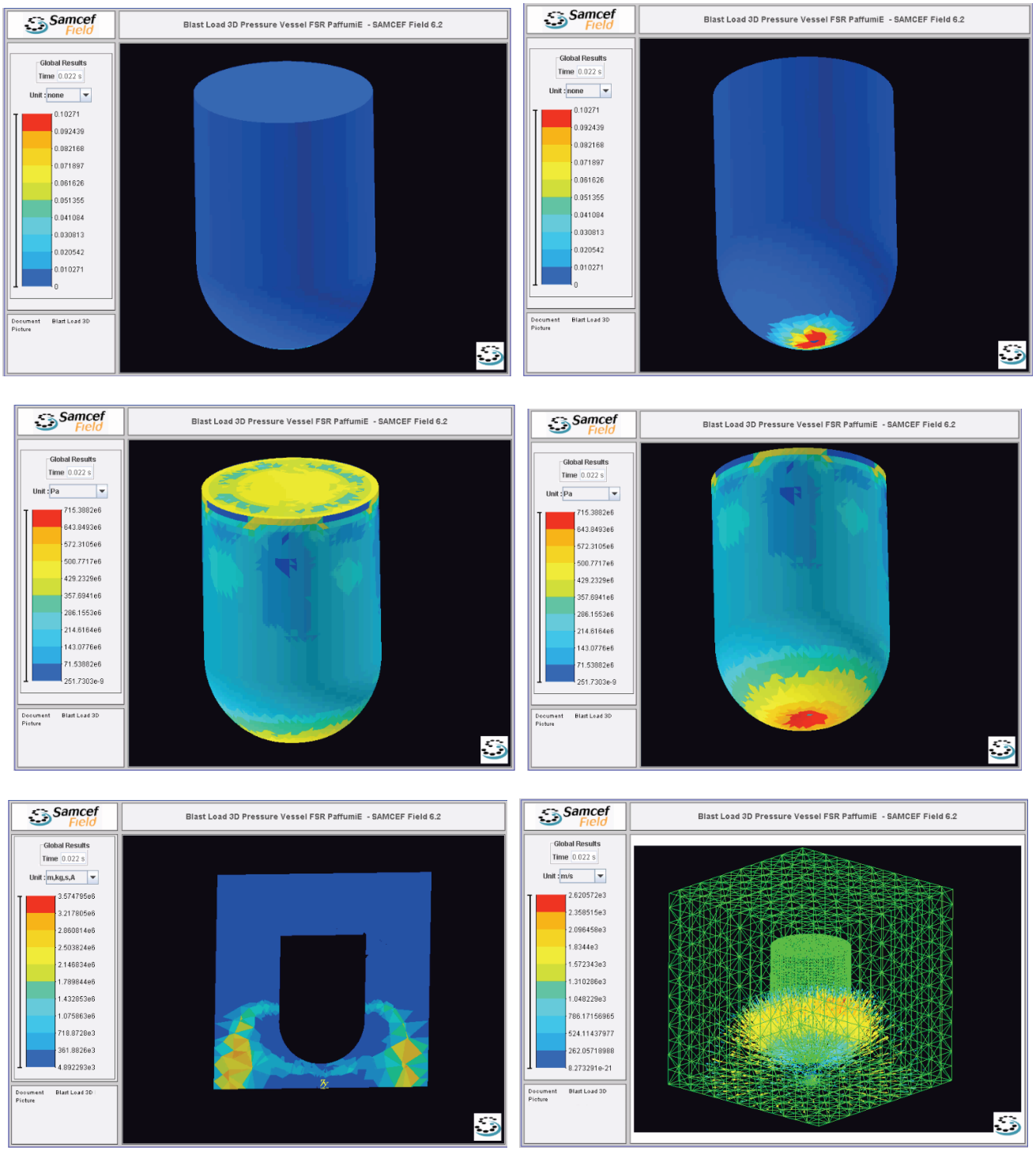

928 kg of explosive material
Equivalent Plastic Strain and Equivalent Stress
Pressure and Nodal Speed: 0.022sec (explosion starts at 20msec)

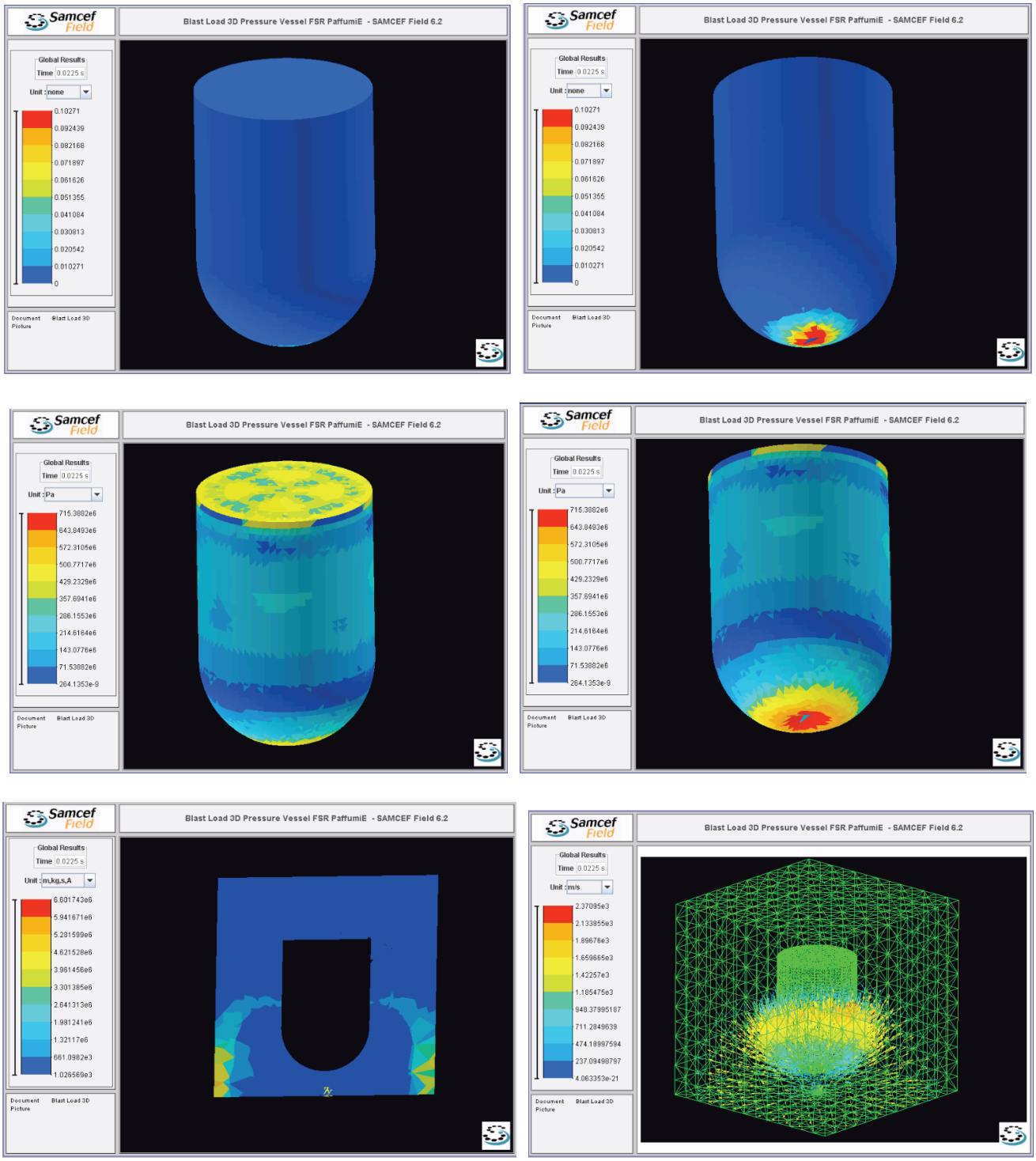

928 kg of explosive material
Equivalent Plastic Strain and Equivalent Stress
Pressure and Nodal Speed: 0.0225sec (explosion starts at 20msec)

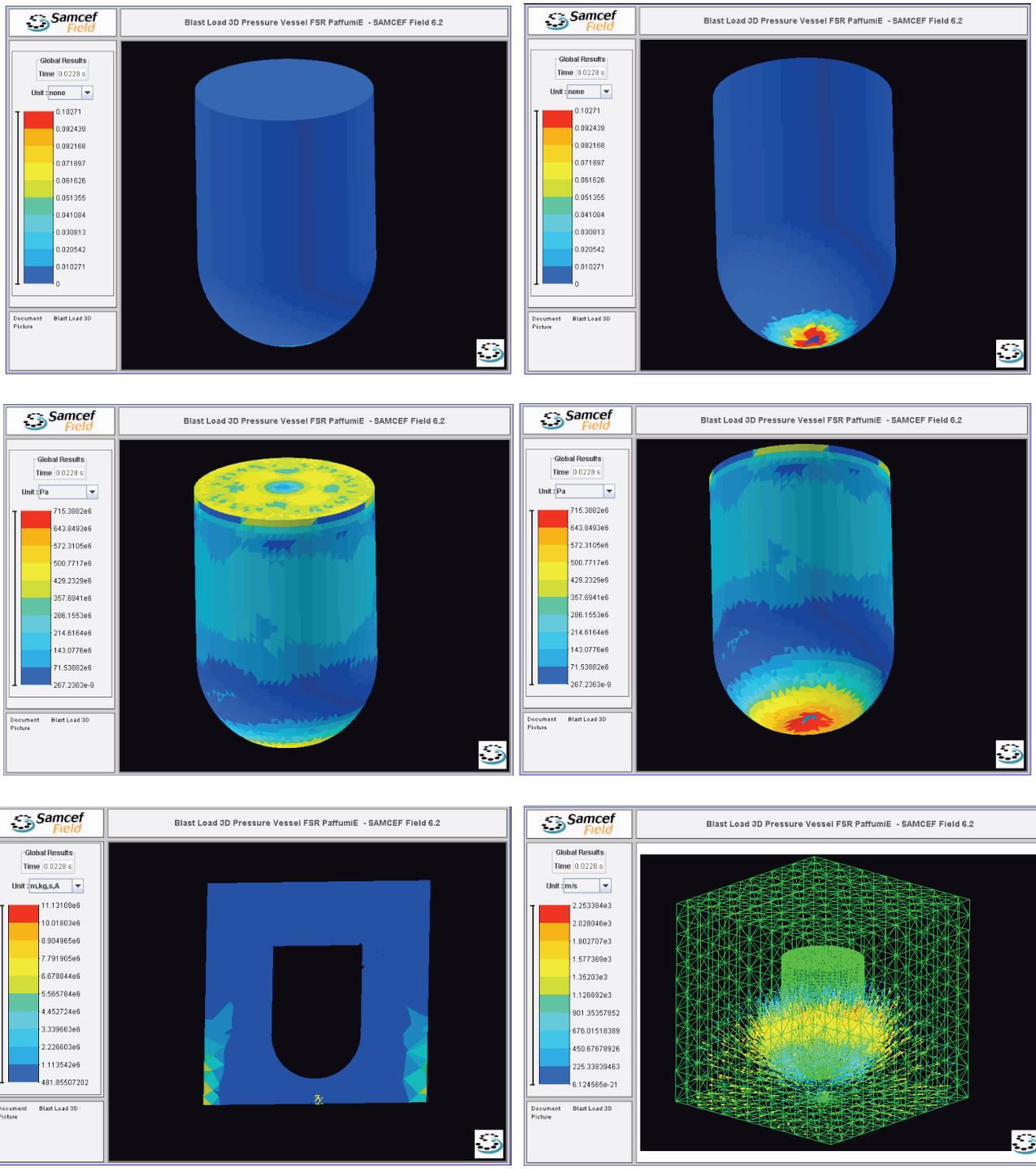

928 kg of explosive material
Equivalent Plastic Strain and Equivalent Stress
Pressure and Nodal Speed: 0.0228sec (explosion starts at 20msec)

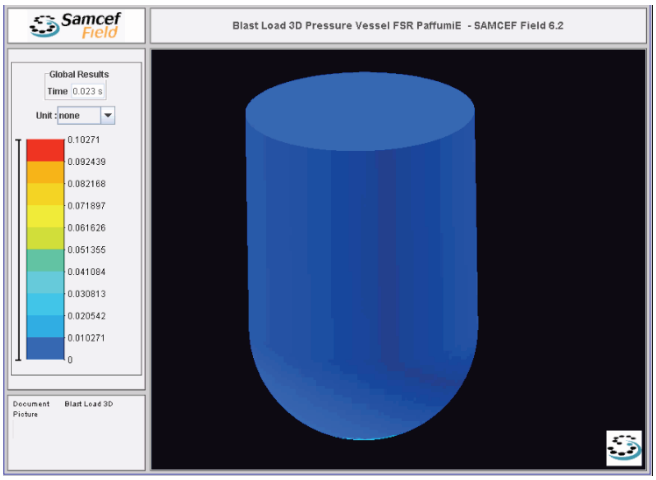

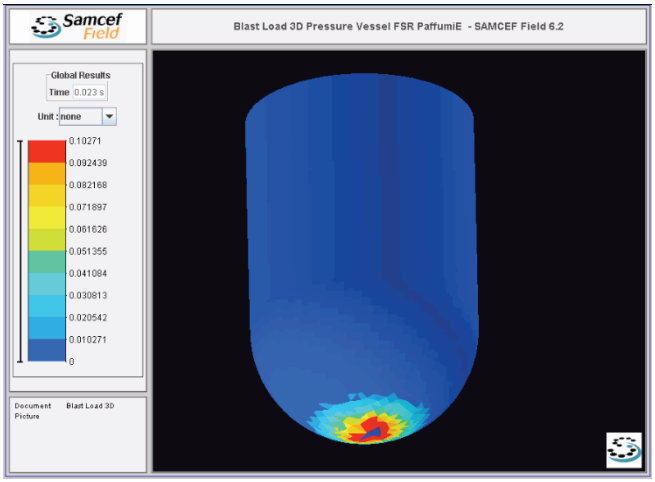

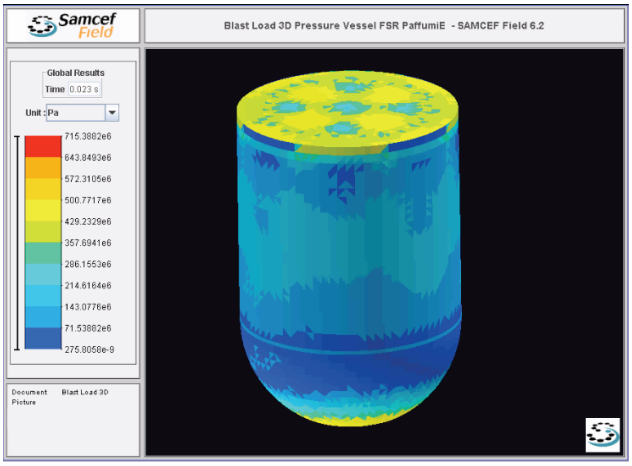

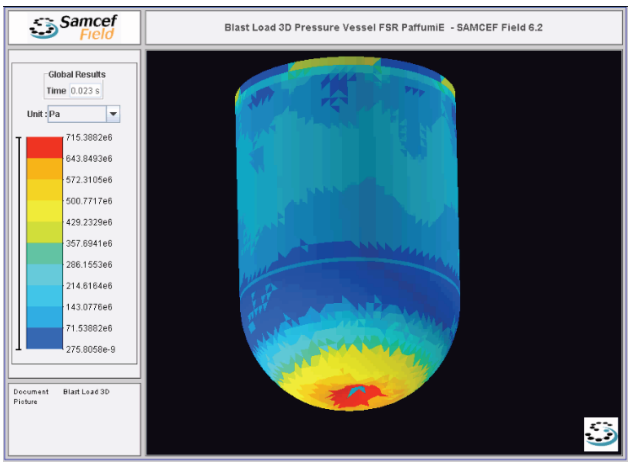

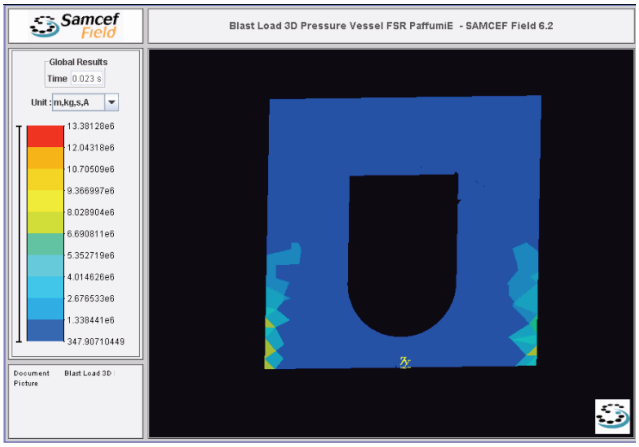

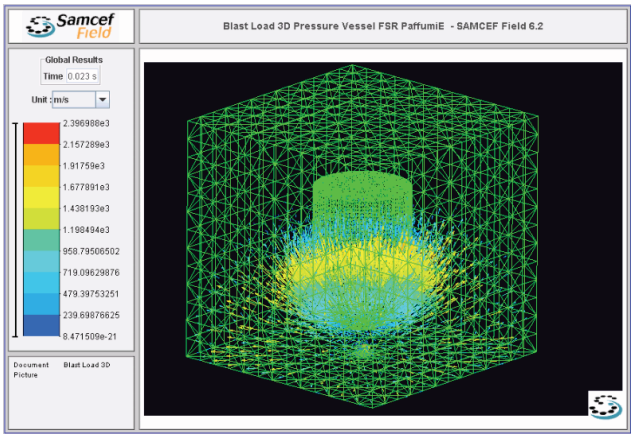

928 kg of explosive material
Equivalent Plastic Strain and Equivalent Stress
Pressure and Nodal Speed: 0.023sec (explosion starts at 20msec)

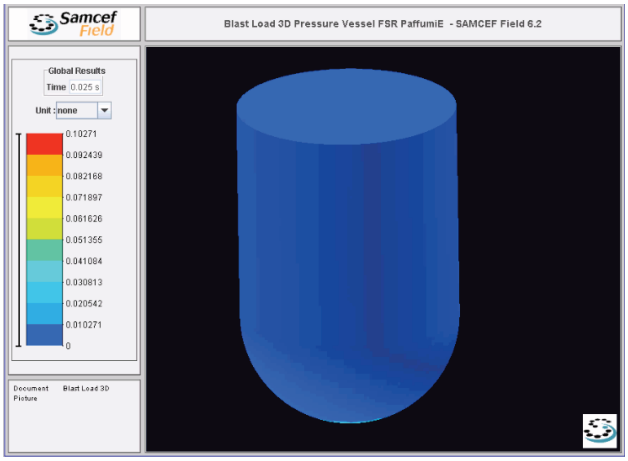

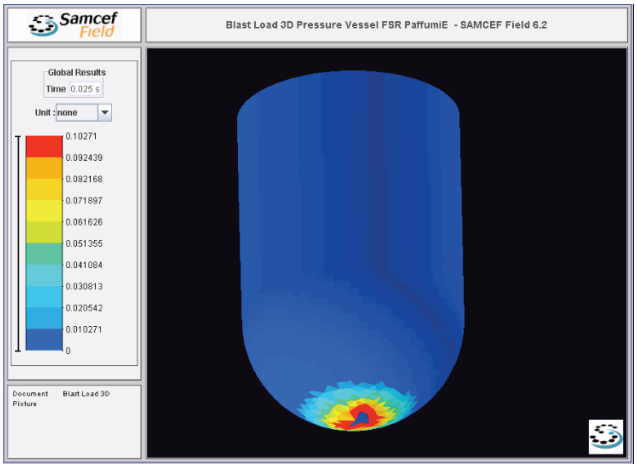

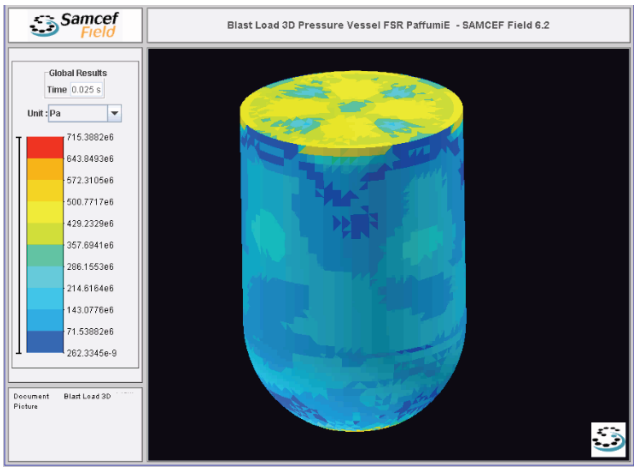

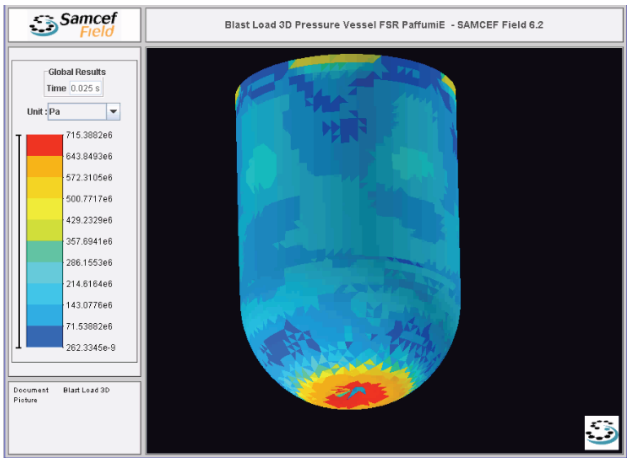

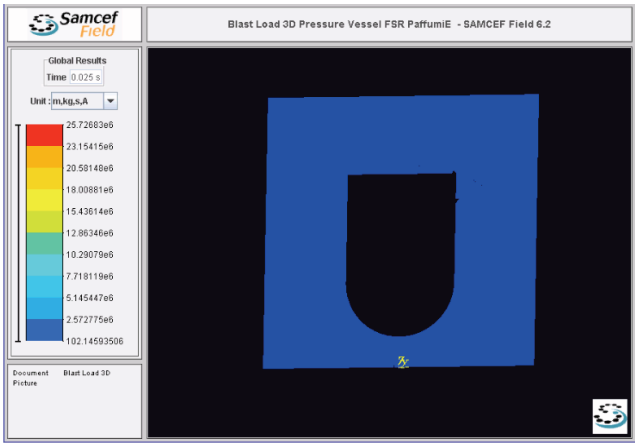

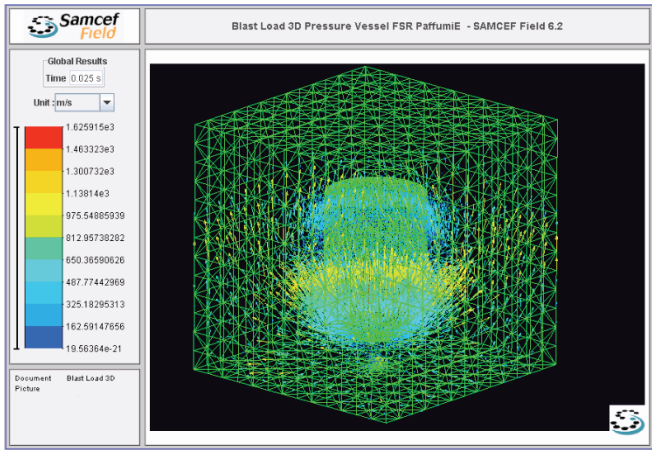

928 kg of explosive material
Equivalent Plastic Strain and Equivalent Stress
Pressure and Nodal Speed: 0.025sec (explosion starts at 20msec)

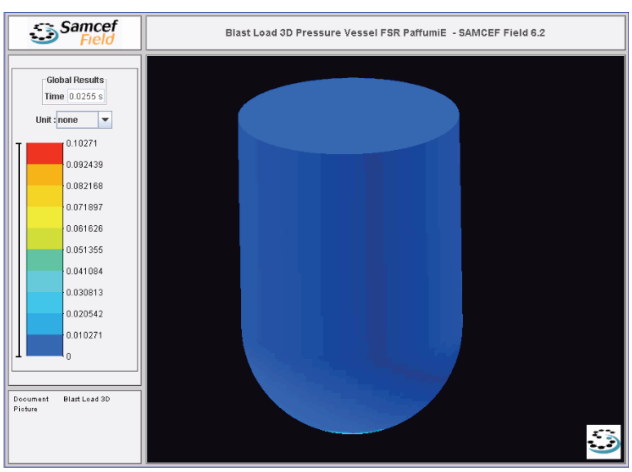

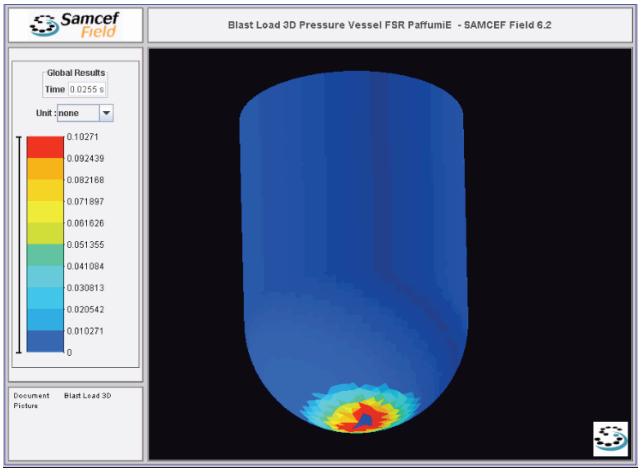

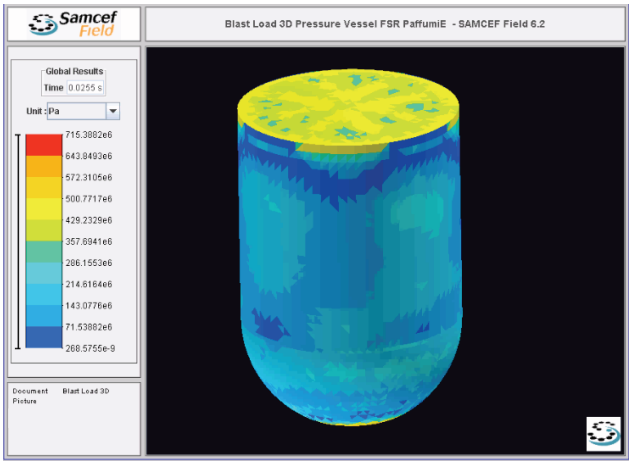

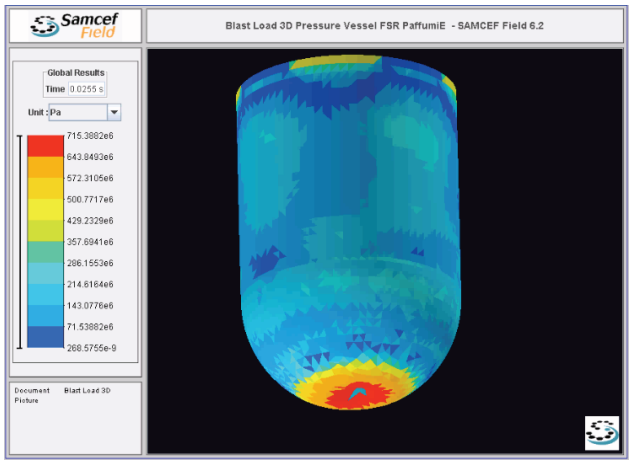

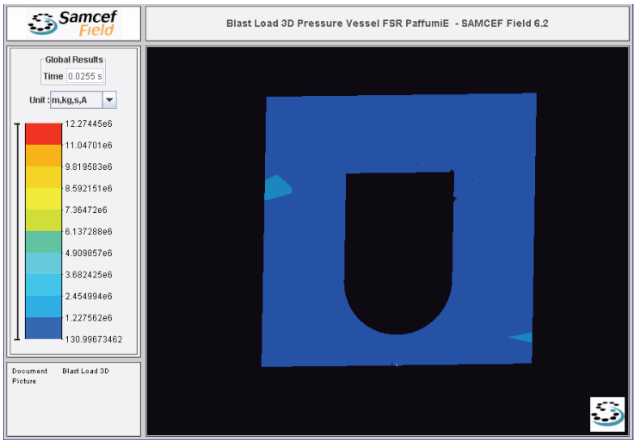

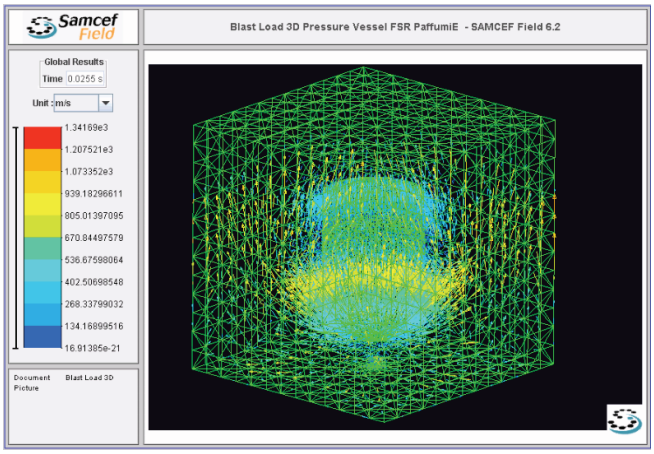

928 kg of explosive material
Equivalent Plastic Strain and Equivalent Stress
Pressure and Nodal Speed: 0.0255sec (explosion starts at 20msec)

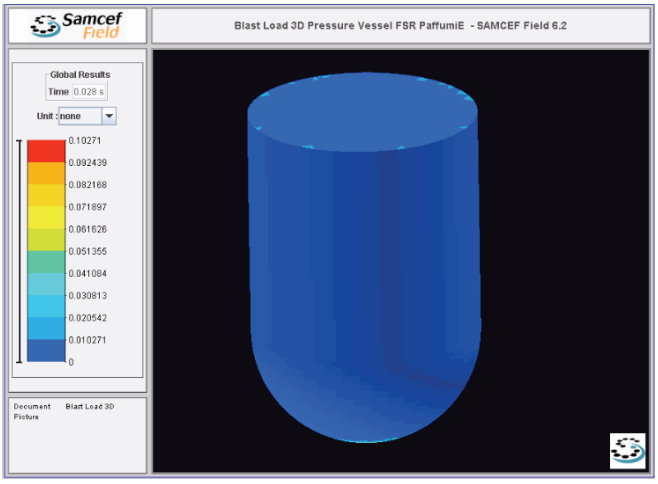

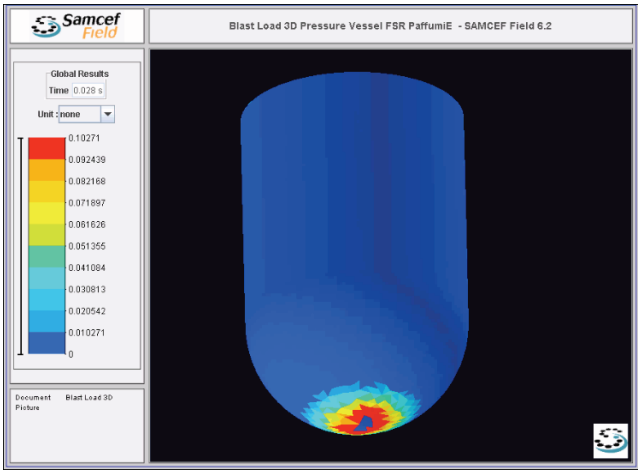

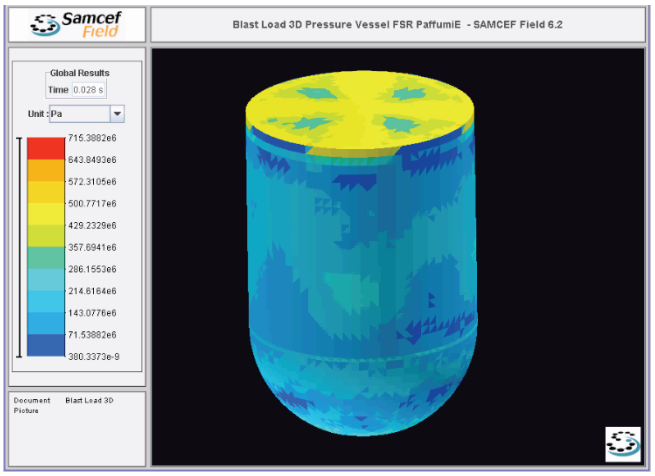

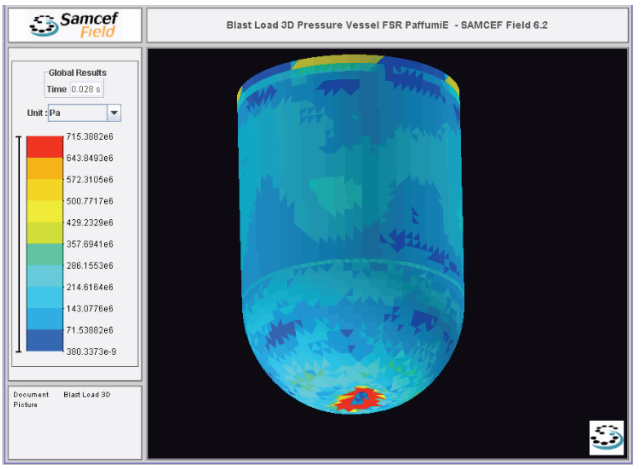

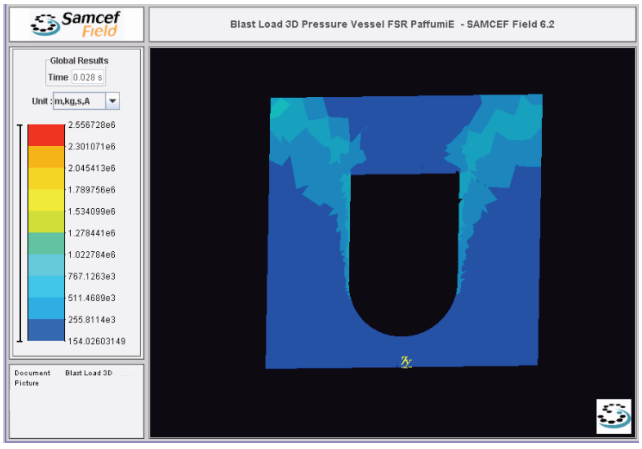

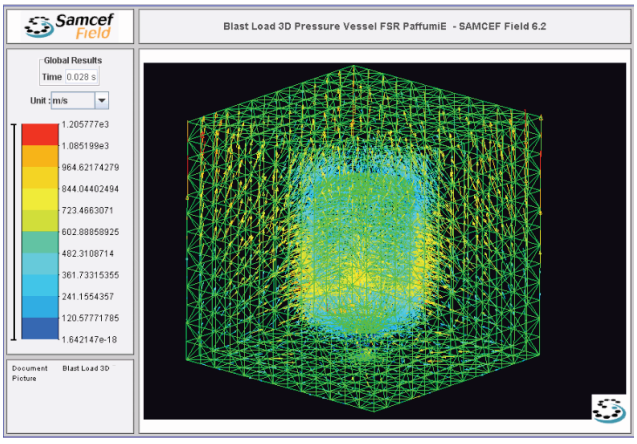

928 kg of explosive material
Equivalent Plastic Strain and Equivalent Stress
Pressure and Nodal Speed: 0.028sec (explosion starts at 20msec)

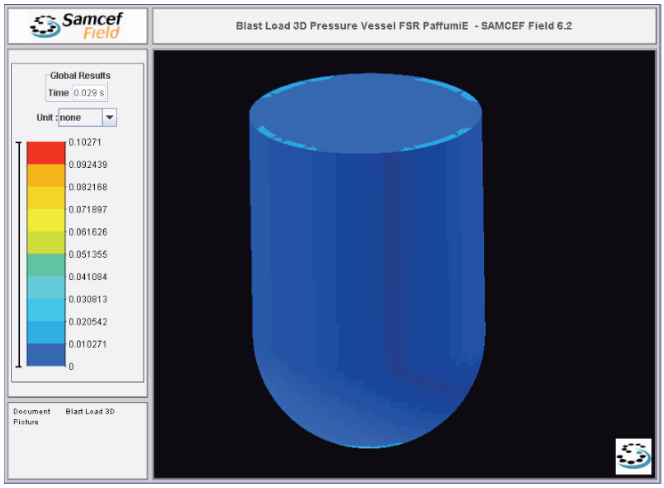

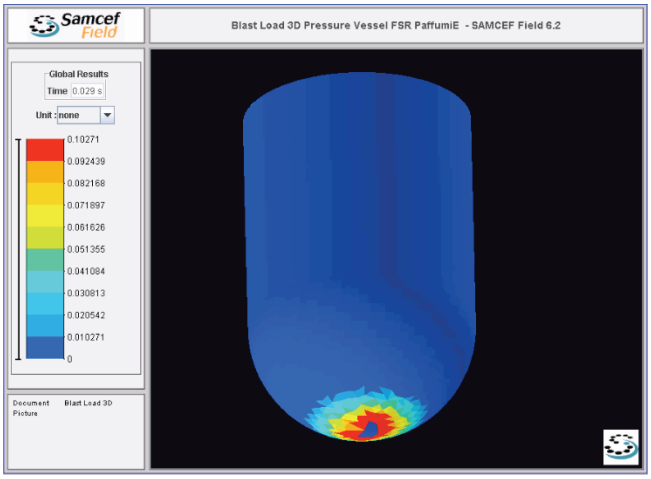

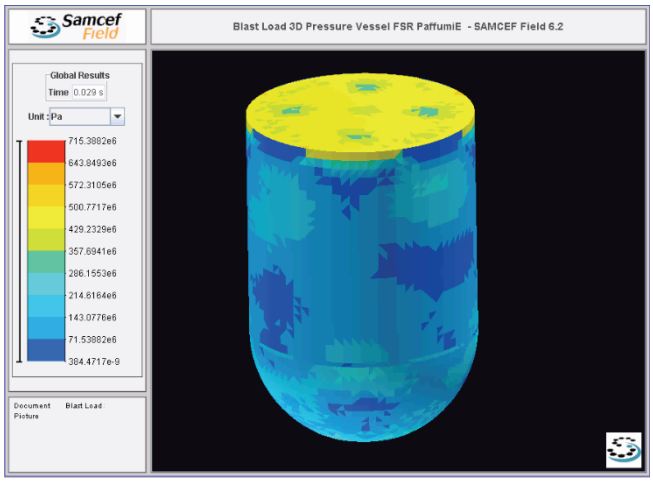

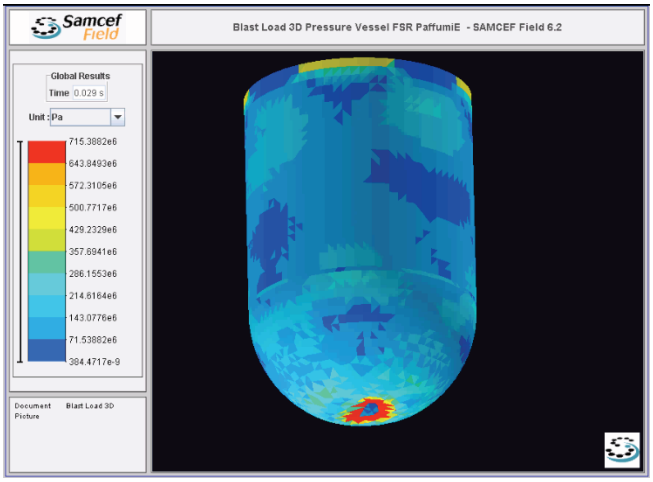

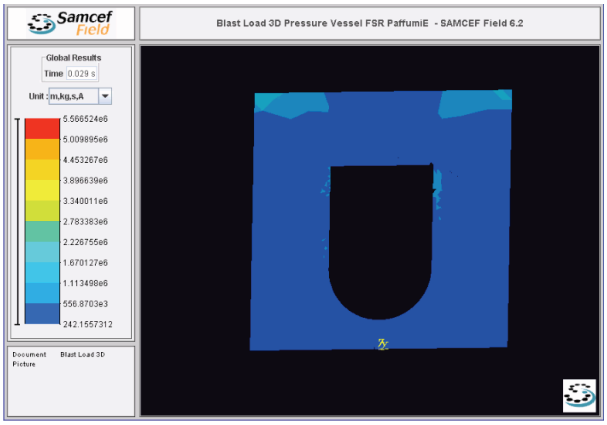

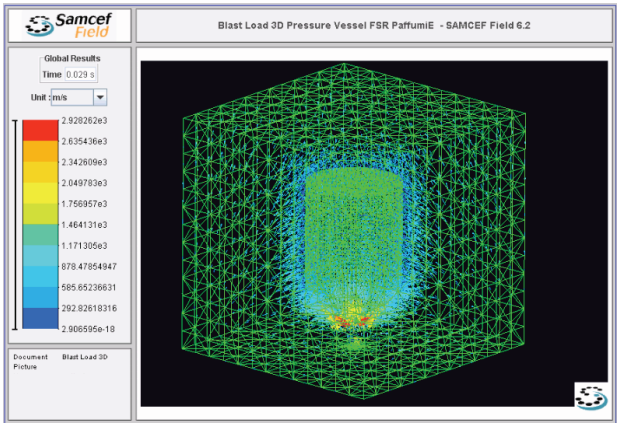

928 kg of explosive material
Equivalent Plastic Strain and Equivalent Stress
Pressure and Nodal Speed: 0.029sec (explosion starts at 20msec)

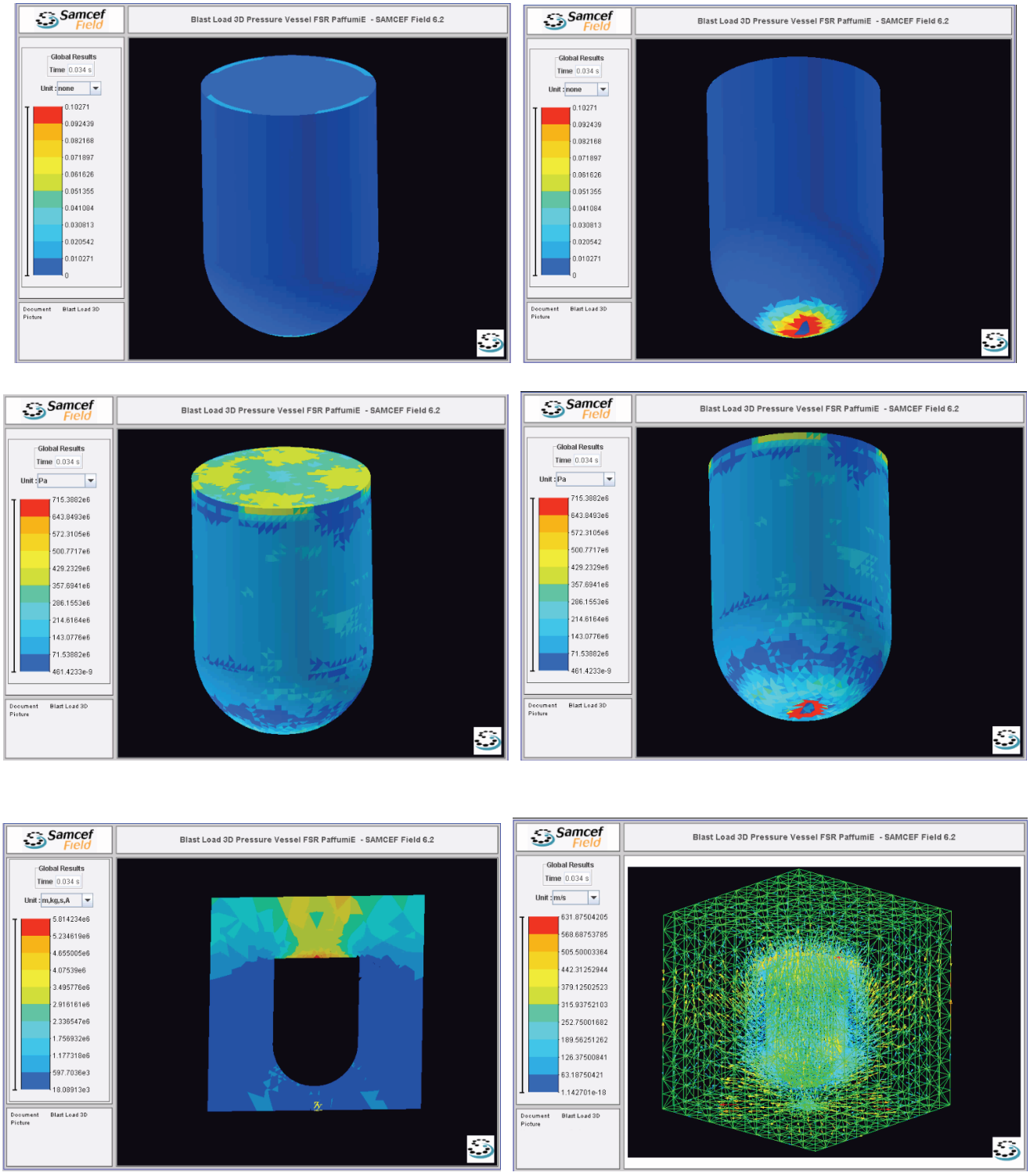

928 kg of explosive material
Equivalent Plastic Strain and Equivalent Stress
Pressure and Nodal Speed: 0.034sec (explosion starts at 20msec)

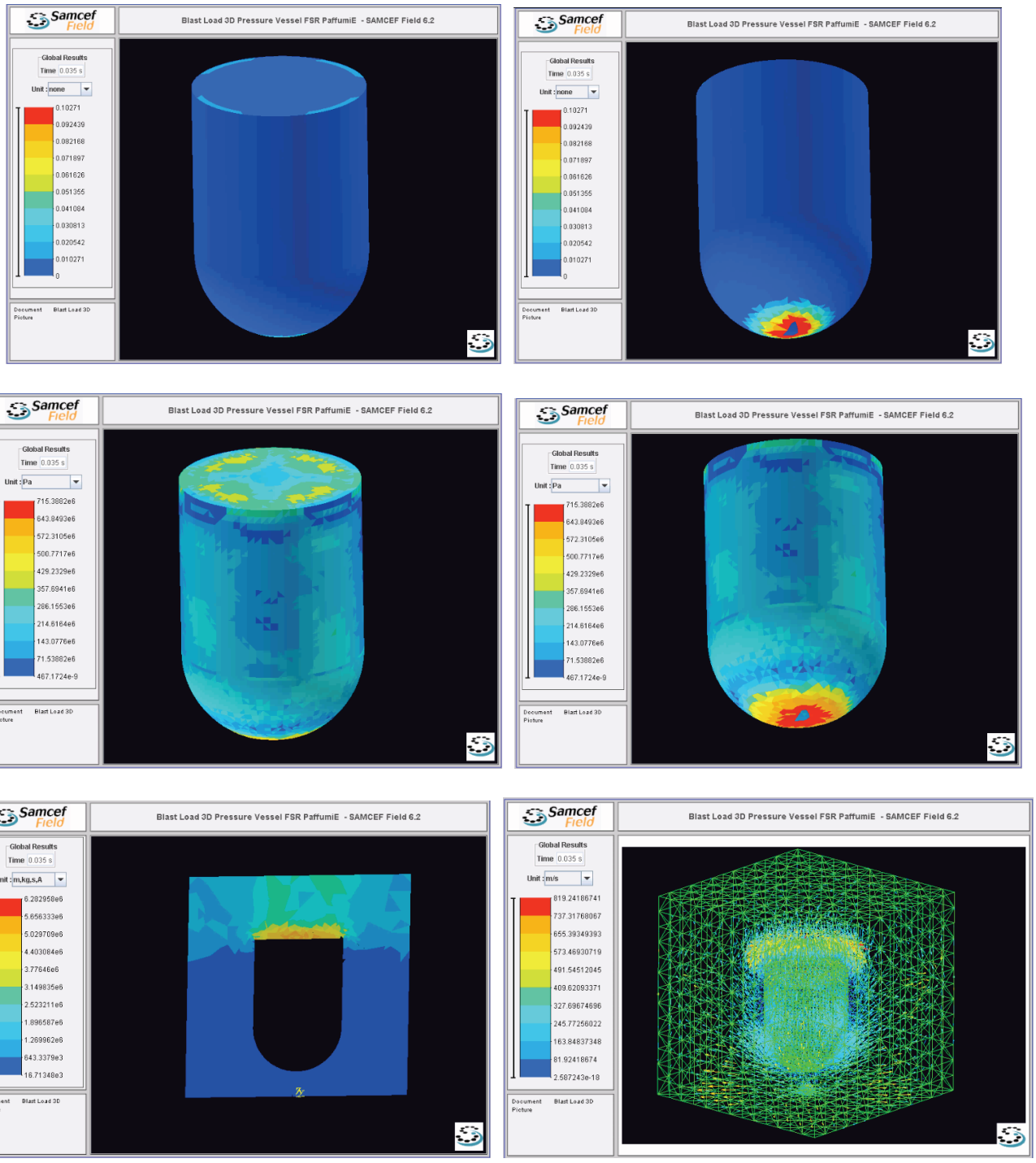

928 kg of explosive material
Equivalent Plastic Strain and Equivalent Stress
Pressure and Nodal Speed: 0.035sec (explosion starts at 20msec)

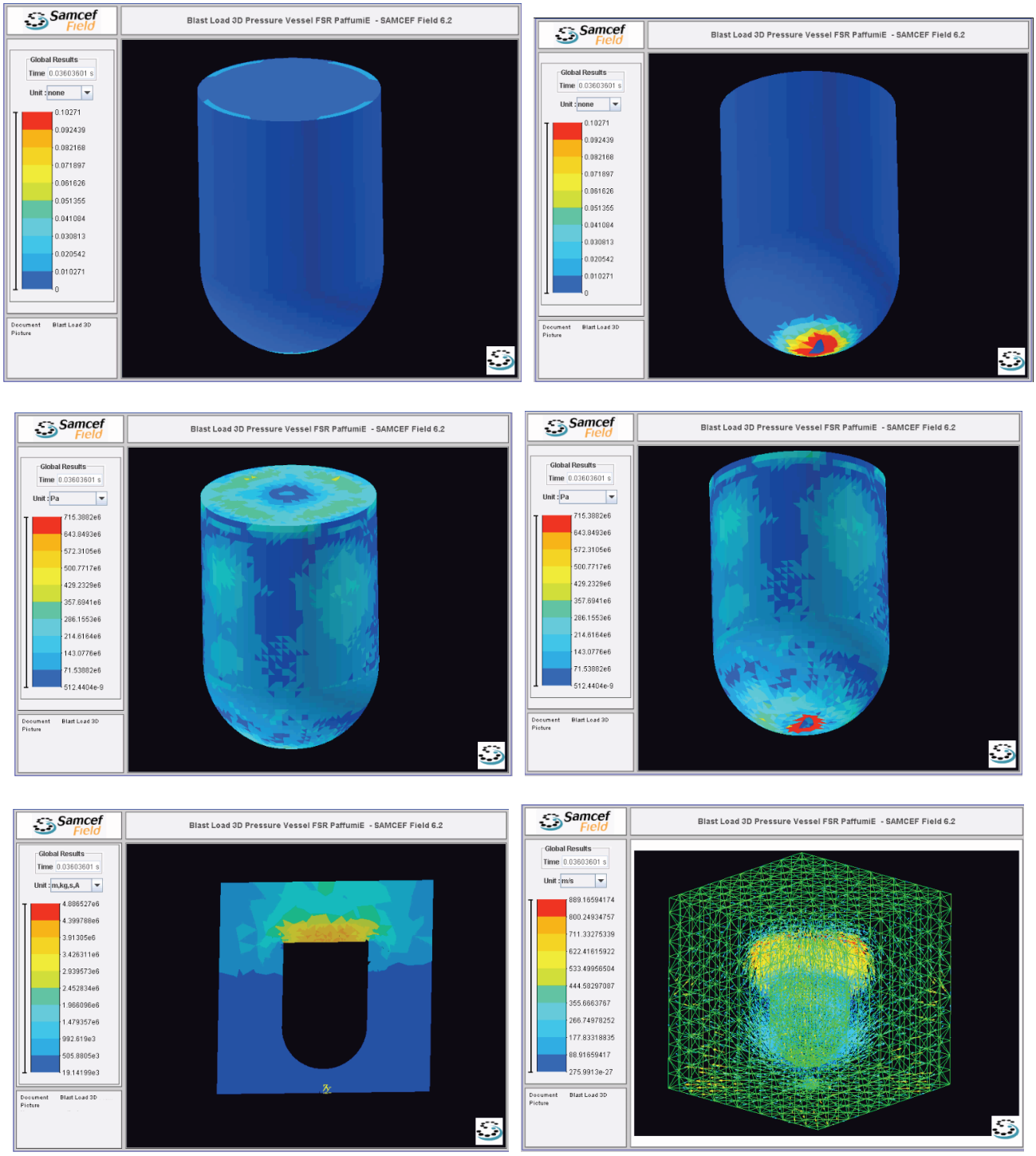

928 kg of explosive material
Equivalent Plastic Strain and Equivalent Stress
Pressure and Nodal Speed: 0.036sec (explosion starts at 20msec)

7 REFERENCES

1. EUROPLEXUS 2007, EUROPLEXUS documentation, A Computer Program for the Finite Element Simulation of Fluid Structure Systems under Transient Dynamic Loading, USER'S MANUAL Version 2007, CAE-DG JRC
2. SAMCEF-FIELD 6.2, 2007
3. Hibbit, Karlson and Sorensen ABAQUS/Standard - Explicit Version 6.6-1 - User's manual, Inc.
4. Elena Paffumi, Nigel Taylor, Structural Response of a Large Pressure Vessel to Dynamic Loading - Feasibility of Fast Transient Dynamic Analysis Methods, European Commission Scientific and Technical Report, DG JRC IE, Dec 2007, Petten, The Netherlands
5. B. Luccioni, D. Ambrosini, R. Danesi, Blast load assessment using hydrocodes, Engineering Structures, Vol. 28, p. 1736-1744, 2006
6. NESC IV Project - Supporting Clad & SA533B-1 Base Material Tensile Data, EC DG JRC IE, 2003
7. Cowper G. R. and Symonds P. S., Strain hardening and strain-rate effects in the impact loading of cantilever beams, Brown University Division of Applied Mathematics Report N.28, September, 1957
8. Symonds P. S., Survey of Methods of Analysis for Plastic Deformation of Structures under Dynamic Loading, Brown University, Division of Engineering Report BU/NSRDC/1-67, June, 1967
9. ASME Nuclear Boiler and Pressure Vessel Code – Section VIII, Division 1, 2004
10. Minnebo Philip, Strain-rate dependent tensile properties for the analysis of the structural response of a pressure vessel to a blast event, JRC Technical Notes, 2007 JRC41364
11. G.R. Johnson, W. H. Cook, A Constitutive Model and Data for Metals Subjected to Large Strains, High Strain Rates and High Temperatures, 7th International Symposium on Ballistics, 1983
12. Tuler R., Butcher B. M, A criterion for time depende of dynamic fracture, Int. Journal of Fracture Mechanics, Vol. 4, 1968, pp. 431-437
13. Baker WE, Cox PA, Westine PS, Kulesz JJ, Strehlow RA. Explosion hazards and evaluation. Amsterdam: Elsevier; 1983.
14. Kinney GF, Graham KJ. Explosive shocks in air. 2nd ed. Berlin: Springer Verlag; 1985.
15. Smith PD, Hetherington JG. Blast and ballistic loading of structures. Great Britain: Butterworth-Heinemann Ltd; 1994.
16. Young L. A., Streit B. K., Peterson K. J. Read D. L., Maestas F. A., "effectiveness/vulnerability assessment in three dimensions (EVA-3D), Versions 4.1F and 4.1C User's manual, Rev. A, Wright Laboratory, U.S. Air Force, Nov. 29, 1995
17. Baker WE, Cox PA, Westine PS, Kulesz JJ, Strehlow RA. Explosion hazards and evaluation, Amsterdam: Elsevier; 1983.
18. Smith PD, Hetherington JG. Blast and ballistic loading of structures. Great Britain: Butterworth-Heinemann Ltd; 1994
19. Schleyer Graham K., Structural Impact, Notes to the course on Structural Impact, Wessex Institute of Technologies, Oct. 2006
20. Ambrosini Daniel, Luccioni Bibiana, Jacinto Abel, Danesi Rodolfo, Location and mass of explosive from structural damage, Eng. Structures, 27, 2005, pp. 167-176
21. Forrestal M. J. and Sagartz M. J., Elastic-plastic response of 304 stainless steel beams to impulse loads, Journal of Applied Mechanics, 45, 685-7,1978
22. Formby S.A, Wharton R. K., Blast characteristics and TNT equivalence values for some commercial explosives detonated at ground level, Journal of Hazardous Materials, 1996, 50:184-98
23. Smith P. D., Rose T. A., Saotonglang E., Clearing of blast waves from building facades, Proceedings of Institution of Civil Engineers, Structures & Buildings, 1999 , 134:193-9

24. MacPherson W.N., Gander M. J., Barton J. s., Jones J. D.C., Owen C.L., Watson A.J. et al., Blast pressure measurement with high bandwidth fibre optic pressure sensor, Measurement Science and Technology 2000, 11:95-102

8 APPENDIX A

EUROPLEXUS JWLS equation: comparison with other computational literature results

The work of Luccioni et al [5] has been used to check and calibrate the results obtained using EUROPLEXUS[2]. This preliminary study has been useful also for estimating mesh size effects when using the JWL/JWLS equation for blast load simulations. It is well known that the accuracy of numerical results is strongly dependent on the mesh size. On the other hand, the mesh size is also limited by the dimensions of the model and the available computer capacity.

In reference [5] the analysis of the blast wave propagation was performed in two stages. In the first part the simulation of the explosion itself from the detonation instant was addressed, while the second part considered the propagation of the blast wave generated by the explosion. The mass of the explosive is defined by TNT masses. The corresponding masses for other explosives can be obtained through the concept of TNT equivalence [21]. During the present study a charge of around 100 kg of TNT has been used.

A box of 4m by 5 m by 10 m was numerically modelled with different mesh sizes (0.05m, 0.1m and 0.25 m) to study the free propagation of blast waves, Figure 88. To simulate a free field explosion, air was allowed flow out of all the model borders.

In reference [5] the initial detonation and expansion of the sphere of high explosive were modelled in a 1D, spherically symmetric model of 1 m radius with a JWL equation of state. To avoid numerical errors partway through the detonation process the material model for the high explosive was modified. The 1D expansion analysis continued until just prior to impingement of the blast wave on the rigid surface. At this time a 1D remap file was created and then imported into a three-dimensional model, allowing the reflection of the blast wave off the ground and walls to be modelled. In EUROPLEXUS, there is no spherical symmetry, only axisymetrical symmetry. So, 2D axisymetrical symmetry was used, assuming that the axial dimension is long enough not to be dominant in the computation. Considering that the mass of TNT is 100 kg, the density is 1630 kg/m3, then the radius described by the sphere of TNT is 0.245 meters. During this work the bubble was designed with a circular shape Figure 89 a) and b). There is a small transition towards a rectangular domain and then the rest of the mesh is rectangular Figure 89b). With this approximation the final mass of the TNT bubble is 106kg. The mesh size tested is the one along the x axis. It should be noted that the modelling of the fluid domain is Eulerian, which is less accurate than in a sophisticated hydrodynamic code but better for estimating loads on structures; the interaction between fluid and deformable structures is better treated.

There are differences between the modelling of the generation of the blast loading in [5] and in the current work. These concern the mesh building and some computational options. Quadratic damping (option amor quad 0.2) has been added in EUROPLEXUS analysis. Without this option there was a problem of convergence, not in the wave front but in the domain just after the wave front that is in compression (while the bubble is growing the problem occurs inside the bubble but not at the boundary where the pressure is maximum). The bubble domain was declared Eulerian to avoid rezoning in this domain.

The most common approach for blast wave scaling is Hopkinson's law [13], which establishes that similar explosive waves are produced at identical scaled distances when two different charges of the same explosive and with the same geometry are detonated in the same atmosphere. Any distance R from an explosive charge W can be transformed into a characteristic scaled distance Z,

[2] The EUROPLEXUS computations for this section have been performed by A. Cheruet from Samtech SA.

$$Z = \frac{R}{W^{1/3}} \tag{32}$$

when W is the charge mass expressed in kilograms of TNT. In reference [5] the results of the 1D analysis of explosive spherical charges ranging from 1 to 500 kg were mapped in the 3D air models at point P with coordinates x = y = z = 2.5 m, indicated with a star in Figure 88 and representing the location of the explosive charge.

Figure 90 shows the time history of the pressure obtained for point A with coordinates x=5.5 m, y = z = 2.5 m, located at 3 m from the 100 kg of TNT explosive charge. In particular, Figure 90a) in from [5], while Figure 90b) shows the results of the current work. It can be seen that there are significant differences between the peaks overpressures obtained for the different mesh sizes. As the mesh is refined, the difference between the results for the different mesh sizes is reduced. It must be noted also that the results obtained with EUROPLEXUS are in rather good agreement with those of the literature reference. Some time delay is present in pressure values from the current work compared to [5]. This refers to an element where the integration point is located exactly 3.025 meters from the centre of the source, but this does not fully explain the difference. Another factor may be the nature of the model at the initial time. In the current case, a realistic volume of the solid phase is modelled and at the initial time this solid part becomes a gas. However since the JWLS option is used, the complete reaction is activated when all the elements of the solid part are activated and only soon after this does the shock wave propagate. So there is a delay time from the moment where the reaction starts at the ignition point and the moment when the reaction has reached all the solid elements. After this, the reaction starts around the explosive bubble. The JWLS model in fact accounts for the propagation of the detonation (at a constant velocity specified by the user) across the solid material starting from an ignition point (also specified by the user). The detonation of each finite element is triggered when the detonation wave (travelling spherically from the ignition point at a constant speed D) reaches the centre of the element. The JWL material model instead assumes that the (solid) explosive detonation is instantaneous and takes place at the same instant in the whole explosive charge. Therefore by using JWL equation instead of JWLS the delay could probably be avoided.

Numerical results for the peak overpressure relative to the ambient pressure, *Ps/Po*, are compared with those obtained with empirical equations [14,15] and by [5] in Figure 91 for different scaled distances, Z, from the explosive charge. In [5] the numerical values are obtained for different points along the line defined by y = z = 2.5 m and are indicated in Figure 88 for different mesh sizes. For EUROPLEXUS only the results obtained with the finer mesh of 5 cm are reported. These are in good agreement with the literature data, especially for low scaled distance values. The literature results [5] better follow the trend predicted by empirical equations at the high-scaled distances. As the scaled distance increases, numerical results depart from empirical ones. In [5] it was noticed that the accuracy of empirical relations in the near field is not guaranteed [15].

The difference with empirical values is more evident for coarser meshes that give lower values for the peak overpressure, but results tend to converge as the mesh is refined. The results for the meshes of 5 and 10 cm are almost coincident in Figure 90. It can be concluded that the mesh of 10 cm gives an accurate solution to the problem, as reported in several other references.

A comparison of the maximum peak overpressures obtained with the finest mesh ftom reference [5], the current work with EUROPLEXUS and experimental results [23,24] is presented in Figure 92. A good agreement among the results is observed, especially for low scaled distance values.

The third part of the reference [5], dealing with the reflection of the pressure waves on surfaces with different incidence angles has not been studied with EUROPLEXUS during this work.

It is possible to draw some conclusions. The accuracy of the numerical results is strongly dependent on the mesh size used for the analysis. A 10 cm mesh is accurate enough for the analysis of wave propagation in open environments. Nevertheless it may be too expensive to model a complete urban block with this mesh size. Alternatively, a coarser mesh can be used in order to obtain qualitative results for comparison of the loads produced by different hypothetical blast events. From [5] it is possible to see that the difference between numerical results for different mesh size increases with decreasing scaled distances. Even for the coarser mesh with a 50 cm element side, the results lie below

those obtained with empirical expressions (neglecting the multiple reflections that take part in actual situations).

Overall EUROPLEXUS has been found to reliably reproduce the values reported in Ref [5], those from empirical equations [14,15] and experimental data [23,24].

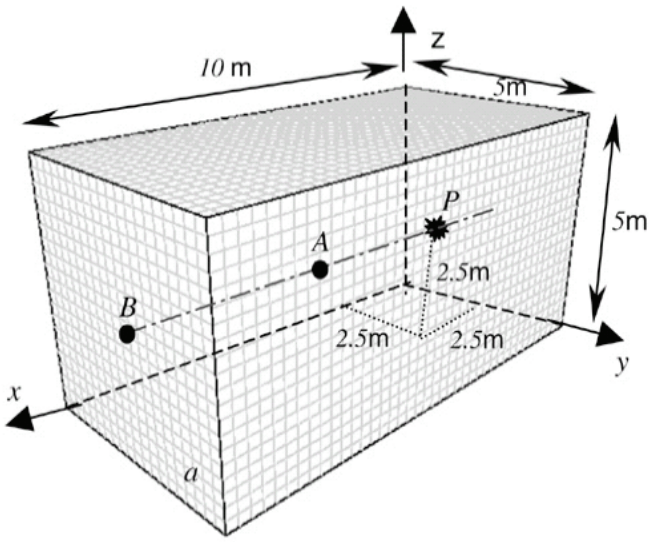

Figure 88 Geometry model for studying the blast wave propagation as taken from [5]. Point *P* is the reference location of the HE charge for the results.

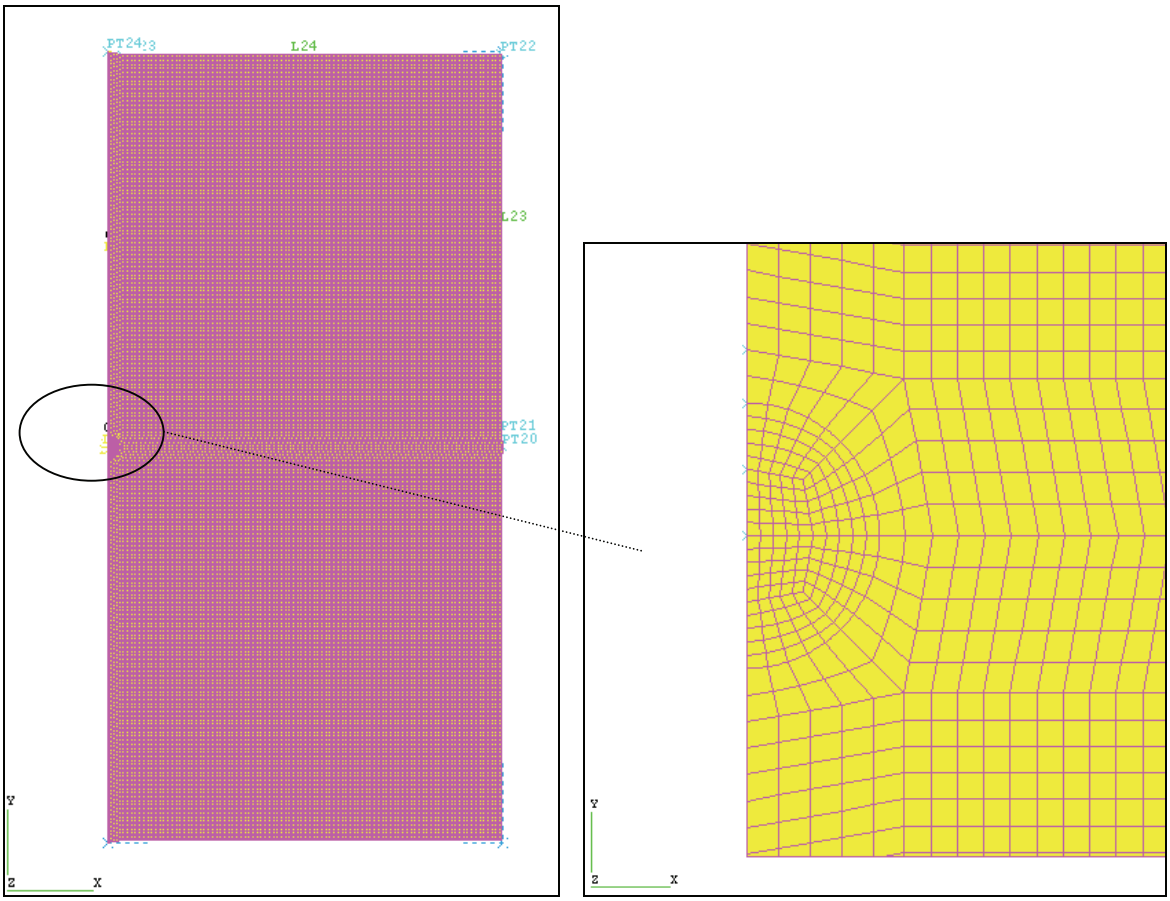

Figure 89 View of the complete mesh a) and detail of the explosive bubble b). Elements size: 0.05m [A. Cheruet, Samtech SA].

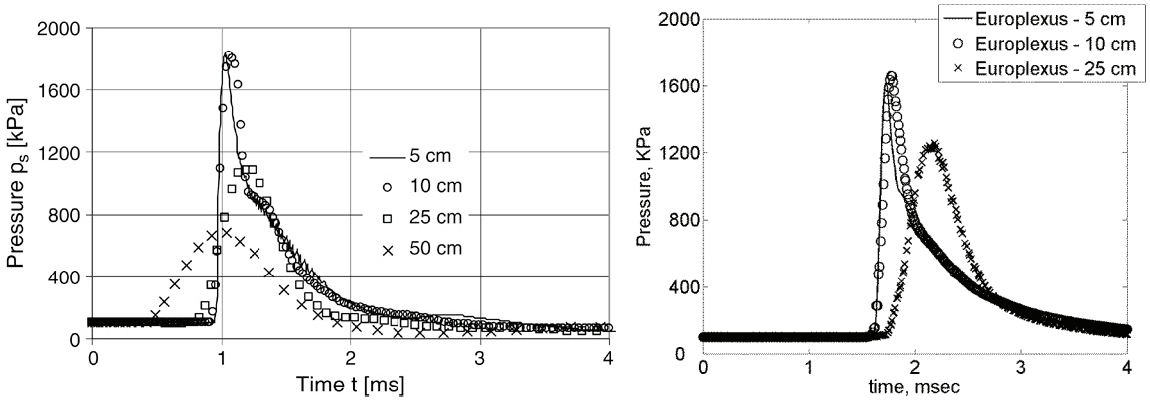

a) b)

Figure 90 Pressure time history for different mesh size a) ref [5] and b) current work [EUROPLEXUS analysis A. Cheruet, Samtech SA] at point *A* (see fig. 12).

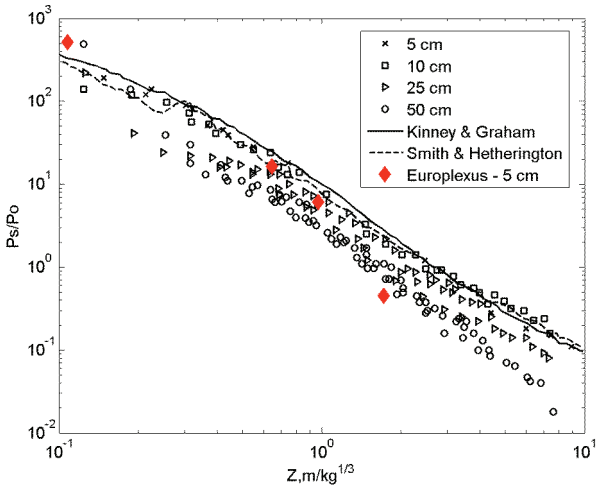

Figure 91 Peak side-on overpressures as a function of scaled distance [EUROPLEXUS analysis A. Cheruet, Samtech SA and [5,14,15] data].

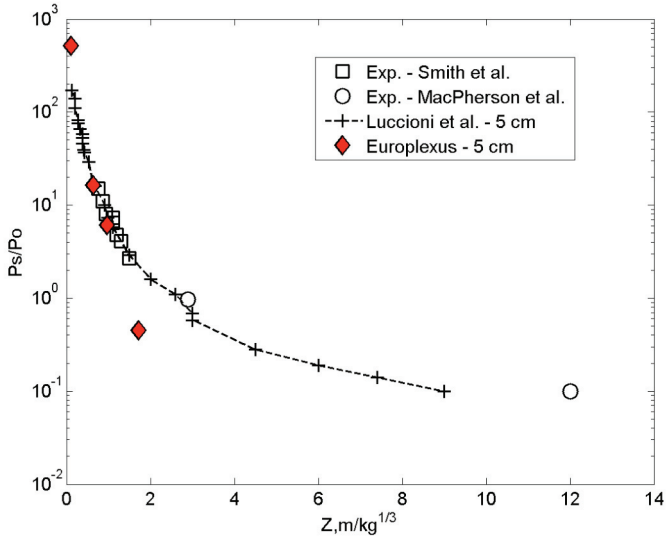

Figure 92 Comparison of numerical and literature experimental values [5,23,24] of peak overpressure [EUROPLEXUS analysis A. Cheruet, Samtech SA].

9 APPENDIX B

The epilogues used during these works are the following.

JWL 3D model – FSR boundary (CEA elements)

```
.hyp group "tank" mindlin
.hyp group "ALE_CELLS" volume
.ael group "ALE_CELLS"  ng 1 1 1
.php group "THICK_162" thick val 0.162
.php group "THICK_200" thick val 0.200
.php group "THICK_125" thick val 0.125

!.ael group "tank" orde 1
.ael group "bubble" orde 1
.ael group "air" orde 1
.ael group "water" orde 1

.FCT CRE FONCTION NOM "F_Harden"
    CRE VAL Y U
    COUPLES
          0.00E+00        4.63E+08
          3.00E-04        4.78E+08
          5.00E-04        4.72E+08
          8.00E-04        4.71E+08
          1.10E-03        4.72E+08
          1.30E-03        4.72E+08
          1.60E-03        4.73E+08
          1.80E-03        4.74E+08
          2.10E-03        4.74E+08
          2.40E-03        4.74E+08
          2.60E-03        4.74E+08
          2.70E-03        4.73E+08
          3.20E-03        4.74E+08
          […]

.MAT NOM "M_Plastic"
    BEHAV "Plastic"
    YT 206.058e09
    NT .3
    M 7800
    VONM
    XIT 1. NF "F_Harden"
    CAUC
.ael group "TANK" mat "M_Plastic"


.MAT NOM "WATER"
   BEHAV "FLUID"
   RO 983.2
   C 1500
   PINI 15.5E06
   PREF 0.E06
.ael group "WATER" mat "WATER"

.FSI
 FSA  group "NODE_FSI"
 FSR  group "NODE_FSR"
 LAGR group "LAGRANGIAN_NODES"
 ALE  group "ALE_CELLS"
```

```
.MOD MAILLE
 ATT 2 group "TANK"
 ATT 3 group "WATER"
 ATT 4 group "AIR" "BUBBLE"

.clm fix group "noe-fix "comp 1 2 3 4 5 6
.sai arch noe i 25078 styp 9163 9173 comp 1 2 3
.sai arch ele i 32898 styp 9671 comp 1 2 3

.sai arch noe i 26787 styp 9163 9173 comp 1 2 3
.sai arch noe i 26786 styp 9163 9173 comp 1 2 3
.sai arch noe i 25115 styp 9163 9173 comp 1 2 3

.sai arch ele i 26507 styp 9390 9391 9392 comp 1
.sai arch ele i 26523 styp 9390 9391 9392 comp 1
.sai arch ele i 26573 styp 9390 9391 9392 comp 1

.sai arch ele i 26507 styp 9380 9381 9382 comp 1
.sai arch ele i 26523 styp 9380 9381 9382 comp 1
.sai arch ele i 26573 styp 9380 9381 9382 comp 1

! new group pressure history
!
.sel group "ele-pression" maille
 38718 38719 38720 38721 38722 38697 38692
 38603 38604 38605 38606 38607 6347

.sai arch group "ele-pression" styp 9339 comp 1


.EPX
MATERIAU
* air: calculated for 1bar
*
   jwls   a 3.738e11   b 3.747e9   r1 4.15   r2 0.90
          omeg 0.35    ros 1630    BETA 0.03
          ro  1.3      pini 1e5    eint 0.21978e6   pref 0.E05
            LECT group "AIR"  TERM
*
**  TNT :
*
   jwls   a 3.738e11   b 3.747e9   r1 4.15   r2 0.90
          omeg 0.35    d 6930      BETA 0.03
          ro   1630   pini 1e5     eint 3.68e6      pref 0.E05
          xdet 0. ydet 0. zdet 0.07142857
            LECT group "BUBBLE" TERM
*
OPTION
 CSTA 0.4
 DTDROP 0.002
 AMOR QUAD 2
CALCUL
 PAS1 1.E-08
```

JWL 3D model – FSR boundary (JRC elements)

```
.hyp group "Vessel_el" mindlin
.hyp group "Water_el"  volume
.hyp group "Air_el"   volume
.hyp group "Bubble_el"   volume
.ael group "Water_el"  ng 1 1 1
.ael group "Air_el"   ng 1 1 1
.ael group "Bubble_el"   ng 1 1 1
```

```
.php group "THICK_162" thick val 0.162
.php group "THICK_200" thick val 0.200
.php group "THICK_125" thick val 0.125

!.ael group "Vessel_el" orde 1
.ael group "Bubble_el" orde 1
.ael group "Air_el" orde 1
.ael group "Water_el" orde 1

.FCT CRE FONCTION NOM "F_Harden"
    CRE VAL Y U
    COUPLES
          0.00E+00        4.63E+08
          3.00E-04        4.78E+08
          5.00E-04        4.72E+08
          8.00E-04        4.71E+08
          1.10E-03        4.72E+08
          1.30E-03        4.72E+08
          1.60E-03        4.73E+08
          1.80E-03        4.74E+08
          2.10E-03        4.74E+08
          2.40E-03        4.74E+08
          2.60E-03        4.74E+08
          2.70E-03        4.73E+08
          3.20E-03        4.74E+08
          […]
.MAT NOM "M_Plastic"
    BEHAV "Plastic"
    YT 206.058e09
    NT .3
    M 7800
    VONM
    XIT 1. NF "F_Harden"
    CAUC
.ael group "Vessel_el" mat "M_Plastic"

.FSI
 FSA  group  "FSI_WATER" "FSI_AIR"
 FSR  group  "FSR_NODES" "BUBBLE_FSR"
 LAGR group  "Vessel_n"
 ALE  group  "Water_el" "Air_el" "Bubble_el"

.MOD MAILLE
 ATT 2 group "Vessel_el"
 ATT 3 group "Water_el"
 ATT 4 group "Air_el" "Bubble_el"

.clm fix group "Clamped_n" comp 1 2 3 4 5 6

.sai ARCHIVE STYP 914 COMP 1 2 3 4 5 6 NOEUD I 671

.sai arch ele i 230758 styp 9671 comp 1 2 3
.sai arch ele i 230759 styp 9671 comp 1 2 3
.sai arch ele i 230760 styp 9671 comp 1 2 3
.sai arch ele i 230761 styp 9671 comp 1 2 3
.sai arch ele i 526000 styp 9671 comp 1 2 3

.sai arch group "N_near_clamp" styp 9163 comp 1 2 3
.sai arch group "N_near_clamp" styp 9173 comp 1 2 3
.sai arch group "N_near_clamp" styp 914 comp 1 2 3 4 5 6

.sai arch ele i 568 styp 9390 9391 9392 comp 1
.sai arch ele i 560 styp 9390 9391 9392 comp 1
```

```
.sai arch ele i 561 styp 9390 9391 9392 comp 1
.sai arch ele i 554 styp 9390 9391 9392 comp 1
.sai arch ele i 1063 styp 9390 9391 9392 comp 1

.sai arch ele i 6058 styp 9390 9391 9392 comp 1
.sai arch ele i 4922 styp 9390 9391 9392 comp 1
.sai arch ele i 6284 styp 9390 9391 9392 comp 1
.sai arch ele i 5361 styp 9390 9391 9392 comp 1
.sai arch ele i 5150 styp 9390 9391 9392 comp 1
.sai arch ele i 6592 styp 9390 9391 9392 comp 1

.sai arch ele i 7100 styp 9390 9391 9392 comp 1

.sai arch ele i 568 styp 9380 9381 9382 comp 1
.sai arch ele i 560 styp 9380 9381 9382 comp 1
.sai arch ele i 561 styp 9380 9381 9382 comp 1
.sai arch ele i 554 styp 9380 9381 9382 comp 1
.sai arch ele i 1063 styp 9380 9381 9382 comp 1

.sai arch ele i 6058 styp 9380 9381 9382 comp 1
.sai arch ele i 4922 styp 9380 9381 9382 comp 1
.sai arch ele i 6284 styp 9380 9381 9382 comp 1
.sai arch ele i 5361 styp 9380 9381 9382 comp 1
.sai arch ele i 5150 styp 9380 9381 9382 comp 1
.sai arch ele i 6592 styp 9380 9381 9382 comp 1

.sai arch ele i 7100 styp 9380 9381 9382 comp 1

! new group pressure history
!
.sel group "ele-pression" maille
 43135 49693 230758 230759 230760 230761 526000
 523115 523128 589243 588369 589066
  571110 553543 580451 580674 570238
  581880 582369 583185 583007

.sai arch group "ele-pression" styp 9339 comp 1

.EPX
MATE
** air: calculated for p=1bar
    flut ro 1.3 eint 0.21978e6 gamm 1.35 PB 0
        ITER 1 ALF0 1 BET0 1 KINT 0 AHGF 0 CL 0.5
        CQ 2.56 PMIN 0 PREF 1.e5 NUM 11
        a 3.738e11 b 3.747e9 r1 4.15 r2 0.90
        ros 1630
        LECT group "Air_el"  TERM

** TNT
*
    flut ro 1630 eint 3.68e6 gamm 1.35 PB 0
        ITER 1 ALF0 1 BET0 1 KINT 0 AHGF 0 CL 0.5
        CQ 2.56 PMIN 0 PREF 1.e5 NUM 11
        a 3.738e11 b 3.747e9 r1 4.15 r2 0.90
        d 6930 pini 1e5
        TDET 20e-3
        xdet 0. ydet 0. zdet 0.0730
            LECT group "Bubble_el"  TERM

    FLUT RO 1000 EINT 0 GAMM 2.1316E9 PB 22.8e6
        ITER 1 ALF0 0.5 RREF 1000 BET0 0
        KINT 1 AHGF 0 CL 0  CQ 0
        PMIN 0 NUM 9 PREF 1.E5
```

```
      LECT group "Water_el"  TERM

OPTION
 CSTA 0.4
 DTDROP 0.002
 AMOR QUAD 2
 NF34
  QUASI STATIQU 59 1 UPTO 20e-3 FROM 60e-3

CALCUL TINI 0 TEND 85e-3
 PAS1 1.E-8
```

JWL 3D model – ABSO boundary (JRC elements)

```
.hyp group "Vessel_el" mindlin
.hyp group "Water_el"  volume
.hyp group "Air_el"   volume
.hyp group "Bubble_el"   volume
.ael group "Water_el"  ng 1 1 1
.ael group "Air_el"   ng 1 1 1
.ael group "Bubble_el"   ng 1 1 1
.php group "THICK_162" thick val 0.162
.php group "THICK_200" thick val 0.200
.php group "THICK_125" thick val 0.125

!.ael group "Vessel_el" orde 1
.ael group "Bubble_el" orde 1
.ael group "Air_el" orde 1
.ael group "Water_el" orde 1

.FCT CRE FONCTION NOM "F_Harden"
    CRE VAL Y U
    COUPLES
          0.00E+00        4.63E+08
          3.00E-04        4.78E+08
          5.00E-04        4.72E+08
          8.00E-04        4.71E+08
          1.10E-03        4.72E+08
          1.30E-03        4.72E+08
          1.60E-03        4.73E+08
          1.80E-03        4.74E+08
          2.10E-03        4.74E+08
          2.40E-03        4.74E+08
          2.60E-03        4.74E+08
          2.70E-03        4.73E+08
          3.20E-03        4.74E+08
          […]

.MAT NOM "M_Plastic"
    BEHAV "Plastic"
    YT 206.058e09
    NT .3
    M 7800
    VONM
    XIT 1. NF "F_Harden"
    CAUC
.ael group "Vessel_el" mat "M_Plastic"

.MAT NOM "ABSO"
   BEHAV "ABSO"
   RO 1
   C 153
```

```
.ael group "ABSO_EL" mat "ABSO"

.FSI
 FSA  group  "FSI_WATER" "FSI_AIR"
 FSR  group  "GROUND_FSR" "BUBBLE_FSR"
 LAGR group  "Vessel_n"
 ALE  group  "Water_el" "Air_el" "Bubble_el"

.MOD MAILLE
 ATT 2 group "Vessel_el"
 ATT 3 group "Water_el"
 ATT 4 group "Air_el" "Bubble_el"

.clm fix group "Clamped_n" comp 1 2 3 4 5 6

.sai ARCHIVE STYP 914 COMP 1 2 3 4 5 6 NOEUD I 671

.sai arch ele i 230758 styp 9671 comp 1 2 3
.sai arch ele i 230759 styp 9671 comp 1 2 3
.sai arch ele i 230760 styp 9671 comp 1 2 3
.sai arch ele i 230761 styp 9671 comp 1 2 3
.sai arch ele i 526000 styp 9671 comp 1 2 3

.sai arch group "N_near_clamp" styp 9163 comp 1 2 3
.sai arch group "N_near_clamp" styp 9173 comp 1 2 3
.sai arch group "N_near_clamp" styp 914 comp 1 2 3 4 5 6

.sai arch ele i 568 styp 9390 9391 9392 comp 1
.sai arch ele i 560 styp 9390 9391 9392 comp 1
.sai arch ele i 561 styp 9390 9391 9392 comp 1
.sai arch ele i 554 styp 9390 9391 9392 comp 1
.sai arch ele i 1063 styp 9390 9391 9392 comp 1

.sai arch ele i 6058 styp 9390 9391 9392 comp 1
.sai arch ele i 4922 styp 9390 9391 9392 comp 1
.sai arch ele i 6284 styp 9390 9391 9392 comp 1
.sai arch ele i 5361 styp 9390 9391 9392 comp 1
.sai arch ele i 5150 styp 9390 9391 9392 comp 1
.sai arch ele i 6592 styp 9390 9391 9392 comp 1

.sai arch ele i 7100 styp 9390 9391 9392 comp 1

.sai arch ele i 568 styp 9380 9381 9382 comp 1
.sai arch ele i 560 styp 9380 9381 9382 comp 1
.sai arch ele i 561 styp 9380 9381 9382 comp 1
.sai arch ele i 554 styp 9380 9381 9382 comp 1
.sai arch ele i 1063 styp 9380 9381 9382 comp 1

.sai arch ele i 6058 styp 9380 9381 9382 comp 1
.sai arch ele i 4922 styp 9380 9381 9382 comp 1
.sai arch ele i 6284 styp 9380 9381 9382 comp 1
.sai arch ele i 5361 styp 9380 9381 9382 comp 1
.sai arch ele i 5150 styp 9380 9381 9382 comp 1
.sai arch ele i 6592 styp 9380 9381 9382 comp 1

.sai arch ele i 7100 styp 9380 9381 9382 comp 1

! new group pressure history
!
.sel group "ele-pression" maille
 43135 49693 230758 230759 230760 230761 526000
 523115 523128 589243 588369 589066
  571110 553543 580451 580674 570238
```

```
 581880 582369 583185 583007

.sai arch group "ele-pression" styp 9339 comp 1

.EPX
MATE
** air: calculated for p=1bar
    flut ro 1.3 eint 0.21978e6 gamm 1.35 PB 0
        ITER 1 ALF0 1 BET0 1 KINT 0 AHGF 0 CL 0.5
        CQ 2.56 PMIN 0 PREF 1.e5 NUM 11
        a 3.738e11 b 3.747e9 r1 4.15 r2 0.90
        ros 1630
        LECT group "Air_el"  TERM

** TNT
*
    flut ro 1630 eint 3.68e6 gamm 1.35 PB 0
        ITER 1 ALF0 1 BET0 1 KINT 0 AHGF 0 CL 0.5
        CQ 2.56 PMIN 0 PREF 1.e5 NUM 11
        a 3.738e11 b 3.747e9 r1 4.15 r2 0.90
        d 6930 pini 1e5
        TDET 20e-3
        xdet 0. ydet 0. zdet 0.0730
            LECT group "Bubble_el"  TERM

    FLUT RO 1000 EINT 0 GAMM 2.1316E9 PB 22.8e6
        ITER 1 ALF0 0.5 RREF 1000 BET0 0
        KINT 1 AHGF 0 CL 0  CQ 0
        PMIN 0 NUM 9 PREF 1.E5
        LECT group "Water_el"  TERM

OPTION
 CSTA 0.4
 DTDROP 0.002
 AMOR QUAD 2
 NF34
  QUASI STATIQU 59 1 UPTO 20e-3 FROM 60e-3

CALCUL TINI 0 TEND 85e-3
 PAS1 1.E-8
```

JWL 3D model – gravity (JRC elements)

```
[…]
.EPX
MATE
** air: calculated for p=1bar
    flut ro 1.3 eint 0.21978e6 gamm 1.35 PB 0
        ITER 1 ALF0 1 BET0 1 KINT 0 AHGF 0 CL 0.5
        CQ 2.56 PMIN 0 PREF 1.e5 NUM 11
        a 3.738e11 b 3.747e9 r1 4.15 r2 0.90
        ros 1630
        LECT group "Air_el"  TERM

** TNT
*
    flut ro 1630 eint 3.68e6 gamm 1.35 PB 0
        ITER 1 ALF0 1 BET0 1 KINT 0 AHGF 0 CL 0.5
        CQ 2.56 PMIN 0 PREF 1.e5 NUM 11
        a 3.738e11 b 3.747e9 r1 4.15 r2 0.90
        d 6930 pini 1e5
        TDET 20e-3
```

```
        xdet 0. ydet 0. zdet 0.0730
           LECT group "Bubble_el"  TERM

    FLUT RO 1000 EINT 0 GAMM 2.1316E9 PB 22.8e6
        ITER 1 ALF0 0.5 RREF 1000 BET0 0
        KINT 1 AHGF 0 CL 0  CQ 0
        PMIN 0 NUM 9 PREF 1.E5
        LECT group "Water_el"  TERM

CHAR CONS GRAV 0 0 -9.80665 LECT group "WATER_N"   TERM
CHAR CONS GRAV 0 0 -9.80665 LECT group "Vessel_n"   TERM
CHAR CONS GRAV 0 0 -9.80665 LECT group "BUBBLE_N_VOLUME" TERM
CHAR CONS GRAV 0 0 -9.80665 LECT group "AIR_NODES"  TERM

OPTION
 CSTA 0.4
 DTDROP 0.002
 AMOR QUAD 2
 NF34
  QUASI STATIQU 59 1 UPTO 20e-3 FROM 60e-3

CALCUL TINI 0 TEND 85e-3
 PAS1 1.E-8
```

Strain rate Cowper-Symond dependence for steel

```
[…]
      .FCT CREE FONCTION  NOM "pressure"
          CREE VALEUR Y U
          COUPLES
           0.       0.
           0.0001   (14e06-1.e05)
           0.1      (14e06-1.e05)
           100.     (14e06-1.e05)
          CREE
      .clm pre group "Vessel_el" val 1. nf "pressure" time

      .MAT NOM "M_Plastic"
          BEHAV "Plastic"
          YT 206.058e09
          NT .3
          M 7800
         VONM
          XIT 1. NF "F_Harden"
          VONMISES
          SYMO 40 5
      .ael group "Vessel_el" mat "M_Plastic"

[…]
```

Pressure load (JRC elements)

```
.hyp group "Vessel_el" mindlin
.hyp group "Air_el"   volume
.hyp group "Bubble_el"   volume
.ael group "Air_el"   ng 1 1 1
.ael group "Bubble_el"   ng 1 1 1
.php group "THICK_162" thick val 0.162
.php group "THICK_200" thick val 0.200
```

```
.php group "THICK_125" thick val 0.125

!.ael group "Vessel_el" orde 1
.ael group "Bubble_el" orde 1
.ael group "Air_el" orde 1

.FCT CRE FONCTION NOM "F_Harden"
    CRE VAL Y U
    COUPLES
          0.00E+00          4.63E+08
          3.00E-04          4.78E+08
          5.00E-04          4.72E+08
          8.00E-04          4.71E+08
          1.10E-03          4.72E+08
          1.30E-03          4.72E+08
          1.60E-03          4.73E+08
          1.80E-03          4.74E+08
          2.10E-03          4.74E+08
          2.40E-03          4.74E+08
          2.60E-03          4.74E+08
          2.70E-03          4.73E+08
          3.20E-03          4.74E+08
          […]

.FCT CREE FONCTION  NOM "pressure"
    CREE VALEUR Y U
    COUPLES
     0.       0.
     0.0001   (15.5e06-1.e05)
     0.100    (15.5e06-1.e05)
     100.     (15.5e06-1.e05)
    CREE
.clm pre group "Vessel_el" val 1. nf "pressure" time

.MAT NOM "M_Plastic"
    BEHAV "Plastic"
    YT 206.058e09
    NT .3
    M 7800
    VONM
    XIT 1. NF "F_Harden"
    CAUC
.ael group "Vessel_el" mat "M_Plastic"

.FSI
 FSA  group  "FSI_AIR"
 FSR  group  "FSR_NODES" "BUBBLE_FSR"
 LAGR group  "Vessel_n"
 ALE  group  "Air_el" "Bubble_el"

.MOD MAILLE
 ATT 2 group "Vessel_el"
 ATT 4 group "Air_el" "Bubble_el"

[….]

.EPX
MATE
** air: calculated for p=1bar
*
    flut ro 1.3 eint 0.21978e6 gamm 1.35 PB 0
        ITER 1 ALF0 1 BET0 1 KINT 0 AHGF 0 CL 0.5
        CQ 2.56 PMIN 0 PREF 1.e5 NUM 11
```

```
        a 3.738e11 b 3.747e9 r1 4.15 r2 0.90
        ros 1630
        LECT group "Air_el"  TERM

** TNT
    flut ro 1630 eint 3.68e6 gamm 1.35 PB 0
        ITER 1 ALF0 1 BET0 1 KINT 0 AHGF 0 CL 0.5
        CQ 2.56 PMIN 0 PREF 1.e5 NUM 11
        a 3.738e11 b 3.747e9 r1 4.15 r2 0.90
        d 6930 pini 1e5
        TDET 20e-3
        xdet 0. ydet 0. zdet 0.0730
            LECT group "Bubble_el"  TERM

OPTION
 CSTA 0.4
 DTDROP 0.002
 AMOR QUAD 2
 NF34
  QUASI STATIQU 59 1 UPTO 20e-3 FROM 60e-3

CALCUL TINI 0 TEND 85e-3
 PAS1 1.E-8
```

Von mises progressive fracture model

```
.hyp group "Vessel_el" mindlin
.hyp group "Air_el"   volume
.hyp group "Bubble_el"   volume
.ael group "Air_el"   ng 1 1 1
.ael group "Bubble_el"   ng 1 1 1
.php group "THICK_162" thick val 0.162
.php group "THICK_200" thick val 0.200
.php group "THICK_125" thick val 0.125

!.ael group "Vessel_el" orde 1
.ael group "Bubble_el" orde 1
.ael group "Air_el" orde 1


.FCT CRE FONCTION NOM "F_Harden"
    CRE VAL Y U
    COUPLES
            0.00E+00        4.63E+08
            3.00E-04        4.78E+08
            5.00E-04        4.72E+08
            8.00E-04        4.71E+08
            1.10E-03        4.72E+08
            1.30E-03        4.72E+08
            1.60E-03        4.73E+08
            1.80E-03        4.74E+08
            2.10E-03        4.74E+08
            2.40E-03        4.74E+08
            2.60E-03        4.74E+08
            2.70E-03        4.73E+08
            3.20E-03        4.74E+08
            […]

.FCT CREE FONCTION  NOM "pressure"
    CREE VALEUR Y U
    COUPLES
```

```
      0.       0.
      0.0001   (14e06-1.e05)
      0.1      (14e06-1.e05)
      100.     (14e06-1.e05)
     CREE
.clm pre group "Vessel_el" val 1. nf "pressure" time

.MAT NOM "M_Plastic"
    BEHAV "Plastic"
    YT 206.058e09
    NT .3
    M 7800
    VONM
    XIT 1. NF "F_Harden"
    DT 0.1027
.ael group "Vessel_el" mat "M_Plastic"

.FSI
 FSA  group  "FSI_AIR"
 FSR  group  "FSR_NODES" "BUBBLE_FSR"
 LAGR group  "Vessel_n"
 ALE  group  "Air_el" "Bubble_el"

.MOD MAILLE
 ATT 2 group "Vessel_el"
 ATT 4 group "Air_el" "Bubble_el"

[….]

.EPX
MATE
** air: calculated for p=1bar
*
    flut ro 1.3 eint 0.21978e6 gamm 1.35 PB 0
        ITER 1 ALF0 1 BET0 1 KINT 0 AHGF 0 CL 0.5
        CQ 2.56 PMIN 0 PREF 1.e5 NUM 11
        a 3.738e11 b 3.747e9 r1 4.15 r2 0.90
        ros 1630
        LECT group "Air_el"  TERM

** TNT
    flut ro 1630 eint 3.68e6 gamm 1.35 PB 0
        ITER 1 ALF0 1 BET0 1 KINT 0 AHGF 0 CL 0.5
        CQ 2.56 PMIN 0 PREF 1.e5 NUM 11
        a 3.738e11 b 3.747e9 r1 4.15 r2 0.90
        d 6930 pini 1e5
        TDET 20e-3
        xdet 0. ydet 0. zdet 0.0730
            LECT group "Bubble_el"  TERM

OPTION
 CSTA 0.4
 DTDROP 0.002
 AMOR QUAD 2
 NF34
  QUASI STATIQU 59 1 UPTO 20e-3 FROM 60e-3

CALCUL TINI 0 TEND 85e-3
 PAS1 1.E-8
```

European Commission

EUR 23451 EN – Joint Research Centre – Institute for Energy
Title: ***Structural Response of a Large Pressure Vessel to Dynamic Loading - Feasibility of Fast Transient Dynamic Analysis Methods***
Author(s): E. Paffumi, N. Taylor
Luxembourg: Office for Official Publications of the European Communities
2008 – 124 pp. – 21 x 29.7 cm
EUR 23451EN – Scientific and Technical Research series – ISSN 1018-5593

Abstract

This report presents a feasibility study on structural analysis of pressure-containing structures subject to external blast loads using finite element and volume simulation software. A basic understanding of the main factors influencing the results of such analyses was established in an earlier study. An extensive series of computations have now been performed and the results are presented and discussed in detail in this report. These involve a 3-D simulation of a large steel vessel of hypothetical design containing pressurised water and subject to an explosive blast from a charge located directly underneath the lower torispherical end. The top is closed by a flat lid arrangement. The properties of the explosive material, the air and water environments and the vessel steel were taken from the literature. For the latter, elastic-plastic material properties at 20˚C have been considered. The vessel is located in a bunker and by using FSR boundary conditions the reflections of the pressure waves on the bunker walls are also considered. To provide a cross-check on the computational results, some simplified analyses were performed using engineering and empirical formulae to estimate the pressure loads need to produce yielding and failure of the vessel, as well as of the corresponding quantities of explosives that would be needed to produce sufficient shock wave pressures.

The mission of the JRC is to provide customer-driven scientific and technical support for the conception, development, implementation and monitoring of EU policies. As a service of the European Commission, the JRC functions as a reference centre of science and technology for the Union. Close to the policy-making process, it serves the common interest of the Member States, while being independent of special interests, whether private or national.

JRC
EUROPEAN COMMISSION

Publications Office
Publications.eu.int